DISSERTATION

Synthesis and Photophysical Characterization of New Cyano-Substituted Aromatic Compounds

Muhammad Zahid

Graz, March 2011

Zur Erlangung des akademischen Grades eines Doktorln der Naturwissenschaften

erreicht an der

Technischen Universität Graz

O. Univ.-Prof. Dipl.-Ing. Dr. rer. nat. Günter Grampp
Institut für Physikalische und Theoretische Chemie
Technische Universität Graz

Deutsche Fassung:
Beschluss der Curricula-Kommission für Bachelor-, Master- und Diplomstudien vom 10.11.2008
Genehmigung des Senates am 1.12.2008

EIDESSTATTLICHE ERKLÄRUNG

Ich erkläre an Eides statt, dass ich die vorliegende Arbeit selbstständig verfasst, andere als die angegebenen Quellen/Hilfsmittel nicht benutzt, und die den benutzten Quellen wörtlich und inhaltlich entnommene Stellen als solche kenntlich gemacht habe.

Graz, am …… ……..
(Unterschrift)

Englische Fassung:

STATUTORY DECLARATION

I declare that I have authored this thesis independently, that I have not used other than the declared sources / resources, and that I have explicitly marked all material which has been quoted either literally or by content from the used sources.

…… ……..
date (signature)

In The Name of ALLAH, The Most Beneficent, The Most Merciful

To my loving family

Acknowledgement

The present work (in fact everything in my life) cannot be possible but with the blessings of ALLAH. Bundle of thanks to Almighty ALLAH for his numerous blessings on me.
Prayers of my parents are always a wonderful source for me to gather my strength and make difficult things pretty easy. Thanks to my parents, my family for their support, guidance and loving care they always have for me. May ALLLAH give me strength to serve them as they have right on me.

I would like express my profound gratitude to Prof. Günter Grampp for giving me a chance to work with him. I have never seen in my life such a wonderful, dynamic and inspirational personality. Your enthusiasm, of always willing to do something when you have time, is a source for great inspiration. During my work tenure, I always find you available when I need help and guidance. Your appreciation especially when I have synthesis problems with the words "you are the expert" has solved many problems, atleast give me a boost to look for solutions…….. Great scientific knowledge in various fields, always helping me actively when I have problems, deep understandings of problems, very polite and friendly attitude, give freedom of thoughts and expressions…… in fact all these qualities create a wonderful environment to perform experiments efficiently. I would also like to thank you for giving me chance and funding for my visit to Mulhouse, France to discuss results with Prof. Patrice.
My special thanks to Prof. Patrice Jacques, for his very fruitful discussions during my stay in Mulhouse, France. I would say him as the real expert of SOLVATOCHROMISM. Many problems related to solvatochromic study are resolved during discussions with Prof. Patrice. I thank him also for giving me opportunity to contact him whenever I need his help and guidance.
I would like to thanks to Ao. Prof. Stephan Landgraf for having discussion on problem related to TCHQ and for managing me to measure lifetimes for some compounds. I am also grateful to him for giving me opportunities to learn from time to time discussion on results which always end up at some interesting ideas from him.

Very special thank for Dr. Arnulf Rosspeintner and Dr. Gonzalo Angulo for their guidance and patience towards my repeatedly disturbances. In fact I would like to say more than thanks because I

think that it would not be easy for me to finish this work without your guideline. The ideas shared by them always result as the solutions of my problems. Special thanks to Ulf for MATLAB programs (makes data treatment so easy), as after getting these programs, I have started some workout on MATLAB which was totally unknown to me before. Thank you for discussions and help related the data treatment. I would say that I did not feel much trouble during my research because of you people.

I would like to thanks Dr. Asim Mansha, Bhabhi jee and chote mian (Mr. Abdullah). I can find many occasions during my stay here in Graz when I would have miss my family but they never give me chance to feel that I am away from my family.

I would like to thank Dr Boryana Mladenova for ESR measurements. I have theoretical knowledge of ESR but with your help I am able to perform ESR experiments, thanks for this. Thanks to Dr. Kenneth Rasmussen for both general and work related help.

I would like to thank to my colleague Dr. Faiza, Dr. Noureen, Dr. Tajamal, Tahir, Kunal, Truong, Kraiwan …… for sharing time, labs and giving me some good memories.
I want to express my thanks to Herbert Lang, Helmut Eisenkölbl, Marion Hofmeister and Hilde Freissmuth for keeping things running administratively and experimentally. Thanks to Hilde Freissmuth for my understanding to German language (though still at very beginning level)…. Vielen Dank!.
Special thanks to my colleagues (The UETIANS in Austria, My MSc classmates) for making my stay here memorable. It's wonderful to have you people around
Very special thanks to Qamar Abaas, Sarfraz Ahmed, Muhammad Tahir Soomro, Kahsif Nadeen, Saeed Khan, Imam Bakhash Abdullah and Mudassir Abbas for sharing their time in hostel (C-15) and long discussions on dining table…….. You all are really wonderful people….. Thanks to all my friends living in Graz to make me feel like I am among my own people.
……. ……. …… …. … .
I would like to thank to NAWI Graz for partial funding to attend conference in USA.
Many thanks to Higher Education Commission (HEC), Pakistan for financial support of my PhD degree.

Abstract

Novel cyano-substituted derivatives of p-phenylenediamine (PPD) and N,N,N',N'-tetramethyl-p-phenylenediamine (TMPPD) have been synthesized. These newly synthesized compounds are structurally characterized using UV-VIS, IR, NMR and mass spectrometry. Photophysical properties (e.g. absorption maxima, fluorescence maxima, fluorescence quantum yield, fluorescence lifetime, Stokes shift, 0-0 transition energy, radiative and non-radiative rate constants) of these compounds (also for PPD and TMPPD) have been thoroughly studied in several solvents. Interactions of the solvent molecules with ground and excited states of the fluorophore have been investigated through linear solvation energy relationship (LSER) using different parameters developed by Kamlet-Taft, Catalan, Reichardt, Gutmann and Onsager. The changes in the photophysical properties with increasing the number of cyano groups on the aromatic ring of the PPDs and TMPPDs are explored. Also the comparison of cyano-substituted PPDs with counter tetra-methylated derivatives (cyano-substituted TMPPDs) have been studied.

Additionally 2,3,5,6-tetracyanohydroquinone (TCHQ) and 2,3,5,6-tetracyanobenzoquinone (cyanil) have also been synthesized. Absorption and emission characteristics of TCHQ are studied in different solvents. The ground and excited state protic equilibria (pK_a and pK_a^*) are also measured for some cyano-substituted aromatic compounds. The substitutions by the electron-withdrawing cyano groups also change the electrochemical behavior of PPDs. Electrochemical properties such as redox potential and diffusion coefficients for cyano-substituted PPDs and TMPPDs are studied by cyclic voltammetry. Qualitative electron spin resonance (ESR) studies for some of these compounds have been investigated.

Zusammenfassung

Neue cyanosubstituierte Derivate von p-Phenylendiamin und N,N,N',N'-Tetramethyl-p-Phenylendiamin wurden synthetisiert. Diese erstmalig synthetisierten Substanzen wurden vermittels UV-Vis, IR, NMR und Massenspektroskopie charakterisiert. Die photophysikalischen Eigenschaften (u.a. Absorptionsmaxima, Fluoreszenzmaxima, Fluoreszenzquantenausbeute, Fluoreszenzlebensdauer, Stokes-Shift, 0-0 Energie, radiative und nicht radiative Geschwindigkeitskonstanten) dieser Substanzen (sowie zusätzlich PPD und TMPPD) in verschiedenen Lösungsmitteln wurden genauestens untersucht. Die Wechselwirkung zwischen den Lösungsmittelmolekülen und dem Grund- und angeregten Zustand der untersuchten Fluorophore wurde mittels „linear solvation energy relationships" (LSER) unter Verwendung verschiedenster Parameter, wie Kamlet-Taft, Catalan, Reichardt, Gutmann und Onsager, untersucht. Der Einfluss der Anzahl an Cyanogruppen im aromatischen Ring von PPD und TMPPD auf die photophysikalischen Eigenschaften wurde ermittelt. Zudem wurde der Einfluss der Methylierung der Aminofunktionalität cyanosubstituierter TMPPDs erprobt.

Zusätzlich wurden 2,3,5,6-Tetracyanohydrochinon (TCHQ) und 2,3,5,6,-Tetracyanobenzochinon (Cyanil) synthetisiert. Die Absorptions- und Emissionscharakteristika von TCHQ wurden in verschiedenen Lösungsmitteln ermittelt. Die protischen Gleichgewichte im Grund- und angeregten Zustand (pKa und pKa*) einiger cyanosubstituierter aromatischer Verbindungen wurden auch untersucht. Das Einbringen elektronenziehender Cyanogruppen in den aromatischen Ring verändert auch das elektrochemische Verhalten der untersuchten p-Phenylendiamine. Die elektrochemischen Eigenschaften, wie Redoxpotential oder Diffusionskoeffizienten, der cyanosubstituierten PPD und TMPPD wurden mittels zyklischer Voltammetrie untersucht. Zudem wurden für einige der angeführten Verbindungen qualitative Elektronenspinresonanz Untersuchungen durchgeführt.

LIST OF FIGURES

LIST OF TABLES

1 INTRODUCTION

Both *p*-phenylenediamine (PPD) and N,N,N',N'-tetramethyl-p-phenylenediamine (TMPPD) have been very well studied in numerous different aspects[1], e.g. photoinduced charge transfer studies [1-4], CIDEP (chemically induced dynamic electron polarization), ESR (electron spin resonance) as well as other magnetic field effects [5-13], electrochemical investigations in various solvents (also ionic liquids) [14-20] etc. Derivatives of PPD and TMPPD constitute an interesting family of molecules because of their useful electrochemical and spectrochemical properties which are governed by the substitution on the aromatic ring [20-24]. Thanks to their low oxidation potential and formation of stable semiquinone radical cations [25], PPD and its derivatives are used in electrochromism, hair coloration and as color developer in color films and paper [26]. Their properties depend on both the position and nature of the substituents and the medium [27-29].

Until recently PPD derivatives were not renowned for being highly fluorescent molecules. Fluorescence properties have been drastically changed by the inclusion of electron withdrawing groups (-CN) on the aromatic ring [30-31]. 2,6-dicyano-N,N,N',N'-tetramethyl-*p*-phenylenediamine (DCTMPPD) and 2,3,5,6,-tetracyano-*p*-phenylenediamine (TCPPD) were found to have fluorescence quantum yields and lifetimes much larger than any formerly known PPD derivatives [32-34]. In case of DCTMPPD, the fluorescence quantum yields in different solvents vary from 0.37 to 0.58 with relatively large fluorescence lifetimes ranges from 12 ns to 23 ns and very low triplet production yield [30]. The significant increase in both fluorescence quantum yield and lifetime is larger in TCPPD compared to that of DCTMPPD. In TCPPD the quantum yield is above 0.7 in most of the solvents and its lifetime is around 20ns (upto 0.89 in ethyl ether with fluorescence lifetime of 23.1 ns).

Another interesting feature is the electrochemical behavior of TCPPD. It is the first PPD derivative which undergoes reversible reduction (−0.72V vs SCE) while not showing reversible oxidation [31].

The solvatochromic studies for the above two cyano-substituted derivatives of TMPPD and PPD have shown that DCTMPPD interacts with solvent molecules mainly through non-

[1] PPD and TMPPD are among the most studied compounds with respect to magnetic, photophysical and

specific interactions while in TCPPD the solvent basicity is responsible for solvatochromic shifts.

The precise role of the nitrile and amino groups in the former two molecules is not yet absolutely clear. Thence, in order to study the depth of the mystery of such dramatic change in the photophysical (in both TCPPD and DCTMPPD) and electrochemical (in TCPPD) properties compared to PPD and TMPPD, some new cyano-substituted PPDs and TMPPDs have been synthesized. The photophysical properties of predecessor molecules (PPD and TMPPD) have also not been studied with special concern of solvent-solute interactions in different solvents. Photophysical properties of PPD, TMPPD and their cyano-substituted derivatives, monocyano-*p*-phenylenediamine (MCPPD); 2,6-dicyano-*p*-phenylenediamine (26DCPPD); 2,3,5,6-tetracyano-*p*-phenylenediamine (TCPPD); monocyano-N,N,N',N'-tetramethyl-*p*-phenylenediamine (MCTMPPD) and 2,6-dicyano-N,N,N',N'-tetramethyl-*p*-phenylenediamine (DCTMPPD)[2] have been studied in about 21 to 25 solvents[3]. Above molecules are divided into two sets: (1) PPD and its cyano-substituted derivatives (PPDs) and (2) TMPPD and cyano-substituted derivatives (TMPPDs). The photophysical properties such as absorption maxima ($\tilde{\nu}_{abs}$), fluorescence maxima ($\tilde{\nu}_{flu}$), Stokes shift ($\Delta\tilde{\nu}$) , 0-0 transition energy (E_{00}), fluorescence quantum yield (Φ), fluorescence lifetime (τ), radiative rate constant (k_r) and non-radiative rate constant (k_{nr}) have been assessed in different solvents. The solvents used in this study encompass polar protic (alcohols and H_2O) highly polar aprotic (DMSO, DMF, HMPA etc.) and apolar to slightly polar aprotic ones (alkanes, aromatics, ethers and esters).

Solvent-solute interactions, which include non-specific (electrostatic) and specific interactions (hydrogen bonding) depend on different parameters. Therefore no single parameter or macroscopic property can be used to characterize the solvent effects on the solute properties. Different solvent parameter sets such as Kamlet-Taft (α, β and π^*) [35-38], Catalan's parameters (SA, SB, Sdp and SP) [39-42], combination of Reichardt polarity parameter (ETN) [43-46] and Gutmann's donor number (DNN) [47] and Onsager polarity parameters $\left(f(n^2), f(D,n^2) \right)$ [48-49] have been used to study solvent-solute interactions. The solvent-solute interactions can be analyzed by using the combination of solvent

[2] Solvatochromic properties of TCPPD and DCTMPPD have already published in literature by our group but, in order to have a same set of solvents and valid comparison, photophysical propertied in some protic solvent and in some esters have been studied which are not studied previously .

[3] This number is reduced due limitation of solute solubility in some solvents and solvent absorption (cut off).

properties in the manner of Linear Solvent Energy Relationships (LSER) that can be expressed as general mathematical form as shown in equation 1-1:

$$ABC = ABC_o + \sum_i x_i X_i \qquad 1\text{-}1$$

where ABC is the solvent dependent property of interest and ABC_o is its value in the gas phase. X_i are the parameters of the solvent, like solvent acidity, basicity, polarizability, di-polarity etc., and x_i stands for the solute sensitivity to the corresponding solvent property. Therefore, in order to disentangle the influence of so many solvent properties in the photophysics of aromatic molecules, a large number of solvents must be studied. Additionally, most solvents show a combined effect and no homogeneous series for each of the parameters in question does really exist. The information thus obtained can be in principle used to predict the behavior of the excited state in a number of environments and it is the starting point for further photophysical characterization works.

The electrochemical properties such as redox potentials and diffusion coefficients for all PPDs and TMPPDs have been studied in acetonitrile. Also the ESR measurements for some of these compounds have been performed. In addition to PPDs and TMPPDs, 2,3,5,6-tetracyanohydroquinone (TCHQ) and 2,3,5,6-tetracyanobenzoquinone (cyanil) have also been synthesized. Cyanil has high redox potential [44] and is of high interest in photoinduced electron transfer reactions studies [50]. Absorption and emission properties of TCHQ have been studied in various solvents. Very interesting concentration dependant absorption and emission properties of TCHQ have been observed. Additionally ground and excited state proton transfer equilibria (pK_a and pK_a^*) have been studied for TCHQ and 26DCPPD.

The description of the present work in the thesis is organised as follow: In chapter 2 the some basics of photophysical process and associated properties have been discussed along with some discussions how absorption and emission is related with the structure of organic molecules. The middle part is dedicated to solvatochromism with emphasis of different solvent scales used to describe the nature of the solvents. At the end of this chapter, few words about cyclic voltammetry to describe the electrochemical characteristics of reversible and irreversible systems. Chapter 3 provides the necessary information about experimental techniques, solvents used, methods for sample preparation, experimental measurement and finally the layout of data treatment. Chapter 4 describes compounds of interest for the present study and different experimental procedures adopted to synthesize them. The results are presents in two parts in chapter 5. In the first section, photophysical properties of

different cyano-substituted aromatic compounds are given along with solvatochromic studies using differ solvent parameters. In second section the electrochemical properties of PPDs and TMPPDs are discussed along with ESR study of some TMPPDs. Finally the short summary of the conclusions those are extracted from the experimental results and a short outlook describing the future interest of the present findings is described in chapter 6. Appendix contains the values of the solvent parameters used in the present study and some supporting figures those might be required for visualize the experimental facts.

In short, the document describes the systematic study of photophysical properties for cyano-substituted PPDs and TMPPDs in adequate number of solvents. The comparison of linear regression coefficients, obtained by using different solvent parameters, helped to get a deep insight of the solvatochromic effects but may lead to many open questions for different solvent scales which may require some more extensive study.

2 THEORETICAL CONSIDERATION

2.1 Photophysical Processes in UV-VIS region

Photoexcitation and subsequent events which lead molecules from one state to another through radiation and radiationless transitions are called photophysical processes. The molecular specie does not undergo any chemical change as a result of light interaction during the photophysical process. Both photochemical and photobiological properties are related to photophysical properties of the molecule. The photophysical processes are divided commonly in unimolecular and bimolecular processes depending upon the number of molecular species involved.

Unimolecular processes are photophysical processes that occur in isolated molecules in gas the phase or in dilute solutions in the transparent medium. Unimolecular photophysical processes result in both, radiative (electronic absorption and photo emission) and non-radiative (internal conversion and intersystem crossing) transitions. The unimolecular photophysical processes are summarized in the Figure 2-1.

2.1.1 Electronic Absorption

A molecule undergoes radiative excitation transitions from a lower electronic state to higher electronic state as a result of absorption of photon. The electronic transition consists of promotion of an electron from a ground state molecular orbital into an unoccupied orbital of the excited state. The photophysical processes that can be involved in absorption are as follow;

i. **Single-singlet absorption;** S_0-S_1 and S_0-S_n absorption are spin allowed processes and constituted the main electronic absorption spectrum.
ii. **Singlet-triplet absorption;** S_0-T_1 and S_0-T_n are spin forbidden transitions.
iii. **Singlet-singlet absorption of S_1 excited state;** S_1-S_n is biphotonic process (as S_1 is achieved by an intense light flash, S_0-S_1) and transient absorption is observed by nanosecond flash photolysis.
iv. **Triplet-triplet absorption of T_1 excited State;** T_1-T_n is also biphotonic process and triplet state T_1 is populated by the intersystem crossing from S_1.The transient absorption is observed during the lifetime of T_1.

Absorption of two photons by the same molecule is termed as a **biphotonic process**. The two photons can be of the same or different energies. Sometimes irradiation by an intense light source, e.g. laser light, can result as the absorption of the second photon by the molecule already in exited state (S_1 or T_1) as in the process (iii) and (iii). Two photons, each of energy less than S_1, may be absorbed at the same time by the same molecule when excited by laser beam (S_0-S_n transition). Higher excited states produced as a result of biphotonic process sometimes have higher energy than that the molecular ionization and thus biphotonic ionization processes occur.

2.1.2 Photoluminescence

Deactivation of a molecule from the higher to a lower electronic state with emission of a photon is called luminescence and luminescence following the absorption of a photon is called photoluminescence. Radiative transition between the two states of same multiplicity is known as fluorescence and those of between the states of different multiplicity is known as phosphorescence. Following photophysical processes are involved in luminescence:

v. **Singlet-Singlet emission;** S_1-S_0 fluorescence is referred as normal fluorescence emission with lifetime of ps to ns.

vi. **Triplet-singlet emission;** T_1-S_0 corresponds to the phosphorescence with longer lifetime μs to ms.

vii. **Singlet-Singlet emission;** S_n-S_0 fluorescence is observed only in very few compounds e.g. in azulene.

viii. **Triplet-singlet emission;** T_n-S_0 phosphorescence is rarely observed luminescence and has been reported for fluoranthene.

ix. **Triplet-triplet absorption;** T_n-T_1 fluorescence is reported for azulene and naphthalene.

x. **Singlet-Singlet emission;** S_n-S_1 fluorescence is also a possible photophysical process.

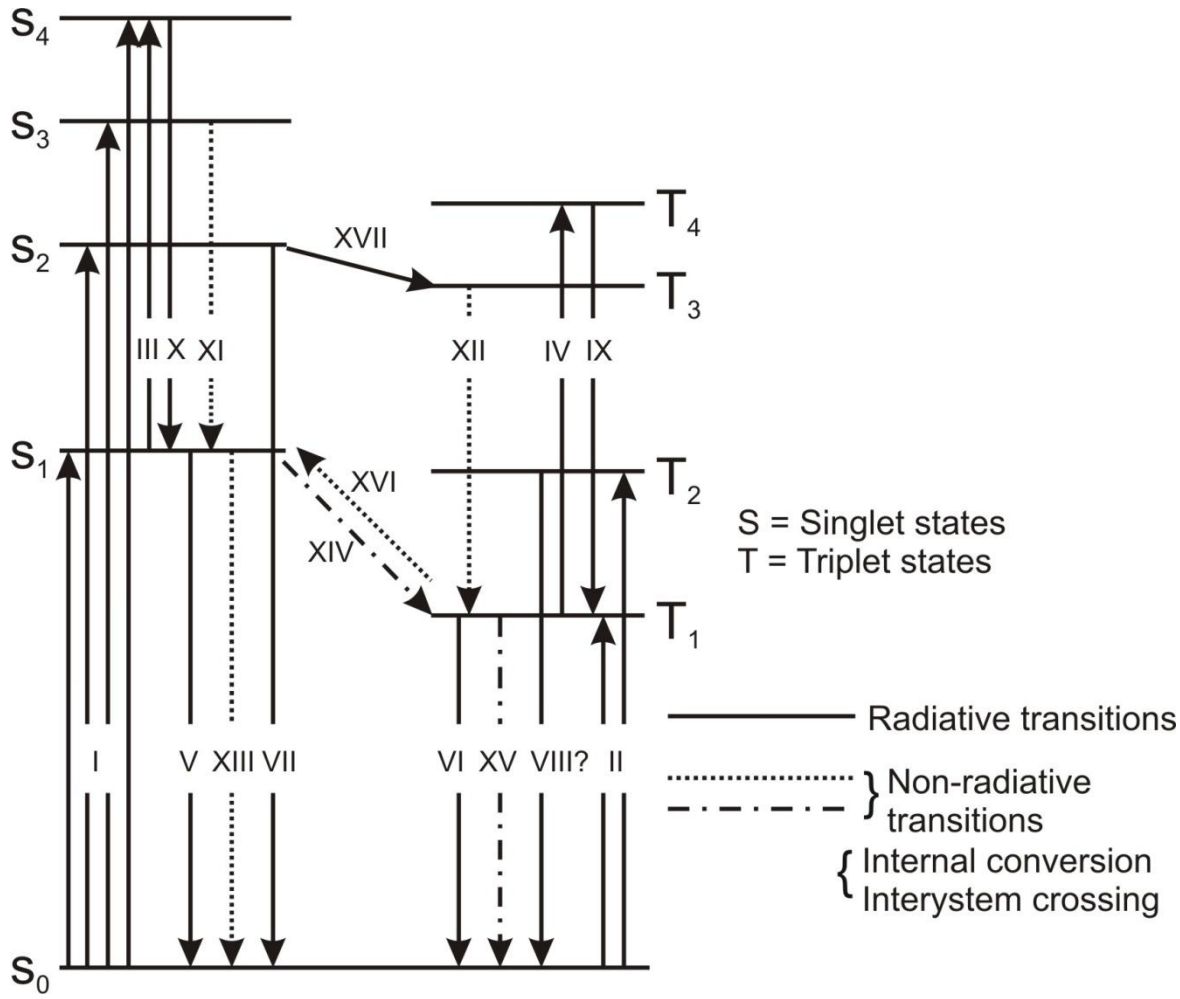

Figure 2-1: Photophysical processes.

2.1.3 Internal conversion and intersystem crossing

Transition between the isoenergetic vibrational levels of different electronic states are preceded by non-radiative thermal activation of the initial electronic state and/or followed by non-radiative thermal deactivation of the final electronic state. Non-radiatve transitions are internal conversion (transition between same multiplicities) and intersystem crossing (transition between the different multiplicities). Following photophysical processes are involved in non-radiative transition;

xi. **S_2-S_1 and S_n-S_{n-1} internal conversion** processes are very fast.

xii. **T_2-T_1 and T_nT_{n-1} internal conversion** processes are also a rapid process.

xiii. **S_1-S_0 internal conversion** process for quenching of first excited singlet state to ground singlet state.

xiv. **S_1-T_1 and S_1-T_n intersystem crossing** processes compete with normal fluorescence.

xv. **T_1-S_0 intersystem crossing** competes with the normal phosphorescence.

xvi. **T_1-S_1 intersystem crossing** may occur due to thermal activation of the T1 state and results in the form of e-type (eosin-type) delayed fluorescence[4].

xvii. **S_n-T_n intersystem crossing** for higher singlet excited states has also been observed in some molecules

In **bimolecular processES**, two molecules are involved in photophysical processes. These two molecules can be either the same specie or of different species. In concentrated solutions, there exist additional interactions with other molecules of the same specie called homopolar bimolecular processes. If the interacting molecules belong to different species, the photophysical processes under these circumstances are referred as heteropolar bimolecular process. Bimolecular process can be divided in the following categories:

1. **Perturbation processes;** sometimes the energy levels of the excited state may be disturbed by the interaction with the neighboring molecule(s)/atom(s) and modify the photophysical behavior. Enhanced intersystem crossing due to interaction with paramagnetic molecule(e.g. oxygen) or molecules bearing heavy atom(s) (external heavy atom effect) are example for perturbation processes.
2. **Excitation migration and transfer processes;** an excited ad unexcited molecular interaction can lead to transfer of excess energy either by a radiative or by a non-radiative process. Exciton migration is excitation energy transfer between the molecules of same species (homopolar process) and lead to delocalization of the excited states.
3. **Ground state complex formation by two unexcited molecules;** ground state complex formation can occur between the molecular of the same species (usually between dye molecule in concentrated solutions, association/aggregation) or between the molecules belong to different species (e.g. aromatic hydrocarbon and some other appropriate molecules like p-chloranil, heteropolar donor-acceptor complexes). Photophysical properties of these ground state complexes are different from the constituent molecules.
4. **Complex formation between an excited and an unexcited molecule;** Molecule in their first excited singlet state are more reactive and sometimes interact with other unexcited molecules. Interaction between the excited and ground state molecules of

[4] The process in which the first excited singlet state becomes populated by a thermally activated radiationless transition from the first excited triplet state. Delayed fluorescence emitting from such excited triplet state is referred E-type delayed fluorescence.

same species form excited dimers, known as excimers. If the excited and ground state molecules belong to different species, then their resulting interaction lead to excited molecular complexes known as exciplexes. Both excimers and exciplexes exhibit their own photophysical characteristics.

5. **Interaction between two excited molecules;** Interaction between the two molecules when both are in the excited states also exists in different molecules. The simplest form triplet-triplet association yields both excited molecules and excimers. The fluorescence of these formed species is known as p-type (pyrene-type) delayed fluorescence[5].

2.2 Structure and electronic transitions

The electronic spectra are valuable aid in understanding the molecular structure because the electronic states depend upon the number of electrons (lone pair and bond pairs) in a molecule and also on the geometry and symmetry of the molecules.

Absorption of a photon of suitable energy results in promotion of an electron from an orbital of molecule in ground to an unoccupied orbital of some higher energy. The usual energy order for the electronic transition is as follow:

$n \rightarrow \pi^* \geq \pi \rightarrow \pi^* > n \rightarrow \sigma^* > \pi \rightarrow \sigma^* > \sigma \rightarrow \pi^* > \sigma \rightarrow \sigma^*$

In some cases the $\pi \rightarrow \pi^*$ transition has become lower in energy compared to $n \rightarrow \pi^*$ transition as discussed in section (transition in some heterocyclic compounds). Also $n \rightarrow \sigma^*$ transitions require a lot of energy and appear normally in far UV region. The energy diagram for these transitions is shown in Figure 2-2.

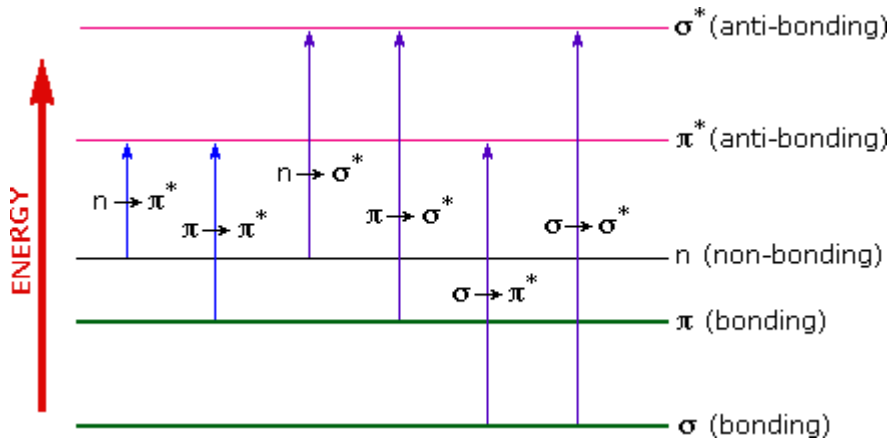

Figure 2-2: Type of electronic transitions in organic molecules.

[5] The process in which the first excited singlet state is populated by interaction of two molecules in the triplet state (triplet-triplet annihilation), delayed fluorescence in such case is called P-type delayed fluorescence.

2.2.1 Selection Rules

Electronic state is characterized by certain basic properties like energy, multiplicity and its symmetry and in centro-symmetric molecules includes parity. These properties formulate the important selection rules which influence the probability of transitions between in different electronic states.

Multiplicity rules: Only those electronic transitions are allowed which occur between same spin multiplicity states i.e. singlet-singlet and triplet-triplet transitions are allowed but triplet-singlet and singlet triplet transition are forbidden. Multiplicity selection rule has major influence of the probability of electronic transition (and thus photophysical process section 2.1) in aromatic molecules. But in reality there is always a week interaction between the wave functions of different multiplicities through spin-orbital coupling. Spin-orbit coupling in aromatic hydrocarbon is small because of the low atomic number of the constituent carbon and hydrogen atom.

Intersystem crossing is possible because of spin orbit interaction. The efficiency of this coupling is related to the fourth power of the atomic number, which is reason why intersystem crossing is favored due to presence of heavy atom at the molecule (internal-heavy atom effect) or in their environment (external-heavy atom effect).

Symmetry rules: Symmetry selection rules also influence the electronic transition between the different states. Electric dipole transitions between electronic states of same symmetry are forbidden. It should be noted that the symmetry forbidden transition can be observable because of vibronic coupling due to molecular vibrations. The molar absorption coefficient for this type of transition is comparatively very small. This is the case with most of $n \rightarrow \pi^*$ transition in solvent that are lake of hydrogen bond forming ability ($\varepsilon \sim 100\text{-}1000$ L mol^{-1} cm^{-1}).

Parity: In parity selection rule, under special case of symmetry selection rule i.e. in centrally symmetric systems, is that electric dipole transitions between same parity states are forbidden. In centro-symmetric molecules (e.g. naphthalene, anthracene and higher polycenes), the states are divide into even (*g* = gerade) and odd (*u* = ungerade) parity, depending on the electronic wave function is symmetric or anti symmetric with respect to reflection of center of gravity. The transitions from *u*-*u* (or *g*-*g*) parities are forbidden and between those of different parities are allowed.

The first excited states (both singlet S_1 and triplet T_1) of polycenes have odd (*u*) parity whereas higher excited states (single S_n and triplet T_n) have even (*g*) parity and transitions

between them are allowed. The transient absorption spectra for such transition can be studied using flash photolysis and provide information for the higher excited states.

2.2.2 Molecular structure and absorption

Energy required for electronic transition from highest unoccupied molecular orbital (HOMO) to the lowest unoccupied molecular orbital (LUMO) is the most probable (energetically favored) transition. In the Figure 2-2 the n→π* transition would require lower energy compared to the other transition. The nuclei determine the strength to hold electrons in the bonds and thus play an important role in determining the energy for the electronic excitation. Hence the characteristic energy absorbed during an electronic transition is the property of group of atom. The group of atoms (sometimes the whole molecule itself) which is responsible for such absorption is called *chromophore*[6]. Originally this term came from dye stuff industry, referred as group of atoms in a molecule that is responsible for its color. Most often the chromophores are of two types, conjugated π system (resonating systems) and metal complexes. Auxochromes are the substituents that increase the intensity, and possibly the wavelength of the principal chromophore. Typical examples of the auxochromes include -CH_3, -OH, -X, and NH_2. There are four different types of effect that a substituent can have on the absorption:

a) **Hyperchromic shift;** an increase in the absorption (or emission) intensity.
b) **Hypsochromic shift;** a decrease in the absorption (or emission) intensity.
c) **Bathochromic shift (red shift);** a shift of absorption (or emission) maxima to longer wavelength (lower energy).
d) **Hypsochromic shift (blue shift);** a shift of absorption (or emission) maxima to shorter wavelength (higher energy).

Thus the structure of the chromophore (thus molecule) has been related to the absorption of the photon of the typical energy.

Effect of conjugation

The conjugation of double and triple bonds to already existed π system will shift the absorption maxima to the longer wavelength (bathochromic shift) as seen in Figure 2-3.

[6]O.N. Witt introduced this term but it had different meaning from that accepted today.
51. Witt, O.N., *Zur Kenntniss des Baues und der Bildung färbender Kohlenstoffverbindungen.* Berichte der deutschen chemischen Gesellschaft, 1876. **9**(1): p. 522-527.

Increase in conjugation not only results as bathochromic shift but also increase the absorption intensity.

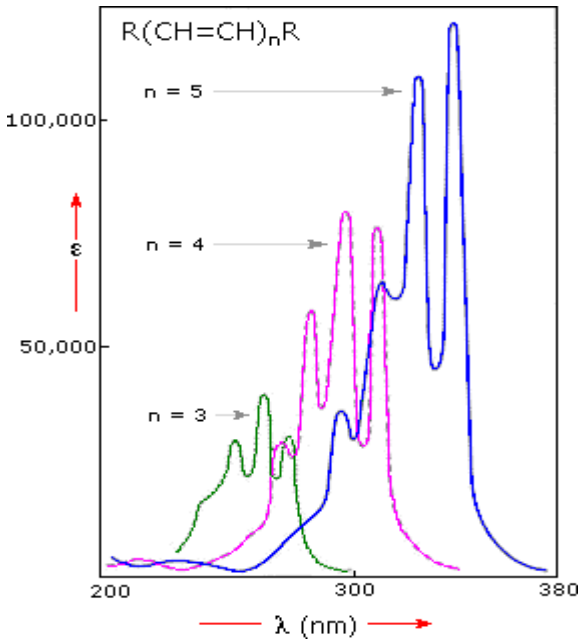

Figure 2-3: Absorption spectra of polyenes illustrating the effect of conjugation.

There are empirical rules called Woodward-Fieser Rules[7] for the estimation of the absorption maxima in an UV-VIS spectrum of the carbonyl compounds, dienes and polyenes.

Aromatic compounds

Aromatic compounds constitute a wide range of organic molecules but the absorption that results the transition in aromatic compounds is very complex. Electronic excitation within the benzene chromophore are basically of the $\pi \rightarrow \pi^*$ type, but they are not as simple as in the case of other chromophores. Due to electron-electron repulsions and symmetry, there are three types of the electronic transitions in the benzene ring. The transitions at 180 and 202 nm are known as primary bands and one at 255 is know as secondary band.

There can be different types of shifts (bathochromic and hyperchromic) caused by the substitution on the benzene ring but these shifts are difficult to predict by some empirical rules as was done for dienes, polyenes and enones. There may be some qualitative understanding of the substitution effects by grouping of certain substituents.

[7] Named after Robert B. Woodward and Louis F. Fieser who introduced these rules.

52. Woodward, R.B., *Structure and the Absorption Spectra of α,β-Unsaturated Ketones.* Journal of the American Chemical Society, 1941. **63**(4): p. 1123-1126.

53. Fieser, L.F., M. Fieser, and S. Rajagopalan, *Absorption spectroscopy and the structures of the diosterols.* The Journal of Organic Chemistry, 1948. **13**(6): p. 800-806.

Substituent with lone-pair of electrons

Substituents containing nonbonding lone-pair of electrons can extend the π-system through conjugation. If the lone pair is more available for conjugation then there will be a shift of the absorption band to longer wavelengths. In such compounds, there is also the possibility of $n \rightarrow \pi^*$ due to presence of these n electrons. The atom (A) from which the electron is excited becomes electron deficient during $n \rightarrow \pi^*$ excitation process. Also the π system (now include A atom as well) contains an extra electron. This result in the form of charge separation and generally represented by the resonance structure as shown in Scheme 2-1. Such an excited state is called an electron transfer or charge transfer excited state. The examples for such substituents include $–NH_2$, -OH, -X, and –OR.

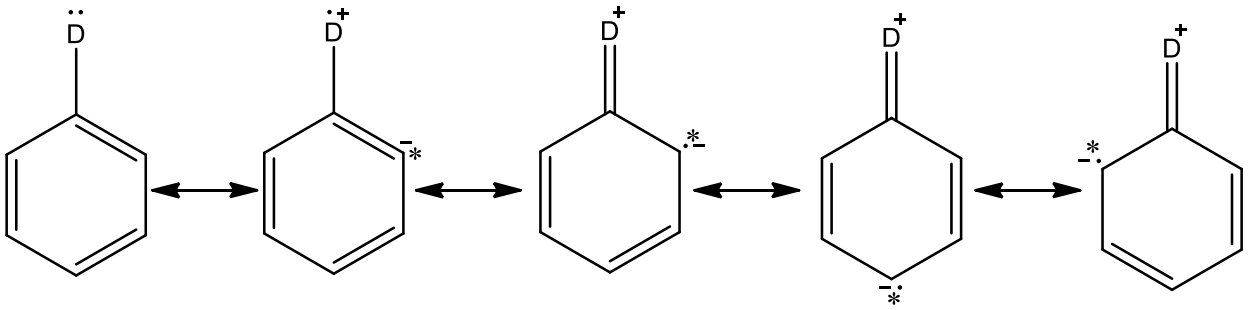

Scheme 2-1

Substituents with pi-conjugation

When benzene ring is substituted with the groups those have π-electrons and are chromophore themselves, there may be interaction between the electrons of the benzene ring and π-electrons of the substituents. Chromophores containing carbonyl groups (-COOH, -CHO, >CO etc) are the examples for such substituents. This can result a new electron transfer band and this band may have high intensity to observe the already existed band of the benzene system. But in this case, in contrast to the previous case, the benzene ring becomes electron deficient as shown in Scheme 2-2.

Scheme 2-2

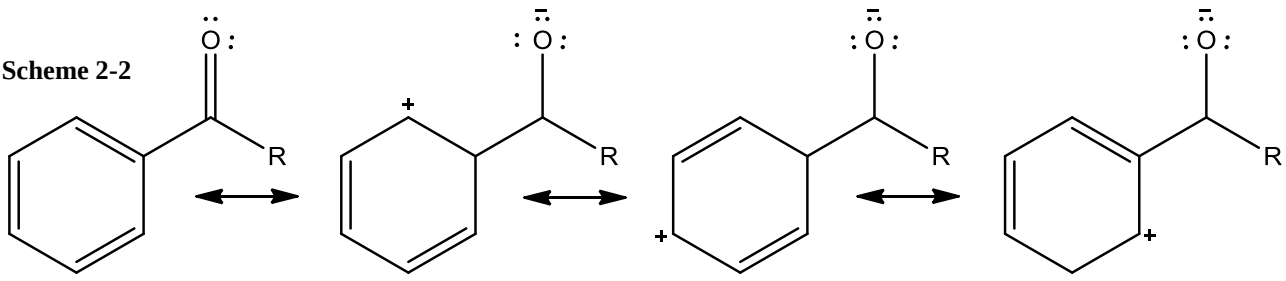

Electron withdrawing and electron releasing effects

The position of the absorption maxima also varies with the nature (electron donating or withdrawing effect) of the substituent. In case of mono substituted benzene derivatives, any substituent (whether electron withdrawing or electron donating effect) shifts the primary band to the longer wavelength. Electron releasing substituent has very little effect on the position of the secondary band unless such substituent also acts as chromophore but electron withdrawing groups increase both the intensity and wavelength of the secondary band.

In di-substituted benzene derivatives, for para di-substituted benzene, there exit two possibilities:

1. If both groups have same (electron donating or withdrawing effect) effect, then the effect is similar as in case of mono-substituted benzene and the group with stronger effect will determine the extent of the shift in absorption band.
2. If one group is electron releasing and other electron withdrawing effect, the magnitude of the shift in absorption is greater than the sum of their individual shift. The reason for such enhanced shift is the possible resonance interaction.

If both groups are either ortho or meta to each other, the magnitude of the shift is the sum of their individual shifts. However the case of more than one substituent on the aromatic ring is much more complex.

Polynuclear aromatic hydrocarbon and heterocyclic compounds

The primary and secondary absorption bands are shifted towards the longer wavelength in case of polyaromatic hydrocarbons. The primary bands that appear in benzene at 184 nm is shifted to 220 nm in case of naphthalene. In general, there is more bathochromic shift as the extent of conjugation increases as shown in Figure 2-3. There exist the characteristic fine structure UV spectra of polynuclear aromatic compounds. The nature of the substituent can be identified by comparing the shape and fine structure of the substitute and unsubstituted polynuclear aromatics.

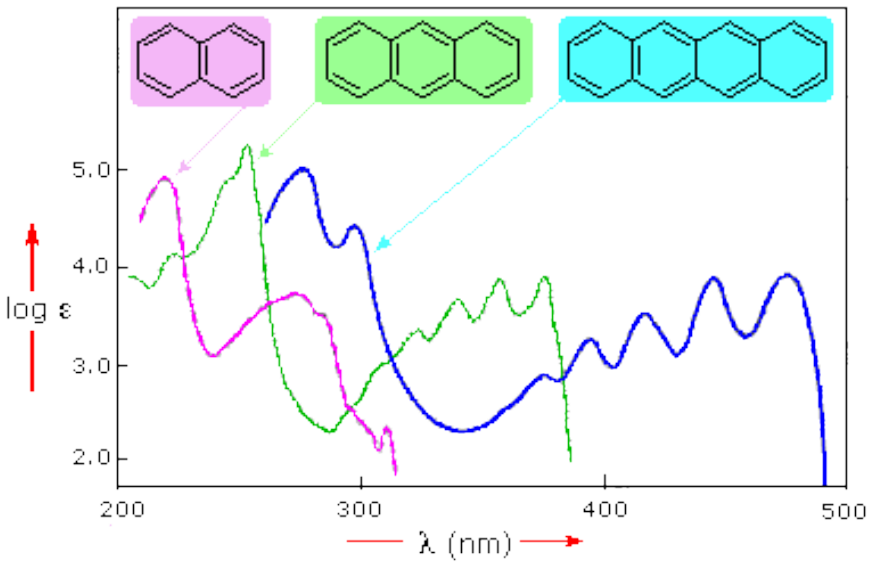

Figure 2-4: Absorption spectra of polycyclic aromatic hydrocarbons.

Heterocyclic compounds have both n- and π-electrons and their UV-VIS spectra constitute the combination of both π→π* and n→π* electronic transitions.

2.2.3 Molecular structure and fluorescence

The π→π* transition is lowest lying transition in the aromatic hydrocarbons. In the presence of heteroatom, an n→π* transition may be lowest lying transition. π→π* transition has molar absorption coefficients are at least 10^2 times higher than those of n→π* transitions. Thus according to Strickler-Berg equation [54] the radiative lifetime for π→π* is at least 100 times longer than that of low-lying n→π* transitions. This can be the reason for the low fluorescence quantum yield of many molecules containing carbonyl groups, nitrogen heterocycles and azo compounds.

Internal Heavy atom effect

The probability of intersystem crossing is related to the substitution of heavy atoms on the molecules. Thus result in decrease of fluorescence quantum yield. Intersystem crossing is favored by presence of heavy atom because of Z^4 dependence of spin-orbital coupling, where Z is atomic number. The heavy atom effect can be small in some case:

- **a.** If fluorescence quantum yield is very large that the de-excitation due to fluorescence emission dominate on other de-excitation processes.
- **b.** If fluorescence quantum yield is so low that relative increase in intersystem crossing is small.
- **c.** No triplet state is energetically close to the fluorescing state, e.g. perylene.

Electron donating substituent

Presence of electron donating substituents (-OH, -OR, -NH_2, -NHR,-NR_2) on the aromatic ring generally increase molar absorption and a shift in both absorption and fluorescence spectra. Nature of n→n* transitions of the parent molecule is not change due to presence of lone pair of the oxygen (in -OR) and nitrogen (in case of –NR_2) atom because such lone pair is directly involved in π–bonding of the aromatic system. Electron donating substitution results as broad and structureless spectra compared to the parent aromatic hydrocarbon. A significant intramolecular charge transfer character is anticipated for aromatic phenols and amines which is confirmed by the presence of broad and structureless fluorescence spectra. The emission properties of phenol and amines also depend on pH of the medium.

Electron withdrawing substituent

Aromatic withdrawing groups are carbonyl, nitrile and nitro groups. The fluorescence properties of aromatic carbonyl compounds are usually complicated and difficult to predict. Aromatic aldehydes and ketones have low fluorescence quantum yields because of the low lying n→π* excited state. The major excited state deactivation process is intersystem crossing (which is close to 1 in case of benzophenone).

The $\pi\rightarrow\pi^*$excited state is low lying excited state (compare to n→p* excited state) in some carbonyl compounds and hence have reasonable fluorescence quantum yield (e.g. fluorenone has 0.12 quantum yield at 77 K). The fluorescence quantum yield strongly depend on the polarity of the medium when $n\rightarrow\pi^*$ excite state is slightly higher in energy compared to π→π*excited state. The $n\rightarrow\pi^*$ can become lower than that of π→π* excited state in some solvent. In the presence of polar medium and/or strong hydrogen bonding interaction the π→π* state shifts to lower energy and n→π* state shifts to higher energy. This is the reason for the weak fluorescence in non-polar solvent and intense fluorescence in polar solvents is observed in case of xanthone.

Photophysical properties due to conformational changes can also be observed in the molecules containing carboxylic groups (-COOH) as a substituent. For example, in case of anthracene-9-carboxylic acid the fluorescence contains no apparent vibronic bands as seen in its absorption spectrum and in both absorption and fluorescence and absorption of its conjugate base. This is due to the fact that the corboxylate (-COO^-) is almost perpendicular to the aromatic ring (π-system) whereas the carboxylic group (-COOH) may be in position to interact with the π-system resulting intermolecular charge transfer to the $\pi\rightarrow\pi^*$ transitions. And charge transfer fluorescence bands are usually broad and structureless.

The fluorescence of nitro group (-NO_2) substituted aromatic hydrocarbons are usually not detectable. The reason is low lying n→π* transition which support efficient intersystem crossing process (e.g. the quantum yield of intersystem crossing for 2-nitronaphthalene is 0.83 in benzene solution at room temperature). Most of the nitro substituted aromatics are phosphorescent. In some cases the intersystem crossing is considerably less that one. There may be the high rate of S_1-S_0 internal conversion due to considerable charge transfer character of excited state because of strong electrophilic power of the nitro group and hence very low fluorescence efficiency. Also many nitro aromatic hydrocarbons undergo photo degradation (e.g. 9-nitroanthracene is transformed into anthraquinone upon irradiation).

Sulfonates

To make fluorophores water soluble, sulfonate groups are substituted on the aromatic molecule. The sulfonate groups slightly affect the fluorescence characteristic of the parent hydrocarbon. Generally, the fluorescence quantum yield is slightly decreased and there is small red shift in the fluorescence spectrum upon substitution of sulfonate group [55].

Heterocyclic compounds

Compounds containing one or more heterocyclic nitrogen atoms are called azarenes (pyridine, quinoline, acridine etc). These compounds have low lying n→π* and have low fluorescence quantum yields in hydrocarbon. Fluorescent properties of these compounds depend largely on the solvent. In protic solvent, fluorescent quantum yield is much higher compared to that in hydrocarbon because of the inversion of the lowest lying n→π* and π→π* states (by hydrogen bonding between nitrogen atom and solvent molecules). Many interesting derivative of the quinoline and acridine have been obtained by different substations (e.g. oxine, 5-sulfonate oxine). Tryptophan is important derivative of indole which has been studied extensively because of fluorescence investigations in proteins. Many other heterocyclic compounds which have practicle interest are known such as coumarines, rhodamines, xanthenes, pyronines, fluoresceine, oxazenes etc [55].

Compounds with more than one substituent

Usually more than one group is substituted on the hydrocarbon molecule and it should be note that the fluorescent properties of aromatic hydrocarbons in such case cannot be simply extrapolated from those of individual substituents. As an example, inspite of the presence of nitro group, ortho/meta nitroaniline and m-nitro-N,N-dimethylaniline exhibit fluorescence.

When an organic compound possesses electron donating group (-NH_2,-NMe_2, -CH_3O) in conjugation with an electron acceptor group (like carbonyl, nitrile), there exist the migration of the charge upon excitation called photoinduced intramolecular charge transfer. In these molecule the excited state reached upon excitation (Frank-Condon state or locally excited state, LE) is not in equilibrium with the surrounding solvent molecules. The solvent molecules rotate during the lifetime of the excited state to achieve a thermodynamic equilibrium between solvent molecule and the fluorophores and a relaxed intramolecular charge transfer (ICT) state is then reached. Such a relaxation due to solvent molecules is responsible for the red shift in the fluorescence spectrum with the increase in solvent polarity.

Relaxation towards an ICT can be accompanied by internal rotation within the fluorophore and such state is called twisted intramolecular charge transfer (TICT) state. The very well studied example for this observation is 4-N,N-dimethylanimo-benzonitrile. This molecule has been studied extensively in past because, inspite of its simplicity, it show dual fluorescence in polar solvents. The dual fluorescence can be explained as emission form two different states i.e. *locally excite* (LE) and *twisted intramolecular charge transfer* (TICT) states.

Internal rotation, accompanying solvent relaxation or not, may occur in many fluorophores but dual fluorescence and right angle twist are exceptional. As a general rule, internal rotations usually provide additional channels for non-radiative dissipation of excited energy. Restricting the internal rotation often increase the fluorescence quantum yield as shown in rhodamine B (Φ_f=0.54) and rhodamine 101 (Φ_ϕ=0.92).

2.3 Photophysical Properties

2.3.1 Absorption and emission spectra

The absorption of light by a molecule in UV region occurs over a wide range of wavelength because an electronic excitation is coupled with many vibrational and rotational excitation modes. The rotational and vibrational energy levels are superimposed by the electronic levels and thus the all three rotational, vibrational and electronic transition occur simultaneously. Because each transition differ slightly from others, the vibrational and rotational energy levels are closely spaced compared to the electronic levels. Because of the above reason the absorption as well as the emission spectrum consists of broad band with peak corresponds to the wavelength of most probable transition. As shown in Figure 2-5

(Jablonski diagram), the emission spectra is always at lower energy compare to the absorption spectra. Absorption and absorption of photon is very fast (~10^{-15} s) but the molecule remains in the excited state for certain time (about 10^{-11} s to 10^{-7} depending upon the medium) before emitting the photon or undergoing some other excitation processes.

Scheme 2-3

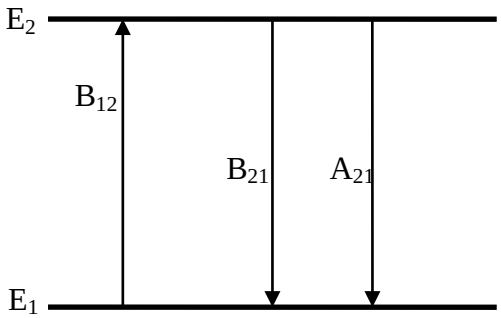

Consider the two energy level of a molecule as E_1 and E_2, the three Einstein coefficients can be shown as in Scheme 2-3.

B_{12} is the induced absorption coefficient.

B_{21} is the induced emission coefficient (stimulated emission, in laser).

A_{21} is the spontaneous emission coefficient.

The Einstein coefficients indicate the probability of transition the molecule between the energy levels E_1 and E_2. The induced absorption and induced emission processes occurs exactly at same rate, so $B_{12}= B_{21}$. Equation 2-1 shows the relation between Einstein coefficients for the induced absorption and spontaneous emission.

$$A_{21} = \frac{8\pi h\nu^3}{c^3} B_{21} \qquad 2\text{-}1$$

where c is velocity of light, h is plank's constant and ν is frequency.

Above equation (ratio A_{21}/B_{21} is proportional to ν^3) explains the reason for spontaneous emission in visible region and for longer wavelength the spontaneous emission is negligible.

The Einstein coefficients of the induced absorption and spontaneous emission are related to transition dipole moment ($\vec{M}_{l\to u}$) as well as modified absorption $\varepsilon(\tilde{\nu})$ and modified fluorescence $F(\tilde{\nu})$ spectra shown by eqs. 2-2 and 2-3 , respectively

$$B_{12} \propto \left|\vec{M}_{1a\to 2b}\right|^2 \propto \tilde{\nu}^{-1}\varepsilon(\tilde{\nu}) \qquad 2\text{-}2$$

$$A_{21} \propto \tilde{\nu}^3 \left|\vec{M}_{2b\to 1a}\right|^2 \propto F(\tilde{\nu}) \qquad 2\text{-}3$$

where *a* vibrational levels for lower (*l or 1*) electronic state and *b* is vibrational levels of upper (*u* or *2*) electronic state.

Rearranging the above equations relates the transition dipole moments with absorption and fluorescence spectra as below:

$$\left|\vec{M}_{2b\to 1a}\right|^2 \propto \tilde{\nu}^{-3}F(\tilde{\nu}) \qquad 2\text{-}4$$

$$\left|\vec{M}_{1a\to 2b}\right|^2 \propto \tilde{\nu}^{-1}\varepsilon(\tilde{\nu}) \qquad 2\text{-}5$$

Equations 2-4 and 2-5 indicate that for correct representation of the absorption and fluorescence spectra together, the fluorescence spectrum, $F(\tilde{\nu})$, should be divided by third power of wavenumber and absorption spectrum, $\varepsilon(\tilde{\nu})$, to be divided by the first power of wavenumber.

Fluorescence is the emission of photon from the excited molecule during its radiative decay from singlet state ($S_u \rightarrow S_l$) to the ground singlet state. Fluorescence spectra correspond to decay from lowest vibrational level of S_1 to the vibrational levels of S_0. Generally differences between the vibrational levels of the ground state are similar to that of the excited state. So the emission spectra are often resembled to the absorption spectra. This is called mirror symmetry or mirror image rule.

2.3.2 Beer-Lambert Law and probability of transition

The molar absorption coefficient or molar absorptivity is the measure of the extent of the absorption of specie. The efficiency of absorption of light is at particular wavelength is characterized by its absorbance (A(λ)) or transmittance (T(λ)) and defined as in eq. 2-6.

$$A(\lambda) = \log\left(\frac{I_0}{I}\right) = -\log T(\lambda) \qquad 2\text{-}6$$

Most of the case the absorption of light follow the Beer-Lambert's law, which is "The absorption of light is directly proportional to the number of molecule in the radiation path, which is related to the concentration and path length". Mathematically it can be written as eq. 2-7

$$A(\lambda) \propto cl \qquad 2\text{-}7$$
$$A(\lambda) = \varepsilon(\lambda)cl$$

where $\varepsilon(\lambda)$ (L $mol^{-1}cm^{-1}$) is the proportionality constant and is called molar absorption coefficient, c (mol L^{-1}) is concentration and l (cm) is path length of absorbing medium.

$\varepsilon(\lambda)$ is calculate from the slope of the plot between the absorbance, A(λ), versus the concentration of the solution measured in the sample holder with constant path length of absorbing light. A straight line is obtained if there is no deviation occurs from Bee-Lambert Law. However the deviation from Beer-Lambert law is observed in certain case where the concentration of the absorbing specie is too high and/or may form aggregates, the solution is

turbid because of partial soluble species as in case of macromolecule and/or the optical density is high and solution is fluorescent (this can be minimized by placing detector at distant from the sample).

Molecular absorption can be described by considering the molecule as oscillation dipole in discussion of classical theory. The term *oscillator strength (f)* is introduced which represent the strength of absorption relative to the completely allowed transition which is related to integral of absorption band as shown in eq.

$$f = 2.303\times10^{3}\frac{mc_o^{\,2}}{N_A\pi e_o^{\,2}n}\int\varepsilon(\tilde{\nu})d\tilde{\nu} = \frac{4.32\times10^{-9}}{n}\int\varepsilon(\tilde{\nu})d\tilde{\nu} \qquad 2\text{-}8$$

where c_o is the velocity of light, e_o and m are charge and mass of the electron, respectively, n is refractive index and λ is wavenumber (in cm^{-1}). The oscillator strength (f) is a dimensionless quantity to express the strength of the transition.

2.3.3 Stokes shift and 0-0 transition energy

Strokes shift is among one of the earliest observation in fluorescence. Stokes shift is named after Sir G. G. Stoke who observed this phenomenon at the University of Cambridge in 1852[56]. From the Jablonski diagram Figure 2-5, it can be seen easily that fluorescence occurs at lower energy than absorption. The factors for Stokes shift are the rapid decay to lower vibrational levels of S_1, decay of excited state S_1 to the higher vibrational levels of S_0, solvent effects, excited state complex formation and/or energy transfer.

The *Stokes shift* is defined as the difference (usually in wavenumber, $\Delta\nu$ (cm^{-1})) between the maxima of the absorption and fluorescence belongs to the same electronic transition i.e. eq. 2-9.

$$\Delta\tilde{\nu} = \tilde{\nu}_{abs} - \tilde{\nu}_{flu} \qquad 2\text{-}9$$

Stokes shift is an important parameter that can provide information about the excited state. The larger red-shift in the fluorescence spectra (hence large Stokes shift) with the increase in the polarity of the medium indicates higher dipole moment in excited state. So it can be helpful in estimating the polarity for the excited state in certain cases and in designing fluorescent polarity probes. Fluorescent species can be detected more easily if the Stokes shift is large.

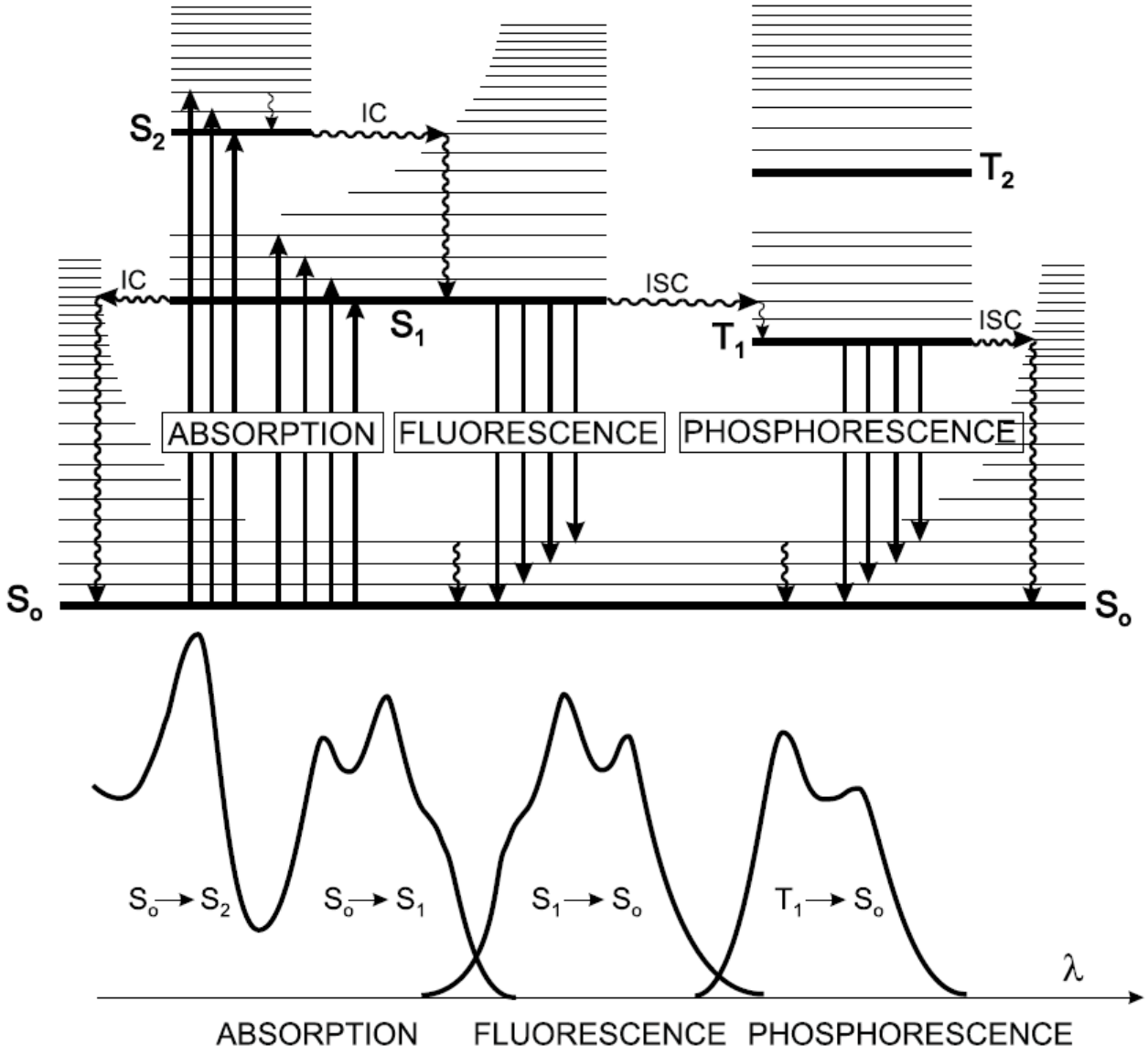

Figure 2-5: Perrin–Jablonski diagram showing absorption, fluorescence and phosphorescence transitions [55].

There are very limited cases where the emitted photon has higher energy (lower emission wavelength) than that of the absorbed photon then Stokes shift value termed as anti-Stokes shift or upconversion and reviewed by F. Auzel [57].

E_{00} is also known as the singlet energy of the fluorophore and is estimated as estimated by the mean value of absorption and fluorescence maxima (eq. 2-10) and corresponds to the energy for the 0-0 transition from S_0 to S_1.

$$E_{00} = \frac{(\tilde{\nu}_{abs} + \tilde{\nu}_{flu})}{2} \qquad 2\text{-}10$$

E_{00} can also be obtained from the intersection of the normalized absorption and fluorescence spectra. E_{00} (either for singlet or triplet state) is important parameter for the estimation of the

driving force (ΔG^o- Free energy change) in charge transfer processes as given by Rehm-Weller equation, eq 2-11:

$$\Delta G^o = E_{ox}(D^+ / D) - E_{red}(A / A^-) - E_{00} + C \qquad 2\text{-}11$$

E_{ox} and E_{red} are oxidation and reduction potentials for donor and acceptor species, respectively and C is the constant that accounts for charge solvation and columbic energy of the formed ion pairs.

2.3.4 Fluorescence quantum yield and lifetime

Fluorescence quantum yield (Φ_{flu}) is in fact the efficiency of the fluorophore to convert the absorbed photon into the emitted photon. Φ_{flu} can be defined as the number of photon emitted (over the whole duration of the decay) per number of absorbed photons as given by eq. 2-12:

$$\Phi_{flu} = \frac{N_{em}}{N_{abs}} \qquad 2\text{-}12$$

N_{em} is number of emitted photon and N_{abs} is the number of absorbed photons. In literature, two different approaches have been applied to determine the fluorescence quantum yield; absolute and relative methods. Absolute methods for the measurement of Φ_{flu} include optical methods, calorimetric methods, photoacoustic spectroscopy, thermal lensing and actinometery. These methods are briefly summarized by Knut Rurack [58] and also this was done by Demas [59].

Quantum yields are commonly determined by using relative method [60]. There is some uncertainty in the fluorescence quantum yield measured by relative methods. The Federal Institute for Materials Research and Testing in Berlin *(Bundesanstalt für Materialforschung und –prüfung, BAM)* is testing a new set of fluorophores in UV-VIS-NIR region on a recently built reference fluorometer which is designed for the determination of absolute fluorescence quantum yields [61-62]. Such measurement of the absolute fluorescence quantum yields and reference standards are likely to gain importance due to an increasing desire for reliable relative and absolute fluorescence quantum yields of different materials that used as NIR fluorophores, in light emitting diodes (LEDs) and organic light emitting diodes (OLEDs)[8] [63].

DeRose, *et al*. have reviewed the classifications and recommendations for the selection and use of the fluorescence standards [62, 64-66]. After absorption of the photon by the ground

[8] LEDs are light emitting diodes and OLEDs are organic light emitting diodes.

state (S_0), molecule is excited to S_1. This excited molecule decays to its ground state and the time for which the molecule remains in the excited state is called the lifetime of the excited state. The excited molecule (in S_1 state) can decay either by radiative, non-radiatived (can be intersystem crossing or internal conversion).

So for the sake of convenience following terminologies are used:

$^{s}k_r$ = rate constant for radiative decay for S_1 to S_0, fluorescence.

$^{s}k_{ic}$ = rate constant for non radiative decay for S_1 to S_0, internal conversion.

k_{isc} = rate constant for non radiative decay for S_1 to T_1, intersystem crossing.

$^{T}k_r$ = rate constant for radiative decay for T_1 to S_0, phosphorescence.

$^{T}k_{nr} = {}^{T}k_{ic}$ = rate constant for non radiative decay for T_1 to S_0, internal conversion.

Both k_{ic} and k_{isc} are rate constant for non-radiative decay and non-radiative decay rate constant for S_1 state can be written combinely as $^{s}k_{nr} = {}^{s}k_{ic}+k_{isc}$

The lifetime for the singlet state (τ_s) and triplet state (τ_T) are given as in equation 2-13 and 2-14, respectively.

$$\tau_s = \frac{1}{{}^{s}k_r + {}^{s}k_{nr}} \qquad 2\text{-}13$$

$$\tau_T = \frac{1}{{}^{T}k_r + {}^{T}k_{nr}} \qquad 2\text{-}14$$

If the only way of de-excitation for the decay of S_1 to S_0 is fluorescence emission then the lifetime ($\tau_s = \frac{1}{{}^{s}k_r}$) is called radiative lifetime (τ_r) and can be theoretically calculated using Strickler-Berg equation (eq. 2-15).

$${}^{s}k_r = \frac{1}{\tau_r} = \frac{8\pi \times 230 c_0 n^2}{N_A} \frac{\int F_{\tilde{\nu}}(\tilde{\nu})d\tilde{\nu}}{\int \tilde{\nu}^3 F_{\tilde{\nu}}(\tilde{\nu})d\tilde{\nu}} \int \left(\frac{\varepsilon(\tilde{\nu})d\tilde{\nu}}{\tilde{\nu}} \right) \qquad 2\text{-}15$$

where n is refractive index of medium, N_A *is Avogadro's number*, $F_{\tilde{\nu}}(\tilde{\nu})d\tilde{\nu}$ is fluorescence per unit wavenumber and $\varepsilon(\tilde{\nu})d\tilde{\nu}$ is molar extinction co-efficient per unit wavenumber.

Strickler-Berg equation 2-15 is often in agreement with the experimental values, but if there is considerable solvent effect or change in excited state geometry then the above equation fails.

Fluorescence lifetime can be measured using different approaches such as direct time-resolved measurements, time correlated single photon counting (TCSPC), modulation or frequency domain methods, streaks camera and up-conversion techniques.

2.3.5 Radiative and non-radiative rate constant

The radiative and non-radiative rate constants are calculated by the combination of both, steady state and time resolved fluorescence measurements. Quantum yield of fluorescence can also be defined as the fraction of the excited molecule (in S_1 state) returned back to the ground state (S_0 state) by the emission of light and this can be expressed as in eq. 2-16.

$$\Phi_{\text{flu}} = \frac{{}^{s}k_r}{{}^{s}k_r + {}^{s}k_{nr}} = {}^{s}k_r \tau_s \qquad 2\text{-}16$$

Rearranging the above equation will give the value of both radiative (eq. 2-17) and non-radiative (eq. 2-18) rate constants, respectively.

$${}^{s}k_r = \frac{\Phi_{\text{flu}}}{\tau_s} \qquad 2\text{-}17$$

$${}^{s}k_{nr} = \frac{1}{\tau_s}\left(1 - \Phi_{flu}\right) \qquad 2\text{-}18$$

It can be seen from equations 2-17 and 2-18 that when fluorescence quantum yield and excited state (S_1) lifetime is measured under the same environment, then respective radiative and non-radiative rate constants can be easily calculated.

2.4 Solvatochromism

It is well known fact that a small change in medium can alter the rate of reaction, position of chemical equilibrium, modify position and intensity of the transition induced by electromagnetic radiations [67]. Both absorption and emission spectra of molecules are influenced by the environment/medium and results in change in shape, intensity and position of absorption band. This effect of medium is termed as solvatochromism by Hantzsch[9]. Early work for the solvent effect on the UV-VIS of various dyes has been reviewed by Sheppard in 1942 [69]. *Solvatochromism is* defined as the pronounced change in the position and sometimes the intensity of absorption or emission band with the change in polarity of the medium as shown in Figure 2-6. Sometimes the solvatochromism can be observed visually by the change in color of solution in solvent of different polarity. The possible changes of the solvent on position as well as intensity are termed as given in section 2.2.2. Figure 2-6 illustrates a very simple model for the solvatochromism. Sometime positive and negative

[9] Now a days *solvatochromism* term has different meaning from the one that is introduced by Hantzsch.
68. Hantzsch, A., *Über die Halochromie und »Solvatochromie« des Dibenzal-acetons und einfacherer Ketone, sowie ihrer Ketochloride.* Berichte der deutschen chemischen Gesellschaft (A and B Series), 1922. **55**(4): p. 953-979.

solvatochromism terms are also used in literature for bathochromic and hysochromic shift, respectively.

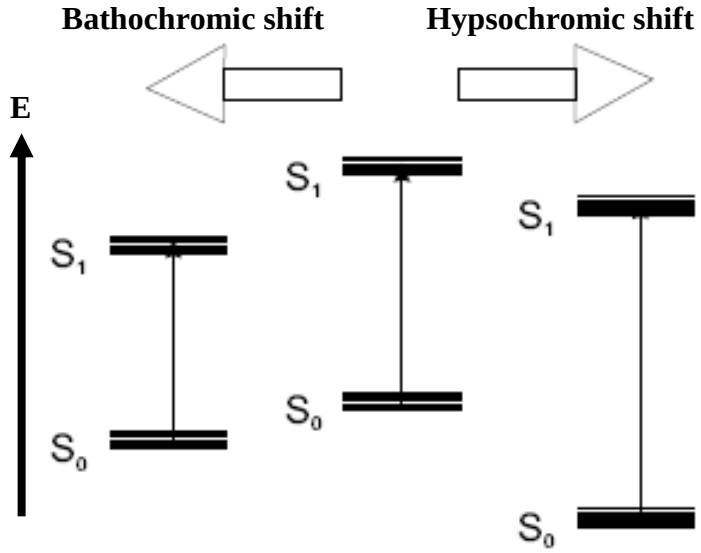

Figure 2-6: Schematic explanation of solvatochromism.

There are different types of interactions between the solvent and solute molecules and led to a century old rule which broadly define as "like dissolve like" and the word like must not narrowly interpreted. In addition to "like dissolve like rule", there are intermolecular interactions that determines the mutual solubility. The interaction between the solvent as well as solute molecule and also there mutual solvent-solute interactions are summarized in Table 2-1. Solvent and solute interactions are broadly divided into two types (a) Specific interactions, section 2.4.2 and (b) Non-specific or general interactions, section 2.4.2.

Table 2-1: Solvent and solute interactions.

Solute A	Solvent B	Type of interaction		
		A---A	B---B	A---B
Non-polar	Non-polar	weak	weak	weak
Non-polar	Polar	weak	strong	weak
Polar	Non-polar	strong	weak	weak
Polar	Polar	strong	strong	Strong

2.4.1 Classification of solvents

Due to large differences in chemical and physical properties between the inorganic and organic solvent, it is difficult to classify them into one single scheme. Physical and chemical properties of large number of solvents are presented in past. The solvents can be classified on the basis of different properties such as:

a) **According to chemical constitution.** In this group the solvents are classified on the basis of their chemical bonds such as (1) Molecular liquids (organic solvents like molecular melts; covalent bond only), (2) Ionic liquids (ionic molten salts; only ionic bonds) and (3) Atomic liquids such as low melting metals (liquid mercury, molten sodium; metallic bond only

b) **Using physical constants.** Here the solvents are grouped together on the basis of same range of physical constant values. The physical constants those can be used to classify the solvents include: melting and boiling points, vapor pressure, refractive index, dipole moment, heat of vaporization, density, viscosity, surface tension, relative permittivity, etc. Physical constants data for extensively large number of solvents are presented in ref. [70-71]

c) **Acid-base behavior.** Solvents can also be classified on the basis of their acidic or basic properties. Acidic solvents are those which can either donates a proton (Brønsted-Lowry Theory of Acids and Bases) or has the ability to accept electron pair (Lewis Acids) and basic solvents have the ability to accept either a proton (Brønsted-Lowry Theory of Acids and Bases) or has the ability to donate a pair of electron (Lewis Bases). Water has the ability to accept as well as to donate the proton and is a prototype to for amphiprotic solvents and all other solvents which have similar acid-base properties are called *neutral* solvent. Solvent with very strong acidic and very weak basic properties compared to water are called *protogenic* properties. *Protophilic* solvents are those which are stronger base and much weaker acids compared to water. Not all solvents can be classified as electron pair donor (EPD) or electron pair acceptor (EPA), e.g. aliphatic hydrocarbons are neither EPD nor EPA. Gutmann introduce donor number (DN) and acceptor number (AN) to measure quantitatively donor and acceptor strength respectively [47, 72].

No single scale of acidity or basicity is equally valid for all the types of solvents. Different acidity and basicity functions have been reviewed [73-74].

d) **Specific solvent-solute interactions.** **S**olvents have been into different groups according to their specific interactions with the solute molecules by Parker [75-85]. Solvents are classified as *dipoar aprotic solvents, apolar aprotic solvents* and *aprotic solvents*. This classification was originated from experimental finding of certain S_N^2 reactions involving anions as nucleophiles are much faster in dipolar aprotic solvent than in protic solvents. The reason for such less reactivity is that in protic solvent most anions are more solvated compared to than in dipolar aprotic solvent.

e) Multivariate statistical methods. Parker [75-85] has divided solvents on the basis of solvent-solute interaction into three groups but there need to be more groups in order to classify a wide range of solvent on the basis of solvent-solute interaction. So multivariate statistical methods have been applied to classify the solvent into certain groups [86-87]. The data set can be composed of physiochemical constant such as boiling point, dipole moment, viscosity, refractive index and molar volumes and sometimes empirical parameters of solvent polarity. The multiple linear regression analysis (MRA), factor analysis (FA) or principal component analysis is done in order to determine the relative importance of each variable [88-90]. The first factor analysis (FA) for classification of solvents was done by Martin and co workers [90] for 18 solvents with 18 physicochemical parameters. They obtained the same classification as was done by Parker [75-85]. Cramer found more than 95% of the variance with only six physical parameters for 114 pure liquids using principal components analysis (PCA) [91-92]. Chastrette and co-worker [86-87] performed the most valuable approach for the classification of the solvents using PCA.

2.4.2 General/non-specific interactions

While describing specific solvent-solute interaction, the fluorophore is considered to be a dipole in a continuous medium of uniform dielectric constant. The interaction between the solvent and solute molecule alter the energy difference of the ground and excited sate. There are solvent-solute interactions which are independent of any fixed stoichiometry or geometry. These interactions can be classified into flowing groups:

- Multipole-multipole interaction
- Multipole (solute)-induced dipole (solvent) interaction
- Multipole (solvent)-induced dipole (solute) interaction “Solvent Stark effect”
- Dispersion interactions
- Transient dipole moment (solute) and the polarizable solvent interaction

The equations for dipole-dipole interaction can be derived if the solute relaxation is short compares to excited state lifetime. The qualitative interpretation of solvent shift is possible if the momentary transition dipole moment is present during optical absorption, the difference in permanent dipole moments between the excited and ground state dipole moments.

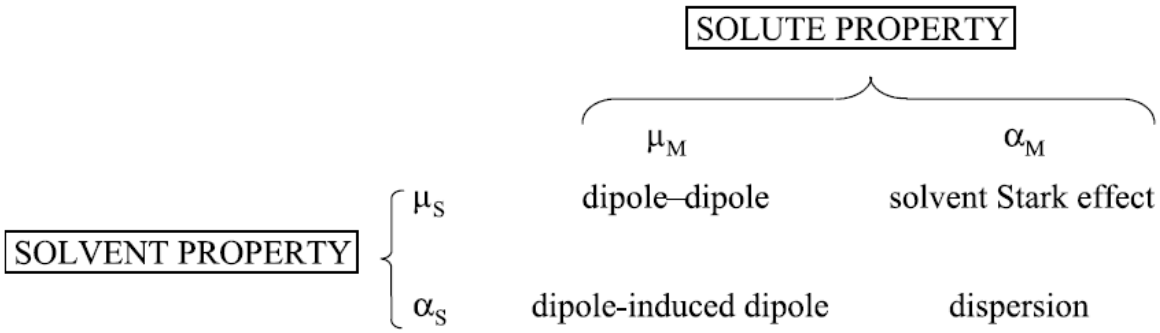

Figure 2-7: Solute–solvent interactions resulting from the dipole moments and average polarizabilities [55].

If the solvent relaxation is complete before emission, under the assumption the dipole moment in FC and relaxed state is equal and taking fluorophore as point dipole with isotropically polarizable spheres, the dipole-dipole interaction equation can be obtained for solvatochromic shift. The solvatochromic shifts in the absorption and emission maxima are related to the macroscopic quantities dielectric constant *(n)* and refractive index *(ε)* as described by equations 2-19 and 2-20.

$$\tilde{\nu}_a = -\frac{2}{a^3 hc}\mu_g.(\mu_e - \mu_g)\Delta f + const. \qquad 2\text{-}19$$

$$\tilde{\nu}_f = -\frac{2}{a^3 hc}\mu_e.(\mu_e - \mu_g)\Delta f + const. \qquad 2\text{-}20$$

where *h* is Plank's constant, *c* is velocity of light, *a* is the fluorophore cavity radius[10], μ_g and μ_e are the dipole moments[11] of ground and excited states and *Δf* is orientational polarizability and defined as:

[10] Cavity radius is very important in the theories of solvent-solute interactions. In simple approaches, the molecule is treated as sphere of radius *a* so the molecular volume is $(4/3)\pi a^3$. An array of sphere always include free volume, so that $(4/3)\pi a^3$ would be "hard volume". The molar volume is $V=M/\rho$, with *M* is molecular mass and ρ is density. The effective volume is $v=V/N_A$ with N_A is Avogadro's number. The best description of cavity radius *a* for solvatochromic shift equations are considering a cubic lattice model as $v=8a^3$. This takes account the free volume and probably the more realistic estimate of Onsager radius. 49. Suppan, P. and N. Ghoneim, Solvatochromism (The Royal Society of Chemistry, Cambridge), 1997.

[11] The dipole moment is defined by the magnitude of change of positive or negative charge and the distance in between as, $\vec{\mu} = q \times \vec{d}$, where q is the charge on individual pole and $\vec{d}$ is the distance between them. It is vector quantity and total dipole moment is the sum of all individual dipole moments, $\vec{\mu} = \sum_i \vec{\mu}_i$.

$$\Delta f = f(\varepsilon) - f(n^2) \qquad 2\text{-}21$$

$$f(\varepsilon) = \frac{\varepsilon - 1}{2\varepsilon + 1} \quad \text{and} \quad f(n^2) = \frac{n^2 - 1}{2n^2 + 1} \qquad 2\text{-}22$$

Δf ranges from 0.001 for cyclohexane to 0.32 in water.

Subtraction of equations 2-19 and 2-20 leads to:

$$\tilde{\nu}_a - \tilde{\nu}_f = \frac{2}{a^3 hc}(\mu_e - \mu_g)^2 \Delta f + const. \qquad 2\text{-}23$$

Equation 2-23 is known as Lippert-Mataga equation [93-95] and its validity is checked by plotting Stokes shift versus *Δf (Lippert plot).* A linear correlation is not always achieved as Lipper equation is only approximation neglecting the solute polarizability and higher order terms. These terms would account for second order effects such as the dipole moments induced in solvent molecules due to excited fluorophore and vice versa. However by choosing the solvent without hydrogen bonding acceptor or donor capability, a linear trend is often observed. The change in the dipole moment $\Delta\mu_{ge} = (\mu_e - \mu_g)$ going from ground state to excited state is estimated from Lippert plot provided that correct estimation of the radius cavity where fluorophore resides is known. For elongated molecules, an ellipsoid form is more appropriate that spherical shape. Furthermore

Similar approach in introduced by McRae [96-97], which is directly evolved from Onsager's reaction field theory [98], including the solute polarizability which is approximated to $a^3/2$. Equation 2-23 is still valid but polarity function *Δf* is replaced by *Δg* given as:

$$\Delta g = \frac{\varepsilon - 1}{\varepsilon + 2} - \frac{n^2 - 1}{n^2 + 2} \qquad 2\text{-}24$$

Suppan [49, 99] derived another useful equation from eqs. 2-19 and 2-20, under the assumption that ground and excited state dipole moments are collinear but without any assumption for the cavity radius or the form of solvent polarity function. This equation 2-25 involve the difference in absorption and emission solvatochromic shift between the two solvents *a* and *b*.

$$\frac{(\tilde{\nu}_{flu})_a - (\tilde{\nu}_{flu})_b}{(\tilde{\nu}_{abs})_a - (\tilde{\nu}_{abs})_b} = \frac{\mu_e}{\mu_g} \qquad 2\text{-}25$$

Equations 2-23 and 2-25 can be used to estimate the excited state dipole moments but they are valid only if *(a)* the cavity radius of fluorophore remain unchanged upon excitation, *(b)*

the dipole moments of the FC and relaxed excited states remain the same and *(c)* the solvent shifts are measured in solvents of same refractive index but different dielectric constants.

The Lippert-Mataga and Suppan approach are not applicable when the excited state undergoes charge transfer because absorption spectrum of the charge transfer state is not known. However in a situation when twisted intramolecular charge transfer (TICT) state is formed, the molecular geometry and the charge distribution must be taken into account. Using only the excited state dipole moment and taking solute polarizability as $a^3/2$, Rettig [100] has developed the following relationship eq. 2-26.

$$\tilde{\nu}_f = -\frac{2}{a^3 hc}\mu_e{}^2 \Delta f'' + const. \qquad 2\text{-}26$$

where $\Delta f'' = \frac{\varepsilon - 1}{\varepsilon + 2} - \frac{n^2 - 1}{4n^2 + 2}$

The Weller's theory for exciplexes (eq. 2-27) takes into account only fluorescence spectra shift and is suitable for the molecules undergo charge transfer in excited state.

$$\tilde{\nu}_f = -\frac{2}{a^3 hc}\mu_e{}^2 \Delta f' + const. \qquad 2\text{-}27$$

where $\Delta f' = \frac{\varepsilon - 1}{2\varepsilon + 1} - \frac{n^2 - 1}{4n^2 + 2}$

The uncertainty for sized and shape of cavity radius along with the assumptions made in the solvatochromic theories explain the inaccuracy of the excited state dipole moment [55].

Liptay has presented another approach for solvent-solute interaction for the case when the molecule in the excited state is relaxed by solvent molecules before emission ($\tau_r \ll \tau_e$). According to Liptay ($\Delta\tilde{\nu}$), the difference of absorption and emission transition can be related to the change in the dipole moment in ground and excited state ($\left|\mu_e - \mu_g\right|$). With the assumption that there is no change in the polarizability of the solute between the ground and excited state, so neglecting the terms depending on polarizability change, the following equation 2-28 is obtained:

$$hc\Delta\tilde{\nu} = hc\left(\tilde{\nu}_{eg}^{sol(abs)} - \tilde{\nu}_{eg}^{sol(flu)}\right) \qquad 2\text{-}28$$

$$= hc\left(\tilde{\nu}_{eg}^{1(abs)} - \tilde{\nu}_{eg}^{0(flu)}\right) + \frac{2}{4\pi\varepsilon_0 a_w^3}\left(\frac{\varepsilon_r - 1}{2\varepsilon_r + 1} - \frac{n^2 - 1}{2n^2 + 1}\right)\left|\mu_e - \mu_g\right|^2$$

where h is Plank's constant, c is speed of light, $\tilde{\nu}_{eg}^{sol(abs)}$ and $\tilde{\nu}_{eg}^{sol(flu)}$ are wavenumbers for absorption and fluorescence transition in solution ($\tilde{\nu}_{eg}^{0(abs)}$ and $\tilde{\nu}_{eg}^{0(flu)}$ are corresponding value in gas phase), a_w is interaction radius of solute molecule.

The equations for dipole-dipole interaction can be derived if the solute relaxation is short compared to the excited state lifetime. The qualitative interpretation of solvent shift is possible if the momentary transition dipole moment is present during optical absorption.

2.4.3 Specific interactions

Specific interaction can be due to hydrogen bonding, acid-base equilibrium reactions, preferential solvation or/and charge transfer interactions by one or more neighboring molecules. The most important contribution of the specific interaction is due to formation of the hydrogen bonding between solvent and solute molecules. Formation of hydrogen bonding (specific interactions) can be observed as the deviation from linearity in a plot relating solvent polarity function *f(D)* with transition energy.

The effect of solvents with specific interaction (alcohols, water and carboxylic acids) on electronic transition of the carbonyl compounds, e.g. benzophenone, is hypsochromic shift (blue shift) in the absorption band corresponds to n→p* band. This is due to lower dipole moment of the ground state compared to the excited state (μ_g=3D and μ_e=1.5) and thus large n→π* transition energy. In case of the hetero atom like nitrogen, the electron density is decreased upon n→π* transition. This results in decrease of hydrogen bond formation capacity and is similar to decrease in dipole moment upon excitation. So, there will be a hypsochromic shift (blue shift) in the absorption band. This criterion is convenient in assigning the n→π* transition and spectral shift can be used to determine the hydrogen bond strength (energy). In case of n→π* transition, emission spectra is always less sensitive to solvent hydrogen bond formation ability than absorption. In fact the n→π* excitation causes the hydrogen bond breaking (e.g. in case of heterocyclic nitrogen, N---HOCH3 hydrogen bond exist in ground state), so there is only very slight effect of the hydrogen bond formation ability of solvent.

In π→π* transition, heteroatom of a heterocycle is often less basic in the ground state than in the excited state. The dipole moment in the excite state is greater than that of the ground state in π→π* transition. This result in stronger hydrogen bond formation ability in the excited state compare to the ground state. So π→π* fluorescence is more sensitive to hydrogen bond formation.

In certain carbonyl compounds, there are two closely spaced states, i.e. n→π* and π→π*. The change in the ability of solvent to form hydrogen bond can affect the lowest lying state (n→π* versus π→π*). When hydrogen bonding ability and polarity of the solvent increases, inversion of these two states can be observed because π→π* shifts to lower energy whereas n→π* state shifts to higher energy. So and increase in the fluorescence quantum yield is observed because π→π* is known to have higher quantum yield than that of n→π*. This is called the polarity induced inversion of n→π* and π→π*.

Specific interactions are determined by the measure of the specific chemical properties of both, solvents and fluorophore. Identification of the specific interaction can be made by examining emission spectra in variety of solvent. Hydroxyl solvents (water and alcohols) are known to have specific interactions. Addition of small amount of hydroxyl solvent to some solvent (with no specific interaction, like hydrocarbons) will dramatically change the emission spectra [101]. Presence of specific interactions sometime leads to misleading information about the polarity of the medium. Also the presence of the specific interactions can be observed by the change in emission maxima with varying the percentage of the polar solvent as seen in 2-acetylanthracene (2-AA) [102]. Very low addition of the methanol (<10%) will result in the loss of structured emission in methanol-hexane mixture as shown in Figure 2-9.

Solvents like 1,4-dioxane, octanol and methanol are used (as polar solvent) in different percentages in addition to non-polar solvent hexane see Figure 2-8. Most of the spectral shift is produced by the addition of 1-2% of the methanol. A smooth shift in fluorescence maxima has been observed on the gradual addition of dioxane. The shift on dioxane addition is probably due to non specific interactions. Specific interaction can occur both in the ground and excited states. If specific interactions occur in ground state only then only absorption spectra will be effect by addition of some polar solvent. If interactions occur only in excited state then addition of polar solvent will affect only emission spectra.

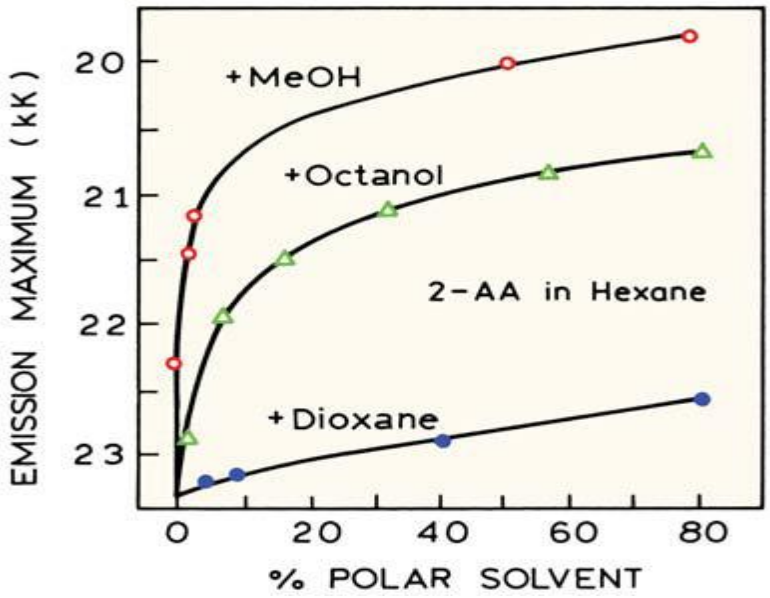

Figure 2-8: Effect of solvent composition on the emission maximum of 2-acetylanthracene. 1 kK = 1000 cm–1 [102].

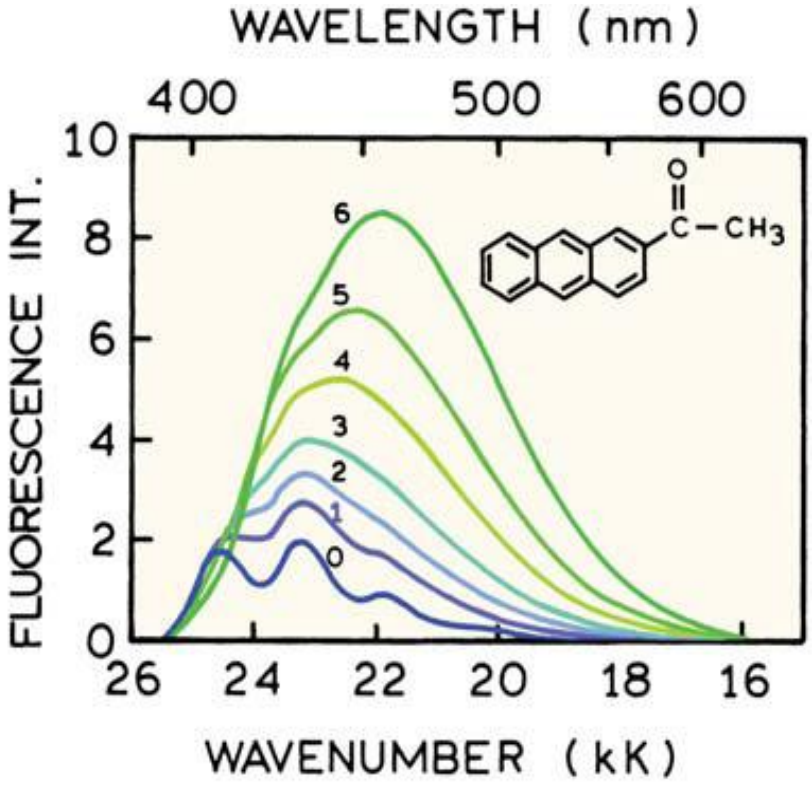

Figure 2-9: Fluorescence spectra of 2-acetylanthracene in methanol–hexane mixtures at 20°C. Concentrations of methanol in mol dm–3: (0) 0, (1) 0.03, (2) 0.05, (3) 0.075, (4) 0.12, (5) 0.2, and (6) 0.34 [102].

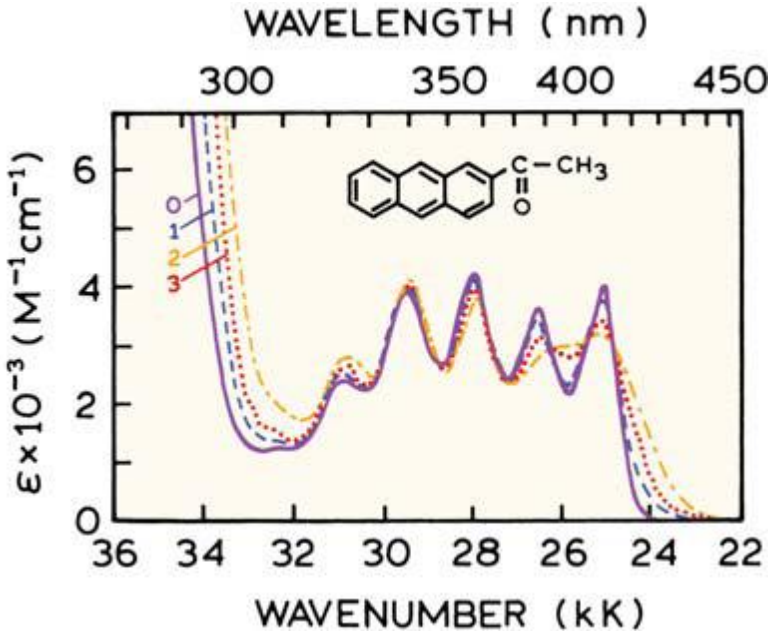

Figure 2-10: Absorption spectra of 2-acetylanthracene in pure hexane (0) and mixtures of methanol and hexane. The concentrations of methanol in mol dm–3 are 0.2 (1) and pure methanol (2). Spectrum 3 (dotted) refers to the H-bonded complex [102].

The absorption spectra of 2-AA showed a red shift and loss of the vibrational structure on addition of methanol as seen in Figure 2-10. This suggest that there exists specific interaction with the ground state of 2-AA as well.

Specific interactions and the Lippert plot: The general observations are that in the presence of (specific interaction), the Stokes shift is larger for solvents with higher power of hydrogen bonding. This larger shift is typically due specific solvent-solute interactions in protic solvents. Such evidence for specific interactions can be seen in Lippert plots. Specific effect prevents the quantitative interpretation of polarity of the medium. Under such circumstance reasonable estimate for the solvent sensitivity can be made. Consider the case of 2-AA, Figure 2-8 has shown that almost equal slopes are found for the region with concentration of the protic solvent greater than 10-15% in case of methanol, octanol and dioxane. These similar slopes indicate similar mechanism, which is general solvent effect and addition of about 10% of protic solvents in hexane will saturate all the specific interaction. So the hexane containing more than the amount where the specific effect is saturated (10% of methanol in 2-AA case) can be used as reference solvent of low polarity and further increase of protic solvent will only corresponds to non-specific interactions. So the emission spectra, where specific as well non-specific interaction occur, can be reasonably

interpreted when compared with reference solvent in which the specific solvent effect is saturated.

2.4.4 Solvent-solute interaction and solvatochromic shift

Both ground and excited state involved absorption or emission transition has been solvated by the solvent molecules. But the solvation energies for these two states are different for different solvent molecules and this result in the shift in the electronic transition called solvatochromic shift. In fact the solvatochromic shift is due to interactions between the solvent and solute molecules in multiple ways like ion-dipole, dipole-dipole, dipole-induced dipole, hydrogen bonding, etc. All these interactions in fact change the energy difference between the ground and excited state involved in absorption or emission transition.

Solvatochromic shift in absorption

The interactions between the solvent and solute molecules can be observed by comparing the spectral changes in absorption transition either going form gas phase (at very low pressure) to the solution or simply changing the polarity of the solvent. In the presence of solvent molecule, both ground and excited states are stabilized due to solvent-solute interaction compare to the ground and excited states in gas phase. Absorption transition only tells about the energy gap between the ground and excited state but not the absolute position of the individual state. Absorption can be affected by both specific and non-specific transition.

Solvent effect on absorption spectra depends on the type of chromophore and nature of transition (discuss in section 2.2.2). The $\pi \rightarrow \pi^*$, $n \rightarrow \pi^*$ and charge transfer absorption are of particular interest to study the solvent effect on absorption electronic transition. The molecules, e.g. aromatic compounds (with no electron donor and/or electron acceptor substitutions; benzene, naphthalene, etc.), polenes (lycopene, carotinoids), polynes (polyacetylenes, symmetrical polymethine dyes) have comparatively small solvatochromic shift in absorption due to no appreciable change in the dipole moment in ground and excited state. The solvatochromic shift in these molecules are very small, for instance in fullerene (aromatic with large π-electron network) has $\Delta\tilde{\nu}$=360 cm^{-1} (in n-hexane to CS_2), β-carotene (polemic π system) has $\Delta\tilde{\nu}$=239cm^{-1} (from solvent cyclohexane to methanol) and heptamethenium cyanide dye (polymethinic π-system) has $\Delta\tilde{\nu}$=304cm^{-1} (from trichlormethane to methanol). Dipolar molecules show dramatic shift in the absorption spectra in different solvents, e.g. merocyanines, mainly due to large change in dipole moments on electronic transitions. Pyridinium N-phenolate betain (also known as

Reichardt's dye) dye is among the one which has one of the largest solvatochromic shift $\Delta\tilde{\nu}$ =9730 cm^{-1} (from diphenyle ether to water). A visible change in the color of solution can be seen in different solvents for this dye. Because of large solvatochromic shift, it has been used to generate an empirical parameter scale, $E_T(30)$ value.

Complexes of electron pair donor and electron pair acceptor also exhibit a large solvatochromic shift due to intermolecular charge transfer (CT). Both the ground and excited states in CT transition also have very different dipole moments. Example for such solvatochromic effect is 1-ethyle-4-(methocycarbonyl)-pyridinium iodide. Organometalic complexes with central metal atom and organic ligands containing π-electron system undergo two types of charge transfer absorptions, (a) metal to ligand charge transfer and (b) ligand to metal charge transfer. Both of these transitions are solvent dependent and often show strong solvatochromic shift.

Generally if the ground state dipole moment is smaller than that of the excited state $(\mu_g < \mu_e)$ then there is red-shift in the absorption is observed with the increase in the polarity of the medium and if the ground state dipole moment is larger than that of the excited state $(\mu_g > \mu_e)$, a blue shift is observed in absorption transition with increase in polarity of the solvent as shown in Figure 2-11. Quantitative calculations for solvent dependence of the UV-VIS absorption transitions has been carried out by Lippert [93], Liptay [103], McRae [96], Abe , Bakhshiev [104], Kawski [105], Suppan [99]. Critical discussions have also been reported for these approaches and reviewed for the theoretical treatments of solvent effects on the electronic spectra [49, 71, 106].

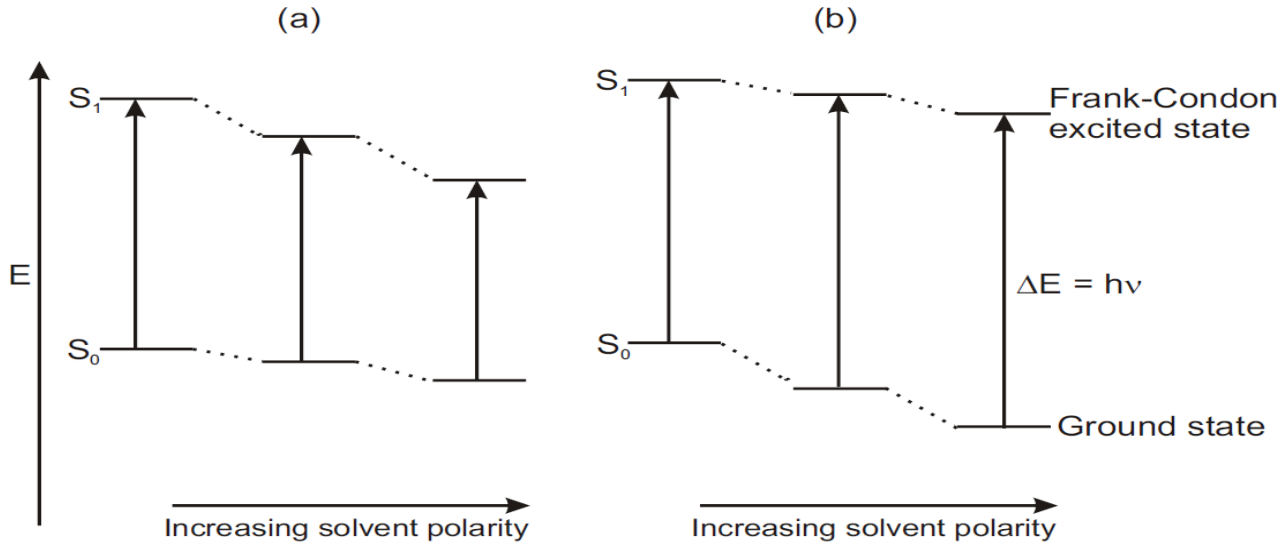

Figure 2-11: Schematic qualitative representation of solvent effects on the electronic transition energy of dipolar solutes in polar solvents (a) $(\mu_g < \mu_e)$ and (b) $(\mu_g > \mu_e)$

Solvatochromic shift in fluorescence

Because of the multiple factor influencing the fluorescence spectra, the effect of solvent on the fluorescence spectra is rather complex. Typically more than one factor will simultaneously affect the fluorophore and to find which effect is prominent is rather difficult. When talking environmental effects, solvent polarity (which itself is combination of different interactions) is the first priority. Following factors can affect the fluorescence spectra:

- Solvent polarity
- Solvent viscosity
- Hydrogen bonding
- Internal charge transfer
- Rate of solvent relaxation
- Rigidity of the local environment
- Interaction within the probes molecules
- Change in radiative and non-radiative rate constant

The variety of interactions of the solute with solvents as well with environmental effect can cause shift in the fluorescence spectra. The solvent dependent shift in emission is also included in the term solvatochromism but sometimes fluorosolvatochromism or solvatofluorochromism terms have also been applied (which are in fact not required because absorption and fluorescence are closely related). According to the Stokes law (section 2.3.3), emission spectra always appear at lower energy than the absorption spectra (because of thermal dissipation of energy among the vibrational levels). The gap between the two maxima is called Stokes shift which provide important information about the excited state. The value of the Stokes shift will increase with the increase in the polarity when the ground state dipole moment is smaller than that of the excited state $(\mu_g < \mu_e)$ as shown in Figure 2-12.

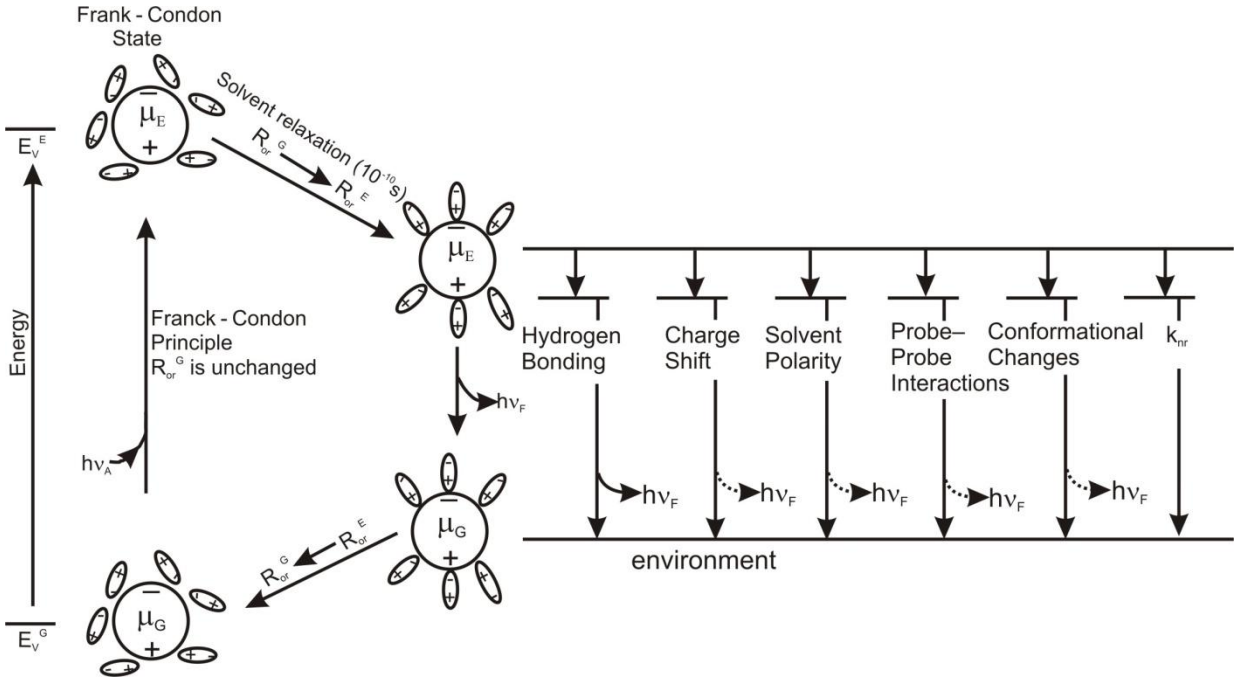

Figure 2-12: Solvent effect on fluorescence.

When the ground and excited state of apolar fluorophore have not so much different dipole moment, only small solvent-solute dispersion interactions occur and very small solvatochromic shift is observed. For instance in benzo[a]pyrene (an apolar planar aromatic) has negligible value for ground and excited dipole moments and has shown no solvent dependent spectral shift [107].

In case of fluorophore which undergo intramolecular charge transfer, $(\mu_g < \mu_e)$, a significant shift in fluorescence band is observed as in 4-(dimethylamino)-4′-nitrostilbene, DNS, (donor-acceptor substituted) whose excited state dipole moment has been increased about four times than that of the ground state [108-110]. Sometime two interconvertible intramolecular charge transfer (ICT) and twister intramolecular charge transfer (TICT) excited states exist and lead to dual fluorescence if both ICT and TICT are fluorescent. 4-dimethlamino-benzonitrile, DMABN, was the first example showing dual fluorescence discovered by Lippert *et al* [109] and later interpreted by Grabowski *et al.* [109, 111], Zachariasse *et al.* [112-113] and Rettig [114-115].

One other well studied example is 6-(arylamino)-2-naphthalene sulfonates (ANS), which has been studied for its solvent dependent dual fluorescence [116-118]. The fluorescence emission of ANS is from two different excited states which are distinctly sensitive to solvent polarity. In non-polar solvent the emission is observed from locally excited state which is not very sensitive to solvent polarity. But in polar solvent the fluorescence emission is mainly

from ICT state (zwitterionic charge transfer excites state) which is also largely sensitive to the solvent polarity.

Highly fluorescent rod-shaped donor-acceptor systems containing electron-donor (D) and -acceptor groups (A) separated by an elongated cycloalkyl spacer, also called ‘‘Fluoroprobe’’. One such example for solvent dependent fluorescence is 1-phenyl-4-(4-cyano-1-naphthylmethylene)piperidine (molecule containing two chromophores, electron donor (D) and electron acceptor(A)). Absorption spectra is solvent independent and resemble to the expected sum of the spectra of two separate chromophores (N,Nidialkylanilin, D, and 1-venylnaphthalene,A,). But the fluorescence spectra is only a single broad band which manifests a large spectral shift $\Delta\tilde{\nu}$=-10160 (from n-hexane to acetonitrile). In addition to high sensitivity of the emission solvatochromism, the bichromophoric piperidine derivative has high fluorescence quantum yield which make it an attractive candidate for solvent polarity probe [119-120]. A number of theoretical and experimental studies for the solvent effect on the fluorescence and/or absorption spectra have been published in literature [43, 49, 70-71, 86, 121-127].

Solvent relaxation: Jablonski diagram Figure 2-5 has shown that the energy of the emitting excited state is always different from that of Frank-Condon (FC) excited state and one reason for this difference is polarity effect called solvent relaxation. In most the dipole moment of the excited molecule (μ_e) is different from that of the ground state molecule (μ_g). The fact is the absorption of the photon by the molecule is very fast (~10^{-15} s) compared to the displacement of the nuclei but redistribution of electron is possible during this period which results as an instantaneous change in dipole moment. Most of the polarity probes have $(\mu_g < \mu_e)$ and undergo ICT upon excitation. So after excitation, reorganization of the solvent molecule (also called solvent relaxation) leads relaxed state to a minimum. The shift in the emission spectra and polarity are related in way that the energy of the relaxed state is lower if the polarity of the solvent is higher leading to a larger red shift in the emission spectra see Figure 2-13.

Rate of solvent relaxation is related to the viscosity of the solvent and also the temperature. The solvent molecules will take finite time (τ_r) to rearrange themselves according to Franks-Condon excited molecule (after electronic transition) and also the lifetime for the excited state (τ_e) have to be taken into account. Usually the fluorescence lifetime (1-100 ns) is much longer compared to the solvent relaxation time (10-100 ps) i.e. $\tau_r \gg \tau_e$, so the emission

corresponds to the solvent relaxed state. If the solvent relaxation rate is of the same order of the excited state lifetime, in such case the first emitted photon will corresponds to the shorter wavelengths than those emitted as longer time. The fluorescence spectrum is shifted under continuous illumination and position of the maxima cannot be related to the polarity of solvent. At low temperature, the rate of relaxation of the solvent molecule can be much lower compared to the room temperature measurements. At low temperature if rate of fluorescence decay is much faster than that of solvent relaxation, the emission will only be observed from the unrelaxed state (F). If the rate of fluorescence decay is much slower than that of solvent relaxation, the emission will only be observed from the relaxed state ($F^{/}$). At intermediate temperature, both emission and relaxation will occur simultaneously and emission from both, the unrelaxed state and relaxed state are observed as shown by dotted line in Figure 2-13. Time-resolved fluorescence techniques can be used to study spectral relaxation.

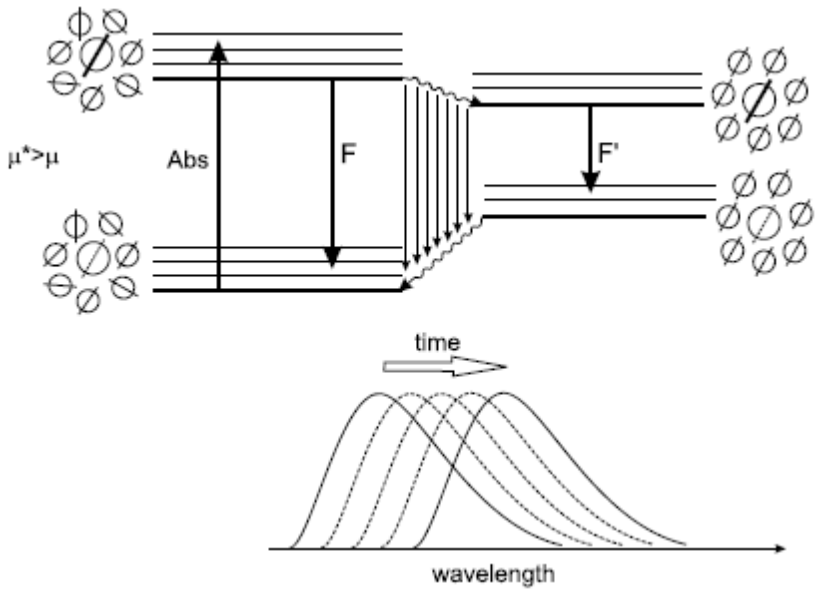

Figure 2-13: Solvent relaxation around a probe that has a weak dipole moment in the ground state and a large dipole moment in the excited state.

2.4.5 Parametric scales for solvents

The effect of the solvent on the spectral properties of a solute can be broadly divided into two categories: non-specific and specific interactions. Non-specific solvent solute interactions include among others dipole-dipole, dipole-induced dipole and induced dipole-induced dipole while specific interactions include hydrogen bonding, complexation, acid-base chemistry and charge transfer interactions among solvent molecules and the fluorophore. Various single empirical parameters have been developed and used to correlate

different physicochemical processes in the past, such as those used for spectroscopic measurements like Z [128], E_T^N[43], AN[129], χ_R and χ_B [130], and many others (reviewed in [45-46, 70-71, 124, 131-132]). About 35 solvent parameters are known out of these only about ten have been found wider application in correlation analysis of solvent-solute interaction. These are Y (Grundwald and Winstein) [133], Z (Kosower)[128], P_y (Dong and Winnik) [134], $E_T(30)$ scale (Reichardt) [43, 45-46, 106], α, β and π^* (Kamlet-Taft)[35-38], DN and AN (Gutmann) [47, 72], SA, SB, SdP and SP (Catalán)[39-42, 135-136]. The applications of most solvent are limited because their values are known for limited number of solvents. The solvent scales extension is restricted due to inherent properties for selected reference process which is sometime difficult (or impossible) to measure for certain solvents. Because spectroscopic technique are easily measurable form a large number of solvent, so the most comprehensive solvent scales are those derived from spectroscopic measurements. A brief introduction of some solvent scales which have been used in the present study is given here.

E_T(30) scale

This is the most widely used single parameter empirical scale developed by Reichardt *et al* [43, 45]. *E_T(30)* scale is based on the solvatochromic shift of the first absorption band of 2,6-diphenyl-4-(2,4,6-triphenyl-1-pyrido) phenoxide and is defined in kcal mol^{-1}. This dye undergoes a strong hypsochromic shift with the increase in the solvent polarity. The scale is named so because the standard dye used to construct this scale by Reichardt and co-workers was numbered 30 in the first publication [137]. *E_T(30)* Betaine dye (also called Reichardt dye) exhibit a absorption maxima at 30.7 kcal mol^{-1} in tetramethylsilane (TMS) and 63.1 kcal mol^{-1} in water. Also the normalized value of this scale (denoted as E_T^N) is used by assigning zero to TMS and unity to water, using the following eq. 2-29 :

$$E_T^N = \frac{\left(E_T(solvent) - E_T(TMS)\right)}{\left(E_T(water) - E_T(TMS)\right)} = \frac{\left(E_T(solvent) - 30.7\right)}{32.4} \qquad 2\text{-}29$$

The E_T^N has values between 0 and one. *E_T(30)* value for more than 300 solvents have been measured. This makes this scale one of the most comprehensive and most widely used at present [45-46, 71, 138-139]. Polarity measure by $E_T(30)$ scale for protic solvent also shows the hydrogen bond donating ability of the solvent in addition to its polarity. So *E_T(30)* scale can successfully describes the solvent-solute interactions for the molecules which are not sensitive for the basicity of the solvent.

Solvent polarity and polarizability

The use of solvatochromic dye as polarity indicator was fist suggested by Brooker *et al.* [140] in 1951 and first comprehensive solvent scale was introduced by Kosower [128] (Z-scale). Several empirical polarity scales have been developed to correlate the solvent-solute interaction and most of them are based on positive or negative solvatochromism of dye molecule. The two interesting and widely used polarity parameters are π^* *scale* and *SPP scale* (later on SPP is splitted into SdP and SP scales).

***π^*-scale*:** This scale was introduced by Kamlet, Taft *et al* [37] to measure the solvent polarity and polarizability at the same time with single scale. The π^*-scale is name so because it is base on the solvent effect on the $\pi \rightarrow \pi^*$ electronic transitions of seven dye of the type D–C_6H_4–A, where *D* is electron donor (e.g. -NMe_2) and *A* electron acceptor (e.g. –NO_2) groups. The solvatochromic shift is normalized between cyclohexane (π^*=0) and DMSO (π^*=1) given as:

$$\pi^*(solvent) = \frac{\tilde{\nu}(solvent) - \tilde{\nu}(cyclohexane)}{\tilde{\nu}(DMSO) - \tilde{\nu}(cyclohexane)} \qquad 2\text{-}30$$

$\tilde{\nu}(x)$ is the maximum of the lowest energy absorption band of the indicator dye measured in solvent *x*. In the initial construction of the π^* -scale, solvent effect on the absorption maxima values of these seven primary solvatochromic indicators were employed, which was then expanded and refined by multiple least squares correlations with additional solvatochromic indicators. So an average π^* -scale was established in this way by Kamlet, Taft and co-workers.

***SPP-scale*:** Catalan *et al* [39, 141] introduced a new scale for solvent polarity/polarizability called *SPP* scale. Two probe, N,N-dimethylamino-7-nitrofluorene (DMANF) and 2-fluoro-7-nitrofluorene (FNF), have been used to construct the SPP scale.

DMANF is chosen as strong candidate, comprehensive analysis of the literature on the choice of probes, for use as a solvent dipolarity/polarizability probe since its absorption is very sensitive to changes in the nature of the solvent. Its dipole moment is largely increased in electronic transition from ground state to the first excited state and the change does not affect the dipole moment direction. Also because of its large, rigid aromatic structure, DMANF is highly polarizable, so its first electronic transition occurs at energies where no appreciable interferences with the cut-offs of ordinary solvents are to be expected.

2-fluoro-7-nitrofluorene (FNF) is chosen as the homomorph because a nitro group at position 7 ensuring the occurrence of the same type of interaction with the solvents and fluorine atom is placed for the $-NMe_2$ group in order to obtain a lower dipole moment relative to DMANF.

A lowest absorption band for both of the above probes behave identical but have much smaller bathochromic shift with increase in solvent polarity in ANF compared to DMANF. The SPP scale is obtained by the difference between the absorption maxima of these two probes which is then normalized between gas phase (SPP=0) and DMSO (SPP=1) given as in equation 2-31.

$$SPP(solvent) = \frac{\Delta\tilde{\nu}(solvent) - \Delta\tilde{\nu}(gas)}{\Delta\tilde{\nu}(DMSO) - \Delta\tilde{\nu}(gas)} \qquad 2\text{-}31$$

$\Delta\tilde{\nu}(x)$ is the difference between the maxima of the lowest energy absorption band of the DMANF and ANF probes in solvent *x*.

The major highlights of *SPP-scale* are the following:

- Cyclohexane (π^*=0) is used as the non-polar reference in many scales but now has a value of 0.557. The polarity gap between the gas phase and cyclohexane is about as wide as that between DMSO and cyclohexane (0.443 SPP units).
- Alkane has a wide range of SPP values up to 0.601, (e.g. 0.214 for perfluoro-n-hexane, 0.479 for 2-methylbutane, 0.542 for n-octane and 0.601 for decalin).
- SPP value of alcohols is increasing upon, e.g. the SPP values for n-propanol, allyl alcohol and propargyl alcohol are 0.847, 0.875 and 0.915, respectively.

As SPP scale has described both the polarity and polarizability but recently SPP scale is divided in two scales, Sdp and SP scales. Sdp scale describes the polarity behavior of the solvent whereas the SP scale describes the sensitivity of the solvent towards solute polarizability [42, 135].

Scales for solvent basicity/hydrogen bond accepting ability

β-scale: Another solvatochromic scale based on the solvatochromic shit in UV-VIS spectral band to measure the hydrogen bond accepting ability of the solvent has been developed by Kamlet and co-workers. This scale is name as Kamlet-Taft *β-scale* [35, 38] and used to evaluate hydrogen bond acceptor (HBA) abilities of the solvents. Solvatochromic shift (

$\Delta\Delta\tilde{\nu}$), in electron pair donor (EPD[12]) solvents, for several protic probes relative to their aprotic homomorphs (structurally similar) are averaged out with the assumption that the non-specific interactions are same for both, protic and aprotic probes. The probes that are originally applied were 4-nitrophenol (protic probe) versus 4-nitroanisol (aprotic probe) and 4-nitroaniline (protic probe) versus 4-nitro-N,N-diethylaniline (aprotic probe). Both protic and aprotic probes have the ability to act as HBA substrate (at the nitro oxygen) in HBD[13] solvents but only protic probes can act as HBD substrates for HBA solvents. The *β-scale* is normalized between the hexamethylphosphoric triamide (β = 1) and cyclohexane (β= 0).

SB-scale: The Catalan and co-workers [40, 136] has introduced a new solvent basicity scale based on difference of the solvatochromic shifts between the two probe (one of them is sensitive to the solvent basicity, has an acid site, and other is not). 5-Nitroindoline (NI) possesses the electronic and structural features that are required for basicity. It has one >NH acid site and rotation is hindered by an ethylene bridge. Substitution of the proton of >NH group with a methyl group (forms >NMe), 1-methyl-5-nitroindoline (MNI), has no more acid site and is insensitive towards the basicity of the solvent. Both NI and MNI have the same sensitivity to solvent polarity, polarizability and acidity but different sensitivity to solvent basicity.

The *SB-scale* is thus constructed by the difference in the absorption maxima of the two probes in measured in the same solvent as in eq. 2-32. The *SB-scale* is normalized between gas phase (SB=0) and tetramethylguanidine,TMG (SB=1).

$$SB(solvent) = \frac{\Delta\tilde{\nu}(solvent) - \Delta\tilde{\nu}(gas)}{\Delta\tilde{\nu}(TMG) - \Delta\tilde{\nu}(gas)} \qquad 2\text{-}32$$

$\Delta\tilde{\nu}(x)$ is the difference between the maxima of the lowest energy absorption band of the MNI and NI probes in solvent *x*.

Some interesting highlights of the *SB-scale* with respect to structural effects on solvent basicity.

- SB values can be tuned by the appropriate substitution in compounds like alcohols and amines; e.g perfluorotriethylamine can be considered non-basic (SB = 0.082), whereas N,N-dimethylcyclohexylamine is at the top of the scale (SB = 0.998). Similarly,

[12] The term electron pair donor (EPD) refers to the ability of the solvent to donate an electron pair to the solute and hence the basicity of solvent. The EPD is also called as "the hydrogen bond acceptor (HBA)" the ability to accept the proton of the hydrogen bond.

[13] The hydrogen bond donor (HBD) refers to the ability to donate the proton for hydrogen bonding. HBD solvents behave as protic solvents.

hexafluoro-2-propanol is non-basic (SB = 0.014), whereas 2-octanol is very near the top (SB = 0.963).

- There is an increase in the SB values of n-alkanols with increase in chain length and levels off beyond octanol,e.g. water (SB=0.025), methanol (SB=0.545), ethanol (SB=0.658), 1-propanol (SB=0.727), 1-butanol (SB=0.809), etc.
- SB value remains almost the same upon, e.g. [n-pentane (SB = 0.073) and cyclopentane (SB = 0.063)] or [n-pentanol (SB = 0.869) and cyclopentanol (SB = 0.836)].
- Solvent basicity is decreased because of the delocalization by a factor of 3.5–5.5, as illustrated by the following couples: pyrrolidine/pyrrole (0.99/0.18), N-methylpyrrolidine/N-ethylpyrrole (0.92/0.22), tetrahydrofuran/furan (0.59/0.11), 2-methyltetrahydrofuran/2-methylfuran (0.56/0.16), cyclohexylamine/aniline (0.96/0.26), N-methylcyclohexylamine/N-methylaniline (0.92/0.21).

***DN-scale*:** The ability of a solvent to donate an electron pair of electrons of one of its donor atoms towards the formation of a coordinate bond with an acceptor atom of a solute is a measure of its Lewis basicity. There are many methods developed to quantify the electron donating ability but only few of them have proved to be viable and of any real usefulness.
One of them is Gutmann's donor number, DN, (Gutman and Vychera 1966) [47, 72]defined as the negative of the standard molar heat of reaction (expressed in kcal mol^{-1}) of the solvent with antimony pentachloride to give the 1:1 complex, when both are in dilute solution in the inert diluent 1,2-dichloroethane.

$$D: + SbCl_5 \underset{Dichloroethane}{\overset{room\ temp.}{\rightleftharpoons}} \overset{\oplus}{D} - \overset{-}{SbCl_5}$$

$$DN = -\Delta H_{D-SbCl_5} / (kcal.mol^{-1}) \qquad 2\text{-}33$$

In order to make it more generally applicable, Marcus (Y. Marcus, J. Sol. Chem. 13, 599 (1984).) has made it normalized, DN^N, by dividing the *DN* value of a given solvent by that of hexamethylphosphoric triamide (HMPA)[14].

[14] The donor number of 38.8 kcal mol^{-1} for HMPT was given by Gutmann. It should be mentioned, however, that a much higher DN value of 50.3 kcal mol^{-1} was subsequently measured for this solvent by Bollinger et al. 142. Bollinger, J.-C., G. Yvernault, and T. Yvernault, *Enthalpies de complexation de quelques phosphoramides avec le chlorure d'antimoine(V). Influence de la structure sur le nombre donneur selon Gutmann.* Thermochimica Acta, 1983. **60**(2): p. 137-147.This shows that serious problems arise in measuring the Lewis basicity of this EPD solvent towards SbCl5.

$$DN^{N} = \frac{DN(solvent)}{DN(HMPA)} = \frac{DN(solvent)}{38.8} \qquad 2\text{-}34$$

This quantity needs to be determined calorimetrically, as was done for a considerable number of solvents at that time.

Scales for solvent acidity/hydrogen bond donating ability

Solvent have also been parameterized on the basis of their hydrogen bond donating ability. Two scale, *α-scale*, and *SA-scale* are most important scales for solvent acidity or hydrogen bond donating ability.

***α-scale*:** Kamlet and Taft (1976) [36] has developed *α-scale* to measure the hydrogen bond donating ability of the solvent. The solvatochromic comparison method is used to evaluate the contribution of the hydrogen bonding in hydrogen bond donor (HBD) solvents for several polarity indicator dyes used to establish the polarity scale (Reichardt's $E_T(30)$, Brooker's χ_R, Kosower's Z). This scale is base on solvatochromic parameters average over several solvatochromic probes.

Linear correlations with other polarity scales like *Z* and E_T^N, taking into account the non-specific interactions by means of π^*values of the solvents, can be also be used [138].

$$\alpha = 0.0485Z - 2.75 - 0.49\pi^* \qquad 2\text{-}35$$

$$\alpha = 2.13E_T^N - 0.03 - 0.76\pi^* \qquad 2\text{-}36$$

The *α-scale* has been normalized between cyclohexane (α = 0) and methanol (α = 1). There is uncertainty of ±0.08 in the *α-scale* values that come from the averaging process [38].

***SA-scale*:** A generalized acidity scale, SA, has been developed on the basis of solvatochromism of o-tert-butylstilbazolium betaine (TBSB) dye and its homomorph o,o′-di-tert-butylstilbazolium betaine (DTBSB) dye [41]. These dyes are chosen in a way that they differ in their sensitivity to acidity but rests of the features (structural and solvatochromic) are similar. In a non-HBD (i.e. one that cannot interact directly with the oxygen lone pair), solvent the first visible absorption band the band is structured; on the other hand, the band loses its structure upon interaction with an HBD solvent. The absorption maxima in different the non-acidic solvents of the probes TBSB and DTBSB correlated using the method of Kamlet and Taft [35-36] eq. 2-37:

$$\tilde{\nu}(TBSB) = 1.408\tilde{\nu}(DTBSB) - 6088.7 \qquad 2\text{-}37$$

with n = 50, r = 0.961 and sd = 43.34 cm^{-1}.

The SA value for a given non-acidic solvents can be obtained from the eq. 2-38 , where ethanol is assigned a value of 0.4, the acid solvatochromic behavior of which is exhibited at 1299.8 cm^{-1}.

$$SA = \frac{[\tilde{\nu}(\text{TBSB})\text{-}(1.409\,\tilde{\nu}(\text{DTBSB})\text{-}6288.7)]}{\tilde{\nu}(\text{ethanol})} \times 0.4 \qquad 2\text{-}38$$

Because of the pK_a (pK~10 for the above probes) problems, the above dyes cannot be used for solvent which are more acidic than methanol. This problem is not exclusive to *SA*; in fact, it affects almost all the acidity scales, which usually provide little information about strongly acidic solvents.

In order to calculate the SA values for the acidic solvent 3,6-diethyltetrazine (DETZ) is used. DETZ molecule has $n\rightarrow\pi^*$ around 500-550 nm in solvents of different acidity. The shift in the $n\rightarrow\pi^*$ band is largely caused by solvent acidity and a little due to polarity of the medium. Kamlet-Taft [35-36] method is used to correlate the absorption maxima of DETZ with solvent polarity (the SPP value). A linear dependence non-acidic solvents, whereas acidic solvents departed from this behavior is obtained. This departure from the linear behavior is quantified by DETZ as described by eq. 2-39:

$$\Delta\tilde{\nu}(DETZ) = 1.015SPP + 17.51 \qquad 2\text{-}39$$

with n = 13, r = 0.983 and sd = 23 cm–1.

The *SA* value of an acidic solvent, using the DETZ probe, has been determined as in eq. 2-40:

$$SA = 0.833\Delta\tilde{\nu}(DETZ) + 0.339 \qquad 2\text{-}40$$

with n = 6 and r = 0.987.

2.4.6 Multiparameter approach

However, none of these single parameters can describe the complex solvation process in its entirety. In order to have a thorough insight into solute-solvent interactions, it is better to make use of linear combinations of different solvent parameters in the manner of Linear Solvent Energy relationships. The general relationship that represents the multiparameter approach is represented in eq. 2-41.

$$XYZ = XYZ_o + \text{Hydrogen bonding term (s)} + \text{di-polarity term} + \text{cavity term} \qquad 2\text{-}41$$

The cavity term in the above equation is the measure of the enthalpy or the free energy necessary to create space for the solute within the solvent molecules. As a result of the multiparameter analysis, the quantitative contribution of different types of interactions can be easily seen

Kamlet-Taft Parameters

One of the most generally applicable and most precisely elaborated approaches was developed by Kamlet, Abboud and Taft (KAT) [35-38]. KAT approach has been successfully applied during the last three decades for illustrating solvent effects in different fields of study. The specific (hydrogen bond donating or accepting ability) and non-specific interactions are separately considered. The commonly used Kamlet-Taft equation used for linear solvation energy relationship is shown in eq. 2-42.

$$A = A_o + a_{\pi^*}\pi^* + b_\alpha\alpha + c_\beta\beta \qquad 2\text{-}42$$

Where A is the measured property (absorption or fluorescence maxima in our case), A_0 the calculated value for the cyclohexane, α is the solvent hydrogen bond donating ability [36], β is solvent hydrogen bond accepting ability [35], and π^* is the solvent polarity/polarizability [37] and the coefficients a_{π^*}, b_α and c_β are respective contribution of the. In the Kamlet-Taft approach, the scale π^* has been described as the combination of both dipolarity and polarizability of a solvent at the same time

Catalán's parameters

Recently Catalán and co-workers [39-42, 71, 135] have developed a new set of solvent parameters based on well defined reference processes. Initially they have introduced three semi empirical parameters; SA (solvent acidity as α in KAT), SB (solvent basicity as β in KAT) and SPP (solvent polarity/polarizability as π^* in KAT). Later on the SPP scale was further split into two: Sdp (solvent dipolarity) and SP (solvent polarizability) scales. This Linear solvation energy relationship (LSER) is now written, eq. 2-43, as a linear combination of four solvent parameters (SA, SB, SdP and SP). Two of these represent the specific interactions (SA and SB) while the other two represent the non-specific interactions (Sdp and SP):

$$A = A_o + a_{S_{dP}} SdP + b_{Sp} SP + c_{SA} SA + d_{SB} SB \qquad 2\text{-}43$$

where A is the measured, A_0 is the calculated value for the gas phase. $a_{S_{dP}}, b_{Sp}, c_{SA}$ and d_{SB} describe the solvent independent quantitative contributions of the solute molecule in solvent-solute interactions for solvent parameters *SdP, SP, SA,* and *SB,* respectively.

Combination of *ETN* and *DNN*

Another multiparameter approaches that can be used to describe the solvent-solute interaction is combination of Reichardt parameter, $E_T(30)$, with Gutmann's donor number, *DN,* in the following way:

$$A = A_0 + aE_T(30) + bDN \qquad 2\text{-}44$$

$E_T(30)$ and DN are the solvent properties whereas *a* and b are corresponding share of the solute molecules. Equation 2-44 is somehow more simplified version of the multiparameter analysis as it includes the two empirical parameters. $E_T(30)$ represents polarity and somehow the hydrogen bond donating ability of the solvent and DN describes the solvent basicity. Thus equation 2-44 is likely to be applied successfully in multiparameter linear regression correlation.

Also the solute-solvent interaction can be analyzed by using physical approach in its simplest form that describe the solvatochromic shift as a combination of non-specific parameters such as relative permittivity $f(\varepsilon)$ and molar polarizability $f(n^2)$. Different dielectric solvent-solute interactions due to polarizability and dipole moment are shown in Figure 2-7.

The multiple parameter equation can be written as [48-49]:

$$A = A_o + Xf(n^2) + Yf(D, n^2) \qquad 2\text{-}45$$

where $f(D.n^2)=f(D)-f(n^2)$ with $f(D) = \dfrac{D-1}{2D+1}$ and $f(n^2) = \dfrac{n^2-1}{2n^2+1}$

$X=(\mu_e^2-\mu_g^2)/2a^3$ (for both absorption and fluorescence) $Y=\mu_g(\mu_e-\mu_g)/a^3$ for absorption

$Y=\mu_e(\mu_e-\mu_g)/a^3$ for fluorescence

μ_g and μ_e are dipole moments for the ground and excited states

a is Onsager radius for solute cavity

A and A_0 are the absorption (or fluorescence) maxima corresponds to the its observed and gas phase values.

If the correlation coefficient is high (r >0.9) and the A_0, X and Y coefficients have low uncertainties, two important information can be obtained from the linear regression of equation 2-45, i.e. μ_e and gas phase absorption (or fluorescence) maxima.

X term reported here is a rough approximation because there are in fact two contributions: (a) variation of solute polarizability, (b) transition dipole moment. Therefore, the μ_e should have to be estimated from Y term in both absorption and fluorescence data analysis. The A_0 is conceptually corresponds to the gas phase value of the property A, but relevance of identifying the constant term A_0 as the gas phase value is under debate [48].

2.5 pH dependence of absorption and fluorescence spectra

Both, the absorption spectra and the emission spectra depend on the acid-base properties of the electronic states involved in electron transition. Proton transfer in the excited state occurs for the compounds containing chromophoric groups like –COOH. -NH_2, -OH, -NR_2, etc. Proton ejection and back recombination depend on the pH of the medium.

2.5.1 Ground state pKa

The ground state pK_a value is calculated using different methods, (a) from the relative intensity of the absorption of the protonated and unprotonated form, (b) using the Henderson-Hasselbalch equation [143-144] and (c) the Benesi-Hildebrand double reciprocal method[30, 145].

Fluorophore molecules (M) exist in the following equilibrium at different pH

$$M + H_3O^+ \underset{k_r}{\overset{k_f}{\rightleftharpoons}} MH^+ + H_2O \qquad 2\text{-}46$$

k_f and k_r are rates of forward and reverse reactions, respectively. Alternatively, the Henderson–Hasselbalch method eq. 2-47 can be applied for the determination of the pK_a value for the above acid-base equilibrium as:

$$pH = pK_a + \log\left(\frac{A - A_{MH^+}}{A_M - A}\right) \qquad 2\text{-}47$$

where A_M and A_{MH+} are the absorbance of the neutral molecule M and its protonated form (MH^+) at a determined wavelength, while A denotes the absorbance due to both neutral and protonated form of organic molecule M. Eventually, from the acid-base equilibrium shown by eq. 2-46, one can formulate the equation 2-48 [30, 145]:

$$A - A_o \cong \left(\varepsilon_{MH^+} - \varepsilon_M\right)\left(\frac{K_c[H^+]}{1+K_c[H^+]}\right) \qquad 2\text{-}48$$

where

$$K_c = [HD^+]/([H^+][D]) = {}^{1}\!/_{K_a}$$

where A and A_o are the absorbance of the organic molecule M at a given pH and that of the unprotonated form, respectively. The value of pK_a can be determined from double reciprocal plot of $(A\text{-}A_o)$ versus $[H^+]$.

2.5.2 Excited state pKa*

Steady state fluorescence titration [146] and Förster cycle [147-149] have been used for the estimation of the excited state pK_a^* value. Steady state fluorescent spectra have been obtained by excitation at the isosbestic point lying at the longest wavelength in aqueous solutions of fluorophore M at different pH. A plot of the relative intensities of both, protonated (I'/I'_o) and unprotonated (I/I_o) forms against different pH and H_o values yields usually two sigmoid curves for protonated MH^+ and unprotonated species M, respectively. The two sigmoidal curves intersect each other at a pH which corresponds to the pK_a^* of the fluorophore. The symmetrical sigmoidal curve can only be obtained if there is no other competing process, e.g. quenching of the excited state.

The estimation of the excited state equilibrium, pK_a^*, by the Förster cycle method is based on ground state thermodynamics and electronic transition energies. Here only the difference in molar enthalpy change (ΔH) of ground and excited states is considered and the difference in the molar entropy change between the ground and excited states (ΔS) is neglected. Equation 2-49 has been used to calculate the pK_a^*.

$$\Delta pK = pK_a - pK_a^* = \frac{E_{AH} - E_{A^-}}{2.303RT} \qquad 2\text{-}49$$

E_{AH} and E_{A-} are the 0-0 transition energies of protonated and unprotonated forms.

Both methods (fluorescence titration and Förster cycle) for the estimation of the pK_a^* value are based on the assumption that the excited state proton transfer is very fast and that the acid-base equilibrium is established during the lifetime of the excited state. However, in the case proton induced fluorescence quenching can compete with the proton transfer reaction in the excited state, the most reliable value for the pK_a^* can only be obtained by a dynamic analysis [150-152].

2.6 Electrochemical Study (Cyclic Voltammetry)

Voltammetry (came from "volt ampere metry") is measurement of the current with the change in voltage of the system. Cyclic voltammetry (CV) is one of the electro-analytical techniques where the potential scan is being reversed at some certain voltage and scanned back toward the initial potential. CV is perhaps the most versatile because of its experimental simplicity and large information contents. It has been widely applied in various fields range from study of simple redox process in organic/inorganic chemistry to the characterization of multi-electron process in supramolecular chemistry and biochemistry. Three differ types of electrode are used in cyclic voltammetry setup.

Working electrode is a place where redox occurs surface area few mm^2 to limit current flow. At high scan rate, the current produced at the electrode surface is large and increased resistance results in distortion so in order to minimized the current and resistance, electrodes with small surface areas (microelectrode or sometime ultramicroelectrodes) are used. **Reference electrode** is an electrode at constant potential and has well-known electrode potential, (e.g. Standard calomel electrode (SCE), Normal hydrogen electrode (NHE), Ag/AgCl, etc.). **Counter electrode** is inert material (Hg, Pt) which does not take part in redox but completes circuit.

In CV experiments, the potential of the working electrode is varied linearly with time, see Figure 2-14 (a), from a potential where no electrochemical change is occurred to a potential where the oxidation or reduction process occurs. After passing the potential region where the electrochemical processes occur, the direction of the linear sweep is reversed. The species formed during the electrochemical process can be detected and studied. The time scale is controlled by the scan rate of the experiment

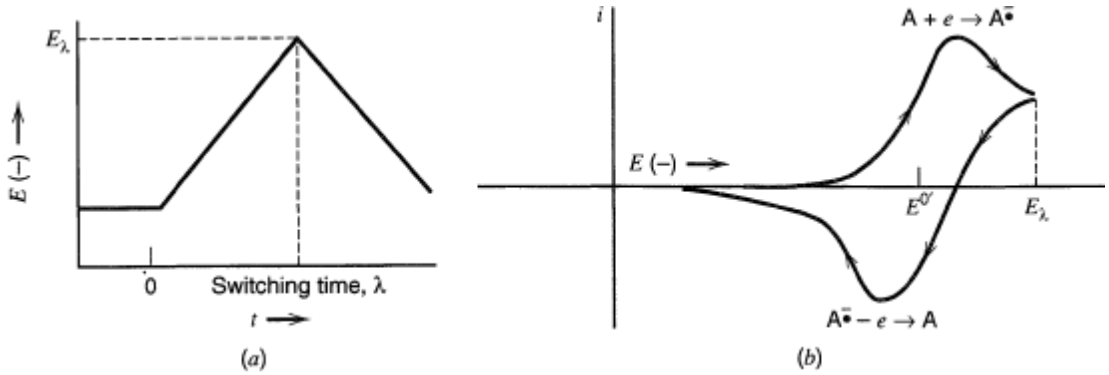

Figure 2-14: linear variation of the electrode potential with time (a) and the change in the current with change in the electrode potential (b) [153].

The cyclic voltammogram is obtained by measuring the current at the working electrode during the potential scan and a displayed as current versus potential, Figure 2-14 (b). Electrode potential is varied linearly with time, so horizontal axis of the voltammogram can be though as time axis. The magnitude of measured current provide information

Electron transfer reaction can be written in very simple form as $ox + ne \rightleftharpoons red$, where *ox* refers to an oxidized from, *n* is the number of electron transferred in an electrode reaction and *red* represents the reduced form generated during an electrode reaction. Some important parameters those are often used to characterize the cyclic voltammetry are the cathodic peak potential, E_{pc}, anodic peak potentials, $E_{Pa,}$ ratio of the anodic and cathodic peak current, i_{pa}/i_{pc}, separation of the peak potential, $\Delta E = E_{pa} - E_{pc}$, half peak potential $E_{p/2}$ and half wave potential $E_{1/2}$. The halfwave potential can be expressed as in classical polarography, see equation 2-50.

$$\mathrm{E}_{1/2} = E^o + \frac{RT}{nF}\ln\left(\frac{D_{red}}{D_{ox}}\right)^{1/2} \qquad 2\text{-}50$$

where E^o is the formal potential referred to the ionic strength of the solution used, *R* is universal gas constant, *T* is temperature, *F* is Faraday's constant, *n* is the number of electron involved in the electrochemical process and D_{red} and D_{ox} are the diffusion coefficient of the reduced or the oxidized form respectively.

2.6.1 Reversible process

Consider the following reversible reaction

$$ox + ne \rightleftharpoons red \qquad 2\text{-}51$$

where *ne* is the number of electrons transferred during electrode process, *ox* and *red* are the oxidized and reduced forms, respectively. In reversible process, the product formed during the electrode process is stable for the time scale of potential scan, the D_{red} and D_{ox} are approximately the same so $E_{1/2}$ has the same values as of E^o and $E_{1/2}$ is given by the average of both potentials:

$$\mathrm{E}_{1/2} = E^o = \frac{E_{pa} + E_{pc}}{2} \qquad 2\text{-}52$$

In CV, the product form during the electrochemical process can be seen directly through magnitude of the current generated on the electrode. For a reversible reaction, the current generated on anode and cathode should be equal to unity, $i_{pc}/i_{ac} = 1$, where i_{pa} is anodic peak current and i_{pc} is cathodic peak current. Deviation of peak current ratio from unity represents

the kinetic or other complexities in the electrode process. In case when the base line for the i_{pa} is difficult to determine, Nicolson suggested that the ratio of the $i_{pa/}$ i_{pc} can be calculated from the uncorrected peak current and the current at switching potential[15], $E_{\lambda,}$ using the equation 2-53:

$$\frac{i_{pa}}{i_{pc}} = \frac{(i_{pa})_0}{i_{pc}} + \frac{0.485(i_{sp})_0}{i_{pc}} + 0.086 \qquad 2\text{-}53$$

where $(i_{pa})_0$ is uncorrected anodic peak current and $(i_{sp})_0$ is current corresponds to E_λ.

The peak separation is also a good criterion to determine the reversibility of the electrochemical redox reaction. For reversible process the separation of the potential peaks can be used to calculate the number of electron transferred in an electrode reaction can be given as:

$$\Delta E_p = E_{pa} - E_{pc} \cong \frac{2.303RT}{nF} \qquad 2\text{-}54$$

At 25^o C

$$\Delta E_p = E_{pa} - E_{pc} \cong \frac{59}{n} mV \qquad 2\text{-}55$$

Peak current for a reversible rate constant can be expressed by Randles-Sevcik equation as:

$$i_p = 0.4463\alpha^{1/2} nFAD^{1/2}C \qquad 2\text{-}56$$

where α is charge transfer coefficient and $\alpha = \left(\frac{nFv}{RT}\right)$

when temperature is taken as 25^oC and A is expressed in cm^2, D in cm^2s^{-1}, C in $molcm^{-3}$, v in Vs^{-1} and i_p in ampere, the equation 2-61 can be written as:

$$i_p = (2.69\times10^5) n^{3/2} ACD^{1/2} v^{1/2} \qquad 2\text{-}57$$

This indicates that the peak current i_p is directly proportional to the square root of the scan rate $v^{1/2}$ and peak potential E_p is given as:

$$E_p - E_{1/2} = E_p - E^o + \left(\frac{RT}{nF}\right)\ln\left(\frac{D_{ox}}{D_{red}}\right) = -1.109\left(\frac{RT}{nF}\right) \qquad 2\text{-}58$$

The peak is sometime broader and is difficult to assign E_p accurately, so it is convenient to relates potential as $i_{p/2}$ which is

[15] The switching potential, $E_{\lambda,}$ is the potential where the direction of the scan in cyclic voltammetry is reversed. The shape of the curve on reversal depends on the switching potential.

$$E_{p/2} = E_{1/2} + 01.09\left(\frac{RT}{nF}\right) = E_{1/2} + \frac{28}{n} \quad \text{at } 25\ ^{o}\text{C} \qquad 2\text{-}59$$

$E_{1/2}$ is about in the midway of E_p and $E_{p/2}$, so the Nernstian wave can be diagnosed as

$$\left|E_p - E_{p/2}\right| = 2.2\left(\frac{RT}{nF}\right) = \frac{56.5}{n} \quad \text{at } 25\ ^{o}\text{C} \qquad 2\text{-}60$$

This is a diagnostic test for the reversibility of the electrode process.

2.6.2 Quasi-reversible process

It is common for a eversible process to become an irreversible process with the change in the scan rate through passing a region known as quasi-reversible region. This transition occurs when the relative charge transfer rate with respect to mass transport is insufficient to maintain equilibrium. For quasi-reversible systems ($10^{-1} > k^o > 10^{-5}$cm s^{-1})[154-155] current is controlled by both mass transfer and charge transport. The Nerst equation is only approximately satisfied.

For one step, the redox reaction is written as $ox + ne \rightleftharpoons red$, the rate constant for the quasi-reversible process can be calculated using the Nicholson equation [156].

$$k^o = \frac{\psi}{\gamma^{\alpha}}\left(\frac{\pi nFvD}{RT}\right)^{1/2} \qquad 2\text{-}61$$

$$\gamma = \sqrt{D_{ox}/D_{red}} \qquad 2\text{-}62$$

ψ is a well know kinetic parameter and value of ψ has been reported by Nicholson[156-157], and also using equation 2-64 [158].

Klinger and Kochi [159] also evaluated the standard rate constant for electron transfer using cyclic voltammetry data as:

$$k_s = 2.18\left(\frac{\beta nFvD}{RT}\right)^{1/2} \exp\left[-\left(E_{pa} - E_{pc}\right)\frac{\beta^2 nF}{RT}\right] \qquad 2\text{-}63$$

The above equation 2-63 is obtained from theory of Nicholson and Shain [157] for totally irreversible reaction by replacing the standard potential with a factor $(1-\beta)E_{pa} + \beta E_{pc}$, where β is transfer coefficient of the electrode process and E_{pa} and E_{pc} are the anodic and cathodic peak potentials. Both procedures, Nicholson[156] and Kochi[159] are valid for different range of $n.\Delta E_p$, for low and high values of peak separation, respectively. The single

empirical relationship has been developed [158] to relate the values of ψ with the peak separation as:

$$\psi = \frac{(-0.6288 + 0.0021 \times n\Delta E_p)}{(1 - 0.017 \times n\Delta E_p)} \qquad 2\text{-}64$$

$n.\Delta E_p$ is peaks separation multiplied by the number of electron transferred in electrochemical reaction and is expressed in *mV*.

2.6.3 Totally irreversible process

In the reversible reaction, one electron reaction is simply shown as $ox + ne \xrightarrow{k_f} red$, the charge transfer has extremely slow ($k^o < 10^{-5}$ cm s^{-1}) and only one of the anodic or cathodic heterogeneous rate constant (depending on the potential) has a measureable rate. Since the surface concentration at the electrode depends on the heterogeneous reaction and current largely controlled by the charge transfer reaction, the Nerst equation cannot be applied in reversible system. The kinetic parameter characterizing such redox reaction can be obtained from equation 2-65 [157]:

$$i = nFAC_{ox}\left(\pi D_{ox} b \chi(bt)\right)^{1/2} \qquad 2\text{-}65$$

where $b = \frac{\beta nFv}{RT}$, function $\chi(bt)$ depends on the potential and is numerically obtained, βn is the symmetry coefficient multiplied by the number of electrons transferred, *F* is Faraday's constant, *R* is the gas constant, *T* is temperature and *v* is the scan rate. The maximum value the current obtained for the function $\chi(bt)\pi^{1/2}$ is 0.4958 [157], so the peak current can be written as in equation 2-66

$$i_p = \left(2.99 \times 10^5\right) n(n\beta)^{1/2} ACD^{1/2} v^{1/2} \qquad \text{at } 25^oC \qquad 2\text{-}66$$

where i_p is expressed in ampere, A in cm^2, D in cm^2s^{-1}, C in $molcm^{-3}$ and *v* in Vs^{-1}. The potential corresponds to the maximum current i_p is E_p, also called the peak potential can be rearranged as

$$E_p = E^o - \left(\frac{RT}{F}\right)\left[\ln\left(\frac{D^{1/2}}{k^o}\right) + \ln\left(\frac{\beta Fv}{RT}\right)^{1/2} + 0.78\right] \qquad 2\text{-}67$$

The above equation shows that the peak potential (E_p) is a function of scan rate(*v*) and shift (for a reduction process) in negative direction by a factor of $1.15RT/RT$ (30 mV at 25 ^oC) for every tenfold increase in *v*.

The peak potential (E_p) and half peak potential ($E_{p/2}$) are related as [157]

$$\left|E_p - E_{p/2}\right| = 1.857\left(RT/\beta nF\right) \qquad 2\text{-}68$$

Knowing the value of E^o, equation 2-67 could be used to calculate the heterogeneous rate constant for irreversible system.

Kochi and Klinger have proposed the following equation to calculated the heterogeneous rate constant which is function of applied potential *E*

$$k(E) = 2.18\left[\frac{\beta nFvD}{RT}\right]^{1/2} \exp\left[\frac{nFv}{RT}\left(E - E_p\right)\right] \qquad 2\text{-}69$$

Where k(E) is potential dependent heterogeneous rate constant and *E* is the applied potential, rest of the parameters have usual meanings. For $E=E_p$ the equation 2-69 becomes as

$$k(E_p) = k_s = 2.18\left[\frac{\beta nFvD}{RT}\right]^{1/2} \qquad 2\text{-}70$$

So the heterogeneous electron transfer rate constant (cm s^{-1}) is related to sweep rate *v* (V s^{-1}) and diffusion coefficient D (cm^2 s^{-1}).

Total reversibility can be manifested by the equation 2-71 through the magnitude of the slope in the E_p or $E_{p/2}$ vs log *v*. The value of slope lies between 0-30 mV per decade for reversible process and beyond 30 mV per decade predicts irreversible process. .

$$E_p = \frac{2.303RT}{2\beta nF}\log v + C \qquad 2\text{-}71$$

Equation 2-71 was first proposed by Delahey [160] and latter Nicholson and Shain [157] have similar equation with different constant value.

Table 2-2: Diagnostic tests for electrode process.

Reversible process	Irreversible process	Quasi-reversible process
$\Delta E_p = E_{pc} - E_{pa} = \frac{59}{n} mV$ $\frac{i_{pa}}{i_{pc}} = 1$ $i_{pa} or\ i_{pc} \propto v^{1/2}$ $\left\|E_p - E_{p/2}\right\| = \frac{56.5}{n} mV$ E_p is independent of *v*	No reverse peak $i_{pc} \propto v^{1/2}$ E_{pc} is shifted -30/(nα) mV for each tenfold increase in *v* $\left\|E_p - E_{p/2}\right\| = \frac{48}{n\alpha} mV$	i_p inceases with $v^{1/2}$ but not proportional to it $\frac{i_{pa}}{i_{pc}} = 1$ provided $\alpha_c = \alpha_c$ =0.50 ΔE_p > 59/n mV and increase with increase in *v*. E_{pc} shifts negatively with increase in *v*

3 EXPERIMENTAL TECHNIQUES AND METHODS

An important part of the research is the technique used to study the specific direction of research and the methods used to analyse the data obtain in different experiments. An overview of the experimental techniques and methods used to study of the photophysical as well as electrochemical properties is presented in this chapter.

3.1 Solvents used

The photophysical properties of various cyano-substituted aromatic compounds have been studied in about 26 solvents. Solvents have been selected in way to to get a true representation of the solvent effect on various photophysical properties and to discuss an ample range of the Kamlet-Taft (a, β and π*) [35-38] and Catalán (SA, SB, Sdp and SP) [39-42, 71, 135] parameter sets and also. The solvents used in this study encompass polar protic (alcohols and H_2O), highly polar aprotic (DMSO, DMF, HMPA etc.) and apolar to slightly polar aprotic ones (alkanes, aromatics, ethers and esters). The halogenated solvents are not used for the present study because of their sensitivity for photochemical reaction. Table 3-2 contains the list of solvents used in the present study.

Ground and excited state proton transfer equilibrium constants (pK_a and pK_a^*) of DCPPD and TCHQ have been calculated by measuring the absorption and fluorescence spectra in H_2O at different pH/H_o values. Citric acid and Na_2HPO_4 have been used in buffer solutions of different pH ranging from pH 2 to 8 [161]. Dilute aqueous solutions of $HClO_4$ have been used in order to perform measurements below pH 2 [162].

The solvent mixtures (H_2O : DMSO) and (H_2O : MeCN) have been also used to study the absorption and emission behavior of 2,3,5,6-tetracyano hydroquinone (TCHQ).

The electrochemical properties for cyano-substituted PPDs and TMPPDs (Cyclic voltammetry measurements) have been studied only in acetonitrile (MeCN).

3.1.1 Solvent purification and handling

Solvents used for photophysical and electrochemical properties are of spectroscopic grade and are purified dynamically (if necessary) using molecular sieves and distilled at ambient pressure under argon (or at reduced pressure). DMSO was purified using recrystallization by 2-3 freeze cycles until no more smell due to dimethylsufide. Bi-distilled water has been

used. It goes without saying that all solvents during purification, sample preparation and measurements are kept under argon to avoid any contact with ambient air (oxygen and moisture).

3.2 Cyano-substituted aromatic compounds

A series of cyano-substituted derivatives of p-phenylenediamine and N,N,N',N'-tetramethyl-p-phenylenediamine (now and onward referred as PPDs and TMPPDs, respectively) have been synthesized to study the photophysical properties and solvatochromism in details. The electrochemical properties of PPDs and TMPPDs have also been studied. Also other cyano-substituted derivatives like 2,3,5,6-tetracyanohydroquinone (THCQ) and 2,3,5,6-tetracyanobenzoquinone (cyanil) have synthesized and their properties have been investigated. The compounds used in the present study are shown in Table 3-1.

Table 3-1: Cyano-substituted aromatic compounds used for photophysical and electrochemical studies.

Sr. No.	Compound Name	Abbreviation	Supplier/purification
1	p-phenylenediamine	PPD	Sigma-Aldrich 98% and purified by sublimation.
2	Monocyano-p-phenylenediamine	MCPPD	Synthesized in the present study and purified by sublimation.
3	2,6-dicyano-p-phenylenediamine	26DCPPD	Synthesized in the present study and purified by recrystallization with methanol.
4	2,3,5,6-tetracyano-p-phenylenediamine	TCPPD	Synthesized for the present study according to ref. [163-165] and purified by column chromatography (ethylacetate).
5	N,N,N',N'-tetramethyl-p-phenylenediamine	TMPPD	Fluka 98% and purified by sublimation.
6	Monocyano-N,N,N',N'-tetramethyl-p-phenylenediamine	MCTMPPD	Synthesized in the present study and purified by sublimation.
7	2,6-dicyano-N,N,N',N'-tetramethyl-p-phenylenediamine	26DCTMPPD	Synthesis and purification was done by A. Rosspeintner in 2002 [164]..
8	2,3,5,6-tetracyano hydroquinone	TCHQ	Synthesized according to reference [44] and purified by recrystallization with glacial acetic acid.
9	2,3,5,6-tetracyano benzoquinone	Cyanil	Synthesize according to reference [44] and purified by recrystallization from CH_2Cl_2.

Table 3-2: List of solvents used.

Ref. No.	Solvent	ABB.	Supplier	drying (sieve)/ Purification	Ref. No.	Solvent	ABB.	Supplier	drying (sieve)/ Purification
1	n-Hexane	NHX	Sigma 99.6%	4A°/distillation	14	Hexamethylphosphor-amide	HMPA	99% Aldrich	Vacuum distillation
2	Cyclohexane	CHX	Sigma 99.6%	4A°/distillation	15	Acetonitrile	MeCN	99.5% ROTH	3A°/distillation
3	p-Xylene	XYL	96% Merck	4A°/distillation	16	Dimethylformamide	DMF	99.8% ROTH	4A°/distillation
4	Benzene	BZN	99.7% Merck	as received	17	Dimethylsulfoxide	DMS	99.5% ROTH	By Freeze cycles
5	Toluene	TOL	99.5% ROTH	4A°/distillation	18	Propylene carbonate	PC	99% Aldrich	Vacuum distillation
6	Ethylbenzene	ETB	95% BDH	as received	19	1-Pentanol	1ptol	99% Sigma	4A°/ vacuum distillation
7	Butylether	NBE	99% Acros	as received	21	1-Butanol	1BOL	99.5% ROTH	as received
8	Diethyl ether	DEE	99.5% ROTH	as received	22	2-Propanol	2PROL	99.7% Merck	as received
9	Propylacetate	PRA	99% Alfa	4A°/distillation	23	1-Propanol	1PROL	99.5% ROTH	as received
10	Ethylacetate	ETA	99.5% Sigma	4A°/distillation	24	Ethanol	EtOH	99.5 % Astr-Alco	3A°/distillation
11	Tetrahydrofuran	THF	99.5% ROTH	4A°/distillation	25	Methanol	MeOH	99.8% Merck	3A°/distillation
12	Acetone	ACT	99.8% ROTH	3A°/distillation	26	Water	H2O	----	bi-distilled
13	Benzonitrile	BCN	99% Alfa	Vacuum distillation					

3.3 Experimental Techniques

Photophysical properties of different cyano-substituted aromatic compounds have been studied using steady state absorption (UV-VIS) spectroscopy, steady state fluorescence spectroscopy and time-resolved fluorescence spectroscopy (in about 26 different solvents shown in Table 3-2). Electrochemical properties have been studies using cyclic voltammetry.

3.3.1 Steady state absorption and fluorescence

The absorption spectra have been recorded by a Shimadzu UV-3101PC UV-VIS-NIR (measureable range 190 nm to 3200 nm) double beam scanning spectrophotometer with a band pass of 1nm. The spectrophotometer is controlled/operated using software *UVPC version 3.9*. Steady state fluorescence measurements (emission and excitation spectra) are recorded using a Jobin–Yvon Spex FluoroMax-2 spectrofluorimeter (scan range 250 nm – 900 nm, band pass 2 nm). FluoroMax is controlled/operated using the software *Datamax version 2.0*. The temperature of spectrofluorimeter sample holder is controlled by an externally attached thermostat.

3.3.2 Time-resolved fluorescence

Time-resolved fluorescence experiments (fluorescence lifetimes) of cyano-substituted PPDs and TMPPDs have been measured using the time-correlated single-photon counting (TCSPC) and modulation techniques.

Time correlated single photon counting (TCSPC)

Time resolved fluorescence measurements have been performed on a home built single photon counting apparatus described elsewhere [166]. The principal behind the TCSPC is to generate a histogram of individual photon emitted by the sample within the decay profile. A simplified scheme of time correlated single photon counting (TCSPC) has been shown in Figure 3-1. The start signal is generated simultaneously by function generator to trigger the pulser for excitation light source (LD or LED). The signal from the trigger is normalized by start CFD (constant fraction discriminator) and sends the signal to the TAC (time to amplitude converter[16]). The 2nd stop signal is reached to TAC because of the emission of a single photon detected by the photomultiplier, after being processed by the stop CFD. On getting excitation pulse (start signal), the capacitor of the TAC is charged till the stop signal

[16] Time to amplitude convertor plays basic role in TCPSC and related to the time laps of the excited molecule

is detected. The charge store by the capacitor is directly proportional to the time elapsed between the start and stop pulse and send this voltage to the multichannel analyzer (MCA). The MCA is directly connected to the computer and displays the resulting histogram on the screen (after many repetitions) which corresponds to decay of the excited state. A more detailed description of instrumental setup and data processing is discussed in ref. [167]. *Maestro program (version 3.2)* is used to control/operate the TCSPC. The different light emitting diodes (LED 340 nm, LED 370 nm and LED 480 nm) have been used as excitation sources depending on the substance under investigation. Proper filters (long pass and interference) have been used for excitation as well as for emission light path to minimize residual excitation light. The dilute LUDOX suspension is used as scattering reference to record the response of the instrument (called instrument response function, *IRF*). All fluorescence measurements (steady state and time resolved) have been performed at 298 K using an external temperature control unit.

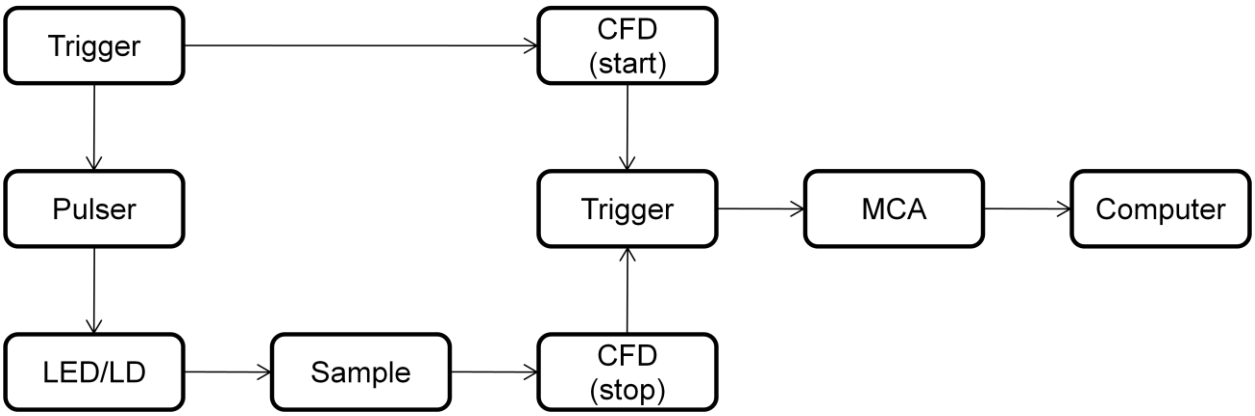

Figure 3-1: Schematic diagram for time TCSPC

3.3.3 Cyclic voltammetry

The cyclic voltammetry measurements are performed using Autolab potentiostat (PGSTAT12/30/302) controlled by software *Gpes version 4.9.007*. Platinum was used as both working and counter electrodes. The reference electrode was Ag/AgCl. The Ag/AgCl electrode was prepared by electrochemical coating of AgCl on the surface of Ag wire by dipping it in 1 N HCl solution and a voltage of 9 V was passed through the solution for half an hour in the dark. The Ag^{+1} ions combine with cloride ions as fast as they were formed at the silver surface The grey layer of AgCl was deposited on the surface of Ag wire (served as reference electrode). The setup for the cyclic voltammetry is shown in Figure 3-2.

3.3.4 ESR spectroscopy

Measurements on the ESR spectra were done using a Bruker ELEXSYS E-500 series spectrometer at 9,5 GHz with 100 kHz field modulation. Temperature was controlled with a Bruker variable temperature controller (ER4131VT) and was kept stable within 0.2 K. All ESR spectra were recorded at 295.5 K temperature. The simulation of ESR spectra, to estimate the hyperfine coupling constants, were made with program *EPR-WINSIM* version 0.98 form NIEHS, USA.

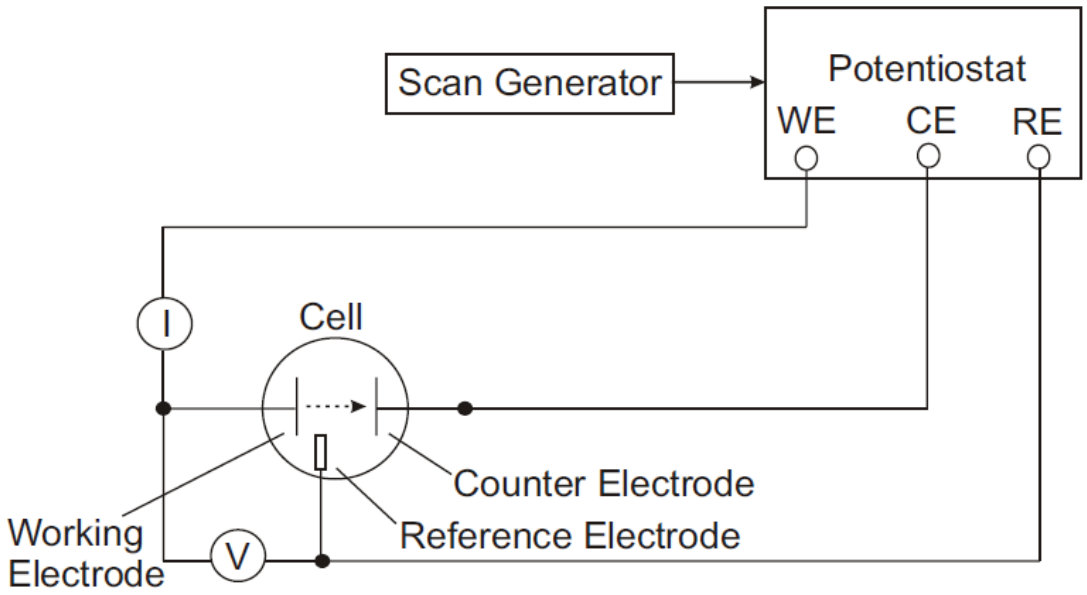

Figure 3-2: Schematic setup for cyclic voltammetry.

3.4 Sample Preparation and measurements

3.4.1 Photophysical Study

The absorption and fluorescence spectra have been recorded using 10 mm quartz cuvette sealed with septum. The concentration of the solution was such that the absorption at the excitation wavelength should not exceed 0.1 at and beyond the excitation wavelength in order to minimize the inner filter effect [168] and reabsorption effect [169]. Each sample is purged with argon for about 15 minutes before each measurement[17]. The measurements were performed in the following sequence; sample in the cuvette → degassing with argon or A blank measurement (solvent only) has also been recorded for both absorption and

[17] The absorption should be taken after degassing because the degassing process may lead to the evaporation of the solvent, hence result in the change in the concentration of solution in the cuvette so the absorption intensity. This contributes error in the quantum yield measurements.

fluorescence spectrum under the similar conditions[18]. The subtractions of sample spectra from the blank lead to the absorption/fluorescence intensity of the substance in that particular solvent. The absorption spectra have been recorded with 1 nm slit width and recorded with "medium" scan speed. The fluorescence spectra have been recorded with the excitation and emission slit width as 2 nm and the scan was started 10 nm after the excitation wavelength till the intensity was again equal to the baseline.

3.4.2 Electrochemical Study

0.1 M solutions of the supporting electrolyte (tetrabutylammonium hexafluorophosphate, $TBAPF_6$) have been prepared in a dry acetonitrile under argon. To a weighed amount of the compound under investigation, a certain volume of 0.1 M solution of $TBAPF_6$ has been added to achieve a concentration between 1 to 5 mM of the compound under investigation (cyano-substituted PPDs or TMPPDs derivative in the present case). Cyclic voltammetry measurements for different cyano-substituted PPDs and TMPPDs has been performed using a sample cell (as shown in Figure 3-3) and 1.6 to 2 mL of solution volume was enough to perform cyclic voltammetry measurements. After transferring the 1.8 mL solution of known concentration, argon gas was bubbled through it for 10-15 minutes to remove dissolved oxygen before starting measurements[19].

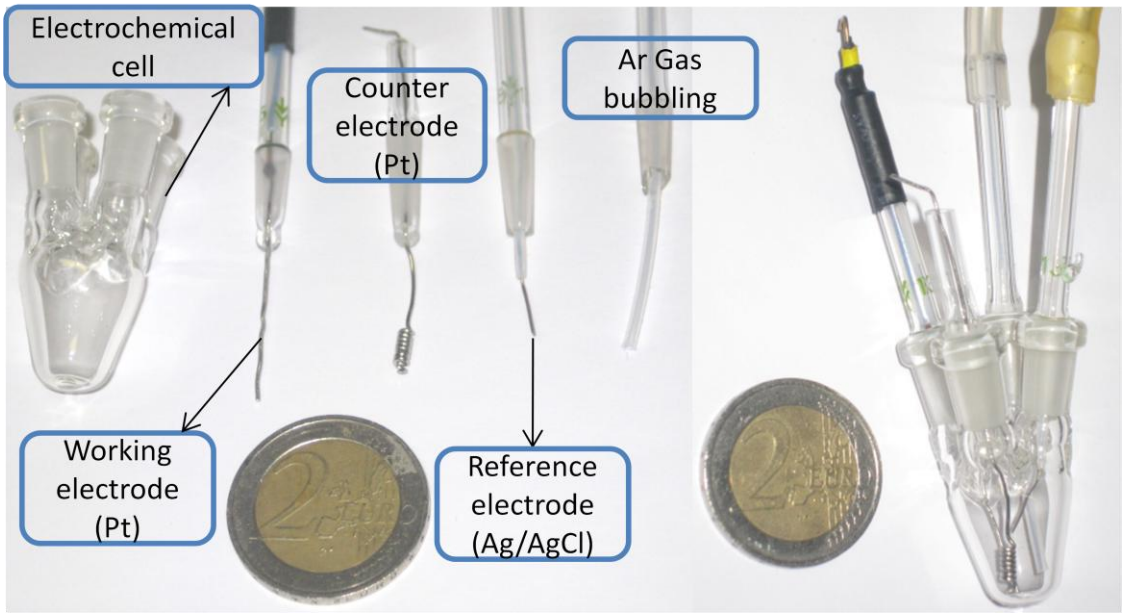

Figure 3-3: Electrochemical cell along with working, reference and counter electrodes.

[18] This is also an additional check to see the purity of solvent in which the photophysical properties are studied.
[19] The flow of argon should be kept slow so that the evaporation of solution during the gas bubbling is negligible.

For reversible systems, the same sample has been used to measure voltammogram at various scan rates (usually 50 to 500 mVs^{-1}). But in case of irreversible system, fresh solution has been used to measure voltammogram for each scan rate (the solution in the cell was used for single scan).

3.4.3 ESR spectroscopy

Acetonitrile was degassed (to remove any dissolve oxygen) by bubbling argon through it for 15 minutes before preparation of solution. $5x10^{-4}$ M solution of nitrosyl perchlorate was prepared and this solution was added in a weighed amount of MCTMPPD or DCTMPPD to get the desired concentration. A very small amoun (about 0.5 ml) was taken to a thin capillary under nitrogen, degassed by freeze-pump-thaw cycles for 4 times to remove molecular oxygen and finally sealed under vacuum. The sealed sample was inserted into 5mm NMR-tube for the ESR measurement.

3.5 Data Treatment

The photophysical properties, such as absorption and fluorescence maxima, Stokes shift, E_{00}, fluorescence quantum yield, fluorescence lifetime and rate constants for both radiative and non-radiative processes have been determined in several solvents. The molar extinction coefficients (ε) were determined by using Lambert-Beer's law. The equation used to calculate these photophysical properties were discussed in chapter 2 (section 2.3).

3.5.1 Absorption and fluorescence spectra

For extracting the absorption and fluorescence maxima, the spectra obtained from the absorption spectrophotometer and fluorimeter were treated (in order to obtain the transition dipole moment representation) in the following ways as [170]:

First fluorescence spectra were corrected by using a wavelength dependent correction factor, which accounts mainly for the wavelength dependence of spectrometer's detector and its light path[20].

Secondly absorption and emission spectra were converted from wavelength scale to the wavenumber scales. For the quantum yield is given as:

[20] Fery-Forgues *et al.* has shown that the quantum yield obtained by integrating the uncorrected emission spectra is 6% lower that obtained from the corrected one.

171. Fery-Forgues, S. and D. Lavabre, *Are Fluorescence Quantum Yields So Tricky to Measure? A Demonstration Using Familiar Stationery Products.* J. Chem. Educ., 1999. **76**(9): p. 1260-1264.

$$\phi = \int_0^\infty I_\lambda(\lambda)d\lambda = \int_\infty^0 I_{\tilde{\nu}}(\tilde{\nu})d\tilde{\nu} \qquad 3\text{-}1$$

where $d\lambda = -\lambda^2 d\tilde{\nu}$ because $\lambda = 1/\tilde{\nu}$

$I_\lambda(\lambda)$ and $I_{\tilde{\nu}}(\tilde{\nu})$ are the fluorescence intensities depends on wavelength and wavenumber, respectively.

Therefore for emission spectra

$$I_\lambda(\lambda).\lambda^2 = I_{\tilde{\nu}}(\tilde{\nu}) \quad \text{or} \quad \frac{I_\lambda(\lambda)}{\tilde{\nu}^2} = I_{\tilde{\nu}}(\tilde{\nu}) \qquad 3\text{-}2$$

and for absorption spectra the molar extinction coefficient is defined as logarithm of a ratio of intensities one gets for the absorption spectra so $\varepsilon(\lambda) = \varepsilon(\tilde{\nu})$.

Thirdly the transition dipole moments ($\vec{M}_{1a\to 2b}$ for absorption and $\vec{M}_{2b\to 1a}$ for emission) are related with absorption and fluorescence intensities as shown below [172]:

$$\left|\vec{M}_{2b\to 1a}\right|^2 \propto \tilde{\nu}^{-3} I_{\tilde{\nu}}(\tilde{\nu}) \qquad 3\text{-}3$$

$$\left|\vec{M}_{1a\to 2b}\right|^2 \propto \tilde{\nu}^{-1} \varepsilon(\tilde{\nu}) \qquad 3\text{-}4$$

The so called transition dipole moment refers to $\tilde{\nu}^{-1}\varepsilon(\tilde{\nu})$ and $\tilde{\nu}^{-3} I_{\tilde{\nu}}(\tilde{\nu})$ {or $\tilde{\nu}^{-1}\varepsilon(\lambda)$ and $\tilde{\nu}^{-5} I_\lambda(\lambda)$ } for absorption and emission, respectively.

3.5.2 Fluorescence quantum yield

Fluorescence quantum yields have been measured using different quantum counters like, quinine sulfate solution in 0.5M H_2SO_4 (Φ =0.53) [173], coumarin 6 in ethanol (Φ =0.78) [174] and rhodamine 6G in ethanol (Φ =0.95) [175]. The absorption intensities of sample as well as quantum reference have not increased more than 0.15 (usually less that 0.1). Fluorescence quantum yields are commonly reported with 10 % error in it [171]. The quantum yields were measured using the equation [172].

$$\Phi_{samp} = \frac{I_{samp}(1-10^{-OD_{ref}})}{I_{ref}(1-10^{-OD_{samp}})}\left(\frac{n_{samp}}{n_{ref}}\right)^2 \Phi_{ref} \qquad 3\text{-}5$$

where Φ represents fluorescence quantum yield, OD represents the optical density at the excitation wavelength, I_x is the intensity calculated from the integrated corrected emission spectrum, n_x is refractive index of corresponding solvent at 25 ^oC, the subscripts 'samp' and 'ref' refer to the sample and quantum reference, respectively.

3.5.3 Linear Solvation Energy Relationship

The multiple parameter regression analysis has been performed by MATLAB program using the absorption and fluorescence maxima obtained as described in section 3.5.1.[21] The MATLAB program is written on the mathematical basis for solving *m* number of equation for *n* variables (for the case when m > n).

3.5.4 Cyclic voltammetry

Area of the working electrode was calculated by measuring the peak current (i_p) for the solution of known concentration (C) of ferrocene for various scan rates (v) at room temperature (25 ^{o}C). The reported value for diffusion coefficient (D) for ferrocene (2.3×10^{-5} cm^2 s^{-1}) [176-179] has been used. The use of the Randles-Sevcik equation allows us to calculate the effective area of the working electrode which was difficult to measure directly otherwise. The Randles-Sevcik equation can be written as:

$$i_p = (2.69\times10^5)n^{3/2}ACD^{1/2}v^{1/2} \qquad 3\text{-}6$$

where A is expressed in cm^2, D in cm^{2}s^{-1}, C in molcm^{-3}, v in Vs^{-1} and measurements were performed at room temperature (25 ^{o}C). The slope of the plot between peak current (I_p) versus square root of the scan rate ($v^{1/2}$) is equal to the effective area of the working electrode. The volume of the solution taken in the electrochemical cell should be same for all the measurements so that area of the working electrode dipped in the solution remain the same. Figure 3-4 shows the anodic and cathodic peak potential (E_{pa} and $E_{pc,}$ respectively) along with their corresponding peak currents (I_{pa} and I_{pc}).

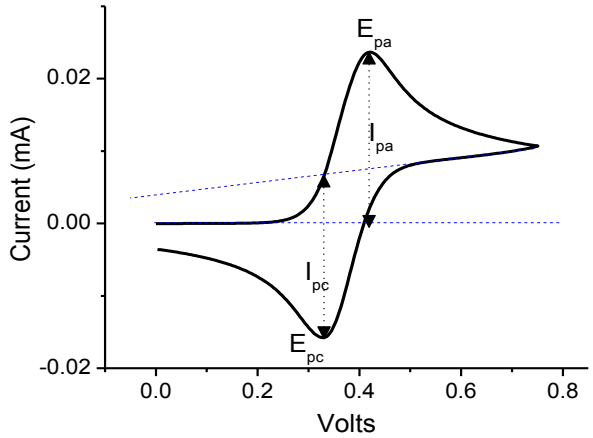

Figure 3-4: Cyclic voltammogram of ferrocene in MeCN with 0.1M TBAPF$_6$ versus Ag/AgCl.

[21] Thanks to A. Rospeintner for MATLAB program for calculating absorption and fluorescence maxima and also for LSER analysis.

4 SYNTHESIS AND STRUCTURAL CHARACTERIZATION

An overview of the synthesis of some novel cyano-substituted aromatic compounds as well as new synthetic strategies for some already synthesized cyano-substituted aromatic compounds have been given in this chapter. Various principal techniques and methods for synthesis of nitrile (cyano-substituted compounds) has been reported by D. T. Mowry [180]. Different possible synthetic routes have been adopted based on the starting material. The final product has been structurally characterized using UV-VIS, IR, NMR-spectroscopy and sometimes mass spectrometry.

4.1 Compounds of interest

Cyano-substituted derivatives of p-phenylenediamine (PPD) and N,N,N',N'-tetramethyl-p-phenylenediamine (TMPPD) are the main target. Our group already have published very interesting photophysical properties of two cyano-substituted PPDs (2,6-dicyano-N,N,N',N'-tetramethyl-p-phenylenediamine (26DCTMPPD) and 2,3,5,6-tetracyano-p-phenylendiamine (TCPPD)) [30-31]. Cyano substitutions result in dramatic changes of the photophysical properties of the parent PPD and TMPPD.

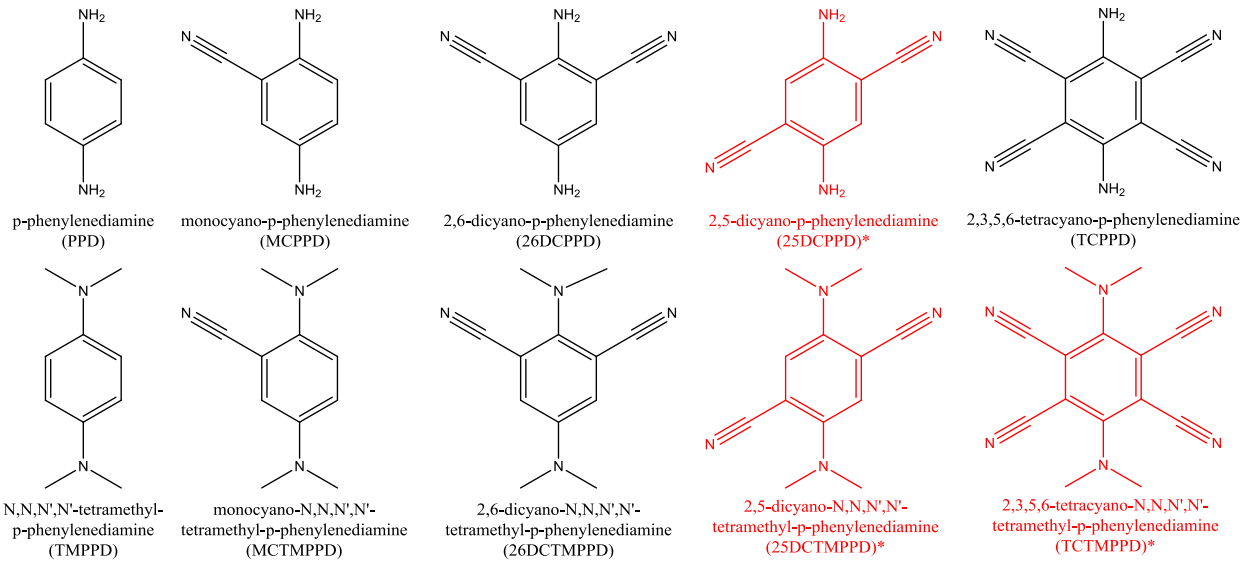

Scheme 4-1: Compounds of interest.
*The synthesis of these compounds has not been successful.

New cyano-substituted derivatives of PPD and TMPPD have been synthesized in order to study the chemistry involved underneath such dramatic change in photophysical behaviour in more detail. The compounds whose photophysical properties are interesting are shown in

Scheme 2-1. PPD and TMPPD have been widely studied for their electrochemical and spectrochemical properties [7-8, 12, 14-15, 20, 181-188] and are commercially available. Some other cyano-substituted aromatic compounds like 2,3,5,6-tetracyano-1,4-hydroquinone (TCHQ) and 2,3,5,6-tetracyano-1,4-benzoquinone (cyanil) have also been synthesized . Photophysical properties of TCHQ have been studied in the next chapter whereas cyanil is of high interest because of its high redox potential [44] and has been used to study the photoinduced electron transfer [50]. The syntheses of some of these compounds (like TCPPD [163, 165] and cyanil [44]) have already been reported in literature with very less product yield. In order to obtain higher product yield of TCPPD some other synthetic routes have been performed.

4.2 Reagent used

Reagent used in synthesis are following (given with purity and supplier):
2-amino-5-nitrobenzonitrile (95%, Alfa Aesar); 2,5-dichloro-p-phenylendiamine (98%, Aldrich); 1,4-dicyanobenzene (98%, Aldrich), 2,5-dimethyl-p-phenylendiamine (96%, ABCR); 2,6-dibromo-4-nitroaniline (98%, Aldrich); 2,6-diiodo-4-nitroaniline (98%, Aldrich); 5-nitroisophthalic acid (98%, Alfa Aesar); 1,2,4,5-tetracyanobenzene; p-phenylenediamine; tetracyanoethylene (97%, Fluka); malononitrile (99%, Aldrich); bromine (99%, Fluka); potassium bromide (99%, Fluka); merceptoacetic acid; 1,2,4,5-tetramethylbenzene (99% Merck); 1,2,4,5-tetrabromo-p-benzoquinone (98% Alfa Aesar); 2,3-dichloro-4,5dicyano-p-benzoquinone (97%, Fluka); sodium cyanide (99%, Fluka); morpholine (99% RdH); pyrene (99%, Fluka); acetic acid (100%, ROTH); cuprous cyanide (99%, Fluka); stannous chloride dehydrate (98% RdH); nitronium tetrafluoroborate (NO_2BF_4, (96%, Fluka)); trifluoromethanesulfonic acid (triflic acid/TfOH, 99%, Fluka); trifluoroacetic anhydride (99%, Merck); fuming nitric acid (100% HNO_3); sulphuric acid (95% Merck), hydrochloric acid (37%, Merck); isoamyl nitrite (97%, ABCR); copper sulphate (99% RdH); Sodium nitrite (98%, Fluka); chromium trioxide (99%, Merck); dimethylsulphate (97%, Fluka); calcium carbonate (99% Merck), ; methyl iodide (99%, Fluka); trimethyl phosphate (99%, Fluka); acetic acid anhydride (99%, Merck); formaldehyde (36.5%, Fluka); formic acid (98%, Merck): P_2O_5 (100%, Fluka), diethylene glycol (99%, ROTH), hydroxylammoniumchloride (98%, Merck), $NaHCO_3$ (99.7%, Riedel-de Haen), $MgSO_4$ (99%, Aldrich) and NH_3 soln. (33%, ROTH), Citric acid (99.5 %, Roth) and Na_2HPO_4 (puris p.a., Fluka) were used as received. $SOCl_2$ (99%, Fluka) was distilled

just before use. Solvents used were of spectroscopic grade (where necessary dried and distilled before using).

4.3 Synthesis of cyano-substituted PPDs

Cyano-substituted PPDs that have been tried to synthesize include monocyano-p-phenylenediamine (MCPPD); 2,5-dicyano-p-phenylenediamine (25DCPPD); 2,6-dicyano-p-phenylenediamine (26DCPPD) and 2,3,5,6-tetracyano-p-phenylendiamine (TCPPD).

4.3.1 Synthesis of monocyano-p-phenylendiamine (MCPPD)

From 2-amino-5-nitrobenzonitrile:

MCPPD has been synthesized by the reduction of 2-amino-5-nitrobenzonitrile using stannous chloride dihydrate ($SnCl_2.2H_2O$) and hydrochloric acid (HCl). The reaction is shown in Scheme 4-2.

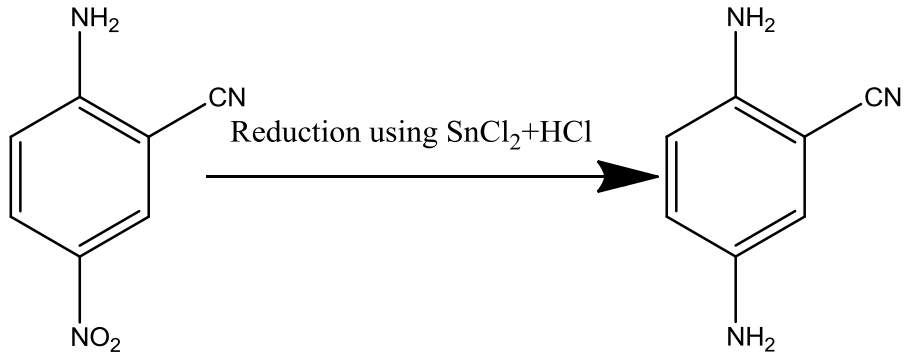

Scheme 4-2: Synthesis of monocyano-p-phenylenediamine (MCPPD)

2 g of 2-amino-5-nitrobenzonitrile has been added slowly portionwise in a solution of 8 g $SnCl_2.2H_2O$ in 15 mL concentrated HCl. During the addition the temperature of the mixture is increased which is lowered by water cooling to about 35 ^oC. After the addition, the mixture is stirred for 10 hrs at room temperature. The colour of the mixture is turned from yellow to offwhite. The precipitates formed are filtered and add to it 50% (w/v) solution of NaOH until the mixture is strongly basic. The MCPPD has been extracted from the mixture using ethyl acetate. The extract is washed with water and dried over $MgSO_4$. Removal of ethyl acetate through rotary evaporator leads to 1.25 g (51 % yield) MCPPC which has been further purified by recrystallization with benzene and also by sublimation. m.p. 89 ^oC. IR (KBr disk) ν/cm^{-1}; 3399 (NH_2), 3222 (NH_2), 3215 (mixed NH_2), 2212 (CN), 1642 (C=C), 1499 (C=C), 1312 (Ar-(NH_2). ^1H NMR (200 MH_z, ^{d6}DMSO) δ/ppm; 6.8 (3H, arom. CH), 4.32 (2H, broad, NH_2), 3.85 (2H, broad, NH_2).

4.3.2 Synthesis of 2,5-dicyano-p-phenylendiamine (25DCPPD)

2,5-dicyano-p-phenylendiamine (25DCPPD) has been tried to synthesize using various starting materials like aryl halide 2,5-dichloro-p-phenylendiamine (25DClPPD), 1,4-dicyanobenzene (DCB) and 2,5-dimethyl-p-phenylendiamine.

Rosenmund–von Braun reaction:

A well known method for the synthesis of aryl nitrile from aryl halide is cyano dehalogenation reaction commonly known as Rosenmund–von Braun reaction [189-190]. According to Rosenmund–von Braun reaction, aryl halides (Ar-X) can be converted into corresponding aryl nitrile using cuprous cyanide (CuCN) in the presence of some polar solvent (shown in Scheme 4-3). Synthesis of aromatic nitriles from corresponding aromatic halides have been has been reviewed by Ellis and Romney-Alexander [191]. Alkali metal cyanides like NaCN and KCN do not react with Ar-X in polar solvent in the same way as CuCN reacts but they do react in the presence of catalyst like nickel, cobalt or palladium complexes [192-195].

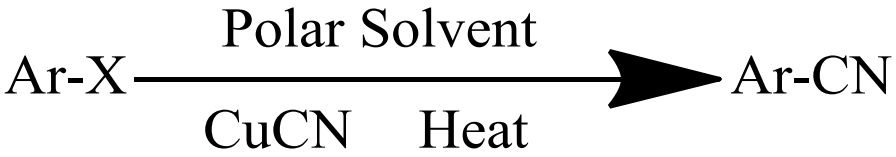

Scheme 4-3: Rosenmund–von Braun reaction.

General Procedure: Aryl halide (2 mmol) is dissolved in about 10 mL of polar solvent. To this solution add portion wise CuCN (> 4 mmol) and heat this mixture to for several hours (vary for 6 hrs to 48 hrs) under Ar. After heating the product formed is separated by two different ways **(a)** to the hot reaction mixture add NH_3/H_2O (30:70) mixture and stir it or further 30 minutes, unreacted CuCN is dissolved in NH_3/H_2O mixture and precipitates formed are filtered off and dried in open air; **(b)** the excess of solvent is removed by rotary evaporator and the product form is extracted by acetone and/or dichloromethane. The final products are analysed using TLC (showing different component) and IR spectroscopy (for the peak around 2200 cm^{-1} which is characteristic for Ar-CN).

From 2,5-dichloro-p-phenylendiamine (25DClPPD):

2,5-dichloro-p-phenylendiamine has been treated for cyano-dehalogenation as reported in Rosenmund–von Braun reaction. The general scheme for the reaction is shown in Scheme

4-4. Different polar solvents like DMF, DMSO, HMPA and NMP have been used [191]. The brief overview for different reactions used to synthesize 25DCPPD is given below.

First reaction has been performed in DMF with mole ratio for of 25DClPPD and CuCN as 1:4, respectively. 2 g (11.30 mmol) of 25DClPPD and 4 g (45 mmol) of CuCN are dissolved in 40 mL of DMF and reflux the reaction mixture for 15 hrs under Ar. The reaction mixture is allowed to cool down to room temperature and cold aqueous ammonia solution (30:70 of ammonia and water respectively) has been added. The reaction content has been stirred vigorously for one hour. The resulting suspension has been filtered through suction and wash thoroughly with ammonia water mixture until no more formation of blue colour. After drying, the crude product is extracted with acetone and latter with CH_2Cl_2. Removal of solvent yields 0.370 g of brown product. The TLC has shown that this the mixture of 4-5 products and IR spectra of this brown product have shown a very small peak in the at 2218 cm^{-1}. The brown product has been tried to separate by column chromatography using 2:3 ethyl acetate and hexane but no successful results have been obtained. Different isolation techniques for the reaction work up as reported by Friedman and Shechter [196] have not been successful. Another reaction is run is the same way as reported above but now instead of adding ammonia water mixture, the solvent (DMF) is removed by rotary evaporator and the solid residue is digested with acetone. Removal of acetone yields the brown solid which has the same component in TLC as obtained after using ammonia/water mixture.

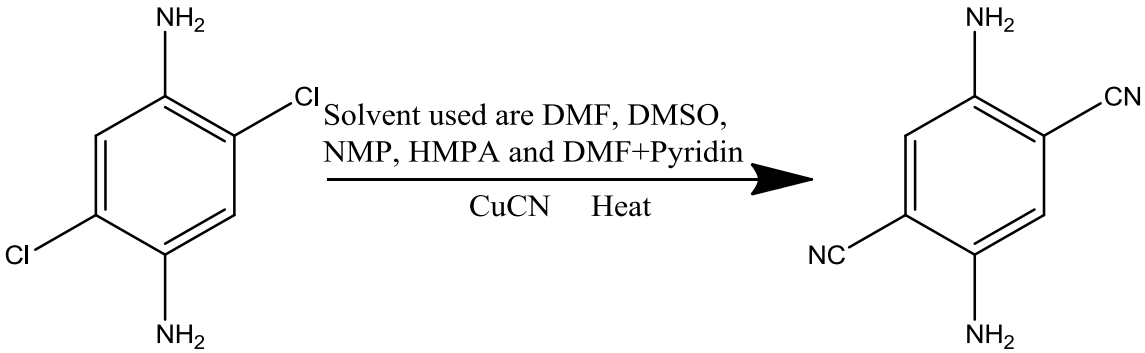

Scheme 4-4: Synthesis of 25DCPPD by the cyano-dehalogenation of 25DClPPD.

Another reaction has been performed as reported by Vagin and co-workers[197]. In place of DMF as solvent, a 60:40 mixture of DMF and pyridine has been used. Other polar solvents that have been applied in the same way as reported above include N-methylpyrolidone (NMP) [198-199], dimethylsolfoxide (DMSO) [200] and hexamethylphsphortriamide (HMPA) [201]. None of the reaction in the above reaction gives the desired 25DCPPD. Both

the increase in amount of CuCN and the reaction time up to 48 hours does not give any fruitful results.

From 1,4-dicyanobenzene:

25DCPPD has also been tried to synthesize using 1,4-dicyanobenzene (DCNB) as starting material. Nitration of DCNB has been tried using different nitration agents like Nitronium tetrafluoroborate (NO_2BF4), Trifluoroacetic anhydride ($(CF_3COO)_2O$) and (CF_3HSO_3).

Nitronium tetrafluoroborate (NO_2BF_4) [202-203]: The reaction is performed in the same way as reported by Olah and Kuhn for the nitration of o-tolunitrile. To a solution of 0.57 g of nitronium tetrafluoroborate in 15 mL of sulfolane, 0.5 g of DCNB has been added in small portions. The reaction mixture is kept under argon during the entire reaction time. The temperature of reaction mixture is increased and is maintained at 120 ^oC for 2 hr. To check the reaction progress 1 mL of the reaction mixture is taken out and add to it excess of water. The precipitates are formed, filtered and dried. The UV-VIS spectrum is identical to that of DCNB. Keep the reaction mixture overnight under Ar at room temperature. Next day 1 mL of reaction sample is taken out and adds to it 15-20 mL of water. The formed precipitates are filtered and dried. Again there is no change in the DCNB as seen by the UV-VIS spectrum.

Trifluoroacetic anhydride ($(CF_3COO)_2O$) [204]: 3.5 mL (17.5 m mole) of trifluoroacetic anhydride is added in 1.1 mL (17.5 mmol) of 100 % nitric acid in a schlenk tube which is dipped in ice water. 2.24 g (17.5 mmol) of DCNB is added and stir continuously at room temperature. In order to check the reaction progress the sample of reaction mixture is take after 3 hrs and pour on ice. The product is separated and dried. The analysis of UV-VIS and IR shows that the product is exactly similar as the starting DCNB. The reaction samples after 23 hr and 46 hr are taken and are analyzed. The melting point, UV-VIS and IR spectra are the same as starting material after 46 hrs which indicate that no reaction is taken place.

Trifluoromethansulfonic acid (CF_3HSO_3) [205]: 4.8 g (32 mmole) of trifluormethansulfoonic acid (CF_3HSO_3) is added in 60 mL of CH_2Cl_2 at room temperature under Ar. To this solution add 1 mL of 100% nitric acid. The reaction mixture is cooled to ~0 ^oC and stirred. White precipitates are formed in the reaction vessel. Then 0.64 g (5 mmole) of DCNB has been added and stirred it for 1.5 hrs at 0-5 ^oC. Take 10 mL of sample of reaction mixture and add to it 15 mL ice cold water. The precipitated formed are extracted with CH_2Cl_2. Removal of solvent give white solid (named as *A*). Remove the ice bath and stirred the reaction mixture for 2.5 hr at room temperature. Again take 10 mL sample and the product obtained after adding water and CH_2Cl_2 extraction is named as *B.* After refluxing the reaction mixture for

20 minutes, another 5 mL sample is taken and processed as mentioned before and named it as *C*. The UV-VIS spectra of all three products *A, B* and *C* are the same as that of DCNB indicating that no nitration of DCNB has been occurred.

The UV-VIS and IR spectra of all the above nitration reaction products are similar to that of DCNB. This shows that nitration of DCNB using the above nitration agents is not a favorable.

From 2,5-dimethyl-p-phenylendiamine:

25DCPPD has also been tried to synthesize using 2,5-dimethyl-p-phenylendiamine (25DMPPD) as starting material. The 25DMPPD has been converted into 2,5-dimethyl-1,4-dinitrobenzene using isoamyl nitrite in acetic acid as reported by Arya and Jebaratnam [206]. The two methyl groups (-CH_3) have been converted into the carboxylic acid groups (-COOH) by oxidation with chromium trioxide as was done by Staab and Haffner [207]. 2,5-dicarboxylic-1,4-dinitrobenzene can be further converted into 25DCPPD by the reaction with $SOCl_2$ (convert –COOH into -COOCl), then with ammonia solution (convert acid chloride into amide). The amide group can be dehydrated to corresponding cyanide group using P_4O_{10} and finally reduction will give us the required 25DCPPD[22].

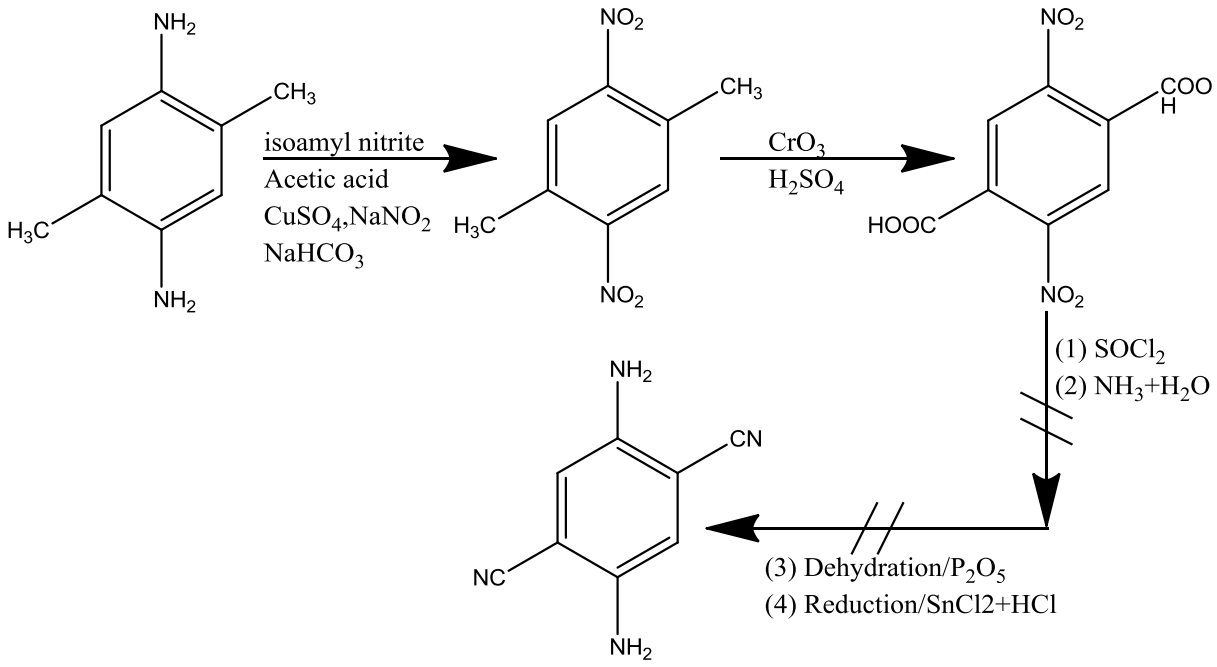

Scheme 4-5: Synthesis of 25DCPPD using 2,5-dimethyl as starting material.

[22] 2,5-dicarboxylic-1,4-dinitrobenzene has been synthesized but further conversion to 25DCPPD has not been performed. But the above reported synthesis is believed to work as the same has been accomplished in the synthesis of 26DCPPD (see section 4.3.3 synthesis 25DCPPD from 5-nitroisophthalic acid)

4.3.3 Synthesis of 2,6-dicyano-p-phenylendiamine (26DCPPD)

From 2,6-dihalo-4-nitroaniline:

Attempts have been made to synthesized 26DCPPD using Rosenmund–von Braun reaction. The starting material used are 2,6-dibromo-4-nitroaniline or 2,6-diiodo-4-nitroaniline. Two reactions (reduction and cyanation) are required to get the final 26DCPPD. Two different approaches have been tried as shown in
Scheme 4-6. In one approach, the dihalo-4-nitroaniline first undergo cyanation and then reduction whereas in the 2nd approach the reduction is the first reaction and then undergo cyanation. The reduction is performed using $SnCl_2.2H_2O$ in HCl as reducing agent (details for this reaction can be seen in section 4.3.1). Substitution of halogen groups is done by following the Rosenmund–von Braun reaction (for details see section 4.3.2). The progress of cyanation reaction is monitored by TLC and also analysed by HPLC. The cyanation reaction does not give a single product but a mixture of products (4 to 6 spots on TLC) and also the yields of the cyanation reactions are low specially in case of cyanation of dihalo substitute PPD (crude mixture yield is less than 10 % by weight) but the IR spectra of the crude product has peak in the range of 2200 to 2250 cm^{-1} (characteristic for aromatic nitriles). Different possible ways to separate the products have been tried but were not successful. Different attempts (such as long reaction time and high mole ratio of CuCN) have been made to improve the reaction yield but were not successful.

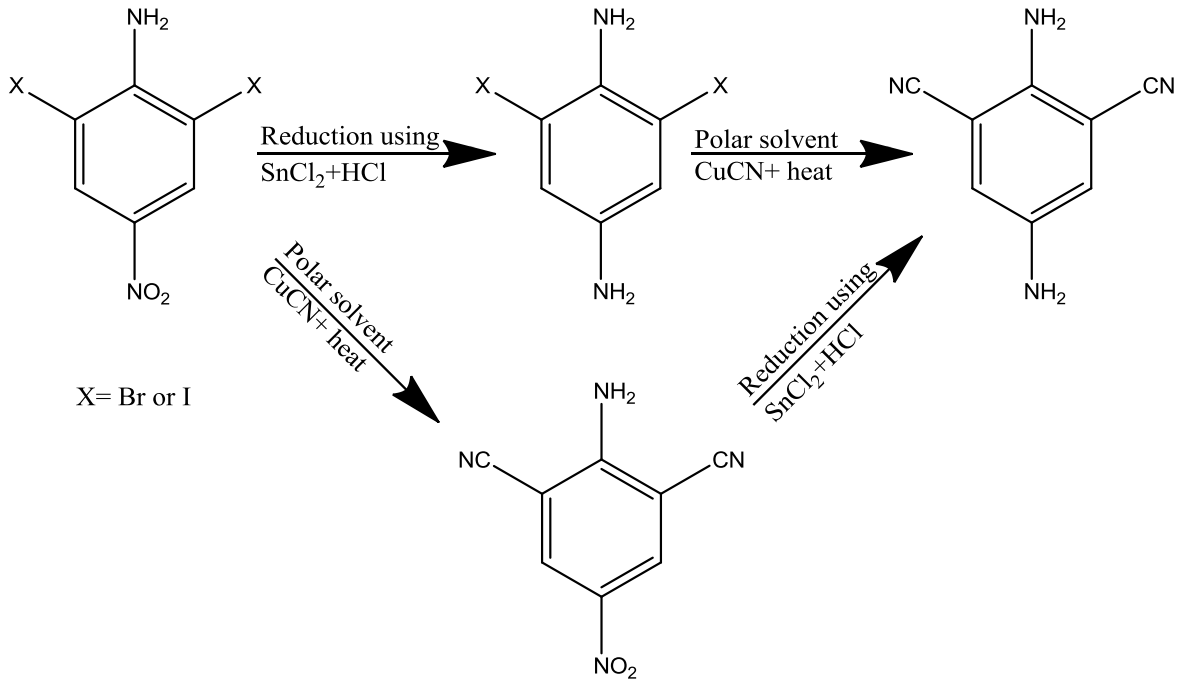

Scheme 4-6: Synthesis of 26DCPPD using 2,6-dihalo-4-nitroaniline as starting material.

From 5-nitroisophthalic acid:

2,6-dicyano-*p*-phenylenediamine (26DCPPD) is synthesized using 5-nitroisophthalic acid as starting material. The carboxylic (-COOH) groups in nitroisophthalic acid are first converted into acid chloride (-COCl), then acid amide ($-CONH_2$), which upon dehydration gives dicyano-nitrobenzene. The amination followed by reduction of dicyano-nitrobenzene gives the desired 26DCPPD. The systematic layout for the synthesis of 26DCPPD starting from 5-nitroisophthalic acid is shown in Scheme 4-7.

Synthesis of 5-nitroisophthalyl chloride:

5-Nitroisophthaloyl Chloride was synthesized using 5-nitroisophthalic acid as starting material. 10 g of 5-nitroisophthalic acid (47.4 mmol) were refluxed with 30 mL of freshly distilled thionyl chloride, $SOCl_2$, until a clear solution was obtained (20 hrs). The solution was filtered to remove undissolved residues. Unreacted $SOCl_2$ was removed by the rotary evaporator, yielding 10.46 g (42.4 mmol; 89%) of 5-nitroisophthaloyl chloride (m.p. 68^{o}C; lit.[208] 66-68 ^{o}C).

Synthesis of 5-nitroisophthalamide:

8.5 g of 5-nitroisophthaloyl chloride (34.4 mmol) were added portion wise with continuous stirring in 50 mL cold solution of (1:1) H_2O and 33% NH_3 aq. soln. This reaction mixture was stirred for 2 hrs. The reaction was exothermic and white precipitates were formed immediately after the addition of NH_3 soln. This turbid mixture was stirred for half an hour to ensure the completion of the reaction. The mixture was then filtered, washed with excess of water and dried at 110°C yielding 7.1 g (33.6 mmol, 98%) of 5-nitroisophthalamide, (m.p. 314-315 ^{o}C; lit.[208] above 300 ^{o}C).

Synthesis of 1,3-dicyano-5-nitrobenzene:

4 g of diamide (2), 19.1 mmol, was very well grinded and mixed thoroughly with 10.5 g of P_2O_5 under Ar to avoid any contact with moisture. To this mixture, 35 mL of *p*-xylene were added. The reaction mixture was refluxed for 9 hrs under Ar and filtered hot. 10 additional mL of *p*-xylene were added to the residue and refluxed again to extract the product formed and filtered. The filtrate was concentrated and 2.43 g (14 mmol; 73%) white crystals of 1,3-dicyano-5-nitrobenzene were formed and recrystallized from *p*-xylene. (m.p. 205 ^{o}C;

lit.[209] 203.5-205.5 ^{o}C). IR (KBr disk) ν/cm^{-1}; 2243 (CN), 1544(NO_2), 1356 (NO_2). ^{13}C NMR (DMSO-d_6) δ/ppm; 114.3 (C_1, C_3), 115.9 (2CN), 132.0 (C_4, C_6), 142.2 (C_2), 148.3 (C_5)

Synthesis of 2,6-dicyano-4-nitroaniline:

3 g of 1,3-dicyano-5-nitrobenzene (3), 17.3 mmol, was dissolved in 54 mL of diethylene glycol by heating at 120 ^{o}C. This mixture was rapidly cooled to room temperature by cooling with ice resulting in some turbidity. 1.3 g of finely grinded hydroxyl ammonium chloride and a solution of 3.4 g KOH in 16 mL methanol were added successively under continuous stirring. The color of the mixture changed to red and the mixture was further stirred for 2 hrs at room temperature. Then 250 mL of ice water were added and allowed to stand for overnight forming very fine brown precipitates. The brownish precipitate was filtrated using a fritted glass funnel, washed with water and dried. 2.45 g (13.0 mmol; 75%) of crude product (1,3-dicyano-5-nitrobenzene) were obtained and recrystallized from pyridine. (m.p. 310 ^{o}C; lit.[210] 310-311 ^{o}C). IR (KBr disk) ν/cm^{-1}; 3385 (NH_2), 3227 (NH_2), 2239 (CN), 1662 (C=C),1591(Ar-(NH_2),1507 (NO_2), 1491 (C=C), 1334 (NO_2), 1320 (Ar-NH_2). ^{13}C NMR (DMSO-d_6) δ/ppm; 96.3 (C_2, C_6), 114.9 (2CN), 135.0 (C_3, C_5), 135.8 (C_4), 155.5 (C_1).

Synthesis of 2,6-dicyano-*p*-phenylenediamine:

3 g of $SnCl_2.2H_2O$ were dissolved in 3 mL concentrated HCl and add to it a solution of 0.5 g (2.7 mmol) of 2,6-dicyano-4-nitroaniline (4), in 6 mL of absolute ethyl alcohol. The mixture was brought to 70 ^{o}C until the starting material is completely dissolved, kept at this temperature for 1.5 hrs, (color of the mixture changes to dark brown) and then cooled to room temperature and poured into 15 mL of ice. The pH of the mixture was made slightly basic by adding 5% $NaHCO_3$ aq. soln. and the reaction product was then extracted with 100 mL ethyl acetate in 25 mL portions. The organic phase was washed with brine, treated with charcoal to remove color impurities and dried over $MgSO_4$. 0.3 g (1.8 mmol; 67%) of the crude 2,6-dicyano-*p*-phenylenedimine were obtained after removal of the solvent and were recrystallized from methanol. m.p. 178^{o}C. IR (KBr disk) ν/cm^{-1}; 3389 (NH_2), 3352 (NH_2), 3195 (mixed NH_2), 2213 (CN), 1665 (C=C), 1575 (Ar-(NH_2), 1490 (C=C), 1312 (Ar-(NH_2). ^{1}H NMR (200 MH_z, CD_3CN) δ/ppm; 7.02 (2H, arom. CH), 4.12 (2H, broad, NH_2), 4.93 (2H, broad, NH_2). ^{13}C NMR (DMSO-d_6) δ/ppm; 99.4 (C_2, C_6), 116.4 (2CN), 123.9 (C_3, C_5), 142.1 (C_4), 144.7 (C_1). Mass (m/z); 158 (M^+, 100 %), 131 ([M-HCN]$^+$, 19%), 104 (M-2HCN]$^+$, 24%).

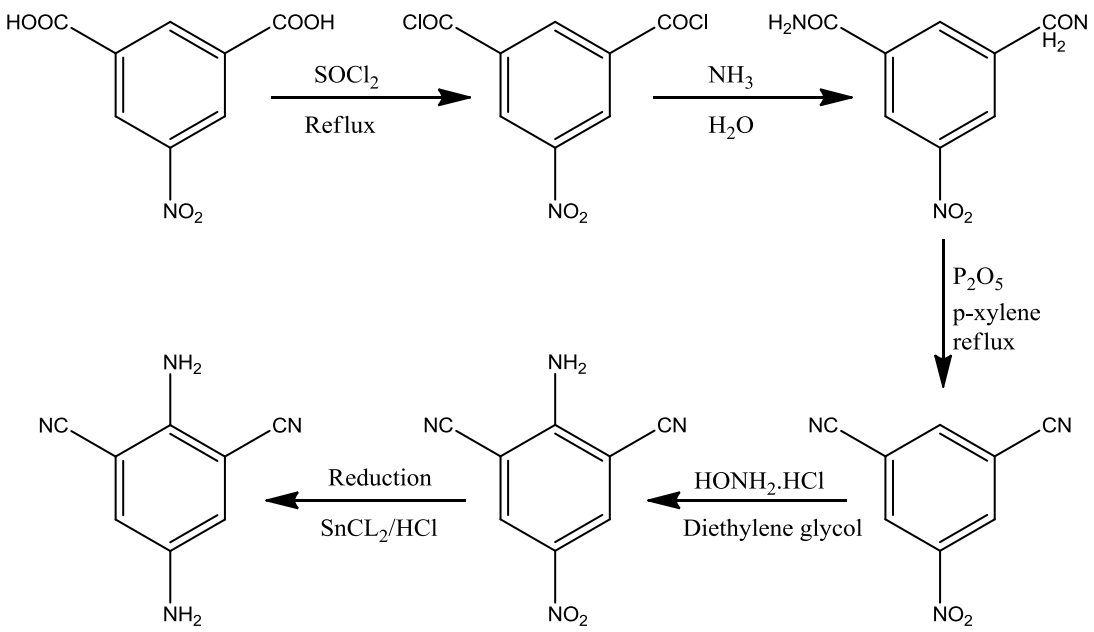

Scheme 4-7: Synthesis of 26DCPPD using 5-Nitro-isophthalic acid as starting material.

4.3.4 Synthesis of 2,3,5,6-tetracyano-p-phenylendiamine (TCPPD)

The synthesis of TCPPD have been reported in literature by Webster and co-workers in 1965 [165] with very low product yield (3.7 %). Different attempts in order to increase the reaction yield have been made by Jakob and maximum yield of 9 % is achieved by using sym-collidine [31, 163]. Different synthetic strategies have been adopted to synthesize TCPPD are given below.

From 1,2,4,5-tetracyanobenzene:

Attempts have been made to synthesize TCPPD from 1,2,4,5-tetracyanobenzene (TCNB). Nitration of TCNB has been tried using different nitration agent like *nitronium tetrafluoroborate* (NO_2BF_4) in sulfolane [202-203] , trifluoroacetic anhydride in 100 % nitric acid [204] and trifluoromethansulfonic acid in 100% Nitric acid [205]. None of these attempts are successful in synthesizing TCPPD. The reason might be the electron withdrawing effect of four cyano groups makes the aromatic ring highly electron deficient. So the substitution of electrophilic nitro group (NO_2^+) is not favored. The other possible option can be substitution of amino group ($-NH_2$) as reported for amination of many heterocyclic reaction (The Chichibabin reaction[23]) [211-214].

[23] The Chichibabin reaction is a method amination of pyridine derivatives by the reaction with sodium amide. It was reported by Aleksei Chichibabin in 1914.

From p-phenylenediamine:

Ottmann has synthesized 2,3,5,6-tetrachloro-p-phenylendiamine by chlorination of p-phenylenediamine (PPD) [215] and same approach has been used by Jakob [163] for the synthesis of 2,3,5,6-tetrabromo-p-phenylendiamine. PPD has been first converted into N,N'-disulfinyl-p-phenylenediamine by reaction with thionyl chloride. The reaction of N,N'-disulfinyl-p-phenylenediamine with Cl_2/Br_2 give N,N'-disulfinyl-2,3,5,6-tetrahalo-p-phenylendiamine which has been converted into 2,3,5,6-tetrahalo-p-phenylendiamine. In the present work we have used cyanogens gas $(CN)_2$ in place of Cl_2 or Br_2 as shown in Scheme 4-8.

Procedure:

5 g (46 mmol) of p-phenylenediamine has been added portion wise in 30 mL of thionyl chloride ($SOCl_2$) over a period of 15 minutes. The temperature of the reaction mixture is maintained at 50-55 ^oC during the addition of PPD and reaction mixture is continuously stirred for two hours at this temperature. The cyanogens gas is produced separately and passes through the reaction mixture for about 4 hrs.

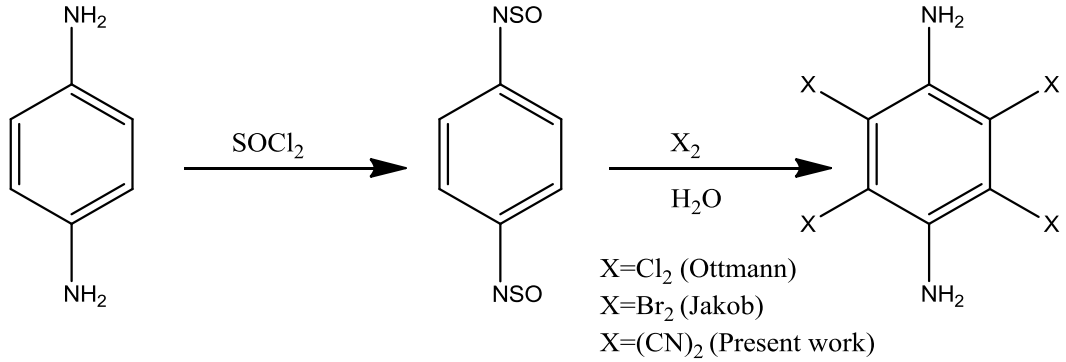

Scheme 4-8: Synthesis of tetrasubstituted-p-phenylenediamine.

Synthesis of cyanogen $(CN)_2$:

The cyanogens gas has been produced using NaCN and CuSO4.5H2O [216-217]. 300 g of copper sulphate ($CuSO_4.5H_2O$) has been taken in 4 neck bottle. The four outlets contain one thermometer to measure the temperature, inlet for the NaCN solution, outlet for $(CN)_2$ gas and one outlet for mechanical stirrer as shown in Figure 4-1. A solution of 120 g of NaCN in 250 mL is added in slowly in the in CuSO4.5H2O. The formation of cyanogen gas has been started as the temperature of the reaction mixture is increased and temperature is maintained around 80-85 ^oC during the production of cyanogens gas. Following reaction occur in the reaction vessel:

$$2CuSO_4 + 4NaCN \longrightarrow 2Na_2SO_4 + 2CuCN + (CN)_2 \qquad 4\text{-}1$$

The cyanogens gas is passed through $AgNO_3$ solution to remove the hydrogen cyanide (if any) during the reaction. Then the cyanogen gas is passed through NaOH column to remove the carbon dioxide and further passes through anhydrous calcium chloride column to remove moisture. Finally the dried cyanogens gas has been bubbled in the reaction mixture of containing N,N'-disulfinyl-p-phenylendiamine. After four hours cyanogen gas bubbling, the precipitates formed have been filtered off and 15% NaOH solution has been added in order to obtain TCPPD. The solid obtained has been filtered and dried in open air. The IR spectra of the final product did not show any peak for the aromatic nitrile (~ 2200 to 2250 cm^{-1}). This shows that the synthesis of TCPPD according to the Scheme 4-8 is unsuccessful.

Figure 4-1: Setup for the synthesis of TCPPD using PPD and cyanogen gas.

From tetracyanoethylene (TCNE):

TCPPD has been synthesized by the method as reported by Webster [165]. TCNE has been synthesized using malononitrile, Br_2 and KBr. The TCNE is then hydrogenated into tetracyanoethane (TCNA) which is further converted into the TCPPD as shown in scheme Scheme 4-9.

Synthesis of TCNE:

50 g malononitrile and 38 g of potassium bromide are dissolved in 450 mL of distilled water. The temperature of this solution is lowered to 5-10 ^{o}C and add to it 80 mL of Br_2 drop wise. The solution is continuously stirred during the addition and temperature is maintained at 5-10 ^{o}C. The addition of Br_2 takes 2 hours and mixture is further stirrered for 2 hours at this temperature. The white precipitates of dibromomalononitrile-potassium bromide complex are formed which have been separated and washed with ice cold water. These precipitates are dried in open air by suction for 1 hour and then kept in dedicator to complete dryness. The weight of dry dibromomalononitrile-potassium bromide complex is 160 g (about 85 % yield).

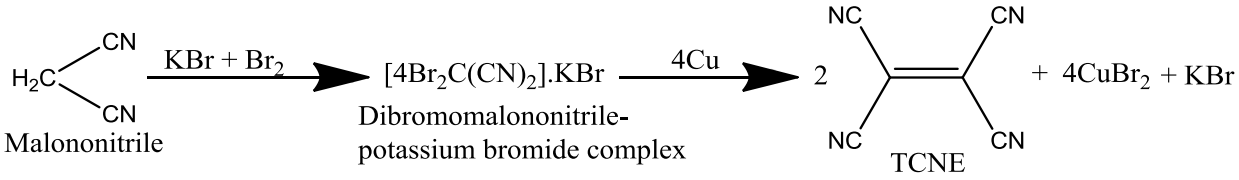

Scheme 4-9: Synthesis of TCNE.

150 g of dry dibromomalononitrile-potassium bromide complex has been added in 600 mL benzene at room temperature. A white milky suspension is obtained and add to it 65 g copper powder in portions wise with continuous stirring. Now heat this mixture to reflux for eight hours with continuous stirring. The colour of the mixture changes to yellow which is indication for the formation of TCNE. The reaction mixture has been filtered while hot to remove any insoluble solids. The filtrate is put in refrigerator for overnight and the precipitate of TCNE has been separated by filtration. The filtrate is concentrated under reduced pressure to 50 mL and put in refrigerator. Again precipitates of TCNE are separated by filtration. Total yield of TCNE synthesized is around 55%. The dried TCNE is purified by sublimation and stored in freezer.

Synthesis of tetracyanoethane:

12.5 g freshly sublimated tetracyanoethylene (TCNE) has been dissolved in 60 mL acetone and cooled this solution with ice bath. 21 mL of merceptoacetic acid ($HSCH_2COOH$) has been added drop wise to this ice cooled solution. The solution is stirred for 1 hour and then pour into 120 mL nitrogen saturated cold water and the precipitates of tetracyanoethane (TCNA) have been separated, filtered, and washed with cold water. The TCNA has been dried in vacuum dessicator over P_2O_5. The final product obtained is 10.6 g (82 % yield) which is decompose at 160-165 ^{o}C without melting (lit. 165-170 ^{o}C [218]).

Synthesis of TCPPD:

10 g of TCNA has been added in portion to ice cold solution of 6 g freshly fused potassium acetate in 50 mL glacial acetic acid and 6 mL acetic acid anhydride. The temperature is slightly increased on addition and a brown slurry has been formed which is stirred for one at ice-bath temperature for one hr and then at room temperature for 24 hrs. The mixture is taken to dryness in rotary evaporator and the residue is mixed in water and filtered it and washed with water. Dry over silica gel in desiccator in vacuum. The dry residue is suspended in acetonitrile and chromatographed over 75 g of acidic alumina. The orange component is the desired TCPPD and is concentrated and removal of solvent yield 300 mg of TCPPD (3.9 % yield) decomposed at 274 ^{o}C (lit. ~275 ^{o}C). The UV-VIS and IR spectra matched with already reported in literature [31, 163].

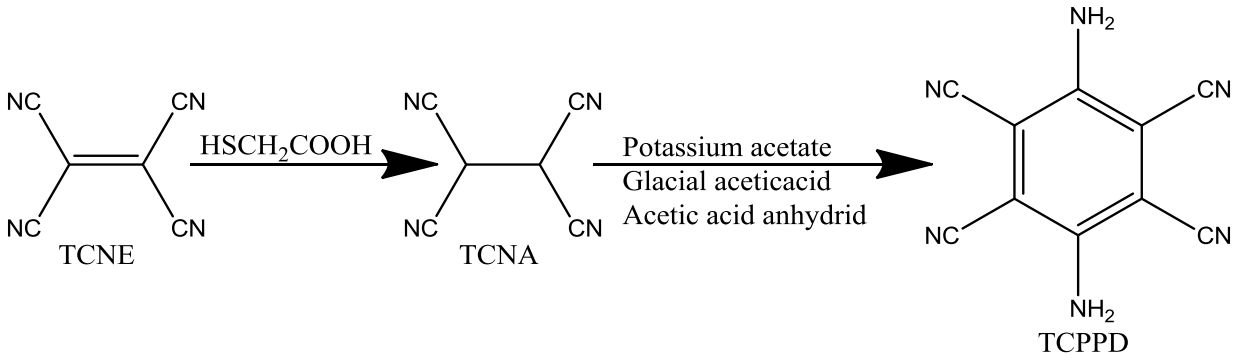

4.4 Synthesis of cyano-substituted TMPPDs

The cyano-substituted TMPPDs like monocyano-N,N,N',N'-tetramethyl-p-phenylendiamine (MCTMPPD), 2, 5-dicyano-N,N,N',N'-tetramethyl-p-phenylendiamine (TCTMPPD) and 2,3,5,6-tetracyano-N,N,N',N'-tetramethyl-p-phenylendiamine (TCTMPPD) have been tried to synthesize. The two different general ways for TMPPDs are **(a)** by the N-methylation of corresponding cyano-substituted PPDs **(b)** by direct synthesis of corresponding cyano-substituted TMPPDs.

4.4.1 Synthesis of monocyano-N,N,N',N'-tetramethyl-p-phenylene-diamine

Monocyano-N,N,N',N'-tetramethyl-p-phenylendiamine (MCTMPPD) has been synthesized by the N-methylation of MCPPD. Several methylating agent like dimethylsulphate ($(CH_3)_2SO_4$), methyl iodide (CH_3I), formaldehyde (HCHO), trimethylphosphate ($(CH_3)_3PO$) have been used to obtain the N-methylated derivative of MCPPD.

Methylation using dimethylsulphate: [24, 219-220]

Dimethylsulphate (DMS) has been used as methylating agent of the methylation of cyano-substituted diamines. 4.5 mmol of diamine is dispersed in 3 mL of water and then add to it 8.4g (100 mmol) $NaHCO_3$. This mixture has been cooled with ice bath and 3.5mL (37 m mole) of DMS has been added drop wise over a period of ~30 minutes. The reaction mixture has been stirred for 1 hr and ice bath is removed to allow th reaction content to come to room temperature. The reaction mixture has been slowly heated to 65 ^oC using oil bath. Vigorous evolution of CO_2 has been observed with continuous stirring of the reaction mixture. The temperature is maintained at 65 ^oC till no more generation of CO_2. 3 mL of cold H2O and 3.5 mL of ethanolamine have been added to the suspension. The reaction mixture is now heated to 120 ^oC and stirred for 1 hr. After cooling to room temperature, the reaction mixture is diluted with 200 mL of water. The contents have been extracted several times with CH_2Cl_2. The CH_2Cl_2 extracts have been combined and dried over $MgSO_4$. The TLC of the final crude product shows 6 components in for the MCPPD as starting material.

Methylation using methyl iodide: [221-222]

A mixture of 0.85 g (6.35 mmol) of diamine, 1.4 g of $CaCO_3$, 7.35 g (3.25 mL) of iodomethane, 10 mL of methanol and 5 mL water has been refluxed under Ar atmosphere. After 10 hrs reflux, the reaction mixture is cooled to room temperature and is diluted with 25 mL of water. Some precipitates have been formed and separated by vacuum filtration. The residue is extracted 4 times with CH_2Cl_2 and dried over $MgSO_4$. Removal of solvent gives 0.2 g of brown solid which also show 6 components on TLC.

Another reaction for the synthesis of MCTMPPD using methyl iodide in THF is added to a mixture of diamine and sodium hydride is used as base. After 10 hrs reflux and work up as described in the above reaction has not produced the desired MCTMPPD.

No promising results have been achieved by increasing the reaction time for the above reaction time up to 30 hrs.

Methylation using formaldehyde: [223-224]

0.6 g of MCPPD is added in a mixture of 2 mL of 36 % formaldehyde in water and 20 mL of 85 % formic acid. The mixture is turned dark brown and refluxed for 18 hrs under Ar. After reflux the reaction mixture is diluted with water and neutralized with dilute aqueous NaOH solution. On neutralization there is some sticky black material is formed. The mixture is extracted with ethyl acetate. A dark brown residue (0.2 g) is obtained on removal of

solvent. The different components are tried to separate using column chromatography using acidic silica and ethylacetyate/n-hexane (4:1) as eluent. Only very small fraction 0.06 g of the desired MCTMPPD is obtained.

Methylation using trimethylphosphate: [225-226]

A mixture of 3 mmol of diamine and 4 mmol of trimethylphosphate along with boiling chips has been heated to reflux in an oil bath for two hrs. The mixture is brought to 50 ^{o}C and add to it 2.5 mL of 20% w/v aqueous solution of NaOH and again the mixture is refluxed for further 1 hr. The reaction mixture is brought to room temperature and poured in 5 mL water. The oily layer of amine is formed which has been extracted with ether. Removal of ether leaves the desired crude product. TLC of the crude product has shown three spots. Pure N,N,N',N'-tetramethylated product has been separated by column chromatography using acidic silica and n-hexan/ethylacetate (4:1) as eluent. The melting point of MCTMPPD is 40 ^{o}C and IR and NMR spectra have no peak for (N-H).

4.4.2 Synthesis of 2,5-dicyano-N,N,N',N'-tetramethyl-p-phenylene-diamine (25DCTMPPD)

Dimethylsulphate has been successfully applied to produced 2,5-dichloro-N,N,N',N'-tetramethyl-p-phenylendiamine (25DClTMPPD) from the 2,5-dichloro-p-phenylendiamine (25DClPPD) in 70% yield (the procedure reported in section 4.4.1). 25DClTMPPD has been used to synthesize 25DCTMPPD in two different approaches shown in Scheme 4-10.

(a) Using Rosenmund–von Braun reaction (as reported in section 4.3.2) for the replacement of chloro groups with cyano group by refluxing (24 hrs) 25DClTMPPD in DMF in the presence of CuCN (mole ratio 1:8 for Ar-X and CuCN respectively). But this reaction is not successful as at the end of reaction there is not substitution of cyano group (indicated by IR) and also there is large amount of starting material is present in the final product (indicated by TLC).

(b) Chlorine atoms of 25DClTMPPD have been tried to replace with iodine atoms. The iodo groups can be more effectively replaced with cyano groups in Rosenmund–von Braun reaction. Gerald an co-workers [24] has reported the replacement of two bromo groups (-Br) in 2,6-dibromo-TMPPD with corresponding iodo groups (-I) to form 2,6-diiodo-TMPPD. Same procedure has been applied to convert replace chloro groups of 25DClTMPPD by

corresponding iodo groups using CuI, KI in HMPA. But halide exchange method did not work for the exchange of chloro group of 2,5-dichloro-N,N,N,N-tetramethyl-p-phenylendiamine.

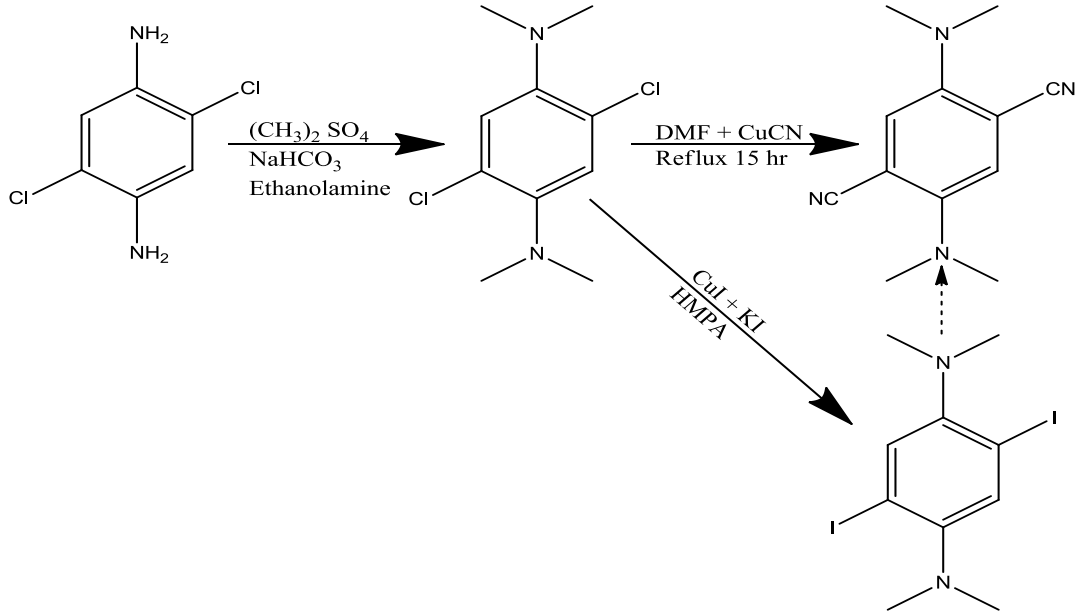

Scheme 4-10: Synthesis of 25DCTMPPD.

The 2,6-dicyano-N,N,N',N'-tetramethyl-p-phenylendiamine has already been synthesized by our group following the procedure given in ref. [24].

4.4.3 Synthesis of 2,3,5,6-tetracyano-N,N,N',N'-tetramethyl-p-phenylene-diamine (TCTMPPD)

Attempts have been made to synthesize the TCTMPPD using the dimethylsulphate, methyl iodide and formaldehyde, but none of the reactions work for the N-methylation of TCPPD. The procedure followed in the same way as given in section 4.4.1.

4.5 Other cyano-substituted aromatic compounds

Two more cyano-substituted aromatic compounds have been synthesized. These are 2,3,5,6-tetracyano-1,4-hydroquinone (TCHQ) and 2,3,5,6-tetracyano-1,4-benzoquinone (TCBQ, also known as cyanil). The formation of 2,3,5,6-tetracyano-1,4-hydroquinone and 2,3,5,6-tetracyano-1,4-benzoquinone starting from p-benzoquinone have been shown in Scheme 4-11.

4.5.1 Synthesis of 2,3,5,6-tetracyano-1,4-hydroquinone

2,3,5,6-tetracyano-1,4-hydroquinone (TCHQ) has been synthesized using 2,3-dichloro-5,6-dicyano-1,4-benzoquinone (DDQ) [227] and 2,3,5,6-tetrabromo-1,4-benzoquinone (bromanil) [44, 227] as starting material. Both the starting materials have been processed in the same way to the final TCHQ however bromanil has given better product yield compared to DDQ.

TCHQ has been synthesized by the replacement of halogen groups (-Cl or –Br) of bromanil or DDQ with cyano groups.

Synthesis of bromanil: 2,3,5,6-tetrabromo-1,4-benzoquinone (bromanil) has been synthesized by the bromination of p-benzoquinone. 5 g of p-benzoquinone has been dissolved in 50 mL acetic acid and heat it to reflux. 1.2 mL of bromine in 10 mL acetic acid is added drop wise to this boiling solution over a period of 30 minutes. The reaction mixture is refluxed for additional two hrs. The reaction is brought to room temperature and small quantity of nitric acid `2 mL is added and heated on a water bath at 50 ^{o}C for 40 minutes. The reaction mixture i brought to room temperature and ice cold water is added to it. The precipitates formed are filtered washed with water and dried. The crude product is recrystallized from acetic acid and 15.4 g (80 % yield) bromanil is obtained. The melting point is 301 ^{o}C (300 ^{o}C in lit. [228]). The IR is as reported in literature.

Synthesis of TCHQ: 5 g of bromanil is added portion wise in solution of 4.6 g NaCN in 400 mL methanol within 30 minutes. The solution is turn red with a little increase in temperature and the reaction mixture is refluxed for 45 minutes. The solution is rapidly cooled to room temperature and HCl gas is bubbled into the reaction mixture until the colour of the reaction mixture is changed from red to brown. This mixture is concentrated to dryness in rotary evaporator and residue is extracted with 250 mL of diethyl ether. The ethereal extracts are combined and morpholine is added to it until no more formation of the precipitates. The morpholine salt is separated by filtration and recrystallized with minimum amount of methanol. 2.4 g of morpholine salt is obtained. The morpholine salt is dissolved in minimum amount of water and HCL gas is bubbled through the solution until the colour of solution is changed from red to brown with the formation of precipitates. This mixture is extracted several times with diethyl ether and dried over $MgSO_4$. The removal of solvent yields yellow solid (0.61 g) which is dissolved in 35 mL of water and filtered to remove any insoluble residue. HCl gas is again bubbled through the filtrate until the formation of yellow precipitates. These precipitates are extracted by diethyl ether. The yellow solid is obtained

(0.45 g) after removal of solvent and dissolved in hot acetic acid (20 mL) and equivalent amount of pyrene dissolved in CH_2Cl_2 is added to hot acetic acid solution. The red pyrene complex is precipitated, filtered, washed with dichloromethane and dried (1.35 g). Hot dioxane is added to this complex and yellow complex of dioxane is formed which is separated by filtration and dried (0.51 g). This yellow solid is dissolve in water, filtered to remove insoluble residue and again bubble HCl gas in the filtrate until the formation of yellow precipitates. The yellow precipitates are extracted with diethyl ether, dried over $MgSO_4$. Removal of solvent leads to crude product of TCHQ which is further purified by recrystallization with acetic acid 0.35 g (14 % yield). The IR spectrum is as reported in literature [44].

4.5.2 Synthesis of 2,3,5,6-tetracyano-1,4-benzoquinone

Silver nitrate solution of 1.15 g in 4 mL H_2O is added quickly in a hot solution of 0.35 g TCHQ in 25 mL of water with continuous stirring. The mixture is turned black and the stirred for 30 minutes. The black precipitates are separated by vacuum filtration while warm and the sample is dried in vacuum.0.70 g. (~ 99% yield). 0.7 g of the disilver salt of TCHQ (QAg_2) is suspended in 40 mL of dry CH_2Cl_2 under Ar[24]. 1.06 g bromine in 2 mL of CH_2Cl_2 is added to the suspension which is further stirred 1 hr at room temperature. The silver bromide precipitates are filtered under nitrogen and washed with 3 times 30 mL of dry CH_2Cl_2. The excess of solvent is removed and the mixture was cooled to room temperature. The yellow precipitates of 2,3,5,6-tetracyano-1,4-benzoquinone (TCBQ) 0.13g (40 % yield) is obtained.

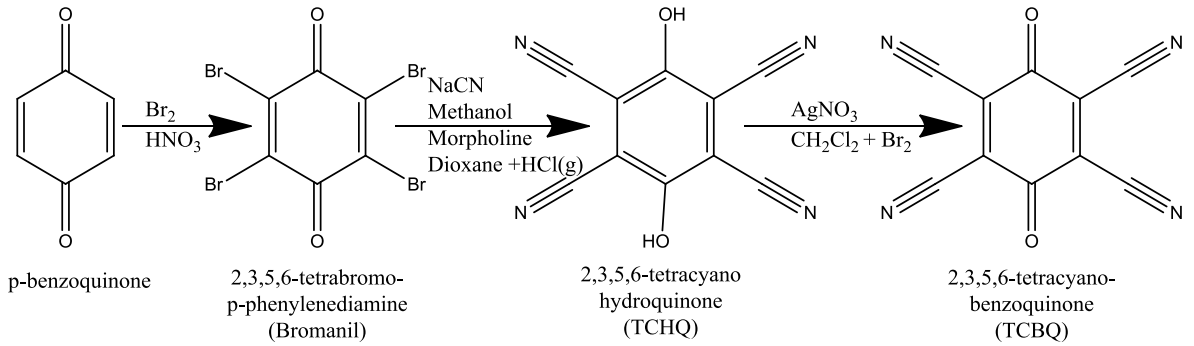

Scheme 4-11: Formation of 2,3,5,6-tetracyano-1,4-hydroquinone and 2,3,5,6-tetracyano-1,4-benzoquinone starting from p-benzoquinone.

[24] CH_2Cl_2 should be totally dried because of the high water sensitivity of 2,3,5,6-tetracyano-1,4-benzoquinone and reaction mixture is kept under Ar throughout the reaction period and also the final product is stored under Ar.

5 RESULTS AND DISCUSSION

Present results comprise of the photophysical and electrochemical investigation of cyano-substituted PPDs and TMPPDs. The absorption and emission characteristics of TCHQ have been studied in different solvents as well as in solvent mixtures. The electrochemical investigations include the measurements of redox potential and diffusion coefficients of these compounds in acetonitrile.

5.1 Photophysical studies

Photophysical studies include the determination of the basic photophysical properties like absorption maxima ($\tilde{\nu}_{abs}$), fluorescence maxima ($\tilde{\nu}_{flu}$), Stokes shift ($\Delta\tilde{\nu}$), 0-0 transition energy (E_{00}), fluorescence quantum yield (Φ), fluorescence lifetime (τ), radiative (k_r) and non-radiative (k_{nr}) rate constant in different solvents. Equilibrium constants for the ground and excited state proton transfer (pK_a and pK_a^*) have been determined for 26DCPPD and TCHQ. Solvent-solute interactions for absorption and emission maxima in different solvents are investigated by LSER analysis.

5.1.1 Photophysical properties of PPDs and TMPPDs

The absorption and fluorescence spectra of cyano-substituted PPDs and TMPPDs have been investigated in different solvents and shift in absorption as well as in fluorescence spectra have been observed for these compounds. Figure 5-1 and Figure 5-2 show the representative shift of absorption and fluorescence maxima in different solvents for MCPPD and 26DCPPD, respectively. The solvatochromic shifts for MCTMPPD and TMPPD have been shown in Figure 5-5 and Figure 5-6, respectively. Normalized absorption spectra (in ethanol) and normalized fluorescence spectra (in ethyl acetate[25]) for four cyano-substituted PPDs are shown in Figure 5-3 and Figure 5-4, respectively. Figure 5-7 and Figure 5-8 show the normalized absorption (complete spectra) and normalized emission spectra of cyano substitute TMPPDs in ethanol. It can be seen in Figure 5-1 to Figure 5-8 that the positions of the absorption and fluorescence band depend on the solvent used.

[25] Ethyl acetate has been used to display all the fluorescence spectra in PPDs because the emission intensity of MCPPD is very low in ethanol.

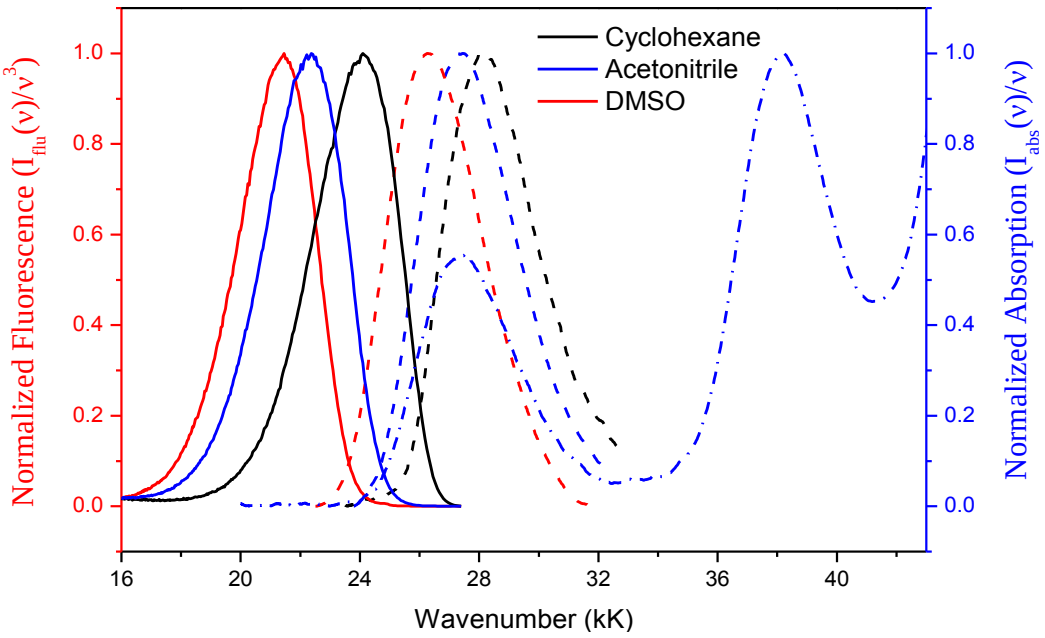

Figure 5-1: Normalized absorption (dashed line) and fluorescence (solid line) spectra of MCPPD in cyclohexane, acetonitrile and DMSO. Dash-dot line is complete normalized absorption spectrum in acetonitrile.

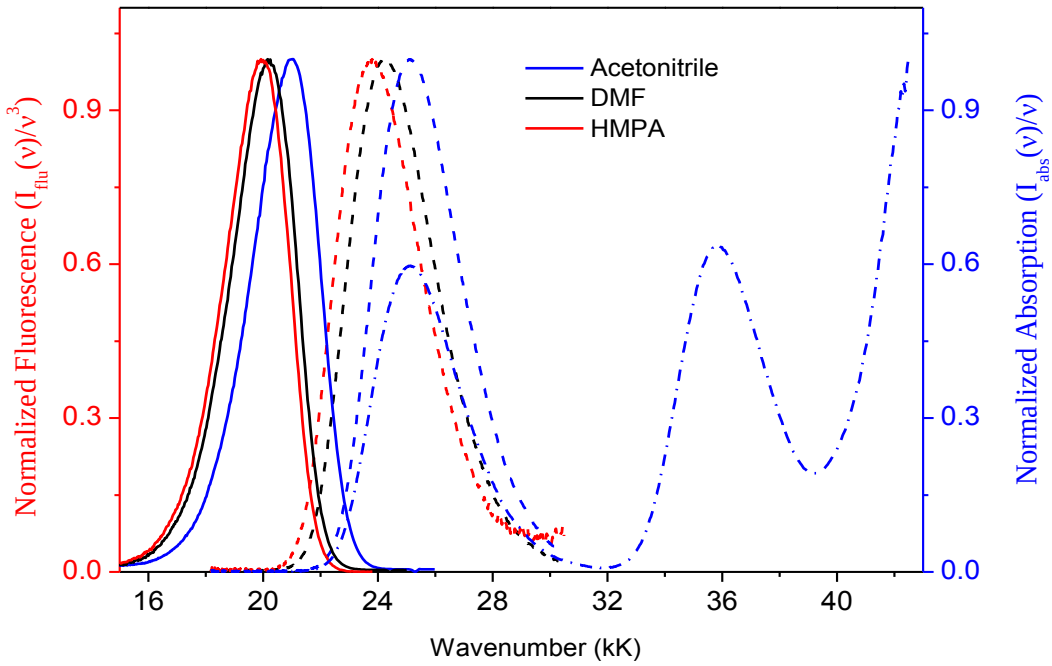

Figure 5-2: Normalized spectra of absorption (dashed line) and fluorescence (solid line) DCPPD in acetonitrile, DMF and HMPA. Dash-dot line is complete normalized absorption spectrum in acetonitrile.

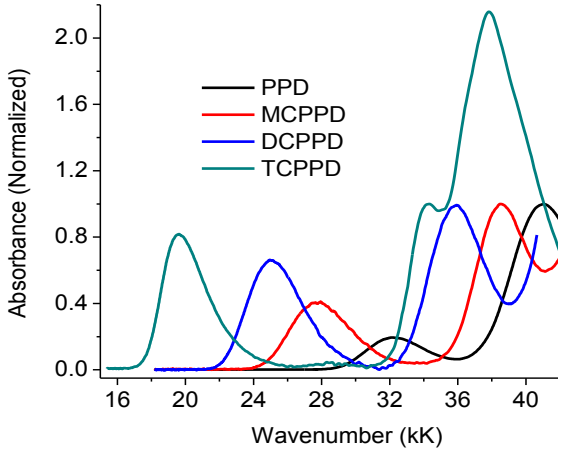

Figure 5-3: Complete (normalized at 2nd absorption band) absorption spectra of cyano-substituted PPDs in ethanol.

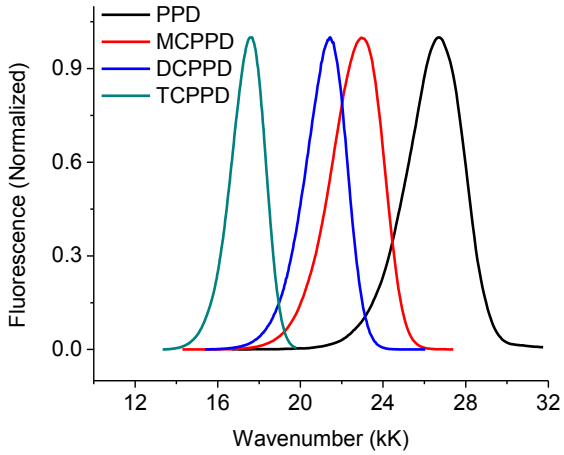

Figure 5-4: Normalized mission spectra of cyano-substituted PPDs in ethyl acetate.

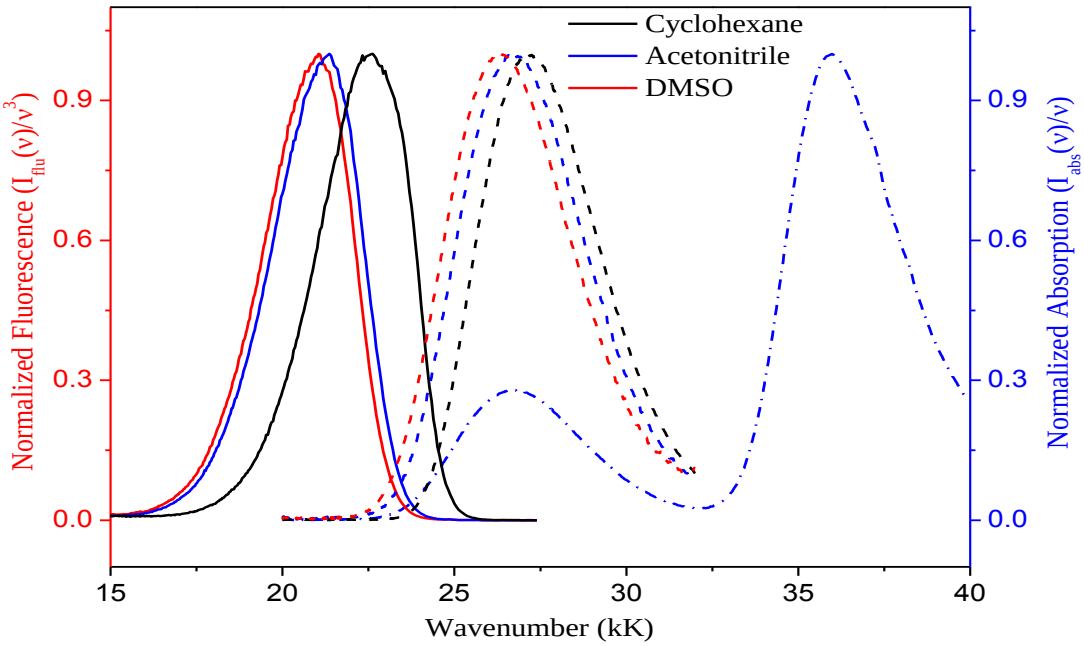

Figure 5-5: Normalized absorption (dashed line) and fluorescence (solid line) spectra of MCTMPPD in cyclohexane, acetonitrile and DMSO. Dash-dot line is complete normalized absorption spectrum in acetonitrile.

The photophysical properties for different cyano-substituted PPDs are compiled from Table 5-1 to Table 5-4. Table 5-4 contains the photophysical properties of TCPPD, most of these properties are already published [31] but photophysical properties of only six new solvents (ethyl acetate, propyl acetate, 1-pentanol, 1-butanol, 2-propanol and 1-propanol) have been measured in order to study the specific solvent-solute interaction as well comparison of the solvatochromic study with other PPDs with same set of solvent used for all compounds.

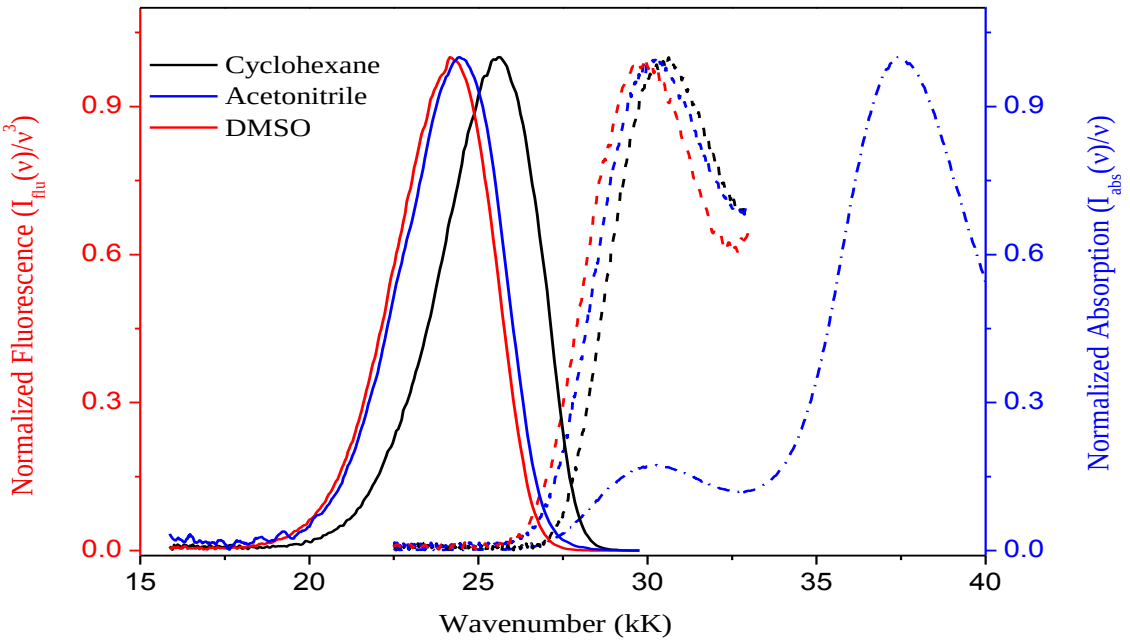

Figure 5-6: Normalized absorption (dashed line) and fluorescence (solid line) spectra of TMPPD in cyclohexane, acetonitrile and DMSO. Dash-dot line is complete normalized absorption spectrum in acetonitrile.

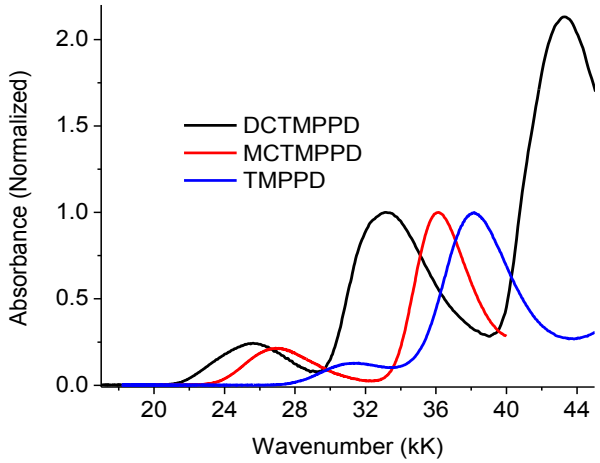

Figure 5-7: Absorption spectra of cyano-substituted TMPPDs in ethanol.

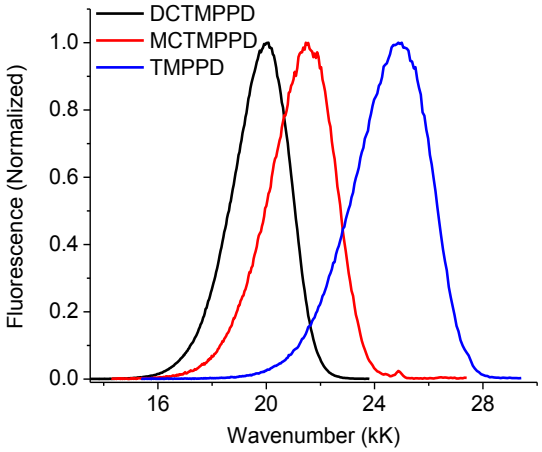

Figure 5-8: Normalized fluorescence spectra of cyano-substituted TMPPDs in ethanol.

The photophysical properties for different cyano-substituted PPDs and TMPPDs are shown from Table 5-5 to Table 5-7. The photophysical properties of TMDCPPD in several solvents are already published [30]. The photophysical properties of DCTMPPD are measured in few more solvents, i.e. ethyl benzene, propyl acetate, 1-pentanol, 1-butanol, 2-propanol and 1-propanol, in order to have nice comparison among different cyano-substituted TMPPDs and also with corresponding analogue of PPD (DCPPD).

Table 5-1: Photophysical properties of PPD in different solvents.

Ref. no.	Solvents	$\tilde{\nu}_{exp,abs}$ kK	$\tilde{\nu}_{exp,flu}$ kK	$\Delta\tilde{\nu}$ cm^{-1}	E_{00} kJ mol^{-1}	Φ	τ ns	k_r $10^7 s^{-1}$	k_{nr} $10^7 s^{-1}$	$\tilde{\nu}_{theo,abs}$ kK	$\tilde{\nu}_{theo,flu}$ kK
1	n-Hexane	31.45	27.01	4438	350	0.11	2.81	3.87	31.70	31.66	27.05
2	Cyclohexane	31.48	26.86	4617	349	0.14	2.89	4.71	29.92	31.58	26.90
4	Benzene	31.00	26.03	4966	341	0.04	0.79	4.54	121.55	31.10	26.02
5	Toluene	31.04	26.08	4959	342	0.05	1.03	4.85	92.24	31.13	26.09
6	Ethylbenzene	31.34	26.05	5298	343	0.01	0.70	2.12	140.74	31.10	26.02
7	Butylether	31.14	26.07	5071	342	0.14	3.63	3.75	23.78	31.09	26.07
8	Diethyl ether	31.44	25.87	5572	343	0.07	2.79	2.38	33.52	31.04	25.98
9	Propylacetate	30.95	25.79	5156	339	0.04	1.00	4.38	95.14	30.88	25.67
10	Ethylacetate	30.93	25.68	5256	339	0.06	1.20	4.68	78.34	30.90	25.71
11	Tetrahydrofuran	30.74	25.55	5191	337	0.12	2.61	4.64	33.68	30.75	25.45
14	HMPA[a]	30.00	24.45	5556	326	---	---	---	---	30.16	24.44
15	Acetonitrile	30.97	25.47	5492	338	0.06	1.49	4.18	62.78	31.15	25.43
16	Dimethylformamide	30.36	24.76	5594	330	0.02	0.50	4.69	195.31	30.39	24.82
17	Dimethyl sulfoxide	30.11	24.41	5694	326	0.19	3.98	4.78	20.38	30.25	24.57
18	Propylene carbonate	30.84	25.37	5475	336	0.26	5.70	4.50	13.05	30.66	25.25
19	1-Pentanol	33.32	25.06	8267	349	0.04	2.90	1.32	33.16	32.22	25.04
21	1-Butanol	32.15	24.97	7180	342	0.11	2.49	4.23	35.86	32.19	24.96
22	2-Propanol	32.14	24.96	7183	342	0.13	2.89	4.39	30.22	32.03	24.97
23	1-Propanol	32.20	24.98	7221	342	0.09	2.30	4.00	39.49	32.10	24.82
24	Ethanol	32.15	24.90	7252	341	0.08	2.05	3.80	44.93	32.24	24.97
25	Methanol	32.34	24.96	7382	343	0.04	1.22	3.60	78.26	32.50	24.97
26	Water	32.77	24.43	8346	342	0.002[b]	---	---	---	32.65	24.48

(a) Time resolved measurements of PPD in HMPA are not performed because of instrumental problem (out of order).

(b) Very low emission.

Table 5-2: Photophysical properties of MCPPD in different solvents.

Ref. no.	Solvents	$\tilde{\nu}_{exp,abs}$ kK	$\tilde{\nu}_{exp,flu}$ kK	$\Delta\tilde{\nu}$ cm^{-1}	E_{00} kJ mol^{-1}	Φ	τ ns	k_r $10^7 s^{-1}$	k_{nr} $10^7 s^{-1}$	$\tilde{\nu}_{theo,abs}$ kK	$\tilde{\nu}_{theo,flu}$ kK
1	n-Hexane	28.08	24.17	3916	312.6	0.61	13.32	4.56	2.95	28.15	24.06
2	Cyclohexane	28.23	24.10	4131	313.0	0.62	12.48	4.93	3.08	28.11	23.90
3	p-Xylene	27.71	23.16	4550	304.3	0.81	14.23	5.71	1.31	27.75	23.08
4	Benzene	27.57	23.02	4553	302.7	0.80	14.20	5.63	1.41	27.75	22.96
5	Toluene	27.64	23.07	4562	303.4	0.79	14.43	5.47	1.46	27.75	23.03
6	Ethylbenzene	27.71	23.00	4715	303.3	0.14	2.72	5.15	31.64	27.72	22.96
7	Butylether	27.49	22.80	4693	300.9	0.63	14.51	4.37	2.52	27.26	22.96
8	Diethyl ether	27.32	22.63	4685	298.8	0.57	14.43	3.95	2.98	27.23	22.86
9	Propylacetate	27.30	22.50	4800	297.9	0.73	16.70	4.38	1.61	27.24	22.54
10	Ethylacetate	27.27	22.45	4821	297.4	0.77	17.81	4.31	1.31	27.19	22.58
11	Tetrahydrofuran	27.01	22.27	4731	294.8	0.64	14.83	4.30	2.44	26.98	22.29
12	Acetone	27.22	22.19	5031	295.5	0.45	10.31	4.37	5.34	27.18	22.25
13	Benzonitrile	27.11	21.91	5199	293.2	0.003[b]	---	---	---	27.17	22.08
14	HMPA[a]	26.12	21.45	4665	284.6	---	---	---	---	26.10	21.16
15	Acetonitrile	27.39	22.22	5168	296.8	0.38	9.44	4.07	6.51	27.45	22.26
16	Dimethylformamide	26.58	21.63	4946	288.4	0.57	12.80	4.45	3.36	26.62	21.60
17	Dimethyl sulfoxide	26.39	21.32	5067	285.4	0.45	9.68	4.65	5.68	26.46	21.33
18	Propylene carbonate	27.18	22.10	5076	294.8	0.39	8.97	4.34	6.81	27.14	22.11
19	1-Pentanol	27.63	21.66	5970	294.8	0.01	0.33	4.18	298.85	27.61	21.65
21	1-Butanol	27.58	21.67	5915	294.6	0.01	0.22	4.38	455.73	27.62	21.57
22	2-Propanol	27.46	21.57	5884	293.3	0.01	0.23	4.08	439.15	27.51	21.60
23	1-Propanol	27.58	21.56	6021	294.0	0.01	0.18	3.87	537.81	27.50	21.41
24	Ethanol	27.68	21.55	6132	294.5	0.005 [b]	0.13	3.76	774.15	27.78	21.60
25	Methanol	27.73	21.36	6375	293.7	0.005 [b]	0.12	3.94	847.85	28.07	21.59
26	Water	28.82	21.15	7672	298.9	0.002 [b]	0.13	0.16	743.44	28.47	21.08

Time resolved measurements has not done because (a) instrumental problem (out of order) and (b) Very low emission (Φ<0.1%).

Table 5-3: Photophysical properties of DCPPD in different solvents.

Ref. no.	Solvents	$\tilde{\nu}_{exp,abs}$ kK	$\tilde{\nu}_{exp,flu}$ kK	$\Delta\tilde{\nu}$ cm^{-1}	E_{00} kJ mol^{-1}	**Φ**	τ ns	k_r $10^7 s^{-1}$	k_{nr} $10^7 s^{-1}$	$\tilde{\nu}_{theo,abs}$ kK	$\tilde{\nu}_{theo,flu}$ kK
1	n-Hexane	26.00	22.75	3251	291.7	0.58	14.0	4.13	3.00	25.87	22.67
2	Cyclohexane	25.81	22.71	3105	290.2	0.60	13.5	4.43	2.98	25.84	22.54
3	p-Xylene	25.39	21.75	3635	282.0	0.69	16.0	4.30	1.94	25.48	21.77
4	Benzene	25.37	21.73	3639	281.7	0.78	15.1	5.14	1.49	25.49	21.68
5	Toluene	25.37	21.76	3614	281.9	0.74	15.5	4.75	1.69	25.49	21.73
6	Ethylbenzene	25.38	21.63	3745	281.2	0.58	11.5	5.04	3.69	25.46	21.67
7	Butylether	25.09	21.39	3700	278.0	0.81	17.5	4.61	1.10	24.94	21.50
8	Diethyl ether	24.95	21.24	3714	276.3	0.77	19.3	4.00	1.19	24.90	21.41
9	Propylacetate	24.92	21.11	3803	275.4	0.81	18.1	4.45	1.07	24.94	21.17
10	Ethylacetate	24.93	21.12	3812	275.5	0.85	18.6	4.59	0.80	24.87	21.19
11	Tetrahydrofuran	24.77	20.86	3909	272.9	0.61	18.5	3.31	2.10	24.66	20.89
12	Acetone	24.90	20.88	4013	273.9	0.82	19.4	4.25	0.91	24.84	20.90
13	Benzonitrile	24.91	20.81	4096	273.5	0.76	15.9	4.77	1.54	24.89	20.79
14	HMPA	23.78	19.96	3818	261.7	0.71	19.7	3.60	1.48	23.74	19.70
15	Acetonitrile	25.09	21.00	4093	275.8	0.82	19.5	4.20	0.94	25.09	20.96
16	Dimethylformamide	24.24	20.17	4074	265.7	0.77	18.9	4.10	1.20	24.30	20.23
17	Dimethyl sulfoxide	24.01	19.86	4155	262.5	0.72	18.3	3.94	1.53	24.14	19.96
18	Propylene carbonate	24.94	20.81	4129	273.7	0.86	17.6	4.91	0.78	24.85	20.80
19	1-Pentanol	24.87	20.26	4613	269.9	0.83	18.6	4.49	0.90	24.95	20.31
21	1-Butanol	24.94	20.25	4691	270.4	0.77	19.0	4.08	1.20	24.96	20.26
22	2-Propanol	24.91	20.30	4608	270.5	0.72	19.7	3.66	1.41	24.88	20.27
23	1-Propanol	24.97	20.27	4704	270.6	0.80	19.3	4.14	1.04	24.84	20.09
24	Ethanol	25.01	20.27	4743	270.9	0.73	19.9	3.65	1.38	25.13	20.32
25	Methanol	25.07	20.27	4805	271.2	0.81	20.5	3.94	0.93	25.39	20.38
26	Water	26.08	20.07	6008	276.0	0.65	15.1	4.34	2.29	25.77	20.05

Table 5-4: Photophysical properties of TCPPD in different solvents.

Ref. no.	Solvents	$\tilde{\nu}_{exp,abs}$ kK	$\tilde{\nu}_{exp,flu}$ kK	$\Delta\tilde{\nu}$ cm^{-1}	E_{00} kJ mol^{-1}	Φ	τ ns	k_r $10^7 s^{-1}$	k_{nr} $10^7 s^{-1}$	$\tilde{\nu}_{theo,abs}$ kK	$\tilde{\nu}_{theo,flu}$ kK
3	p-Xylene	20.27	18.05	2220	229	0.87	22.9	3.80	0.57	20.32	18.03
4	Benzene	20.30	18.10	2200	230	0.73	20.0	3.65	1.35	20.30	17.95
5	Toluene	20.32	18.03	2290	229	0.72	21.1	3.41	1.33	20.32	18.00
6	Ethylbenzene	20.31	18.08	2230	230	0.75	20.6	3.64	1.21	20.28	17.94
7	Butylether	19.87	17.62	2250	224	0.74	21.1	3.51	1.23	19.88	17.69
8	Diethyl ether	19.68	17.40	2280	222	0.89	23.1	3.85	0.48	19.83	17.60
9	Propylacetate[a]	19.80	17.36	2441	222	0.69	21.0	3.29	1.48	19.79	17.40
10	Ethylacetate[a]	19.79	17.28	2513	222	0.68	21.2	3.21	1.51	19.75	17.40
11	Tetrahydrofuran	19.39	17.04	2350	218	0.73	21.4	3.41	1.26	19.52	17.10
12	Acetone	19.68	17.12	2560	220	0.74	22.2	3.33	1.17	19.64	17.15
13	Benzonitrile	19.71	17.19	2520	221	0.74	18.0	4.11	1.44	19.65	17.07
14	HMPA	18.62	15.97	2650	207	0.36	16.4	2.20	3.90	18.56	15.88
15	Acetonitrile	19.95	17.22	2730	222	0.75	22.1	3.39	1.13	19.81	17.25
16	Dimethylformamide	18.99	16.38	2610	212	0.61	19.3	3.16	2.02	19.09	16.46
17	Dimethyl sulfoxide	18.71	16.09	2620	208	0.46	17.4	2.64	3.10	18.91	16.19
18	Propylene carbonate	19.84	17.13	2710	221	0.77	19.7	3.91	1.17	19.63	17.07
19	1-Pentanol[a]	19.46	16.64	2822	216	0.51	18.0	2.83	2.72	19.47	16.64
21	1-Butanol[a]	19.50	16.65	2853	216	0.49	18.2	2.69	2.80	19.47	16.60
22	2-Propanol[a]	19.57	16.73	2844	217	0.48	18.1	2.65	2.87	19.42	16.59
23	1-Propanol[a]	19.55	16.66	2888	217	0.51	18.4	2.77	2.66	19.34	16.42
24	Ethanol	19.54	16.64	2900	216	0.58	19.5	2.97	2.15	19.60	16.69
25	Methanol	19.51	16.64	2870	216	0.65	19.2	3.39	1.82	19.78	16.78
26	Water	19.92	16.44	3480	218	0.33	13.2	2.50	5.08	19.94	16.58

(a) Measured during the present study , photophysical properties of other solvents taken from [31]

Table 5-5: Photophysical properties of TMPPD in different solvents.

Ref. no.	Solvents	$\tilde{\nu}_{exp,abs}$ kK	$\tilde{\nu}_{exp,flu}$ kK	$\Delta\tilde{\nu}$ cm^{-1}	E_{00} kJ mol^{-1}	Φ	τ ns	k_r $10^7 s^{-1}$	k_{nr} $10^7 s^{-1}$	$\tilde{\nu}_{theo,abs}$ kK	$\tilde{\nu}_{theo,flu}$ kK
1	Hexane	30.59	25.74	4844	337.0	0.17	4.28	4.01	19.36	30.44	25.78
2	Cyclohexane	30.60	25.69	4913	336.7	0.18	4.21	4.32	19.45	30.46	25.64
4	Benzene	30.07	24.77	5293	328.1	0.54	7.75	6.9	6.00	30.49	24.92
5	Toluene	30.15	24.98	5172	329.8	0.4	7.19	5.52	8.38	30.47	25.00
6	Ethylbenzene	30.41	25.02	5392	331.6	0.05	1.0	5.34	94.66	30.47	24.95
7	Butylether	30.42	25.44	4977	334.2	0.18	4.45	3.96	18.49	30.18	25.40
8	Ethyl ether	30.51	25.41	5094	334.5	0.15	3.71	4.09	22.88	30.19	25.32
9	Propylacetate	30.41	25.08	5332	332.0	0.25	6.46	3.83	11.64	30.28	24.94
10	Ethylacetate	30.4	25.05	5354	331.7	0.26	6.87	3.83	10.74	30.24	25.05
11	Tetrahydrofuran	30.38	25.06	5313	331.7	0.19	3.86	4.92	20.97	30.19	24.92
15	Acetonitrile	30.30	24.5	5794	327.8	0.03	1.04	2.64	93.89	30.63	24.67
16	Dimethylformamide	30.09	24.53	5562	326.8	0.2	4.4	4.44	18.29	30.15	24.48
17	Dimethyl sulfoxide	30.35	24.31	6034	327.0	0.28	8.76	3.17	8.25	30.12	24.33
18	Propylene Carbonate	30.10	24.4	5694	326.0	0.34	8.8	3.82	7.54	30.33	24.55
19	1-Pentanol	31.24	24.52	6723	333.6	0.26	5.49	4.73	13.48	31.40	24.64
21	1-Butanol	31.25	24.53	6728	333.7	0.28	7.47	3.8	9.58	31.42	24.55
22	2-Propanol	31.26	24.53	6727	333.8	0.27	7.53	3.55	9.73	31.29	24.58
23	1-Propanol	31.35	24.46	6886	333.9	0.28	7.4	3.76	9.76	31.39	24.48
24	Ethanol	31.35	24.5	6841	334.1	0.25	7.16	3.46	10.51	31.53	24.45
25	Methanol	31.58	24.31	7277	334.3	0.1	3.68	2.82	24.34	31.81	24.31
26	Water	33.00	23.7	9303	339.2	0.01	0.15	4.00	662.67	32.34	23.56

Table 5-6: Photophysical properties of MCTMPPD in different solvents.

Ref. no.	Solvents	$\tilde{\nu}_{exp,abs}$ kK	$\tilde{\nu}_{exp,flu}$ kK	$\Delta\tilde{\nu}$ cm^{-1}	E_{00} kJ mol^{-1}	Φ	τ ns	k_r $10^7 s^{-1}$	k_{nr} $10^7 s^{-1}$	$\tilde{\nu}_{theo,abs}$ kK	$\tilde{\nu}_{theo,flu}$ kK
1	Hexane	27.23	22.59	4641	298	0.58	14.6	3.98	2.87	27.03	22.57
2	Cyclohexane	27.17	22.42	4748	297	0.60	14	4.27	2.87	27.03	22.42
3	p-Xylene	26.68	21.79	4892	290	0.86	16.7	5.14	0.85	26.95	21.78
4	Benzene	26.57	21.59	4989	288	0.77	16.6	4.66	1.36	26.97	21.65
5	Toluene	26.66	21.76	4899	290	0.70	16.7	4.17	1.82	26.96	21.73
6	Ethylbenzene	26.68	21.6	5082	289	0.25	5.9	4.26	12.69	26.95	21.67
7	Butylether	27.00	22.17	4831	294	0.62	15.7	3.95	2.42	26.61	22.07
8	Ethyl ether	27.05	22.06	4987	294	0.66	17.3	3.84	1.94	26.61	21.99
9	Propylacetate	26.87	21.68	5193	290	0.69	19	3.63	1.63	26.69	21.61
10	Ethylacetate	27.54	22.84	4694	301	0.12	4.27	2.86	20.56	26.64	21.71
11	Tetrahydrofuran	26.81	21.7	5111	290	0.72	18.8	3.85	1.47	26.55	21.55
12	acetone	26.73	21.37	5368	288	0.70	19.5	3.59	1.54	26.68	21.43
15	acetonitrile	26.72	21.16	5555	286	0.76	23.8	3.19	1.01	26.85	21.34
16	Dimethylformamide	26.55	21.18	5376	286	0.77	20.8	3.71	1.10	26.44	21.07
17	Dimethyl sulfoxide	26.33	20.88	5449	282	0.81	19.9	4.05	0.98	26.38	20.89
18	Propylene Carbonate	26.58	21.05	5525	285	0.76	21.4	3.55	1.12	26.70	21.21
19	1-Pentanol	26.74	21.19	5545	287	0.22	5.6	3.93	13.92	26.92	21.27
21	1-Butanol	26.76	21.16	5600	287	0.18	4.5	3.90	18.32	26.94	21.18
22	2-Propanol	26.78	21.18	5602	287	0.27	7.2	3.68	10.20	26.88	21.21
23	1-Propanol	26.84	21.07	5777	287	0.13	3.5	3.56	25.01	26.89	21.10
24	Ethanol	26.83	21.08	5751	287	0.10	2.6	3.86	34.60	27.05	21.10
25	Methanol	26.92	20.93	5992	286	0.03	0.85	3.31	114.34	27.23	20.98
26	Water	28.39	20.46	7939	292	0.00	0.18	1.98	553.57	27.59	20.27

Table 5-7: Photophysical properties of DCTMPPD in different solvents.

Sr. No.	Solvents	$\tilde{\nu}_{abs,cog}$ kK	$\tilde{\nu}_{flu,cog}$ kK	$\tilde{\nu}_{flu,\max}$ kK	$\Delta\tilde{\nu}$ cm^{-1}	E_{00} kJ mol^{-1}	**Φ**	τ ns	k_r $10^7 s^{-1}$	k_{nr} $10^7 s^{-1}$	$\tilde{\nu}_{theo,flu,cog}$ kK	$\tilde{\nu}_{theo,flu,\max}$ kK
1	Hexane	25.86	20.25	20.87	5610	276	0.38	12.7	2.99	4.88	20.26	20.86
2	Cyclohexane	25.81	20.17	20.79	5640	275	0.37	12.5	2.96	5.04	20.10	20.66
4	Benzene	25.27	19.25	19.78	6020	266	0.57	17.9	3.18	2.40	19.27	19.67
5	Toluene	25.3	19.35	19.88	5950	267	0.55	17.5	3.14	2.57	19.36	19.79
6	Ethylbenzene[a]	25.16[b]	19.26	20.00	----	----	0.50	---	---	---	19.30	19.72
7	Butylether	25.8	19.91	20.58	5890	273	0.45	16	2.81	3.44	19.79	20.43
8	Ethyl ether	25.6	19.71	20.24	5890	271	0.46	16.6	2.77	3.25	19.70	20.33
9	Propylacetate[a]	25.61	19.26	19.98	---	----	0.48	---	---	---	19.27	19.78
10	Ethylacetate	25.66	19.26	19.82	6400	269	0.49	19.1	2.57	2.67	19.39	19.94
11	Tetrahysrofuran	25.61	19.3	19.86	6310	269	0.54	18.8	2.87	2.45	19.23	19.78
12	Acetone	25.65	19.05	19.48	6600	267	0.51	21.3	2.39	2.30	19.10	19.60
13	Benzonitrile	25.04	18.9	19.32	6140	263	0.50	19.5	2.56	2.56	18.76	19.13
15	Acetonitrile	25.58	18.87	19.27	6710	266	0.53	21.8	2.43	2.16	19.01	19.46
16	Dimethylformamide	25.41	18.73	19.19	6680	264	0.57	21.8	2.61	1.97	18.73	19.20
17	Dimethyl sulfoxide	25.2	18.58	19.02	6620	262	0.55	22.9	2.40	1.97	18.54	19.00
18	Propylene Carbonate	25.35	18.78	19.2	6570	264	0.58	22	2.64	1.91	18.83	19.23
19	1-Pentanol[a]	25.36[b]	19.02	19.69	----	----	0.48	---	---	---	19.10	19.75
21	1-Butanol[a]	25.39[b]	18.96	19.65	----	----	0.51	---	---	---	19.00	19.62
22	2-Propanol[a]	25.46[b]	18.97	19.66	----	----	0.48	---	---	---	19.01	19.64
23	1-Propanol[a]	25.44[b]	18.95	19.64	----	----	0.47	---	---	---	18.92	19.54
24	Ethanol	25.53	18.93	19.34	6600	266	0.51	21.3	2.39	2.30	18.89	19.46
25	Methanol	25.49	18.85	19.22	6640	265	0.52	22.2	2.34	2.16	18.77	19.28
26	Water	25.85	18.01	18.38	7840	262	0.47	22	2.14	2.41	17.99	18.26

(a) Absorption and emission characteristics for these solvent are measured during present study while values for other solvents are taken from [30] and $\tilde{\nu}_{flu,\max}$ values are obtained from the author of [30].

(b) Absorption maxima.

5.1.2 Photophysical properties of 2,3,5,6-tetracyanohydroquinone.

Photophysical characteristics of 2,3,5,6-tetracyanohydroquinone (TCHQ) have not been studied in as many solvent as for PPDs and TMPPDs. But the absorption as well as emission behaviour of TCHQ in different solvents is very interesting and vary with concentration of TCHQ in solution. Both absorption and emission characteristic also depend on the type of solvent used. TCHQ is not soluble in apolar solvents like cyclohexane, n-hexance, benzene, toluene etc. So absorption and emission spectra has been obtained from slightly polar (ethers) to highly polar solvent like H_2O, DMSO.

Concentration dependence of the absorption spectra

It has been observed that there is large change in the absorption spectra with the change in concentration of TCHQ in solution and this change in absorption spectra also depends on the nature of solvent used. In very low polar solvents like diethyl ether and n-butyl ether. The absorption spectra show only one peak at 398 nm for different concentration. A very small rise in intensity around 460 nm in dilute solution of TCHQ in ethyl ether has been observed, which cannot be assigned a peak as shown in inset of Figure 5-9.

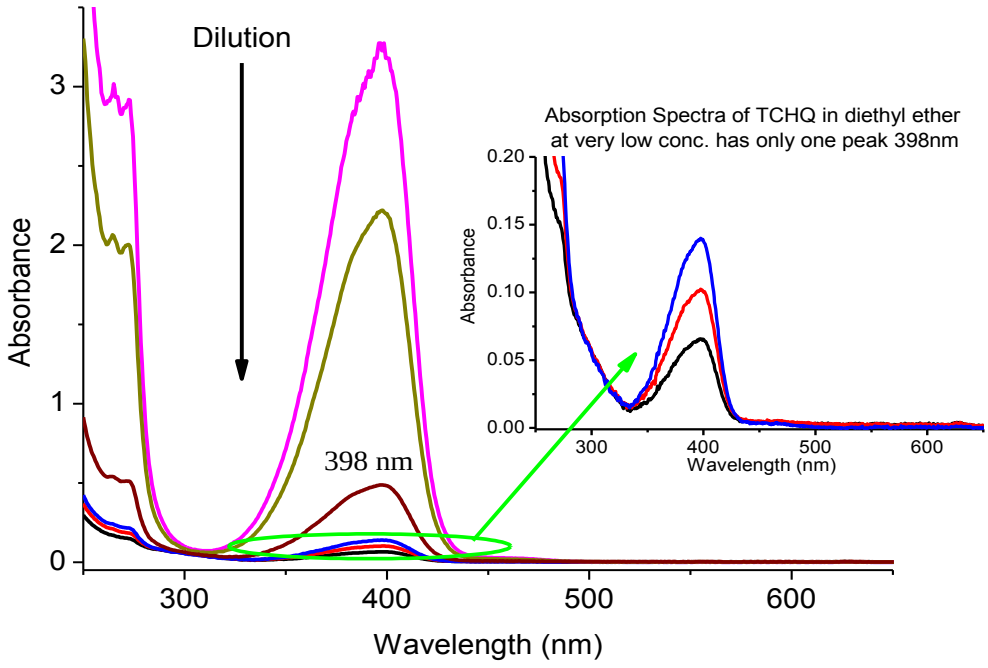

Figure 5-9: Absorption Spectra of TCHQ in diethyl ether at different concentrations.

Two peaks have been observed in the range of 300 to 600 nm for moderately polar solvents like acetone (Figure 5-10) and acetonitrile (Figure 5-11). The first peak is in the range of

390-400 nm and the second peak is around 505 nm. The peak at shorter wavelength is decreased sharply compare to the peak at longer wavelength with decrease in the concentration of TCHQ in both acetone and acetonitrile.

In acetonitrile, the two peaks are appeared at 392 nm and 502 nm. For solutions with conc. of TCHQ greater than $1x10^{-5}$ M, the intensity of the peak at 392 nm is higher compared to the peak at 502 nm. But in very dilute solutions conc. < $1x10^{-5}$ M, the intensity of the peak at 502 nm is higher compared to the one at shorter wavelength (392 nm) in acetonitrile. This non-linear decrease in the absorption intensity at two different wavelengths (392 nm and 502 nm) has been shown clearly in the Figure 5-12 (a) and Figure 5-12 (b) for the various concentration of TCHQ in acetonitrile.

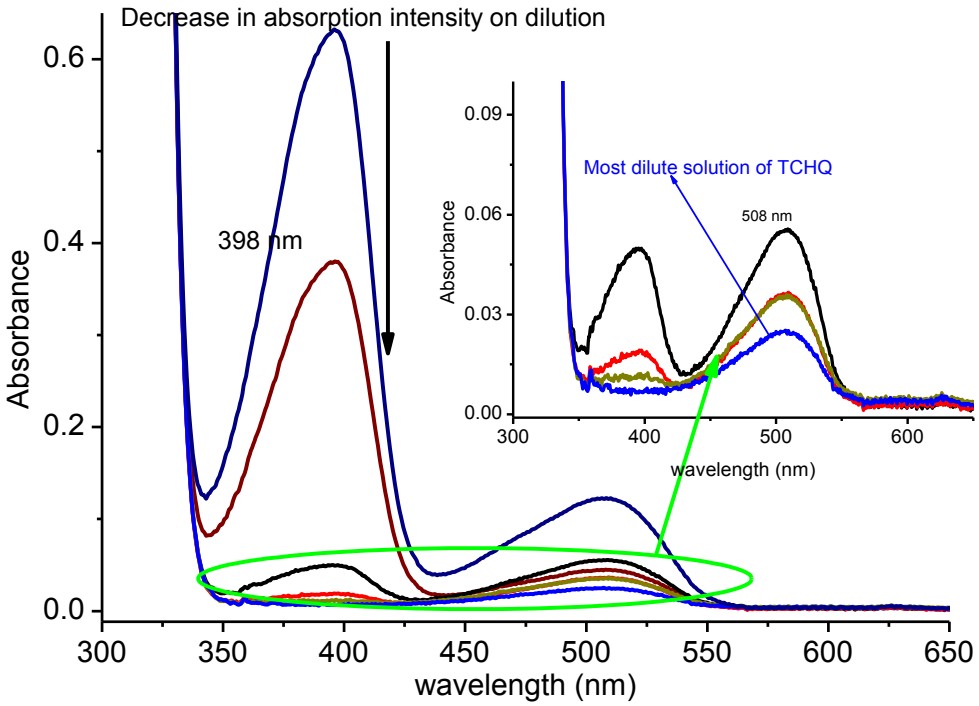

Figure 5-10: Absorption spectra of TCHQ in acetone at different concentrations.

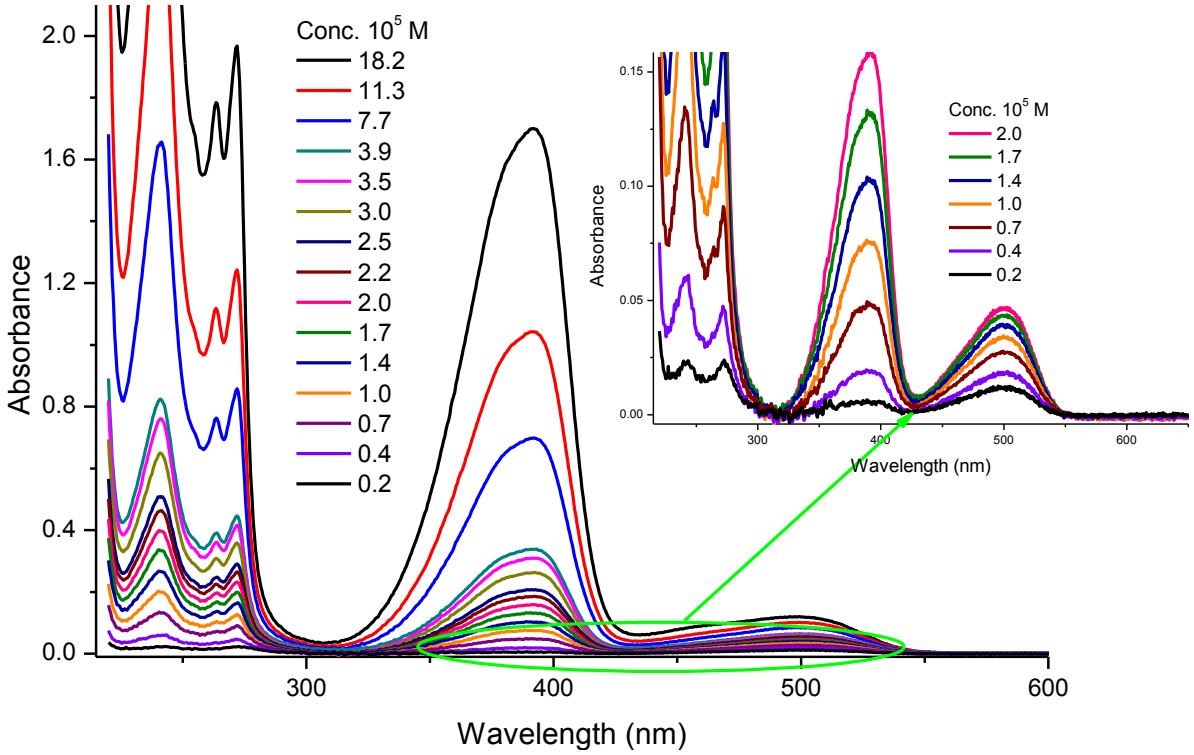

Figure 5-11: Absorption spectra of TCHQ in acetonitrile at different concentrations.

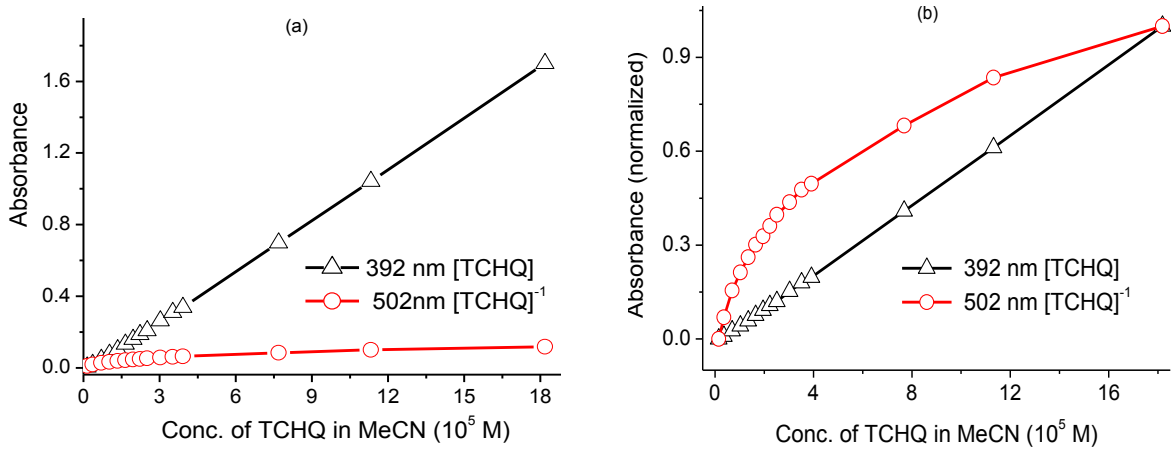

Figure 5-12: Absorbance (a) and normalized absorbance (b) of TCHQ in acetonitrile for different concentrations at 392 and 502 nm.

In DMSO again there are two peaks at 514 nm and 657 nm. In very dilute solutions with conc. less than $7x10^{-6}$ only one peak at 657nm appear, whereas in solutions with conc. > $7x10^{-6}$ M, there exist only one peak at 514 nm as shown in Figure 5-13. As discussed earlier for acetonitrile, non-linear decrease in absorption has been seen when plotting absorbance (at 514nm and 657nm) versus concentration of TCHQ in DMSO as shown in Figure 5-14.

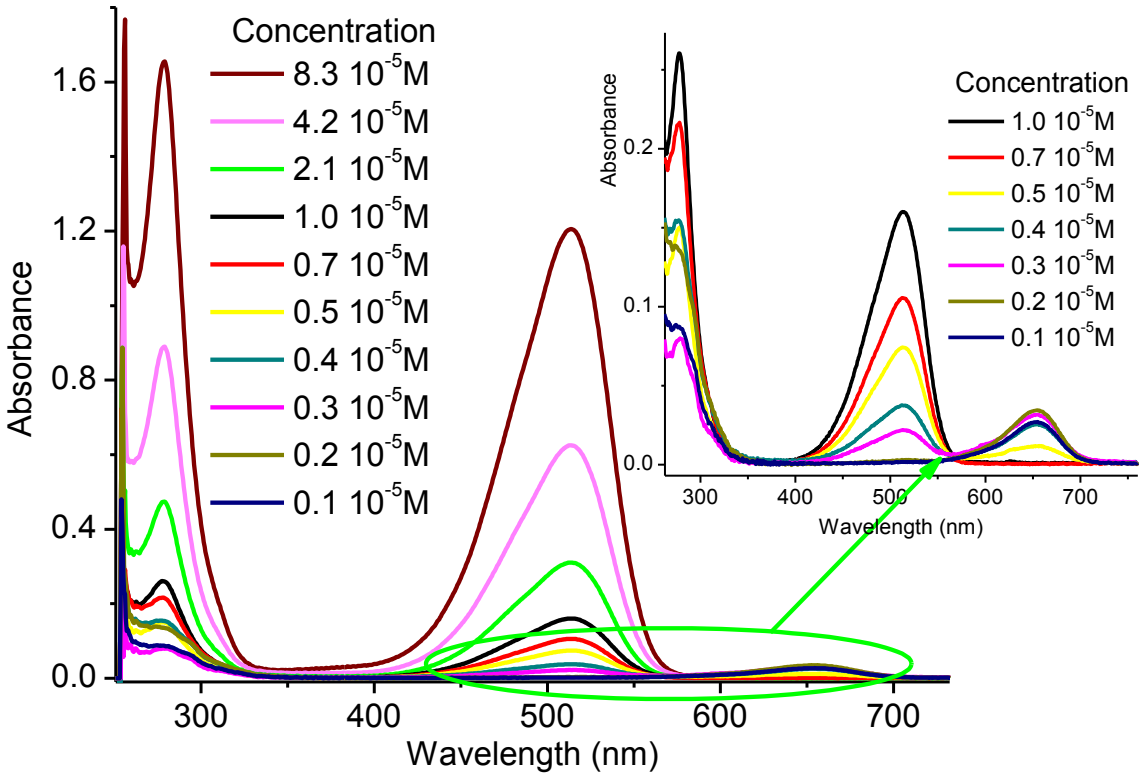

Figure 5-13: Absorption Spectra of TCHQ in DMSO at different concentrations.

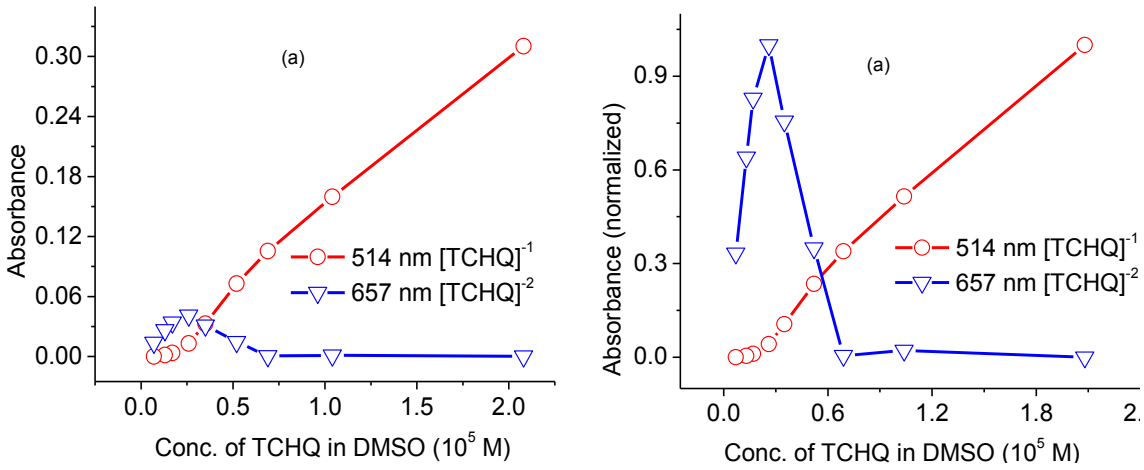

Figure 5-14: Absorbance (a) and normalized absorbance (b) of TCHQ in DMSO for different concentrations at 515 and 657 nm.

In water, TCHQ have been existed with two peaks for most of the concentration except very dilute one (conc. < $1x10^{-5}$ M). The two peaks for TCHQ in H_2O have been appeared at 460 nm and 520 nm which are also observed while measuring at different pH (section 5.2.1). So we are sure that the different peaks for TCHQ at different concentrations are in fact the deprotonated forms (mono-anion and di-anion) of TCHQ. Intensity of the peak at about 460

nm has been decreased rapidly compared to the peak at 520 nm, with the decrease in concentration of the TCHQ in H_2O as shown in Figure 5-16.

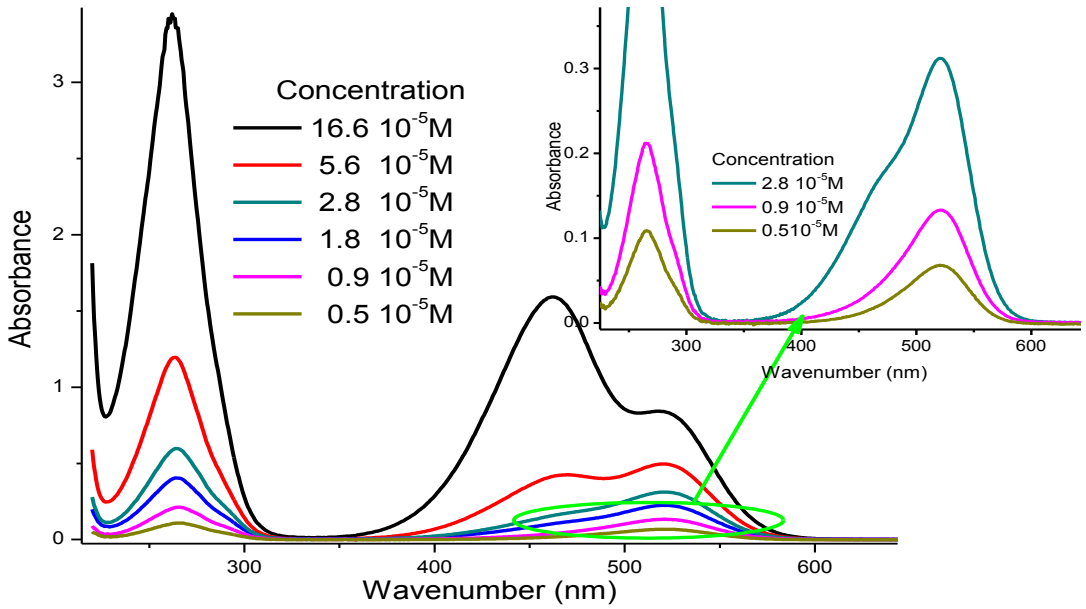

Figure 5-15: Absorption Spectra of TCHQ in H_2O at different concentrations.

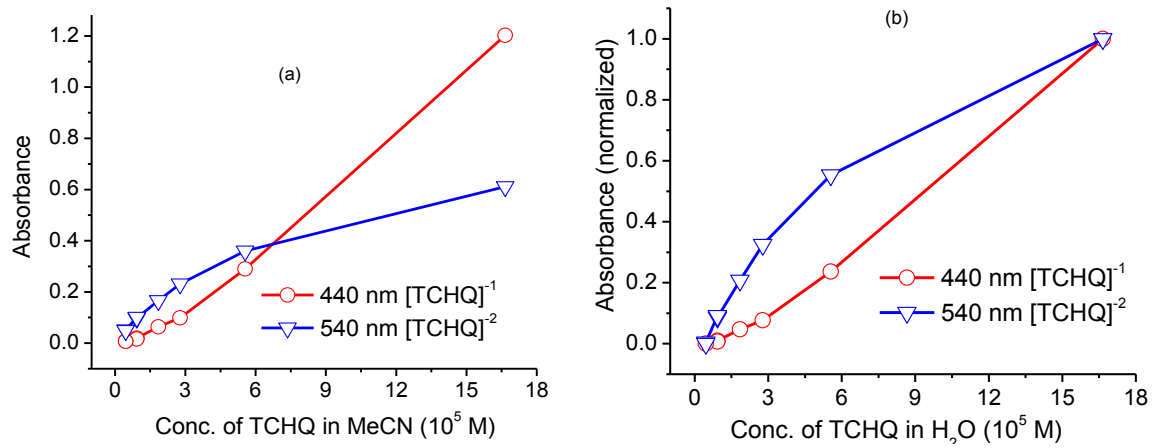

Figure 5-16: Absorbance (a) and normalized absorbance (b) of TCHQ in H_2O for different concentrations at 440 and 540 nm.

Two peaks (at 403nm and 473 nm) exist for the for different concentrations of TCHQ in absolute ethanol except for very dilute solutions (conc. < $5x10^{-6}$ M) which have only one peak at 473 nm as shown in Figure 5-17. The decrease in intensity of both peaks is not proportional to the concentration, but the intensity of peak at 403 nm decreases more sharply compared to that of the peak at 473 nm with decrease in concentration of TCHQ, as depicted in Figure 5-18.

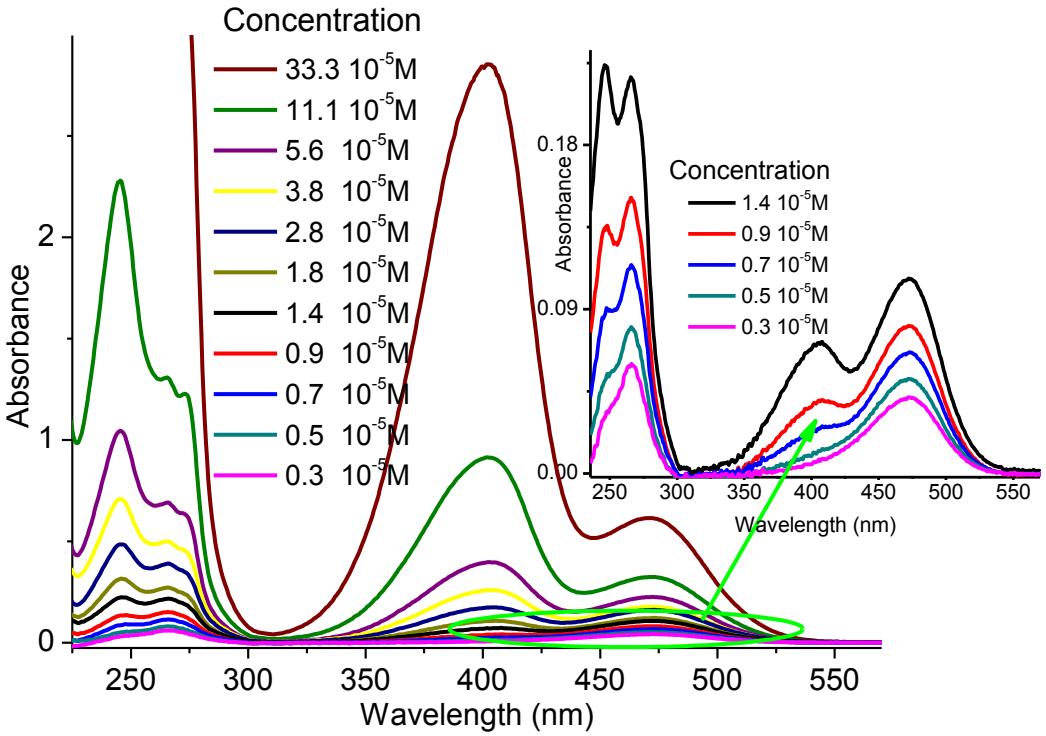

Figure 5-17: Absorption Spectra of TCHQ in absolute ethanol at different concentrations.

An additional peak at longer wavelength (543 nm) has been appeared by the addition of very small amount of water (less that 2%) into the dilute solution of TCHQ in absolute ethanol. This peak is probably due to di-anion of TCHQ which is formed in dilute solution of TCHQ in H_2O.

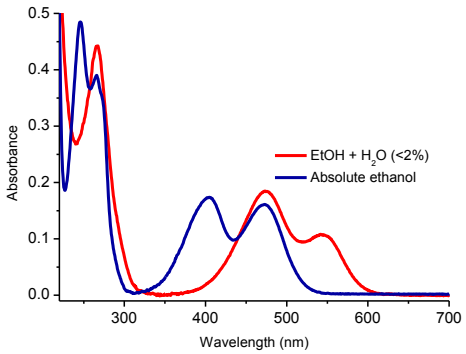

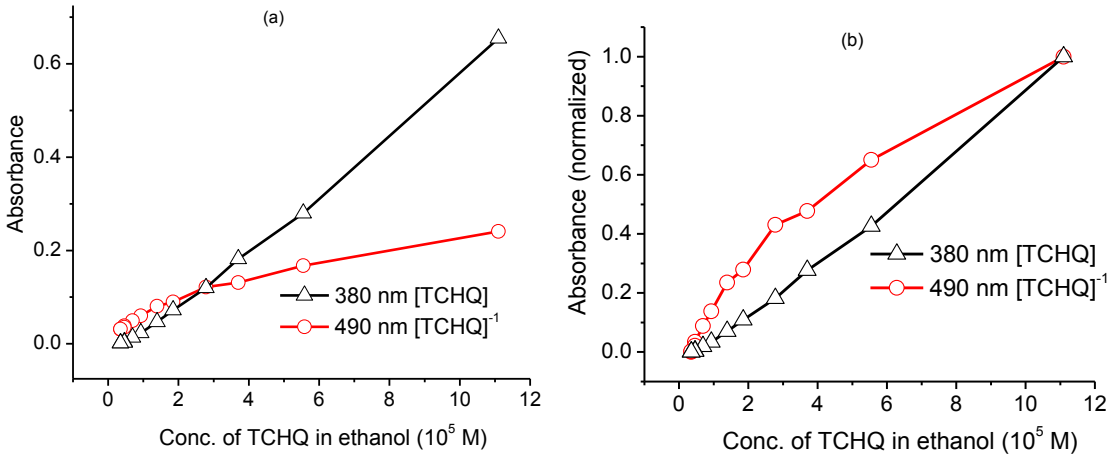

Figure 5-18: Absorbance (a) and normalized absorbance (b) of TCHQ in absolute ethanol for different concentrations at 380 and 490 nm.

TCHQ exist in two forms at different concentration in the solvents either as TCHQ and $TCHQ^{-1}$ (in acetone acetonitrile, ethanol) or $TCHQ^{-1}$ and $TCHQ^{-2}$ (DMSO and H_2O). But only one peak (the one at longer wavelength) is observed in very dilute solutions of TCHQ in acetone, acetonitrile, ethanol, DMSO and H_2O. When dilute solutions are concentrated by the addition of small quantity of TCHQ, a new peak at shorter wavelength has been appeared in addition to already existed peak. Sometimes the peak at longer wavelength is disapeared as in case of DMSO. This means that the effect of concentration is reversible.

The TCHQ exist in three forms in ground state in different solvents at various concentrations as shown by the absorption spectra. In ethers (diethylether and n-butylether), TCHQ exists more or less in the neutral form (λ_{max} 398 nm) which has also been seen in absorption of TCHQ in very acidic aqueous medium (H_o < -1), section 5.2.1. In moderately polar solvent (acetone, acetonitrile and ethanol), the absorption spectra show two peaks in concentrated solutions (absorbance >0.1) and in very dilute solution there exist only one peak. The two peaks correspond to the neutral and mono-anionic forms of TCHQ. In highly polar solvents (water and DMSO), no neutral form of TCHQ exist in concentrated solution. In water TCHQ has two peaks (461 nm and 520 nm for mono-anionic and di-anionic form of TCHQ, respectively) at reasonable concentrated solution (absorbance > 0.2), which have also been observed between the pH range 0-8 (see section 5.2.1). The peak position of absorption bands in different solvents are summarized in Table 5-8.

Fluorescence spectra in non-aqueous solvents

It has been shown by the absorption spectra that there exist more than one species at different concentration of TCHQ in solution. The fluorescence spectra in individual solvents, after exciting at various λ_{ext}, are shown in Figure A-1 to Figure A-7 in appendix. In dilute concentrations there is only one emission maxima is observed but in relatively concentrated solutions, emission by two species can be seen either in the form of additional peak (DEE and MeCN) or in the form of shoulder of the already existed peak (NBE, DMSO). So a more rigorous work is required to calculate the quantum yields for each of the specie (TCHQ, $TCHQ^-$ and $TCHQ^{2-}$). The aim is to show the various emission peaks from TCHQ and its anionic forms. The fluorescence maxima for these three species along with respective excitation wavelength λ_{ext} are summarized in Table 5-8. The normalized fluorescence spectra for the three species of TCHQ in different solvents have been shown in figure Figure 5-19. In this figure there exist different fluorescence maxima for TCHQ in different solvents.

TCHQ along with its mono-anionic and di-anionic forms, emit over a wide range (400nm to 750nm) of visible region of the light spectra.

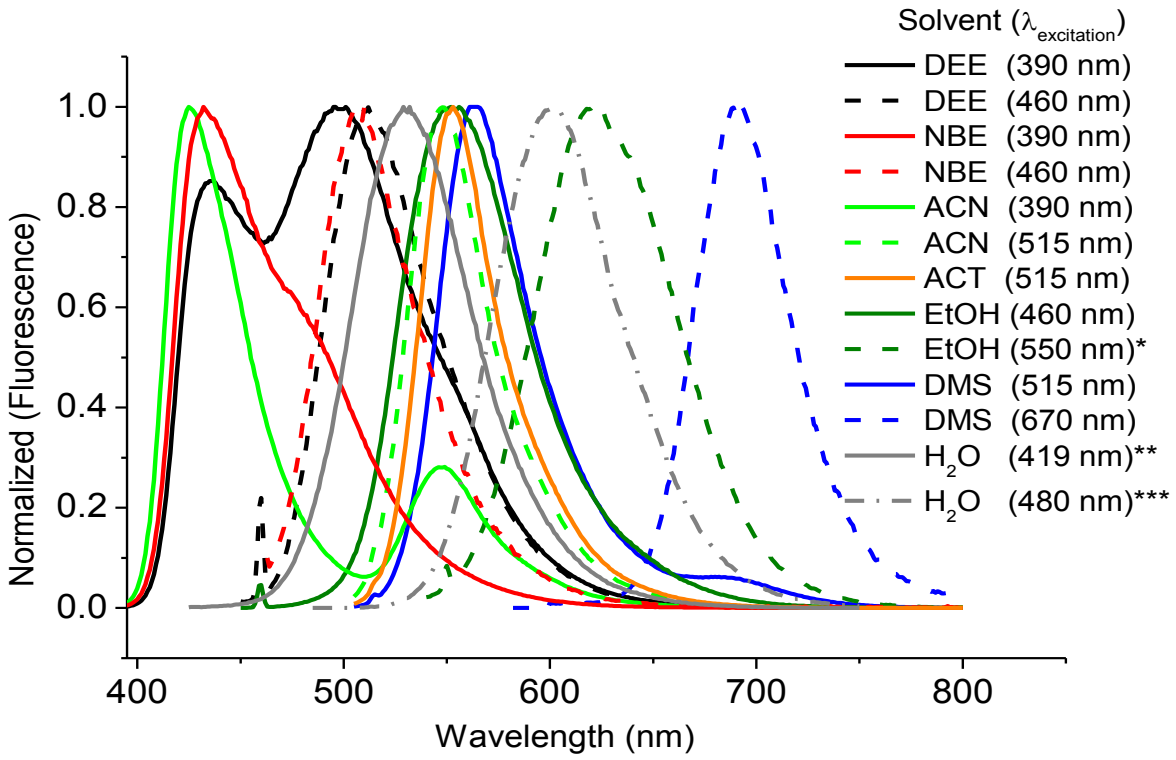

Figure 5-19: Fluorescence Spectra in different solvents; the solid line is comparatively concentrated solution of TCHQ than the dotted line in same solvent.
DEE (diethylether), NBE (n-butyleether), MeCN (acetonitrile), ACT (acetone), EtOH (ethanol), DMSO (dimethylsulfoxide). * add <2% H2O in EtOH **H2O at -3.6Ho and *** H2O at pH 7.8

Table 5-8: Absorption and fluorescence maxima of TCHQ, $[TCHQ]^{-1}$ and $[TCHQ]^{-2}$ in different solvents.

Solvents	Absorption maxima (λ_{abs})			Fluorescence maxima(λ_{flu})[(a)]		
	[TCHQ] (nm)	$[TCHQ]^{-1}$ (nm)	$[TCHQ]^{-2}$ (nm)	[TCHQ] (nm)	$[TCHQ]^{-1}$ (nm)	$[TCHQ]^{-2}$ (nm)
DEE	398	……	……	436,500(390)	511(460)	…
NBE	398	…..	……	433(390)	507(460)	…
MeCN	392	502	……	425(390)	548(515)	…
ACT	396	508	…..	…	553(515)	…
EtOH	403	473	543*	…	553(460)	621(550)*
H2O	398**	460	520***	…	532(419)**	601(481)***
DMSO	……	513.5	654	…	563(515)	692(670)

DEE (diethylether), NBE (n-butyleether), MeCN (acetonitrile), ACT (acetone), EtOH (ethanol), DMSO (dimethylsulfoxide). *EtOH + H2O (<2%) ** at Ho < -1 *** H2O at pH 7.8

(a) The values in parenthesis correspond to the excitation wavelength.

Absorption spectra of TCHQ in binary mixtures

In order to know more about the absorption characteristics of TCHQ, the absorption spectra of TCHQ have been measured in two different solvent binary mixtures. In these binary mixtures one part is chosen as H_2O where as the second partners are acetonitrile and DMSO. The concentration of TCHQ remains the same while varying the volume ratio of water in the binary mixture.

In case of water and DMSO solvent mixture, the concentration of the TCHQ is $2.8x10^{5}$ M. The absorption spectra at various volume ratios of binary mixture have been shown in fig. It has been observed that in pure DMSO there is only one peak at 514 nm. The intensity of this peak has been decrease and shifted hypsochromically with increase in the water volume ratio upto 20%, as shown by the Figure 5-20. A new peak has been appeared at longer wavelength with further increase in water contents (greater than 20%) in the solvent mixture. In the solution which contains only 2% of DMSO, there are two peaks at 521 nm and 469 nm.

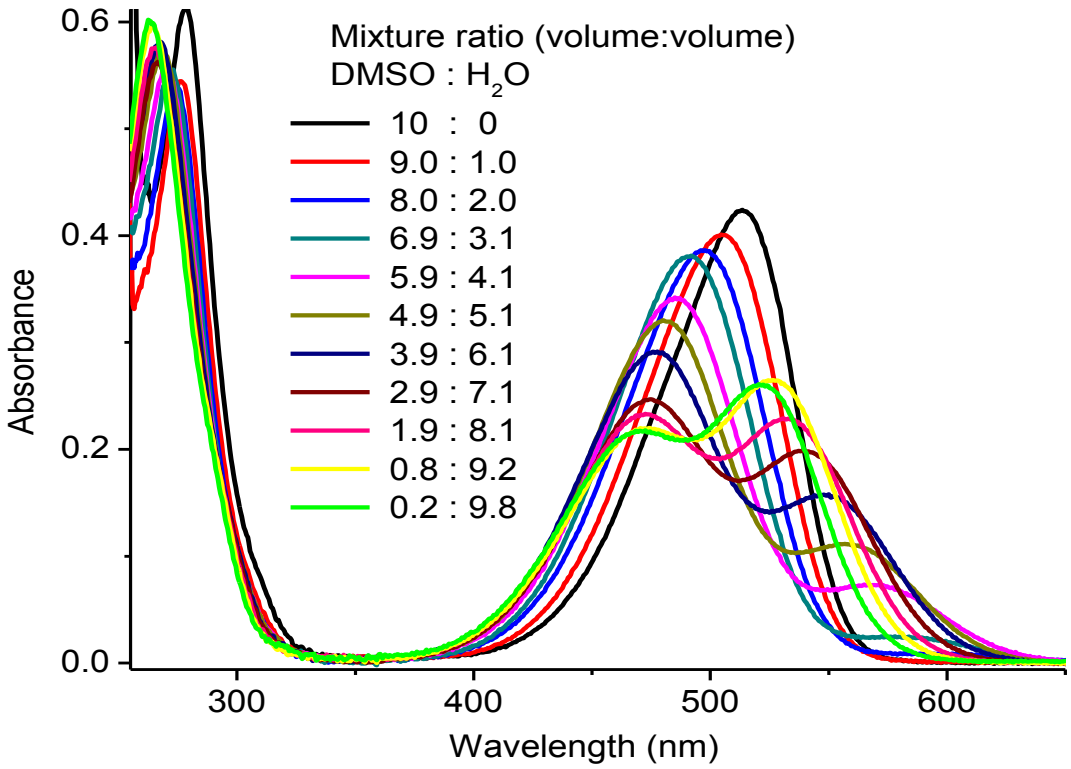

Figure 5-20: Absorption spectra of TCHQ (conc. 2.8x10-5 M) in DMSO-water mixture (vol. by vol.)

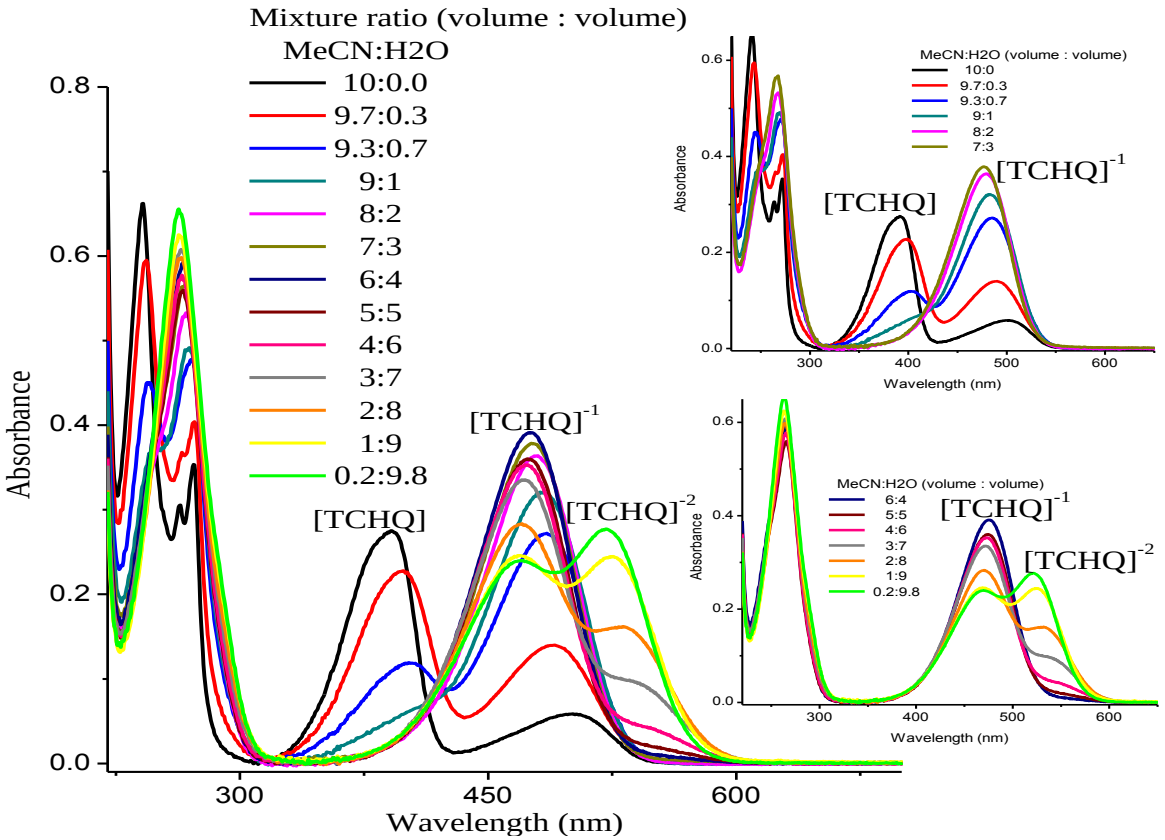

Figure 5-21: Absorption spectra of TCHQ (3x10-5M) in acetonitrile-water mixture (vol. by vol.).

In acetonitrile-water mixture, three different peaks have been seen by changing the volume ratio of the two solvents. The concentration of TCHQ for this solvent mixture is $3x10^5$ M. In pure acetonitrile there are two peaks at 392 nm and 502 nm. A red shift in the peak at 392 nm and a blue shift in the second peak (at 502 nm) have been observed with a small addition of water. The peak at 392 nm has been vanished at about 10% of water contents in the solvent mixture, as shown by Figure 5-21. From about 15% to 50% volume of water contents there is only one peak which is shifted hypsochromically with increasing aqueous component of mixture. A new peak has been appeared at the longer wavelength of already exited peak and shifted hypsochromically with further increasing water contents (more than 50%),

The absorption spectra of TCHQ in different solvent mixtures also show that the TCHQ exist in DMSO-water mixture, at a reasonably concentrated solution ~ $3x10^5$ M, in only mono-anionic form (λ_{max} 514 nm) in pure DMSO (have high proton accepting ability, β), which changes to two peaks for mono-anionic and di-anionic forms on addition of water. In case acetonitrile-water mixture, pure acetonitrile contains two peaks for the neutral TCHQ and its anion at concentration of about $3x10^{-5}$ M. Very small addition of water have changed

the neutral TCHQ by into its mono-anion by donate proton to water molecules. Further increase in water contents have led to the formation of di-anion form of TCHQ by giving away both of its protons to water.

5.2 Ground and excited state proton transfer equilibrium

In order to determine the acid-base equilibrium constants for the ground and excited state proton transfer, the absorption and fluorescence spectra of solute have been determined at different pH/H_o values. Ground and excited state proton transfer equilibrium studies have been performed for TCHQ and 26DCPPD.

5.2.1 Ground and excited state pKa for TCHQ

Absorption spectra of TCHQ in aqueous solution with concentration of about 10^{-5} M (absorbance at $\lambda_{max} \cong 0.1$) has been determined at different pH/H_o values. The absorption spectra show three different peaks at 398, 460 and 520 nm, and in between these, three peaks there are two isosbestic points at 419 and 480 nm at different pH/H_o values as shown in Figure 5-22. The ground state pK_a values have been estimated by plotting the relative intensities of the unprotonated, mono-protonated and di-protonated species at various pH/H_o values as shown in Figure 5-23. The two pK_a values, i.e. pK_{a1} 0.8 (for TCHQ and its mono-anion) and pK_{a2} 3.8 (for mono-anion and di-anion) have been obtained as shown in Scheme 5-1. From pH = 7.8 to pH = 5.0, there exists only one peak at 520 nm for the di-anion of TCHQ ($TCHQ^{2-}$). A new peak at 460 nm start appearing with further decrease in pH of solution and at pH 2 there is again a single peak at 460 nm which corresponds to the mono-anion of TCHQ ($TCHQ^{1-}$). Further increase in $[H^+]$, by using different dilutions of $HClO_4$, a new peak at 398 nm is start rising and in very strong acidic solutions (at $H_o < 2$) there exists again one peak which is in fact the neutral TCHQ. A small shift in absorption spectra below H_o -2.5 has been seen which is probably due to high concentration of $[H^+]$ in the medium.

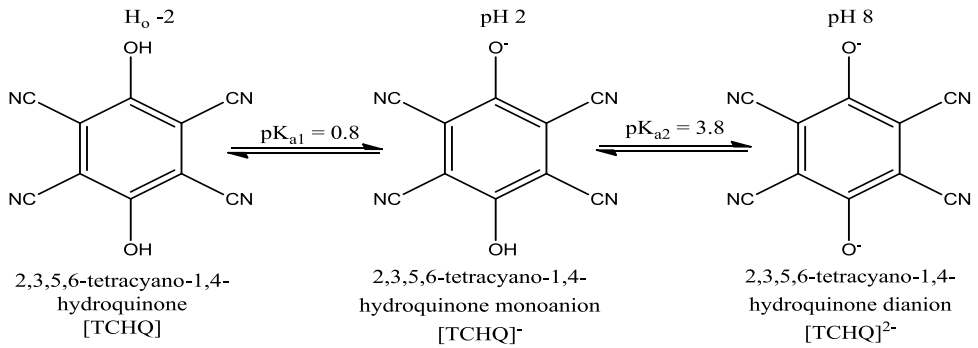

Scheme 5-1

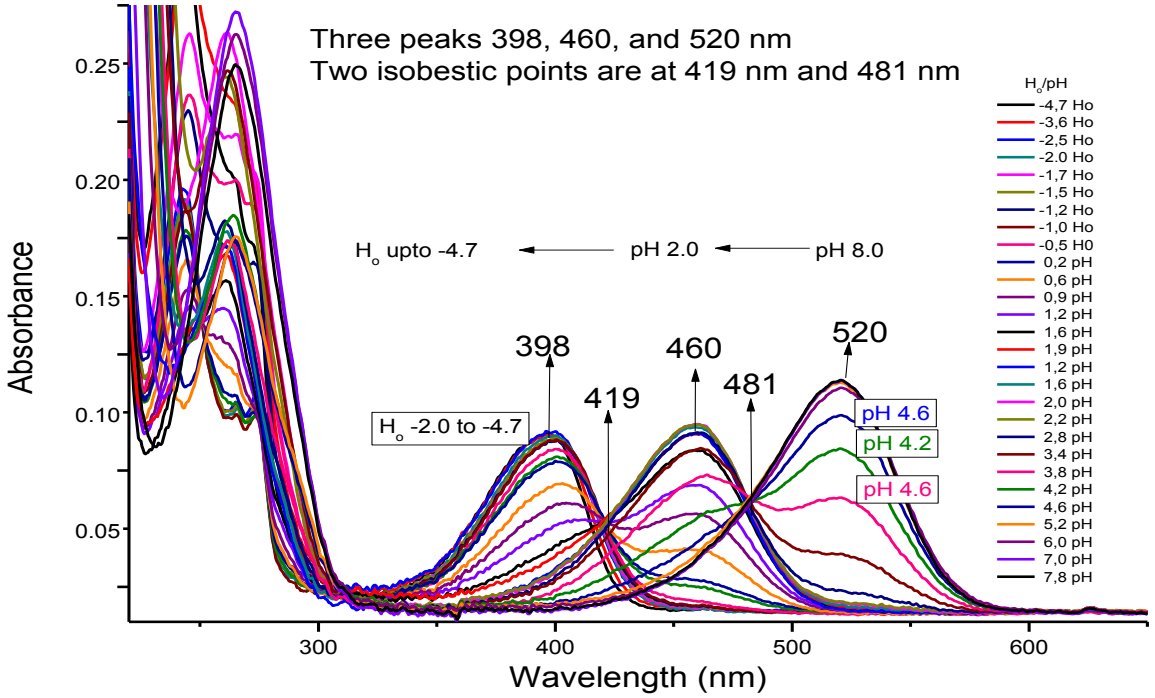

Figure 5-22: Absorption spectra of TCHQ at different pH and H_o values.

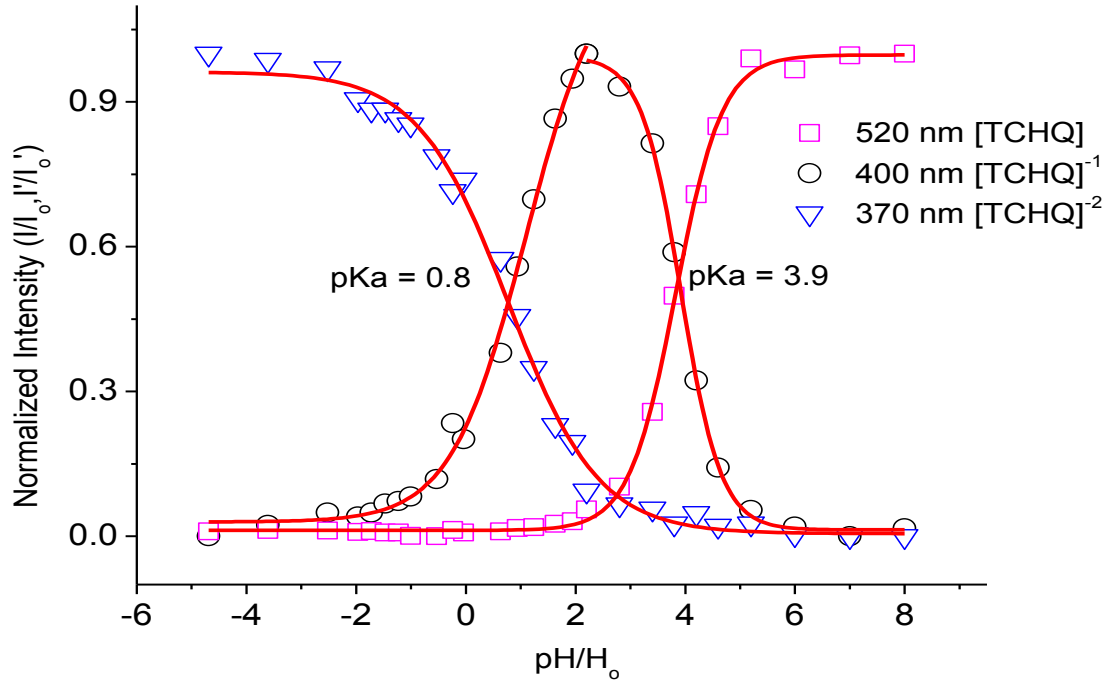

Figure 5-23: Normalized absorption intensity of TCHQ and its mono and di-anion measured at different pH and H_o values.

Excited state acid-base equilibrium constant, pK_a^*, has been estimated from the fluorescence spectra determined at different pH/H_o values. The two isosbestic points (419 nm and 480 nm) have been chosen as excitation wavelengths. The fluorescence spectra, after excitation

at 419 nm, at different pH/H_o values of solution give rise to the two different peaks at 601 nm and 532 nm as shown in Figure 5-24. This shows the fact that two different species are emitting when exciting at 419 nm for solution of TCHQ at different pH/H_o. When excited at 480 nm, only one peak (at 601 nm and is similar to the one of the peaks observed after excitation at 419 nm) has been observed for different pH values. The intensity of this peak (601 nm) is decreased with decreasing the pH/H_o value of the solution Figure 5-25 and this decrease in emission intensity is due to the fact that less number of molecules are available in the ground state for these pH/H_o values when excited at 480 nm i.e. due to lower absorption. The decrease in absorption intensity (at 419 nm) due to shift of absorption band for H_o < -2.5 has been compensated by multiplying the relative amount of light absorbed when plotting the normalized fluorescence for 419 nm. The normalized fluorescence intensities at two different wavelengths, 523 nm & 640 nm, for excitation at 419 nm and at wavelength 640 nm for exciting at 480 nm have been obtained. The value for pK_a^* has been estimated by plotting the relative normalized fluorescence intensity versus pH/H_o values as shown in Figure 5-26.The point of intersection for two sigmoidal curves for 523 nm and 640 nm (after excitation at 419 nm) corresponds to the pKa* value which is -1.1 and other midpoints for the sigmoidal curves for 640 nm at pH 1.0 (after excitation at 419 nm) and for 640 nm at pH 3.9 (after excitation at 480 nm) are just the pK_a values of TCHQ.

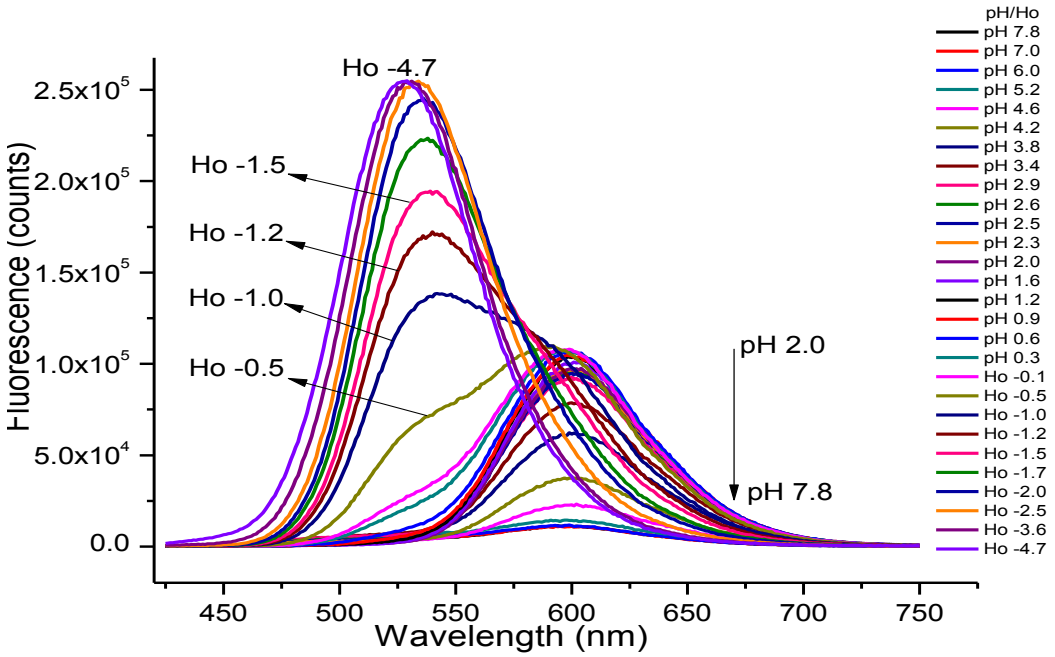

Figure 5-24: Fluorescence spectra of TCHQ measured at different pH and H_o values after exciting at 419 nm.

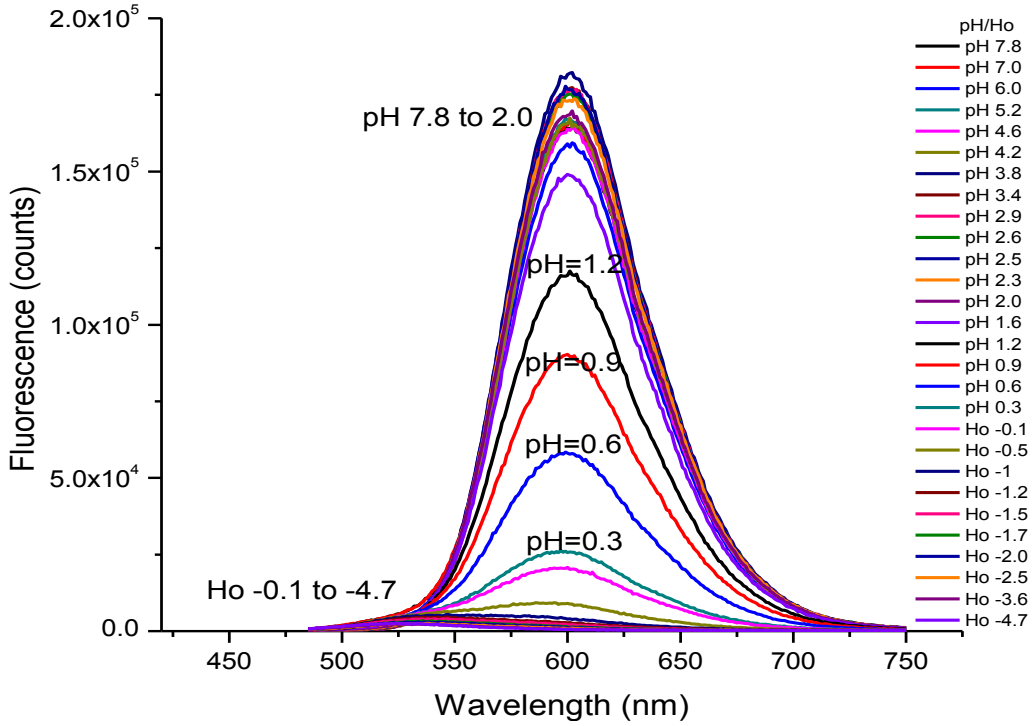

Figure 5-25: Fluorescence spectra of TCHQ measured at different pH and H_o values after exciting at 480 nm.

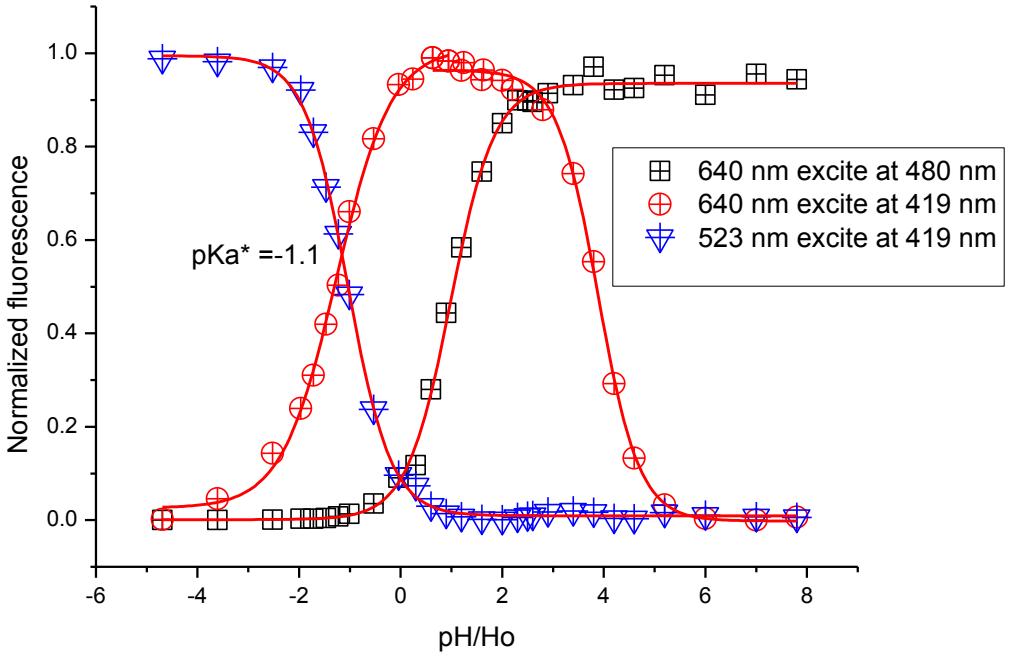

Figure 5-26: Normalized fluorescence intensity of TCHQ mono-anion and di-anion measured at different pH and H_o values.

The absorption and emission of TCHQ in 0.1N solution is NaOH is similar to that measured for pH 7.8 (not shown here). Only one pK_a^* value (pK_a^*= -1.1) for TCHQ has been obtained in aqueous solution at various values of pH and H_o as shown in Scheme 5-2.

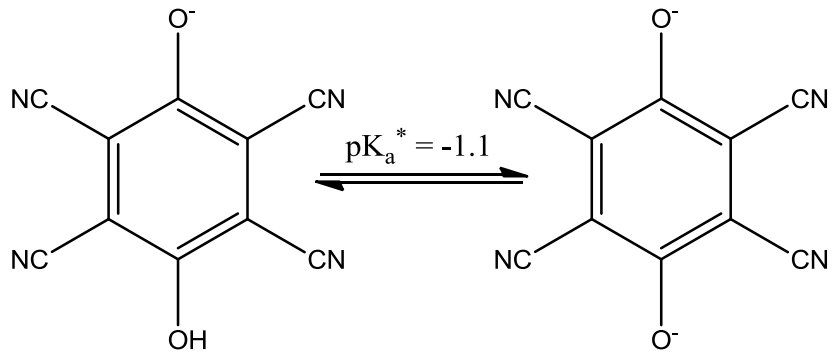

2,3,5,6-tetracyano-1,4-hydroquinone monoanion $[TCHQ]^-$

2,3,5,6-tetracyano-1,4-hydroquinone dianion $[TCHQ]^{2-}$

Scheme 5-2: pK_a^* of TCHQ.

5.2.2 Ground and excited state pK_a for 26DCPPD

The absorption and fluorescence spectra have been recorded at different *pH* (from 1 to 8) and H_0 scale (up to -5). A plot of absorption spectra at different *pH* is shown in Figure 5-27. Going from pH=1 to H_0= -4.7, there is no further change in the absorption spectra of DCPPD. The formal concentration of DCPPD is strictly the same in solutions at different *pH*. Three isosbestic points (at 265nm, 303nm and 370nm) are clearly observed. There are two species in the *pH* range from 6 to H_0 -4.69 in the ground state.

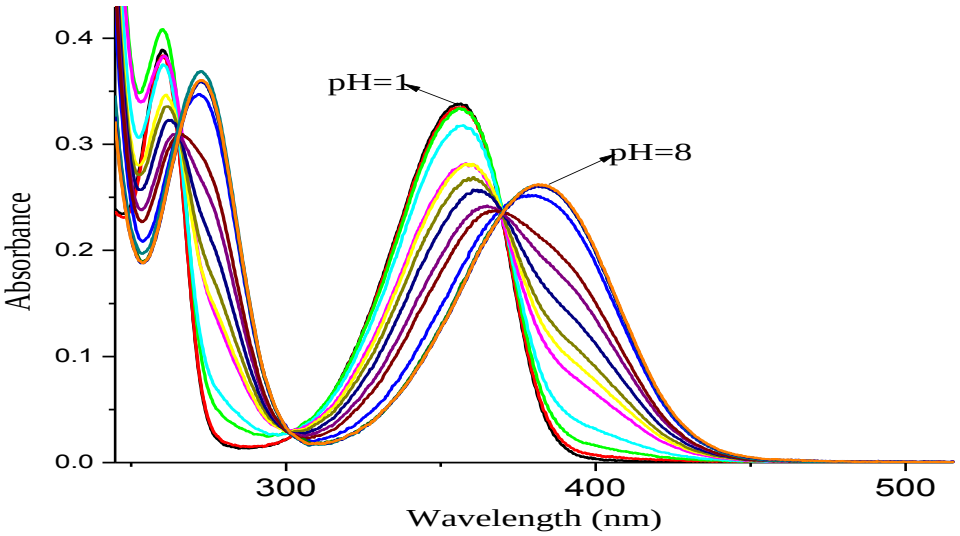

Figure 5-27: Absorption of DCPPD at pH=8 to pH=1 showing three isosbestic points (265nm, 303nm and 370nm).

The ground state pK_a value is calculated using different methods, (a) from the relative intensity of the absorption of the protonated and unprotonated form, (b) using the Henderson-Hasselbalch method.

Figure 5-28 shows the titration curves with the relative absorbance intensities of the two species, protonated (I'/I'_o) and unprotonated (I/I_o) involved in the acid-base equilibrium upon changing the *pH* of the solution. There is a decrease in the intensity of the unprotonated form (λ_{max} = 382 nm) with a corresponding increase in the intensity of the protonated form (λ_{max} = 356 nm) as the *pH* goes from 8 to 1. Both sigmoidal curves intersect at a *pH* of 3.5 which is the pK_a value for DCPPD.

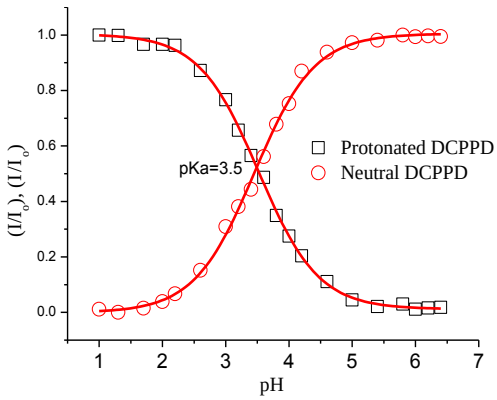

Figure 5-28: Relative absorption intensities of the protonated and unprotonated or neutral DCPPD measured at different pH values.

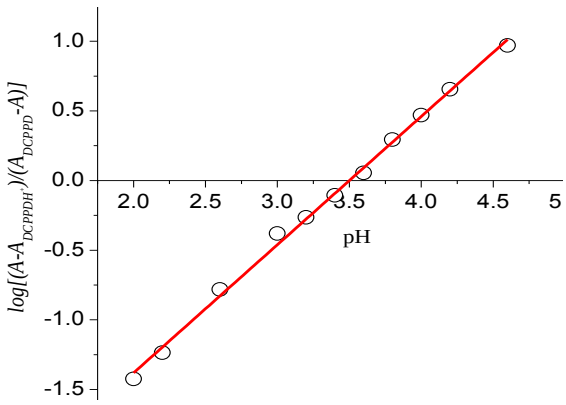

Figure 5-29: Evaluation of pH dependence of absorption spectrum of using Henerson-Hasselbach equation.

DCPPD exists in the following equilibrium at different pH

$$DCPPD + H_3O^+ \underset{k_r}{\overset{k_f}{\rightleftharpoons}} DCPPDH^+ + H_2O$$

k_f and k_r are rates of forward and reverse reactions, respectively. Additionally, the Henderson–Hasselbalch method (eq. 5-1, shown in Figure 5-29) has been applied for the determination of the pK_a value for the above acid-base equilibrium.

$$pH = pK_a + \log\left(\frac{A - A_{DCPPDH^+}}{A_{DCPPD} - A}\right) \qquad 5\text{-}1$$

where A_{DCPPD} and $A_{DCPPDH+}$ are the absorbance of the neutral DCPPD and its protonated form at a determined wavelength, while *A* denotes the absorbance due to both neutral and protonated form of DCPPD.

Steady state fluorescence titration and Förster cycle [147-149, 229] have been used for the estimation of the excited state pK_a^* value. Steady state fluorescence spectra have been obtained by excitation at the isosbestic point lying at the longest wavelength, 370 nm. Fluorescence spectra of DCPPD at different *pH* are shown in Figure 5-30. The titration

curves of fluorescence for the relative intensities of both protonated (I'/I'_o) and unprotonated (I/I_o) forms against different *pH* and H_0 values are shown in Figure 5-31.

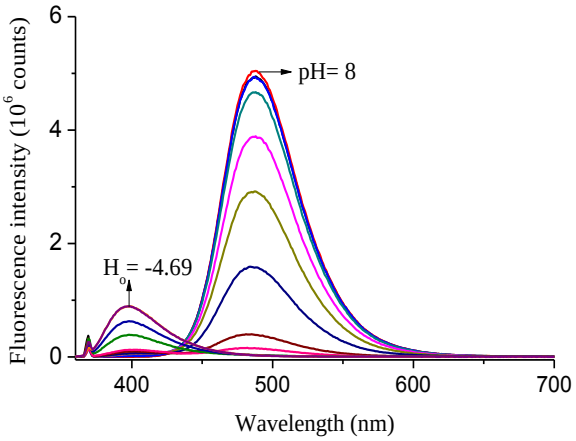

Figure 5-30: Fluorescence spectra of DCPPD at different pH and Ho values (pH=8 to Ho= -4.69) excited at 370nm.

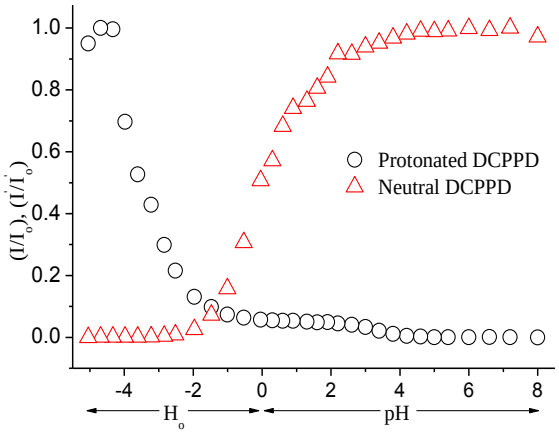

Figure 5-31: Relative emission intensities of protonated and unprotonated DCPPD at different pH and Ho values.

Two curves obtained are not at all symmetrical respect to each other. The emission intensity of the unprotonated form decreases but no corresponding increase in the emission intensity of the protonated form is observed in the same range of pH/H_0. This may indicate the quenching of the excited state at higher proton concentrations. Such a quenching behavior has been observed for other amino (-NH_2) substituted aromatic compounds [230-235] and also for phenylendiamines [236]. We have tried to simulate these curves with a single set of kinetic equations taking into account the quenching processes but we did not succeed so far to reproduce the experimental observations. Additional experiments have to be performed to clarify this quite unusual situation. The third non-emissive excited state species cannot be excluded as there is no clear isostilbic point (*cf.* Figure 5-30). One of the possible pathways for excited state equilibrium is shown Scheme 5-3.

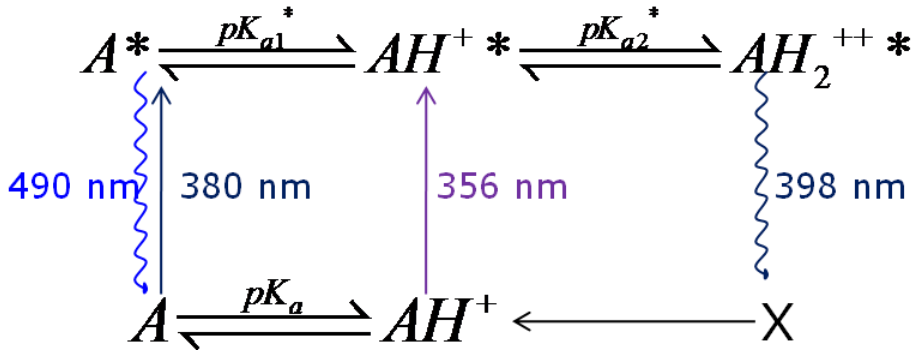

Scheme 5-3

There is no other emission from any third species has been found by exciting the solution of 26DCPPD (at H_o= -2.1) for the whole absorption band (310 to 390 nm) as shown in Figure 5-32.

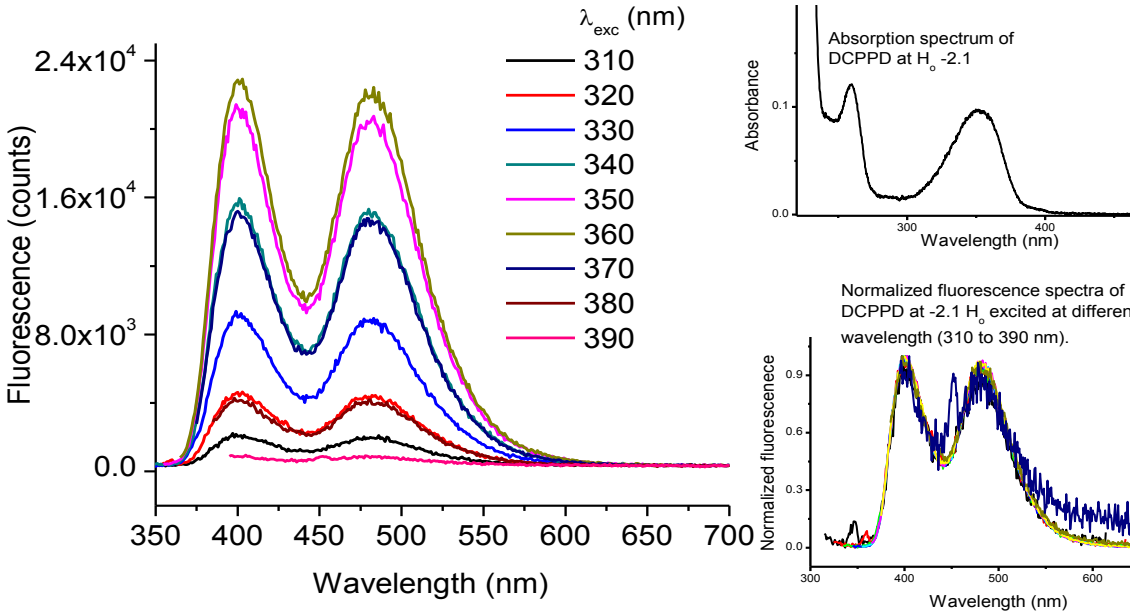

Figure 5-32: Fluorescence spectra of DCPPD at H_o = -2.1 by exciting at different wavelengths (310 to 390 nm).

Anyhow, the estimation of the excited state equilibrium constant, pK_a^*, can be obtained by using the Förster cycle method [148]. It is based on ground state thermodynamics and electronic transition energies. Equation (6) has been used to calculate the pK_a^*.

$$\Delta pK = pK_a - pK_a^* = \frac{E_{AH} - E_{A^-}}{2.303RT} \qquad (6)$$

E_{AH} and E_{A-} are the *0-0* transition energies of protonated and unprotonated forms. Using eq. 6 the calculated *pKa** value is -3.9 which does not coincide at all with the inflection point of the *AH* form titration curve, placed around *pH* = 0.

Both methods (fluorescence titration and Förster cycle) for the estimation of the pK_a^* value are based on the assumption that the excited state proton transfer is very fast and that the acid-base equilibrium is established during the lifetime of the excited state, and that there are no deformations of the excited state forms –no large entropic differences between the ground and excited state processes [149, 237]. However, we want to insist that in the present case proton induced fluorescence quenching can compete with the proton transfer reaction in the excited state and other excited state species cannot be ruled out. Under such conditions, the most reliable value for the pK_a^* can only be obtained by a dynamic analysis [150-152].

5.3 Solvatochromic study

The solvatochromic studies have been performed using individual parameter like *ETN* or set of parameters like Kamlet-Taft parameters (*α, β and* π^*), Javier Catalan parameters (*SA, SB, Sdp and Sp*), combination of *ETN* & *DNN* and Onsager polarity parameters, $f(n^2)$ and $f(D, n^2)$. The Onsager parameters depend on the refractive index and dielectric constant of the solvents as shown by below:

$$f(D,n^2) = f(D) - f(n^2)$$

$$f(n^2) = \frac{n^2-1}{2n^2+1} \qquad \text{and} \qquad f(D) = \frac{D-1}{2D+1}$$

Linear solvation energy relationship (LSER), using multiparameter approach, as discussed in chapter 2, has been applied to study the interaction between the solvent and solute molecules. Three different types of such as, (a) semi-empirical using Kamlet-Taft and Catalan's parameters (b) empirical using ETN& DNN parameters and (c) physical using Onsager polarity parameters, have been applied.

5.3.1 Semi-empirical correlation

Both Kamlet-Taft and Javier Catalan parameter sets have been applied to relate both, the absorption as well as emission maxima of different cyano-substituted derivatives of PPD and TMPPD, with the solvent properties like solvent acidity (*α* or *SA*), solvent basicity (*β* or *SB*) and solvent polarity/polarizability (*π** or *Sdp* and Sp). The theoretically calculated values of absorption or fluorescence maxima (obtained from LSER analysis) were plotted against the corresponding experimentally obtained values. These plots for cyano-substituted PPDs are shown in Figure 5-33 (LSER for PPD), Figure 5-34 (LSER for MCPPD), Figure 5-35 (LSER for 26DCPPD) and Figure 5-36 (LSER for TCPPD). The coefficients of $\tilde{\nu}_0$, *α, β* and *π** obtained after applying the Kamlet-Taft parameters are summarized in Table 5-9 and those of $\tilde{\nu}_0$, *SA, SB, Sdp* and *Sp* obtained using Catalan parameters are given in Table 5-10. LSER analysis, using Kamlet-Taft and Catalan parameters, for cyano-substituted TMPPDs are shown from Figure 5-37 to Figure 5-39. The values for LSER coefficients are collected in Table 5-11 (for TMPPD and MCTMPPD) and in Table 5-12 (for DCTMPPD). LSER analysis for DCTMPPD is performed for fluorescence maxima $\tilde{\nu}_{flu,\max}$ and fluorescence center of gravity $\tilde{\nu}_{flu,cog}$. No correlation for absorption for DCTMPPD has been performed.

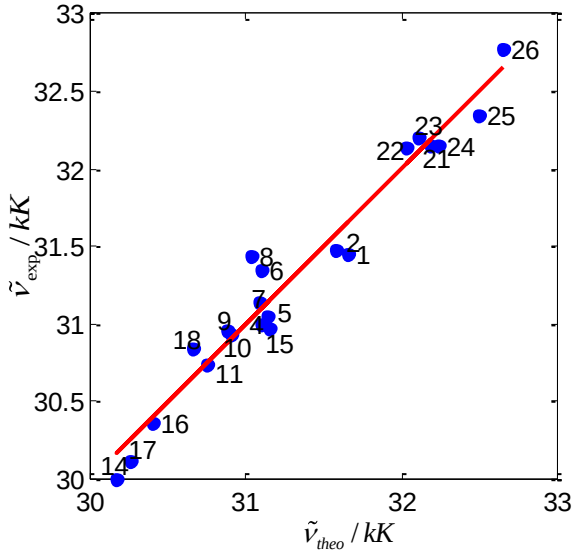

(a) LSER analysis for the absorption maxima $(\tilde{\nu}_{abs})$ of PPD using Kamlet-Taft parameters.

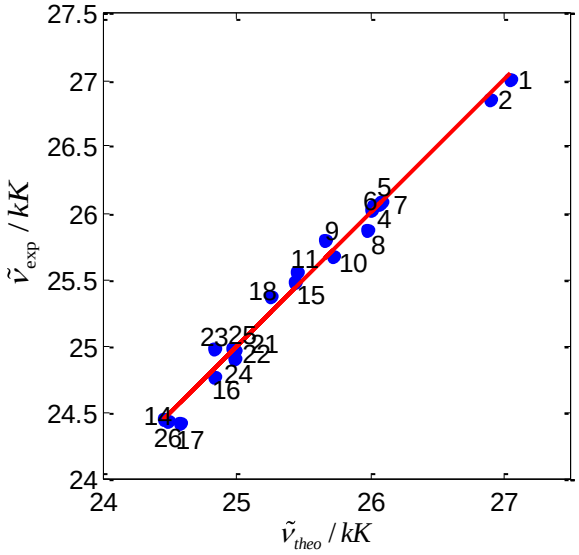

(c) LSER analysis for the fluorescence maxima $(\tilde{\nu}_{flu})$ of PPD using Kamlet-Taft parameters.

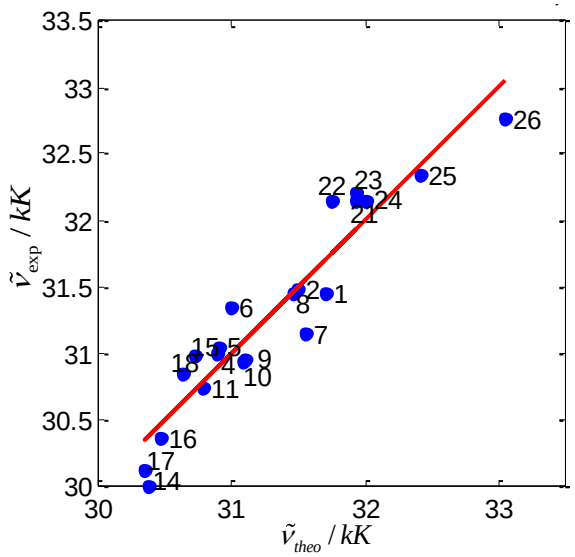

(b) LSER analysis for the absorption maxima $(\tilde{\nu}_{abs})$ of PPD using Catalan's parameters.

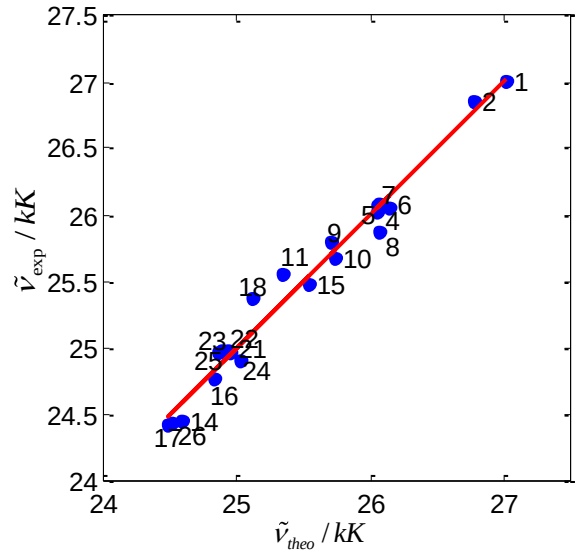

(d) LSER analysis for the fluorescence maxima $(\tilde{\nu}_{flu})$ of PPD using Catalan's parameters.

Figure 5-33: Linear solvation energy relationship (LSER) for the absorption (a and b) and fluorescence (c and d) maxima of PPD using Kamlet-Taft (a and c) as well as Catalan (b and d) parameters for 21 solvents.

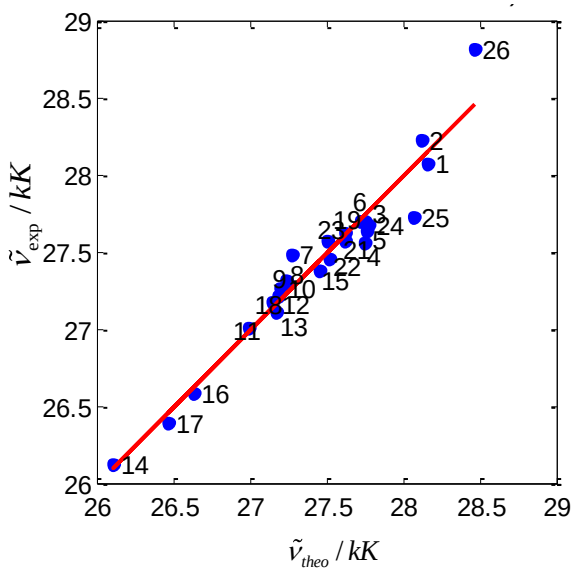

(a) LSER analysis for the absorption maxima $(\tilde{\nu}_{abs})$ of MCPPD using Kamlet-Taft parameters.

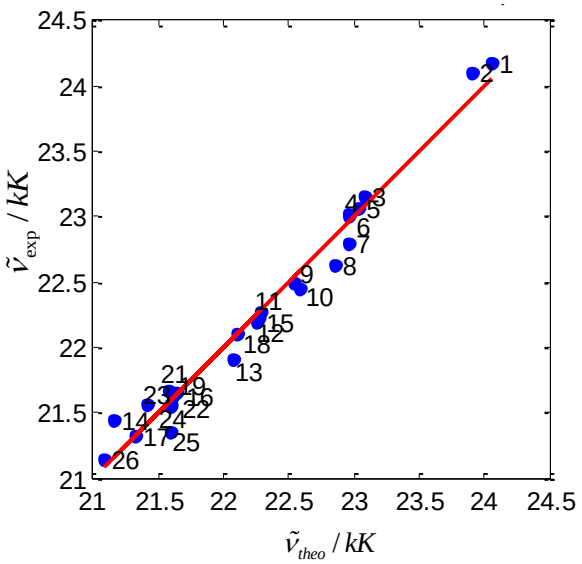

(c) LSER analysis for the fluorescence maxima $(\tilde{\nu}_{flu})$ of MCPPD using Kamlet-Taft parameters.

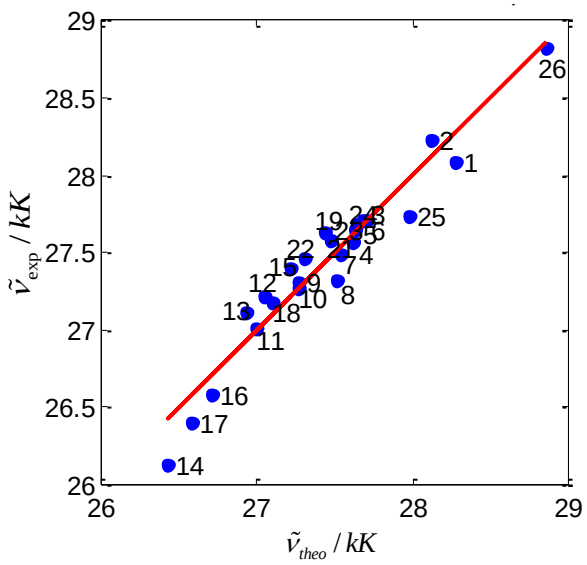

(b) LSER analysis for the absorption maxima $(\tilde{\nu}_{abs})$ of MCPPD using Catalan's parameters.

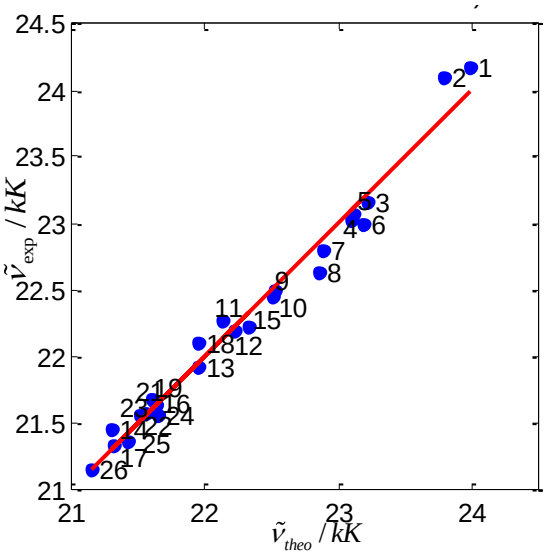

(d) LSER analysis for the fluorescence maxima $(\tilde{\nu}_{flu})$ of MCPPD using Catalan's parameters

Figure 5-34: Linear solvation energy relationship (LSER) for the absorption (a and b) and fluorescence (c and d) maxima of MCPPD using Kamlet-Taft (a and c) as well as Catalan (b and d) parameters for 25 solvents.

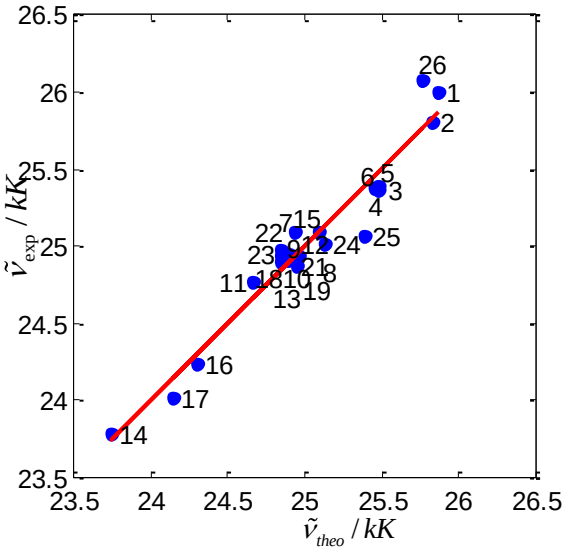

(a) LSER analysis for the absorption maxima $(\tilde{\nu}_{abs})$ of DCPPD using Kamlet-Taft parameters.

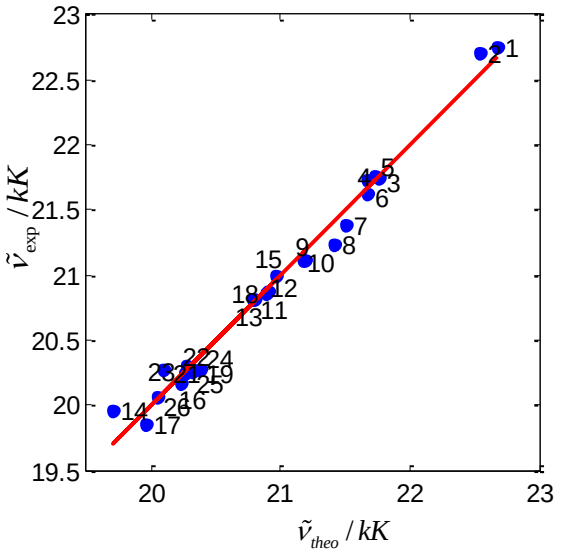

(c) LSER analysis for the fluorescence maxima $(\tilde{\nu}_{flu})$ of DCPPD using Kamlet-Taft parameters.

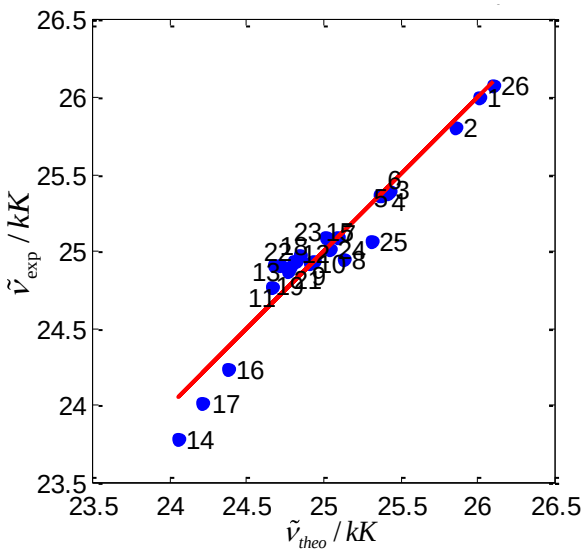

(b) LSER analysis for the absorption maxima $(\tilde{\nu}_{abs})$ of DCPPD using Catalan's parameters.

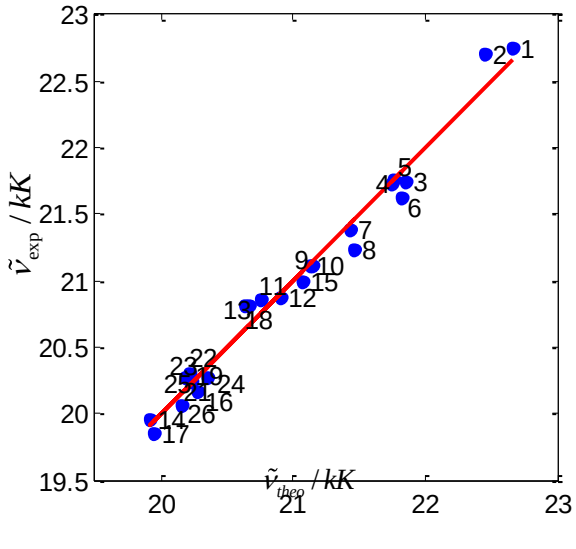

(d) LSER analysis for the fluorescence maxima $(\tilde{\nu}_{flu})$ of DCPPD using Catalan's parameters.

Figure 5-35: Linear solvation energy relationship (LSER) for the absorption (a and b) and fluorescence (c and d) maxima of DCPPD using Kamlet-Taft (a and c) as well as Catalan (b and d) parameters for 25 solvents.

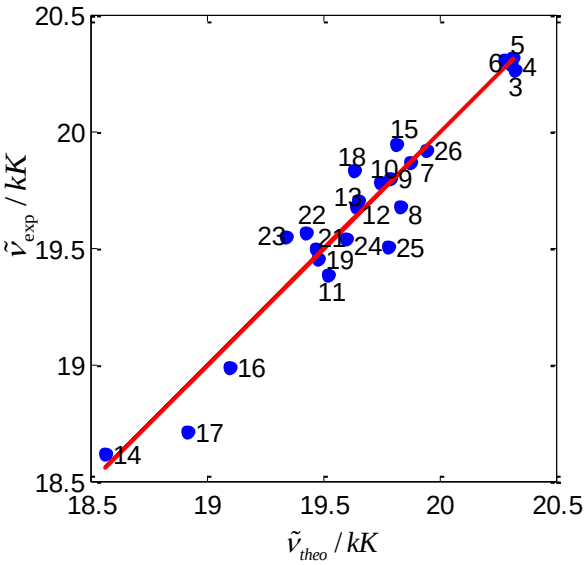

(a) LSER analysis for the absorption maxima $(\tilde{\nu}_{abs})$ of TCPPD using Kamlet-Taft parameters.

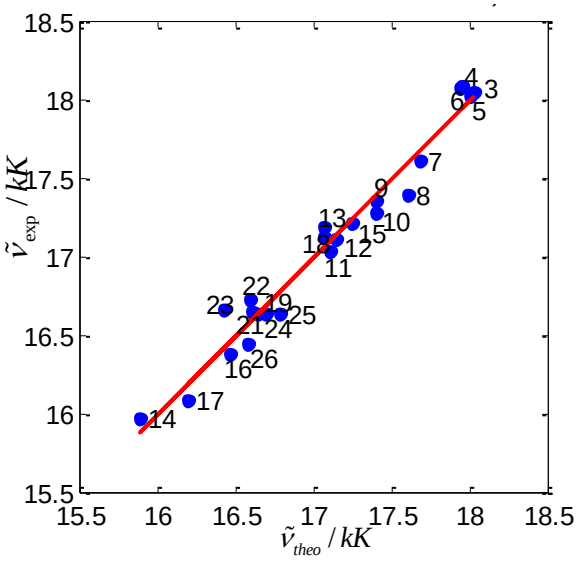

(c) LSER analysis for the fluorescence maxima $(\tilde{\nu}_{flu})$ of TCPPD using Kamlet-Taft parameters.

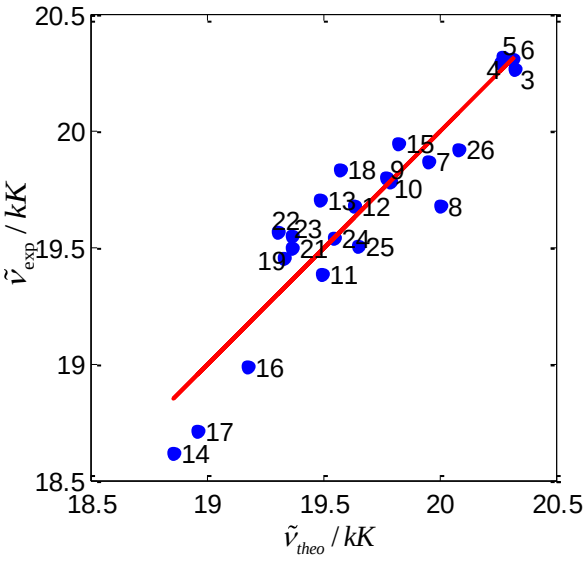

(b) LSER analysis for the absorption maxima $(\tilde{\nu}_{abs})$ of TCPPD using Catalan's parameters.

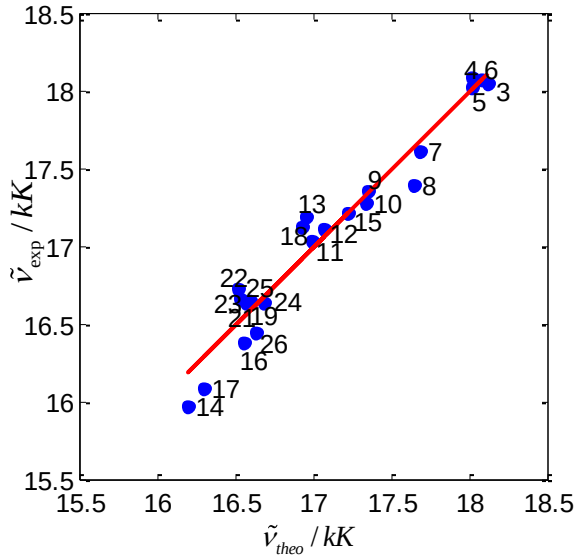

(d) LSER analysis for the fluorescence maxima $(\tilde{\nu}_{flu})$ of TCPPD using Catalan's parameters.

Figure 5-36: Linear solvation energy relationship (LSER) for the absorption (a and b) and fluorescence (c and d) maxima of TCPPD using Kamlet-Taft (a and c) as well as Catalan (b and d) parameters for 23 solvents.

Table 5-9: LSER analysis for cyano-substituted PPDs containing the coefficients of α, β and π* using Kamlet-Taft parameters.

LSER for absorption maxima						LSER for fluorescence maxima					
		PPD (n=21)						PPD (n=21)			
		value	SD	t-value	R			value	SD	t-value	R
Absorption	$\tilde{\nu}_0$	31.58	0.08	374.41	0.978	Fluorescence	$\tilde{\nu}_0$	26.90	0.04	642.23	0.995
	α	1.91	0.10	18.76			α	-0.28	0.05	-5.46	
	β	-0.78	0.16	-4.88			β	-1.26	0.08	-15.85	
	π*	-0.74	0.15	-5.07			π*	-1.38	0.07	-19.12	
		MCPPD (n=25)						MCPPD (n=25)			
		value	SD	t-value	R			value	SD	t-value	R
Absorption	$\tilde{\nu}_0$	28.11	0.07	416.92	0.972	Fluorescence	$\tilde{\nu}_0$	23.90	0.06	371.36	0.989
	α	1.32	0.08	16.02			α	-0.47	0.08	-6.01	
	β	-1.71	0.12	-13.76			β	-1.49	0.12	-12.62	
	π*	-0.36	0.11	-3.23			π*	-1.44	0.11	-13.68	
		DCPPD (n=25)						DCPPD (n=25)			
		value	SD	t-value	R			value	SD	t-value	R
Absorption	$\tilde{\nu}_0$	25.84	0.06	404.98	0.972	Fluorescence	$\tilde{\nu}_0$	22.54	0.05	449.06	0.993
	α	0.96	0.08	12.39			α	-0.26	0.06	-4.21	
	β	-1.83	0.12	-15.65			β	-1.76	0.09	-19.04	
	π*	-0.30	0.10	-2.91			π*	-1.25	0.08	-15.16	
		TCPPD (n=23)						TCPPD (n=23)			
		value	SD	t-value	R			value	SD	t-value	R
Absorption	$\tilde{\nu}_0$	20.77	0.09	234.47	0.965	Fluorescence	$\tilde{\nu}_0$	18.76	0.08	225.46	0.984
	α	0.49	0.08	6.52			α	-0.05	0.07	-0.69	
	β	-1.74	0.12	-14.58			β	-1.90	0.11	-16.95	
	π*	-0.54	0.12	-4.51			π*	-1.13	0.11	-9.97	

n = number of solvents used for LSER analysis; R = regression coefficient.

Table 5-10: LSER analysis for cyano-substituted PPDs containing the coefficients of SA, SB, Sdp and Sp using Catalan parameters.

LSER for absorption maxima						LSER for fluorecence maxima					
		PPD (n=21)						PPD (n=21)			
		value	SD	t-value	R			value	SD	t-value	R
Absorption	$\tilde{\nu}_0$	33.55	0.75	44.52	0.950	Fluorescence	$\tilde{\nu}_0$	29.19	0.36	80.72	0.988
	SA	2.52	0.28	8.95			*SA*	-1.13	0.14	-8.36	
	SB	0.38	0.28	1.37			*SB*	-1.02	0.13	-7.66	
	Sdp	-1.12	0.24	-4.58			*Sdp*	-1.13	0.12	-9.64	
	Sp	-3.05	1.06	-2.88			*Sp*	-3.42	0.51	-6.74	
		MCPPD (n=25)						MCPPD (n=25)			
		value	SD	t-value	R			value	SD	t-value	R
Absorption	$\tilde{\nu}_0$	29.55	0.38	77.21	0.967	Fluorescence	$\tilde{\nu}_0$	25.68	0.32	80.79	0.990
	SA	1.50	0.15	10.03			*SA*	-1.36	0.12	-11.01	
	SB	-0.81	0.14	-5.66			*SB*	-1.26	0.12	-10.65	
	Sdp	-0.90	0.12	-7.37			*Sdp*	-1.27	0.10	-12.57	
	Sp	-1.99	0.52	-3.81			*Sp*	-2.62	0.44	-6.01	
		DCPPD (n=25)						DCPPD (n=25)			
		value	SD	t-value	R			value	SD	t-value	R
Absorption	$\tilde{\nu}_0$	27.37	0.35	77.61	0.968	Fluorescence	$\tilde{\nu}_0$	24.49	0.30	80.88	0.990
	SA	0.86	0.14	6.27			*SA*	-1.16	0.12	-9.87	
	SB	-1.18	0.13	-8.96			*SB*	-1.49	0.11	-13.22	
	Sdp	-0.73	0.11	-6.49			*Sdp*	-1.14	0.10	-11.81	
	Sp	-2.09	0.48	-4.32			*Sp*	-2.83	0.41	-6.82	
		TCPPD (n=23)						TCPPD (n=23)			
		value	SD	t-value	R			value	SD	t-value	R
Absorption	$\tilde{\nu}_0$	22.33	0.52	42.54	0.931	Fluorescence	$\tilde{\nu}_0$	20.12	0.44	46.05	0.975
	SA	0.03	0.18	0.14			*SA*	-0.82	0.15	-5.54	
	SB	-1.25	0.18	-6.88			*SB*	-1.35	0.15	-8.93	
	Sdp	-0.79	0.15	-5.20			*Sdp*	-1.21	0.13	-9.58	
	Sp	-2.14	0.68	-3.16			*Sp*	-2.02	0.56	-3.60	

n = number of solvents used for LSER analysis; R = regression coefficient.

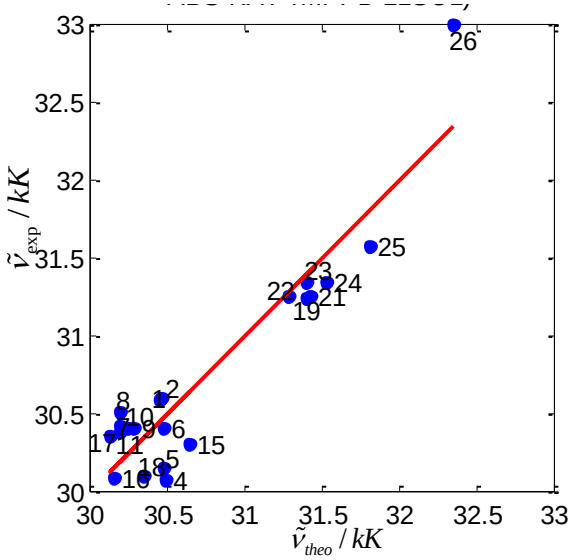

(a) LSER analysis for the absorption maxima ($\tilde{\nu}_{abs}$) of TMPPD using Kamlet-Taft parameters.

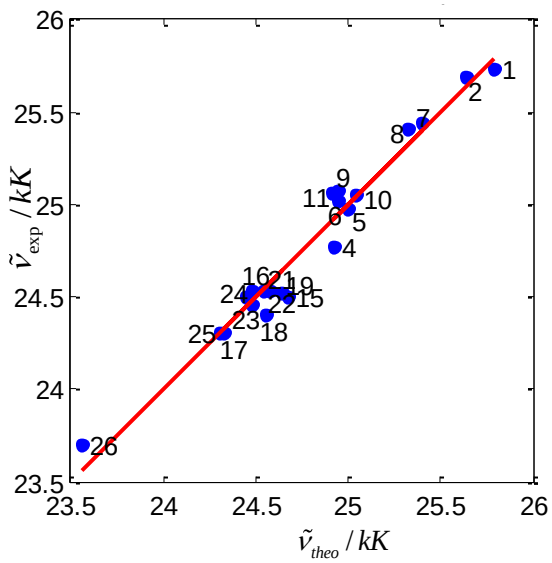

(c) LSER analysis for the fluorescence maxima ($\tilde{\nu}_{flu}$) of TMPPD using Kamlet-Taft parameters.

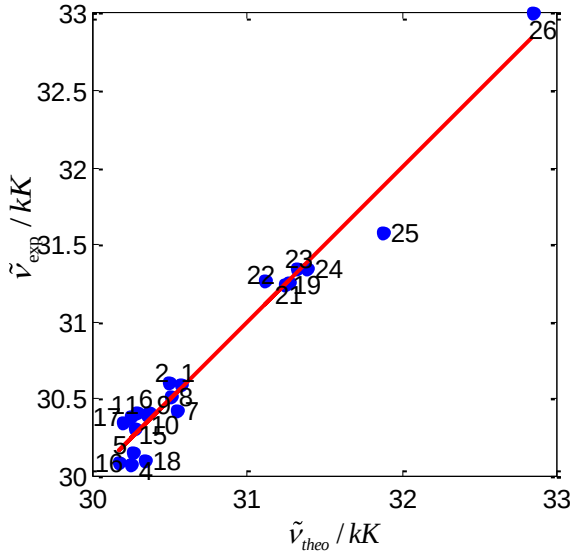

(b) LSER analysis for the absorption maxima ($\tilde{\nu}_{abs}$) of TMPPD using Catalan's parameters.

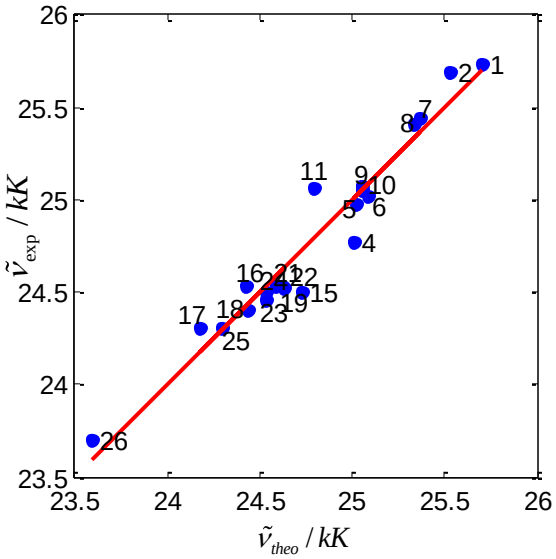

(d) LSER analysis for the fluorescence maxima ($\tilde{\nu}_{flu}$) of TMPPD using Catalan's parameters.

Figure 5-37: Linear solvation energy relationship (LSER) for the absorption (a and b) and fluorescence (c and d) maxima of TMPPD using Kamlet-Taft (a and c) as well as Catalan (b and d) parameters for 25 solvents.

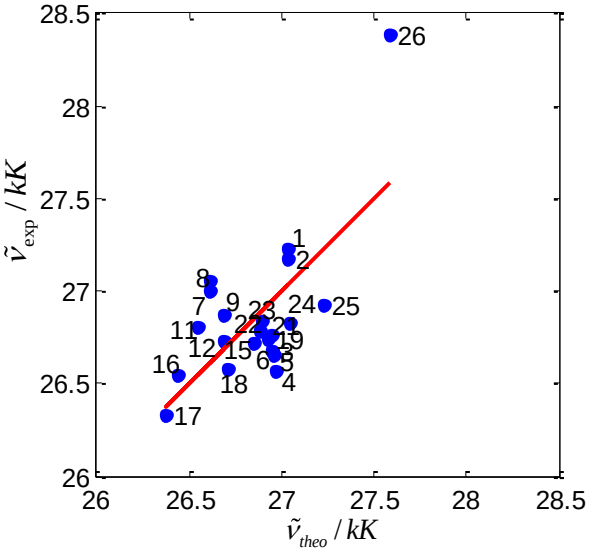

(a) LSER analysis for the absorption maxima ($\tilde{\nu}_{abs}$) of MCTMPPD using Kamlet-Taft parameters.

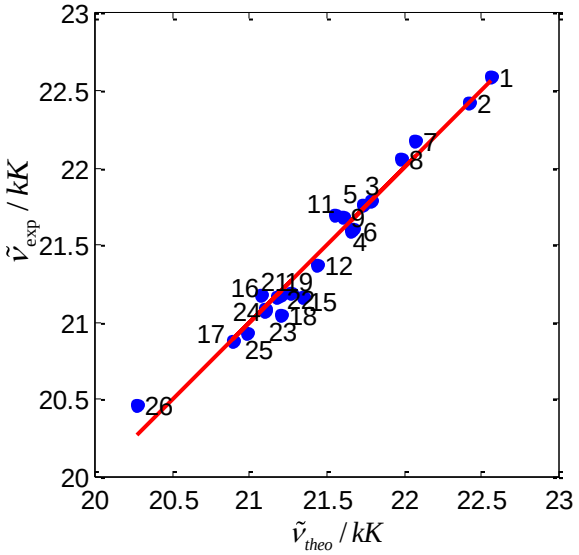

(c) LSER analysis for the fluorescence maxima ($\tilde{\nu}_{flu}$) of MCTMPPD using Kamlet-Taft parameters.

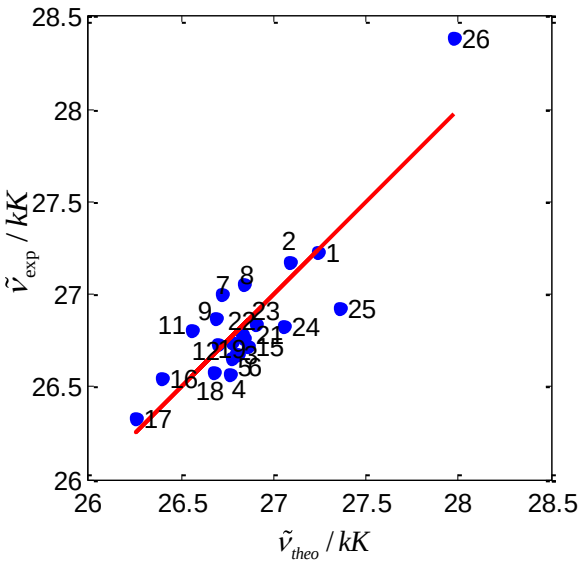

(b) LSER analysis for the absorption maxima ($\tilde{\nu}_{abs}$) of MCTMPPD using Catalan's parameters.

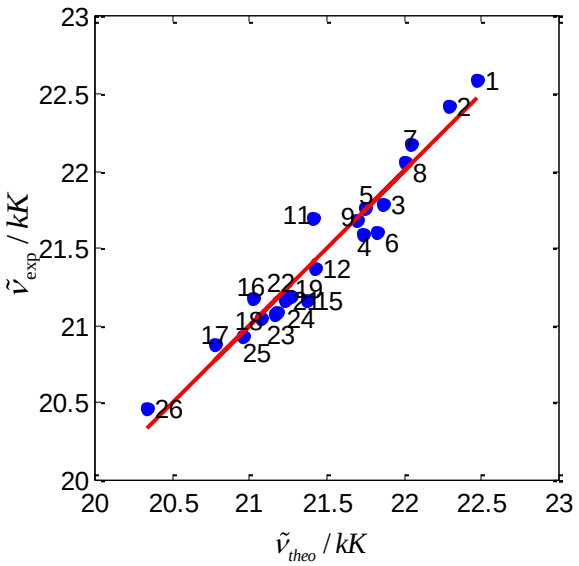

(d) LSER analysis for the fluorescence maxima ($\tilde{\nu}_{flu}$) of MCTMPPD using Catalan's parameters.

Figure 5-38: Linear solvation energy relationship (LSER) for the absorption (a and b) and fluorescence (c and d) maxima of MCTMPPD using Kamlet-Taft (a and c) as well as Catalan (b and d) parameters for 25 solvents.

Table 5-11: Coefficients of LSER analysis for TMPPD and MCTMPPD for Kamlet-Taft and Catalan parameters.

LSER analysis using Kamlet-Taft parameters										
LSER for absorption maxima						**LSER for fluorescence maxima**				
		TMPPD (n=21)						**TMPPD (n=21)**			
		value	SD	t-value	R			value	SD	t-value	R
Absorption	$\tilde{\nu}_0$	30.46	0.15	207.54	0.930	**Fluorescence**	$\tilde{\nu}_0$	25.64	0.05	485.05	0.983
	α	1.72	0.18	9.29			α	-0.55	0.07	-8.32	
	β	-0.67	0.29	-2.29			β	-0.02	0.10	-0.16	
	π*	0.17	0.24	0.73			π*	-1.30	0.09	-15.32	
		MCTMPPD (n=22)						**MCTMPPD (n=22)**			
		value	SD	t-value	R			value	SD	t-value	R
Absorption	$\tilde{\nu}_0$	27.03	0.16	168.21	0.677	**Fluorescence**	$\tilde{\nu}_0$	22.42	0.05	448.74	0.985
	α	0.80	0.21	3.82			α	-0.49	0.07	-7.50	
	β	-0.94	0.32	-2.92			β	-0.23	0.10	-2.32	
	π*	0.05	0.26	0.20			π*	-1.35	0.08	-16.41	
LSER analysis using Catalan's parameters											
LSER for absorption maxima						**LSER for fluorescence maxima**				
		TMPPD (n=21)						**TMPPD (n=21)**			
		value	SD	t-value	R			value	SD	t-value	R
Absorption	$\tilde{\nu}_0$	31.30	0.41	76.02	0.983	**Fluorescence**	$\tilde{\nu}_0$	27.30	0.39	70.59	0.971
	SA	2.65	0.15	17.33			*SA*	-1.03	0.14	-7.16	
	SB	0.22	0.14	1.60			*SB*	-0.06	0.13	-0.49	
	Sdp	-0.44	0.13	-3.32			*Sdp*	-0.86	0.12	-6.90	
	Sp	-1.22	0.58	-2.11			*Sp*	-2.58	0.54	-4.78	
		MCTMPPD (n=22)						**MCTMPPD (n=22)**			
		value	SD	t-value	R			value	SD	t-value	R
Absorption	$\tilde{\nu}_0$	28.60	0.59	48.29	0.873	**Fluorescence**	$\tilde{\nu}_0$	24.09	0.38	62.58	0.971
	SA	1.02	0.22	4.70			*SA*	-0.95	0.14	-6.77	
	SB	-0.63	0.20	-3.10			*SB*	-0.18	0.13	-1.35	
	Sdp	-0.23	0.18	-1.29			*Sdp*	-0.97	0.12	-8.36	
	Sp	-2.14	0.81	-2.64			*Sp*	-2.61	0.53	-4.95	

n = number of solvent used for LSER analysis; R = regression coefficient.

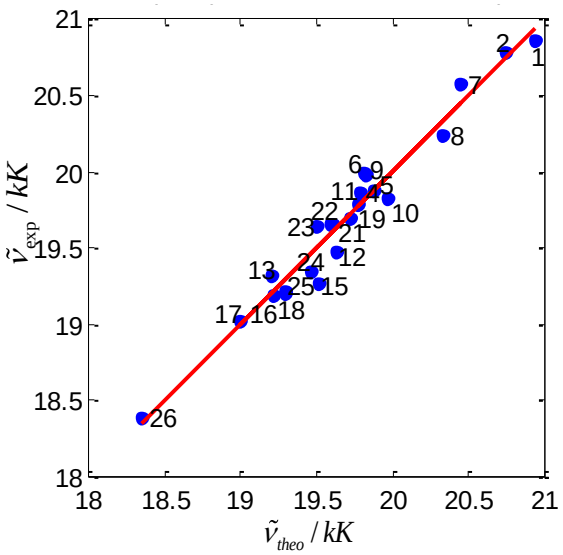

(a) LSER analysis for the fluorescence maxima ($\tilde{\nu}_{flu,\max}$) of DCTMPPD using Kamlet-Taft parameters.

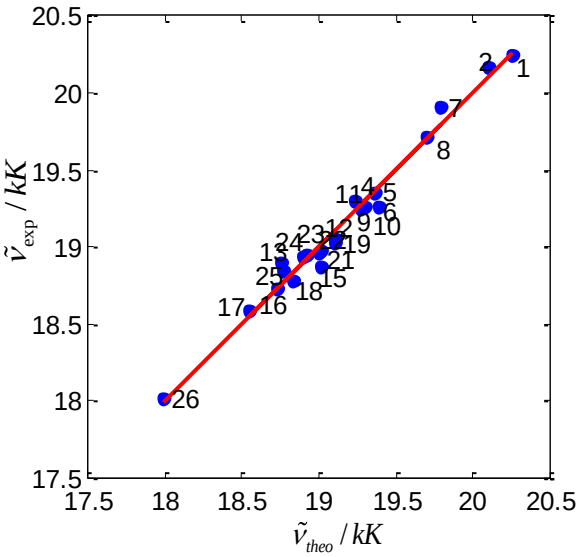

(c) LSER analysis for the fluorescence center of gravity ($\tilde{\nu}_{flu,cog}$) of DCTMPPD using Kamlet-Taft parameters.

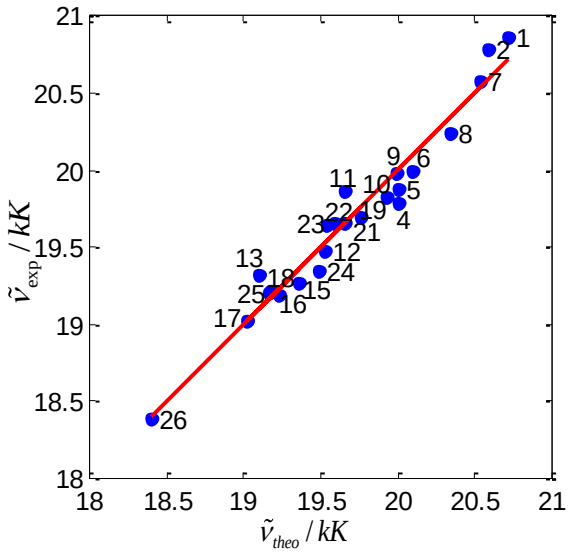

(b) LSER analysis for the fluorescence maxima ($\tilde{\nu}_{flu,\max}$) of DCTMPPD using Catalan's parameters.

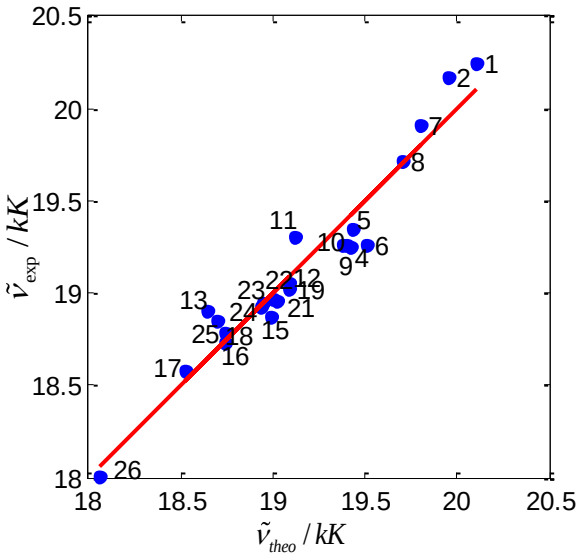

(d) LSER analysis for the fluorescence center of gravity ($\tilde{\nu}_{flu,cog}$) of DCTMPPD using Catalan's parameters.

Figure 5-39: Linear solvation energy relationship (LSER) for the fluorescence maxima (a and b) and fluorescence center of gravity (c and d) of DCTMPPD using Kamlet-Taft (a and c) as well as Catalan (b and d) parameters for 25 solvents.

Table 5-12: Coefficients of LSER analysis for DCTMPPD fluorescence maxima and center of gravity (COG) for Kamlet-Taft and Catalan parameters.

LSER analysis using Kamlet-Taft parameters										
LSER for fluorescence maxima						**LSER for fluorescence center of gravity**				
Fluorescence (maxima)		**DCTMPPD (n=23)**				**Fluorescence (COG)**		**DCTMPPD (n=23)**			
		value	SD	t-value	R			value	SD	t-value	R
	$\tilde{\nu}_0$	20.66	0.08	253.09	0.968		$\tilde{\nu}_0$	20.10	0.04	510.64	0.990
	SA	-0.44	0.10	-4.31			α	-0.38	0.05	-7.81	
	SB	0.23	0.16	1.41			β	-0.10	0.08	-1.31	
	Sdp	-1.83	0.12	-14.69			π*	-1.48	0.06	-24.67	

LSER analysis using Catalan parameters										
LSER for fluorescence maxima						**LSER for fluorescence center of gravity**				
Fluorescence (maxima)		**DCTMPPD (n=23)**				**Fluorescence (COG)**		**DCTMPPD (n=23)**			
		value	SD	t-value	R			value	SD	t-value	R
	$\tilde{\nu}_0$	22.01	0.33	66.54	0.978		$\tilde{\nu}_0$	21.52	0.36	60.37	0.967
	SA	-0.78	0.13	-6.01			*SA*	-0.81	0.14	-5.81	
	SB	0.29	0.12	2.38			*SB*	0.01	0.13	0.07	
	Sdp	-1.37	0.11	-12.54			*Sdp*	-1.04	0.12	-8.86	
	Sp	-2.11	0.46	-4.61			*Sp*	-2.29	0.49	-4.65	

n = number of solvents used for LSER analysis; R = regression coefficient.

5.3.2 Empirical correlation using ETN and ETN+DNN

Linear solvation energy relationship (LSER) analyses using ETN parameter and also the combination of ETN & DNN parameters have been performed for all cyano-substituted PPDs and TMPPDs. Plots of the experimentally determined values of absorption and fluorescence maxima verus the correspongding theroretical values are shown in from Figure 5-40 to Figure 5-43 for the cyano-substituted PPDs and Figure 5-44 to Figure 5-46 for cyano-substituted TMPPDs. The corresponding values of LSER coefficients are summarized in Table 5-13 (using ETN only) Table 5-14 (using ETN and DNN) for the PPDs. And values of LSER coefficients for TMPPDs are given in Table 5-15 (TMPPD and MCTMPPD) and Table 5-16 (DCTMPPD).

LSER analyses for the absorption maxima ($\tilde{\nu}_{abs}$) of PPD and cyano-substituted PDDs using only ETN parameter (shown in (a) of Figure 5-40 to Figure 5-43) have shown that the data points are not spread over the x-axis (theoretically calculated values) as these are for y-axis (experimental values) and hence the values for the regressions coefficients, R, for these analyses are very poor (shown in Table 5-13). The reason for such observation is that ETN parameter infact represents the combination of acidity and polarity properties of the solvents. In case of absorption of PPD and its cyano-substituted derivatives, both acidity and polarity shift the absorption maxima in opposite to each other (opposite sign in Kamlet-Taft and Catalan's analysis). So the combined effect of acidity and polarity subtract each other and almost no net variation in theoretical values when using only ETN parameter. The value of R is improved largely, see Table 5-14, in case of absorption maxima (and also for emission maxima) by adding another parameter DNN, describing the basicity of the solvent. This indicates a large dependence of absorption maxima (and also emission maxima) on the solvent basicity which coincides with the results found earlier using Kamlet-Taft and Catalan's parameters.

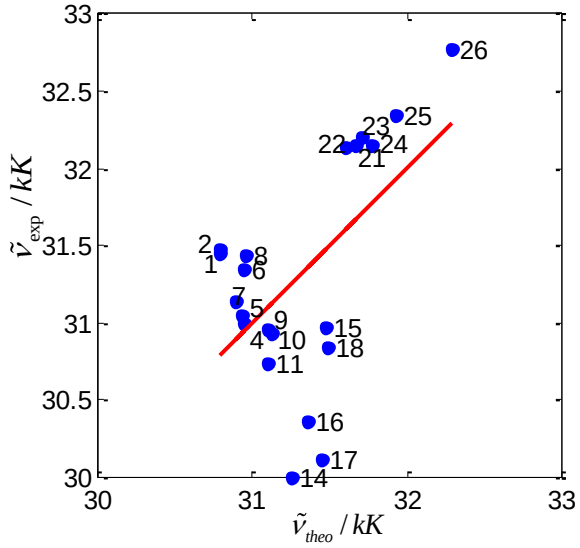

(a) LSER analysis for the absorption maxima ($\tilde{\nu}_{abs}$) of PPD using ETN parameter.

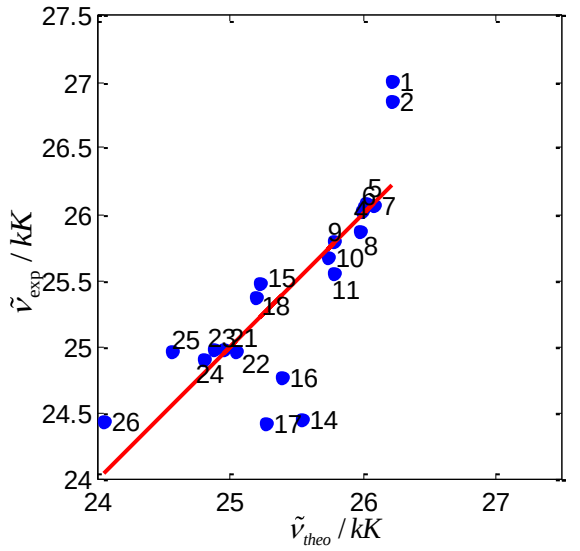

(b) LSER analysis for the fluorescence maxima ($\tilde{\nu}_{flu}$) of PPD using ETN parameter.

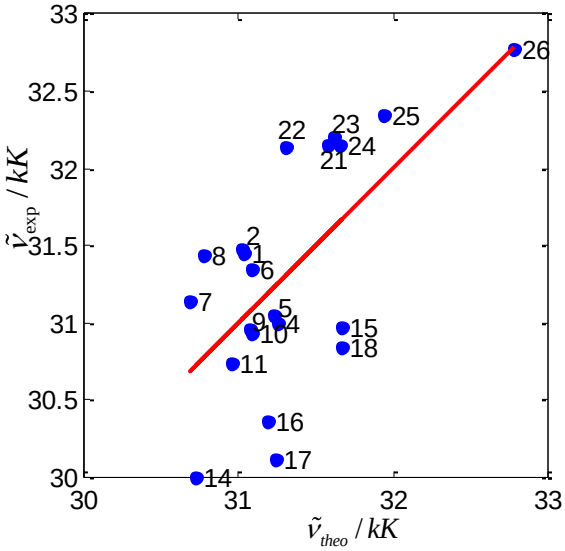

(c) LSER analysis for the absorption maxima ($\tilde{\nu}_{abs}$) of PPD using ETN and DNN parameters.

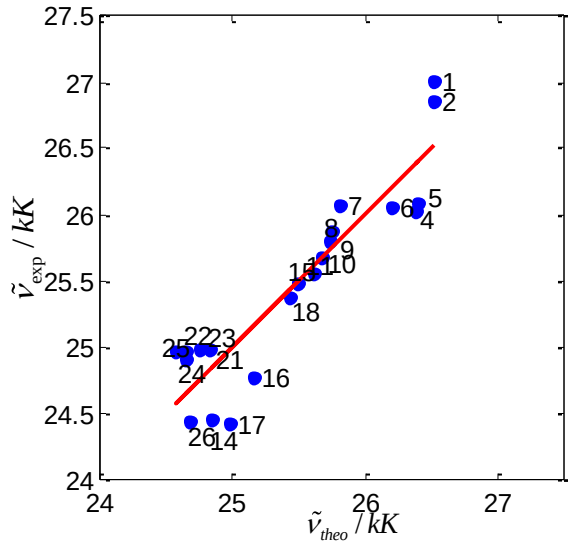

(d) LSER analysis for the fluorescence maxima ($\tilde{\nu}_{flu}$) of PPD using ETN and DNN parameters.

Figure 5-40: Linear solvation energy relationship (LSER) for the absorption (a and c) and fluorescence (b and d) maxima of PPD using ETN (a and b) as well as ETN+DNN (c and d) parameters for 21 solvents.

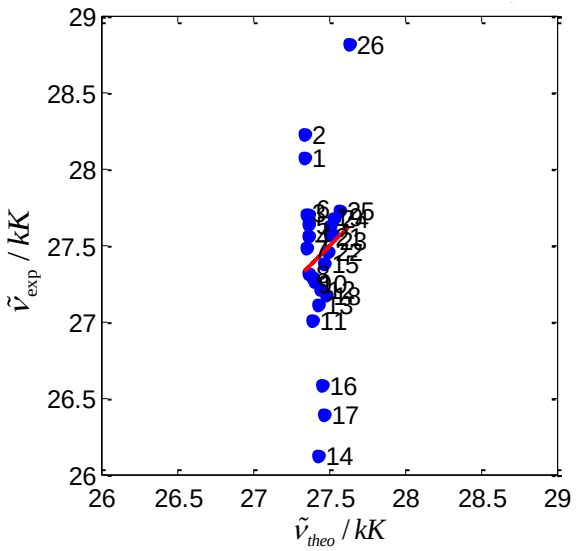

(a) LSER analysis for the absorption maxima ($\tilde{\nu}_{abs}$) of MCPPD using ETN parameter.

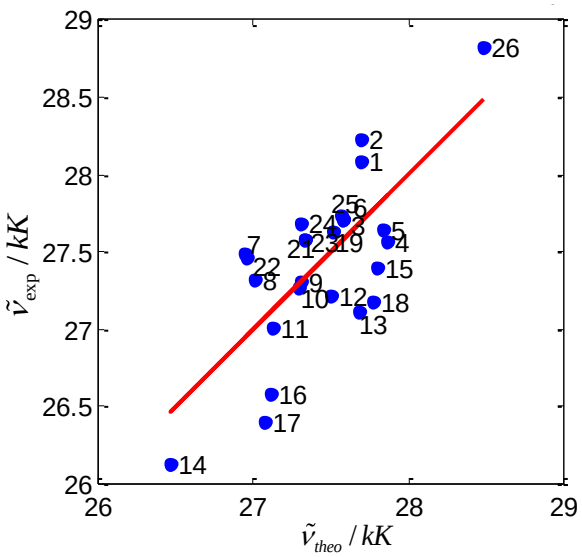

(c) LSER analysis for the absorption maxima ($\tilde{\nu}_{abs}$) of MCPPD using ETN and DNN parameters.

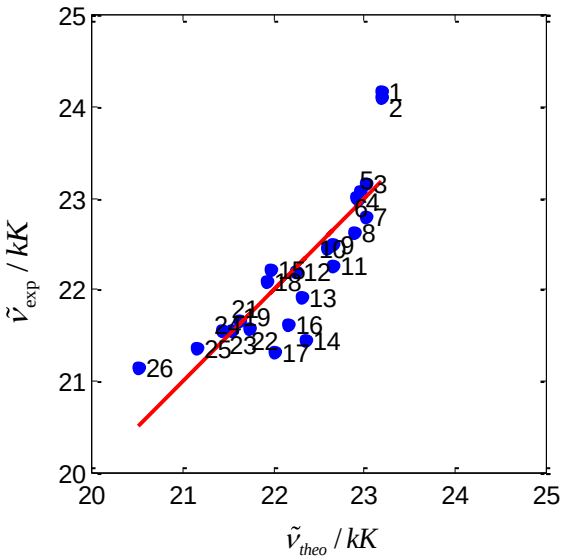

(b) LSER analysis for the fluorescence maxima ($\tilde{\nu}_{flu}$) of MCPPD using ETN parameter.

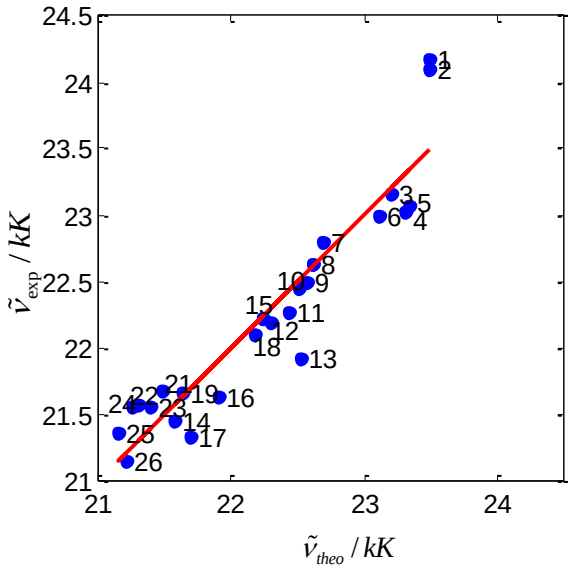

(d) LSER analysis for the fluorescence maxima ($\tilde{\nu}_{flu}$) of MCPPD using ETN and DNN parameters.

Figure 5-41: Linear solvation energy relationship (LSER) for the absorption (a and c) and fluorescence (b and d) maxima of PPD using ETN (a and b) as well as ETN+DNN (c and d) parameters for 25 solvents.

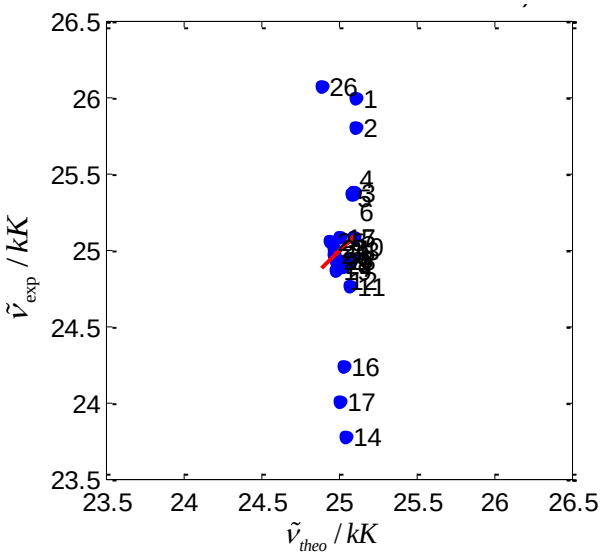

(a) LSER analysis for the absorption maxima ($\tilde{\nu}_{abs}$) of DCPPD using ETN parameter.

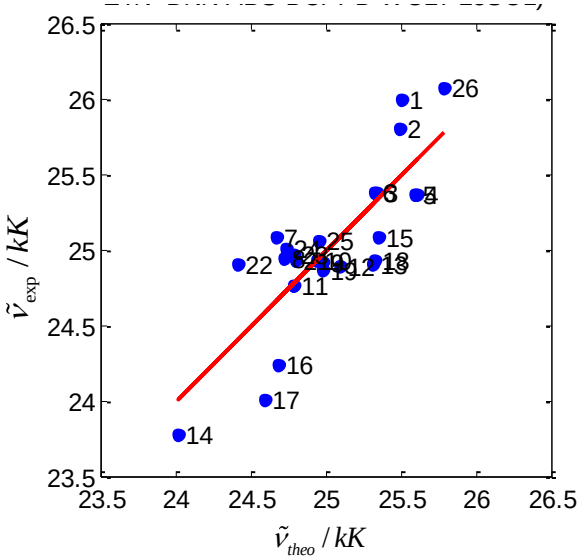

(c) LSER analysis for the absorption maxima ($\tilde{\nu}_{abs}$) of DCPPD using ETN and DNN parameters.

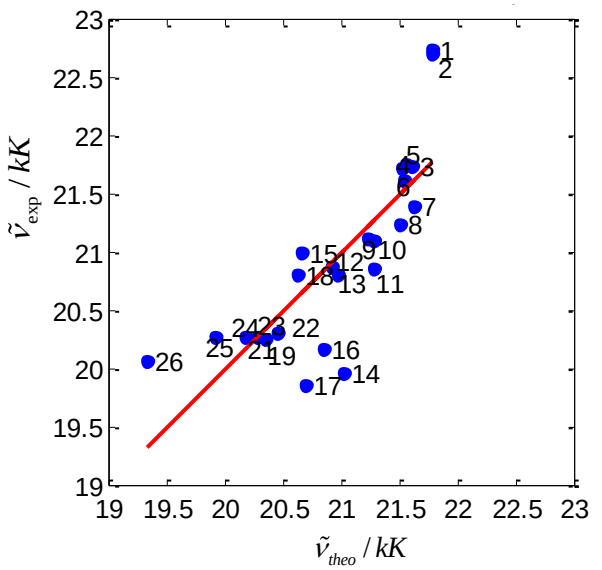

(b) LSER analysis for the fluorescence maxima ($\tilde{\nu}_{flu}$) of DCPPD using ETN parameter.

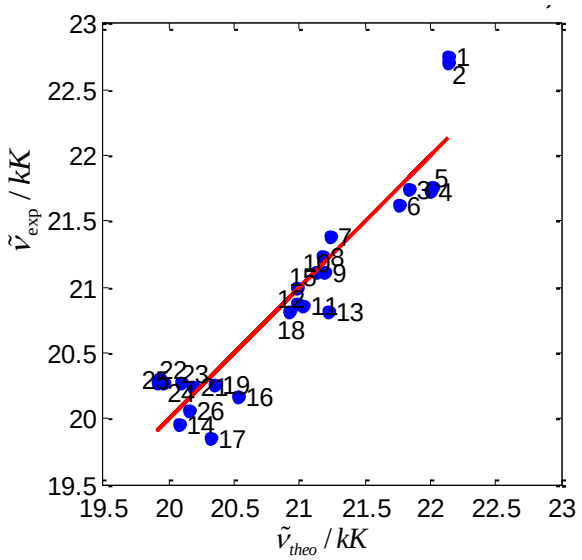

(d) LSER analysis for the fluorescence maxima ($\tilde{\nu}_{flu}$) of DCPPD using ETN and DNN parameters.

Figure 5-42: Linear solvation energy relationship (LSER) for the absorption (a and c) and fluorescence (b and d) maxima of DCPPD using ETN (a and b) as well as ETN+DNN (c and d) parameters for 25 solvents.

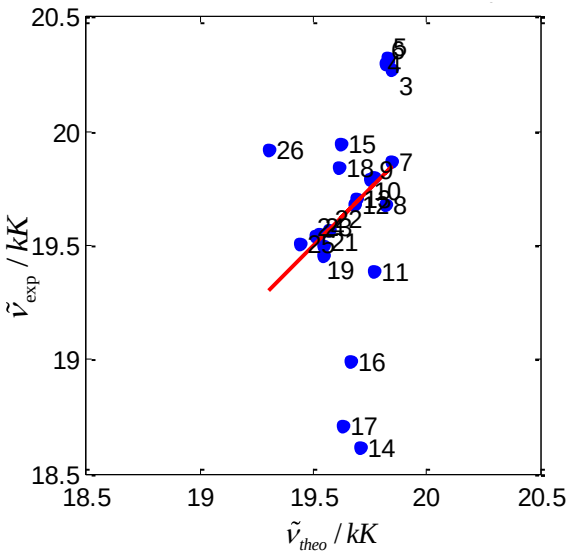

(a) LSER analysis for the absorption maxima ($\tilde{\nu}_{abs}$) of TCPPD using ETN parameter.

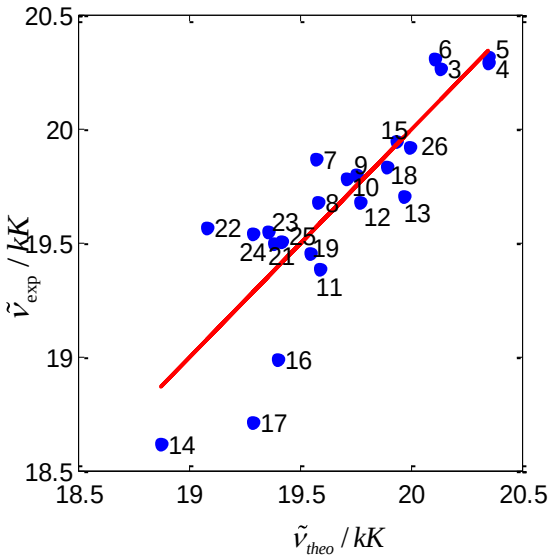

(c) LSER analysis for the absorption maxima ($\tilde{\nu}_{abs}$) of TCPPD using ETN and DNN parameters.

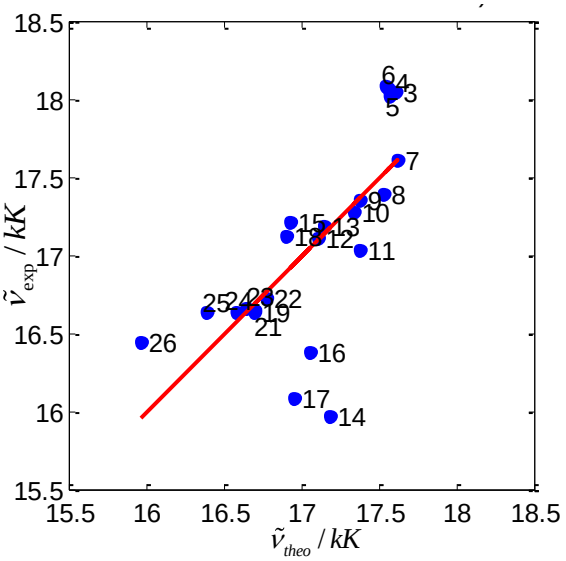

(b) LSER analysis for the fluorescence maxima ($\tilde{\nu}_{flu}$) of TCPPD using ETN parameter.

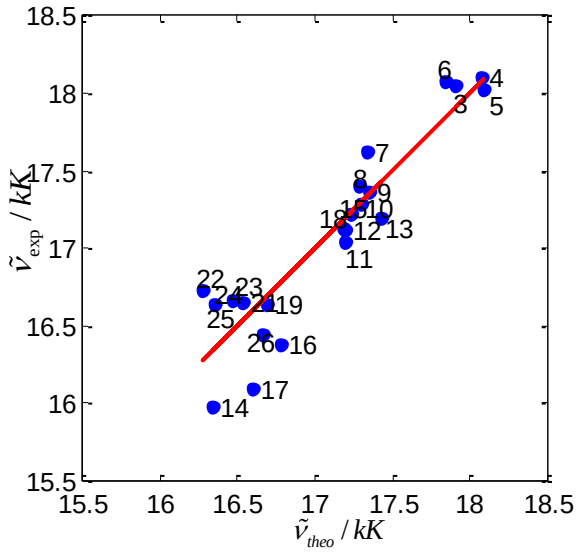

(d) LSER analysis for the fluorescence maxima ($\tilde{\nu}_{flu}$) of TCPPD using ETN and DNN parameters.

Figure 5-43: Linear solvation energy relationship (LSER) for the absorption (a and c) and fluorescence (b and d) maxima of TCPPD using ETN (a and b) as well as ETN+DNN (c and d) parameters for 23 solvents.

Table 5-13: LSER coefficients for cyano substitute PPDs using single parameter ETN.

LSER analysis for absorption maxima						LSER analysis for fluorescence maxima					
		PPD (n=21)						PPD (n=21)			
		value	SD	t-value	R			value	SD	t-value	R
Absorption	$\tilde{\nu}_0$	30.78	0.23	131.59	0.549	Fluorescence	$\tilde{\nu}_0$	26.24	0.16	160.93	0.808
	ETN	1.51	0.53	2.86			ETN	-2.20	0.37	-5.97	
		MCPPD (n=25)						MCPPD (n=25)			
		value	SD	t-value	R			value	SD	t-value	R
Absorption	$\tilde{\nu}_0$	27.32	0.19	143.00	0.143	Fluorescence	$\tilde{\nu}_0$	23.21	0.15	154.49	0.853
	ETN	0.31	0.44	0.69			ETN	-2.72	0.35	-7.83	
		DCPPD (n=25)						DCPPD (n=25)			
		value	SD	t-value	R			value	SD	t-value	R
Absorption	$\tilde{\nu}_0$	25.11	0.18	139.24	0.114	Fluorescence	$\tilde{\nu}_0$	21.80	0.17	131.65	0.804
	ETN	-0.23	0.42	-0.55			ETN	-2.48	0.38	-6.48	
		TCPPD (n=23)						TCPPD (n=23)			
		value	SD	t-value	R			value	SD	t-value	R
Absorption	$\tilde{\nu}_0$	19.89	0.17	116.94	0.319	Fluorescence	$\tilde{\nu}_0$	17.74	0.17	102.31	0.712
	ETN	-0.58	0.38	-1.54			ETN	-1.79	0.38	-4.65	

n = number of solvent used for LSER analysis; R = regression coefficient.

Table 5-14: LSER coefficients for cyano substitute PPDs using ETN and DNN parameters.

Analysis using ETN and DNN						Analysis using ETN and DNN					
		PPD (n=21)						PPD (n=21)			
Absorption		value	SD	t-value	R	Fluorescence		value	SD	t-value	R
	$\tilde{\nu}_0$	31.01	0.26	121.36	0.638		$\tilde{\nu}_0$	26.54	0.13	201.56	0.916
	ETN	2.23	0.64	3.48			ETN	-1.26	0.33	-3.81	
	DNN	-0.99	0.55	-1.79			DNN	-1.30	0.28	-4.56	
		MCPPD (n=25)						MCPPD (n=25)			
Absorption		value	SD	t-value	R	Fluorescence		value	SD	t-value	R
	$\tilde{\nu}_0$	27.68	0.15	181.48	0.733		$\tilde{\nu}_0$	23.50	0.11	205.30	0.939
	ETN	1.61	0.41	3.96			ETN	-1.65	0.31	-5.40	
	DNN	-1.74	0.35	-4.96			DNN	-1.42	0.26	-5.39	
		DCPPD (n=25)						DCPPD (n=25)			
Absorption		value	SD	t-value	R	Fluorescence		value	SD	t-value	R
	$\tilde{\nu}_0$	25.49	0.12	209.51	0.817		$\tilde{\nu}_0$	22.14	0.11	195.73	0.937
	ETN	1.15	0.32	3.55			ETN	-1.22	0.30	-4.03	
	DNN	-1.84	0.28	-6.57			DNN	-1.67	0.26	-6.45	
		TCPPD (n=23)						TCPPD (n=23)			
Absorption		value	SD	t-value	R	Fluorescence		value	SD	t-value	R
	$\tilde{\nu}_0$	20.31	0.11	178.41	0.854		$\tilde{\nu}_0$	18.17	0.12	154.95	0.921
	ETN	0.42	0.26	1.63			ETN	-0.77	0.27	-2.91	
	DNN	-1.57	0.23	-6.82			DNN	-1.59	0.24	-6.72	

n = number of solvent used for LSER analysis; R = regression coefficient.

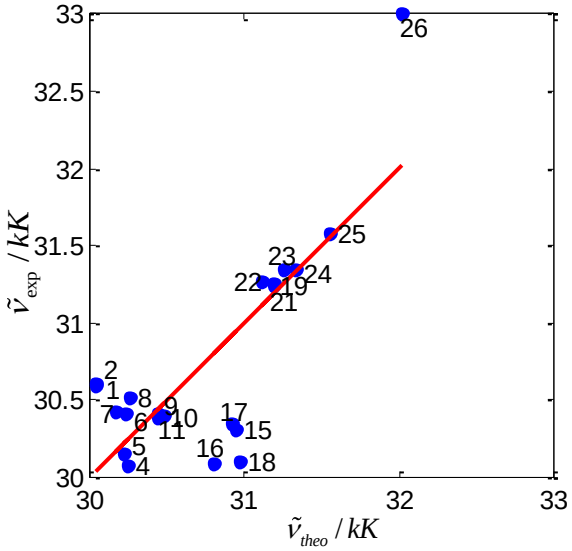

(a) LSER analysis for the absorption maxima ($\tilde{\nu}_{abs}$) of TMPPD using ETN parameter.

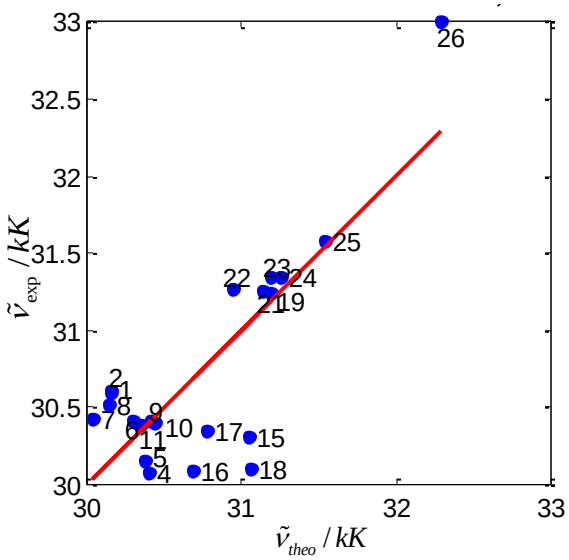

(c) LSER analysis for the absorption maxima ($\tilde{\nu}_{abs}$) of TMPPD using ETN & DNN.

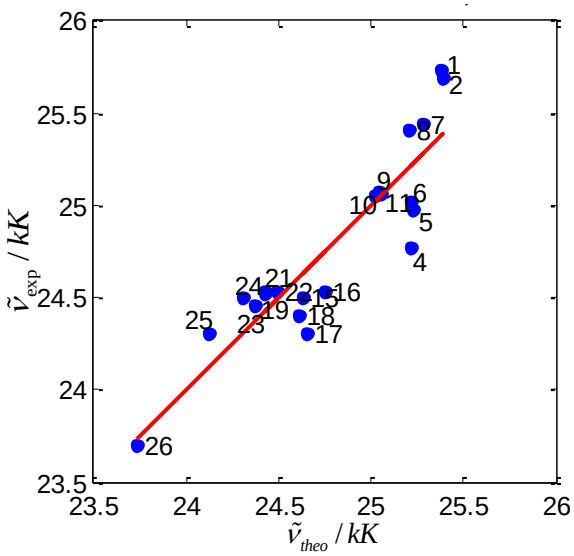

(b) LSER analysis for the fluorescence maxima ($\tilde{\nu}_{flu}$) of TMPPD using ETN parameter.

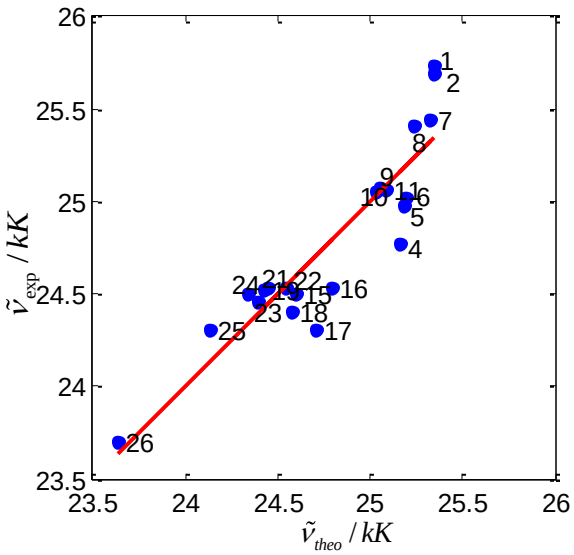

(d) LSER analysis for the fluorescence maxima ($\tilde{\nu}_{flu}$) of TMPPD using ETN & DNN.

Figure 5-44: Linear solvation energy relationship (LSER) for the absorption (a and c) and fluorescence (b and d) maxima of TMPPD using ETN (a and b) as well as ETN+DNN (c and d) parameters for 21 solvents.

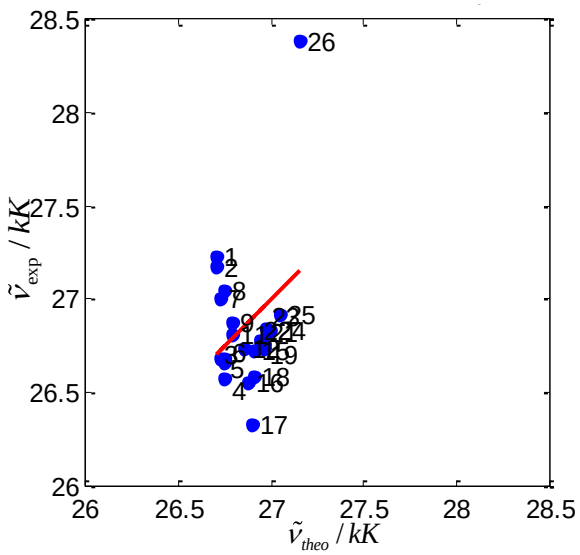

(a) LSER analysis for the absorption maxima ($\tilde{\nu}_{abs}$) of MCTMPPD using ETN parameter.

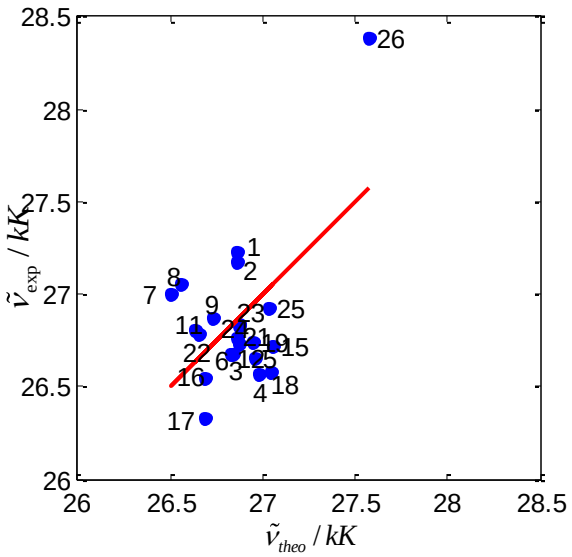

(c) LSER analysis for the absorption maxima ($\tilde{\nu}_{abs}$) of MCTMPPD using ETN & DNN.

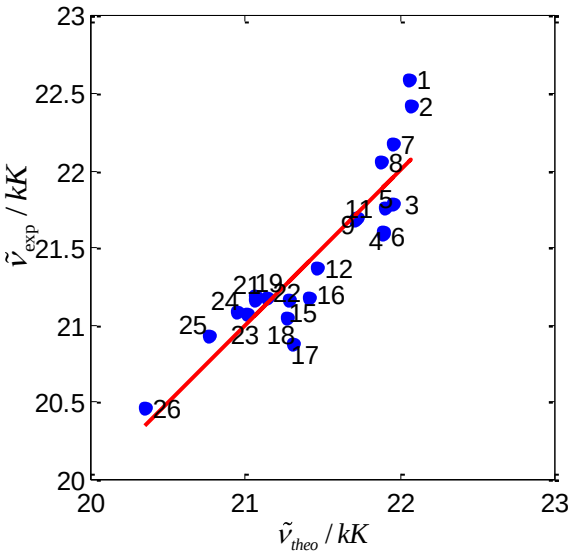

(b) LSER analysis for the fluorescence maxima ($\tilde{\nu}_{flu}$) of MCTMPPD using ETN parameter.

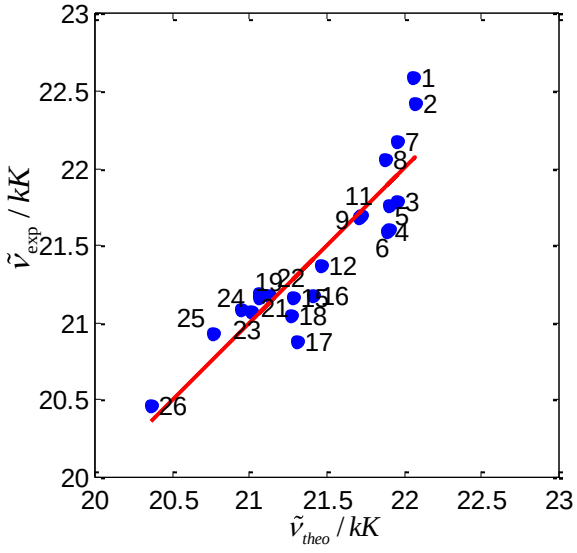

(d) LSER analysis for the fluorescence maxima ($\tilde{\nu}_{flu}$) of MCTMPPD using ETN & DNN.

Figure 5-45: Linear solvation energy relationship (LSER) for the absorption (a and c) and fluorescence (b and d) maxima of MCTMPPD using ETN (a and b) as well as ETN+DNN (c and d) parameters for 22 solvents.

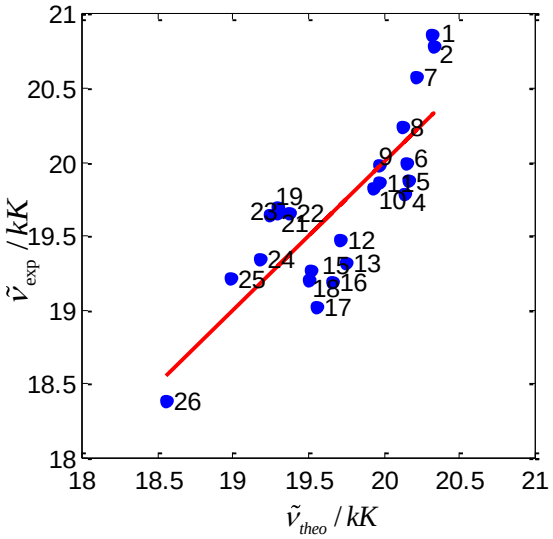

(a) LSER analysis for the fluorescence maxima $(\tilde{\nu}_{flu,\max})$ of DCTMPPD using ETN parameter.

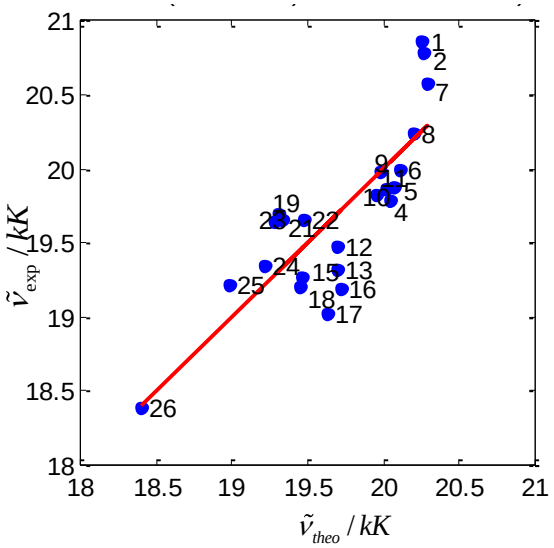

(c) LSER analysis for the fluorescence maxima $(\tilde{\nu}_{flu,\max})$ of DCTMPPD using ETN & DNN parameters.

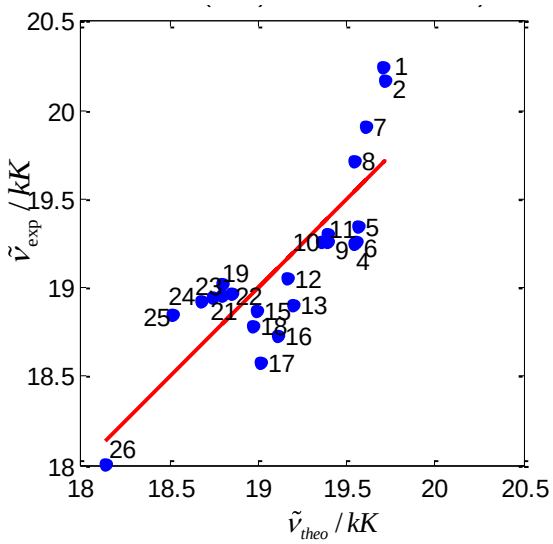

(b) LSER analysis for the fluorescence center of gravity $(\tilde{\nu}_{flu,cog})$ of DCTMPPD using ETN parameter.

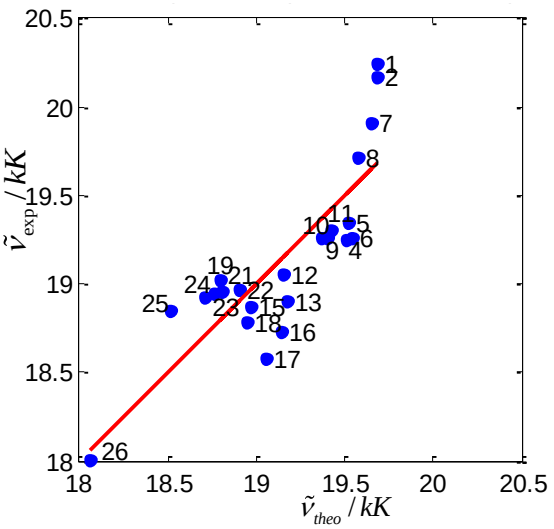

(d) LSER analysis for the fluorescence center of gravity $(\tilde{\nu}_{flu,cog})$ of DCTMPPD using ETN & DNN parameters.

Figure 5-46: Linear solvation energy relationship (LSER) for the fluorescence maxima (a and c) and fluorescence center of gravity (b and d) of DCTMPPD using ETN (a and b) as well as ETN+DNN (c and d) parameters for 23 solvents.

Table 5-15: LSER coefficients for TMPPD and MCTM PPD using ETN and DNN parameters.

Analysis using ETN						Analysis using ETN					
		TMPPD (n=21)						TMPPD (n=21)			
		value	SD	t-value	R			Value	SD	t-value	R
Absorption	$\tilde{\nu}_0$	30.02	0.16	183.24	0.79	Fluorescence	$\tilde{\nu}_0$	25.40	0.08	313.68	0.91
	ETN	2.00	0.36	5.56			ETN	-1.66	0.18	-9.35	
		MCTMPPD (n=22)						MCTMPPD (n=22)			
		value	SD	t-value	R			Value	SD	t-value	R
Absorption	$\tilde{\nu}_0$	26.70	0.14	194.13	0.31	Fluorescence	$\tilde{\nu}_0$	22.08	0.08	265.52	0.90
	ETN	0.45	0.31	1.48			ETN	-1.73	0.19	-9.33	
Analysis using ETN and DNN						**Analysis using ETN and DNN**					
		TMPPD (n=21)						TMPPD (n=21)			
		value	SD	t-value	R			Value	SD	t-value	R
Absorption	$\tilde{\nu}_0$	30.13	0.19	161.82	0.80	Fluorescence	$\tilde{\nu}_0$	25.36	0.09	270.33	0.91
	ETN	2.41	0.49	4.88			ETN	-1.81	0.25	-7.26	
	DNN	-0.55	0.46	-1.20			DNN	0.19	0.23	0.84	
		MCTMPPD (n=22)						MCTMPPD (n=22)			
		value	SD	t-value	R			Value	SD	t-value	R
Absorption	$\tilde{\nu}_0$	26.85	0.14	192.34	0.56	Fluorescence	$\tilde{\nu}_0$	22.08	0.10	229.15	0.90
	ETN	1.13	0.39	2.87			ETN	-1.72	0.27	-6.36	
	DNN	-0.87	0.36	-2.40			DNN	-0.01	0.25	-0.03	

n = number of solvent used for LSER analysis; R = regression coefficient.

The plot of the theoretical values obtained by using ETN (also using ETN+DNN) versus the corresponding experimental values for the cyano-substitute TMPPDs are shown from Figure 5-44 to Figure 5-46 for cyano-substituted TMPPDs. The corresponding values of LSER coefficients are summarized in Table 5-15 (TMPPD and MCTMPPD) and (DCTMPPD).

First observation is that there no improvement in the regression coefficient R by the use of two parameter (ETN and DNN) instead of single parameter ETN as shown in Table 5-15 and Table 5-16. This observation indicates that solvent basicity term has no influence on the absorption as well as emission maxima of TMPPDs. Secondly absorption maxima of TMPPD can be seen in two distinct set of data points, one for the protic and other for aprotic as shown in . This is because the absorption maxima of TMPPD largely depend on the solvent acidity (high coefficients of α and SA have already discussed) and which is reduced after substitution of cyano group on aromatic ring as manifested by lower value for ETN coefficient in absorption of MCTMPPD compare to TMPPD. The LSER analysis for

fluorescence maxima is very well described by using ETN parameter only (R > 0.9). This is due to that fact that emission maxima of TMPPDs depends on the solvent acidity and solvent polarity (as found in LSER analysis using Kamlet-Taft and Catalan's parameter) and both of these are described by single ETN parameter.

Table 5-16: LSER coefficients for fluorescence of DCTM PPD using ETN and DNN parameters.

Analysis using ETN						Analysis using ETN					
Fluorescence (maxima)		DCTMPPD (n=23)				Fluorescence (COG)		DCTMPPD (n=23)			
		value	SD	t-value	R			value	SD	t-value	R
	$\tilde{\nu}_0$	20.34	0.12	166.00	0.82		$\tilde{\nu}_0$	19.72	0.10	193.26	0.84
	ETN	-1.78	0.27	-6.49			ETN	-1.59	0.23	-6.97	
Analysis using ETN and DNN						**Analysis using ETN and DNN**					
Fluorescence (maxima)		DCTMPPD (n=2)				Fluorescence (COG)		DCTMPPD (n=23)			
		value	SD	t-value	R			value	SD	t-value	R
	$\tilde{\nu}_0$	20.27	0.14	144.65	0.83		$\tilde{\nu}_0$	19.69	0.12	166.23	0.84
	ETN	-2.03	0.38	-5.32			ETN	-1.71	0.32	-5.31	
	DNN	0.33	0.35	0.93			DNN	0.15	0.30	0.52	

n = number of solvent used for LSER analysis; R = regression coefficient.

5.3.3 Correlation using Onsager polarity parameters

LSER analysis for cyano-substituted PPDs and TMPPDs have also been performed using Onsager polarity parameters $f(n^2)$ and $f(D,n^2)$. Due to specific solvent-solute interactions, the absorption and fluorescence maxima are modified in a way to subtract the contributions of specific interactions for each solvent by using the following equation:

$$\tilde{\nu}_{onsager} = \tilde{\nu}_{\exp} - a\alpha - b\beta \qquad \textbf{5-2}$$

where $\tilde{\nu}_{onsager}$ is the absorption (or emission) maxima used for LSER analysis, $\tilde{\nu}_{\exp}$ is absorption (or emission) maxima values obtained from experimental measurements, *a & b* are the theoretical contribution of solute obtained after applying LSER analysis using Kamlet-Taft parameters, α is solvent acidity and β is solvent basicity.

The LSER graphs for cyano-substituted PPDs are shown from Figure 5-47 to Figure 5-50 and corresponding data is summarized in Table 5-17 whereas the LSER plot for cyano-substituted TMPPDs are shown from Figure 5-51 to Figure 5-53 with data for LSER coefficients are compiled in Table 5-18.

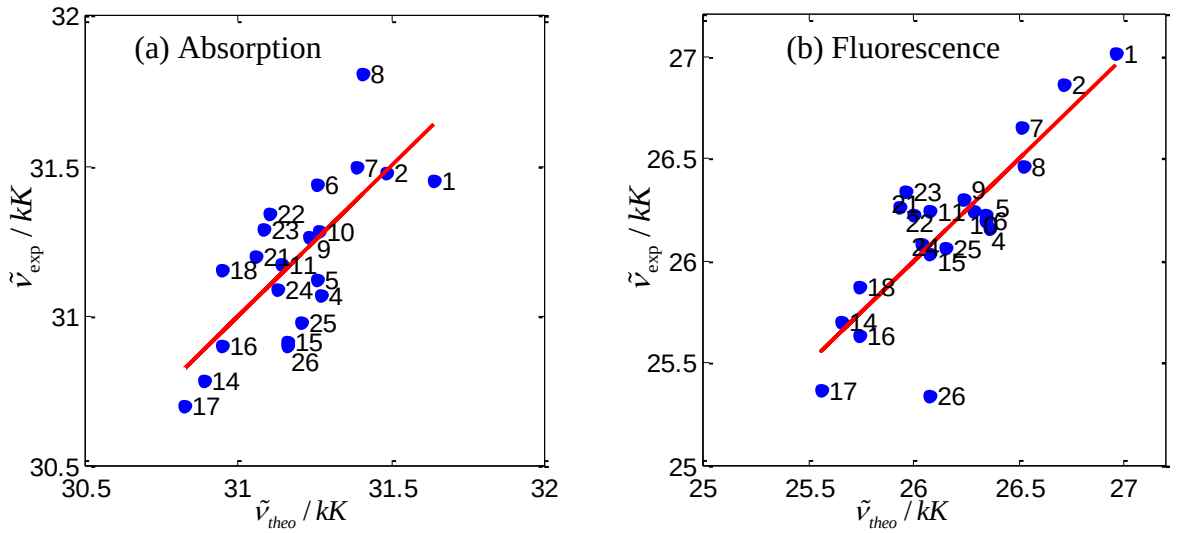

Figure 5-47: Linear solvation energy relationship (LSER) for the absorption (a) and fluorescence (b) maxima of PPD using Onsager polarity parameters for 21 solvents.

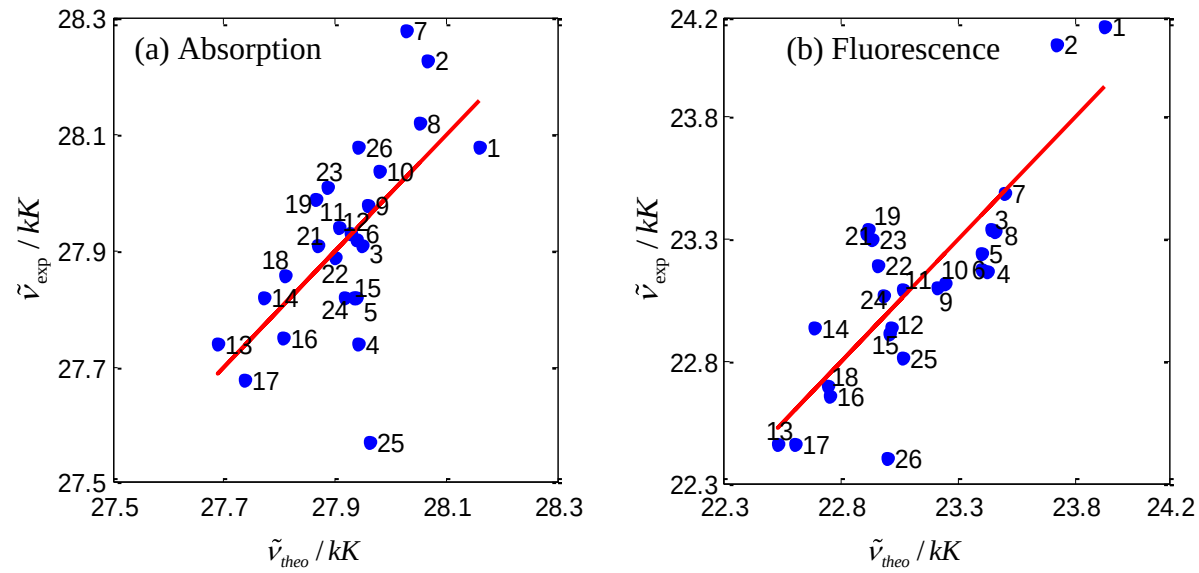

Figure 5-48: Linear solvation energy relationship (LSER) for the absorption (a) and fluorescence (b) maxima of MCPPD using Onsager polarity parameters for 25 solvents.

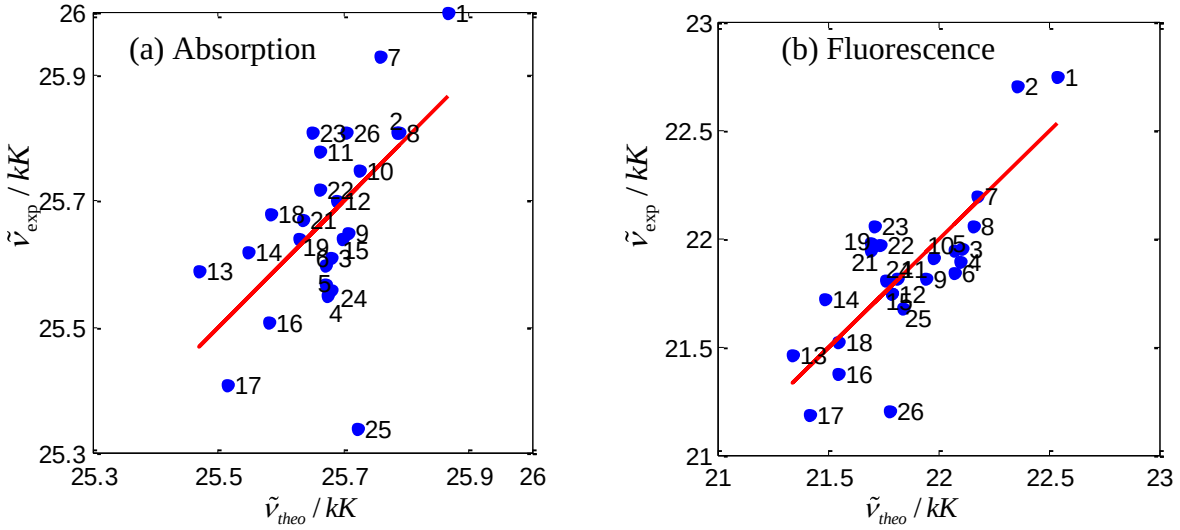

Figure 5-49: Linear solvation energy relationship (LSER) for the absorption (a) and fluorescence (b) maxima of DCPPD using Onsager polarity parameters for 25 solvents.

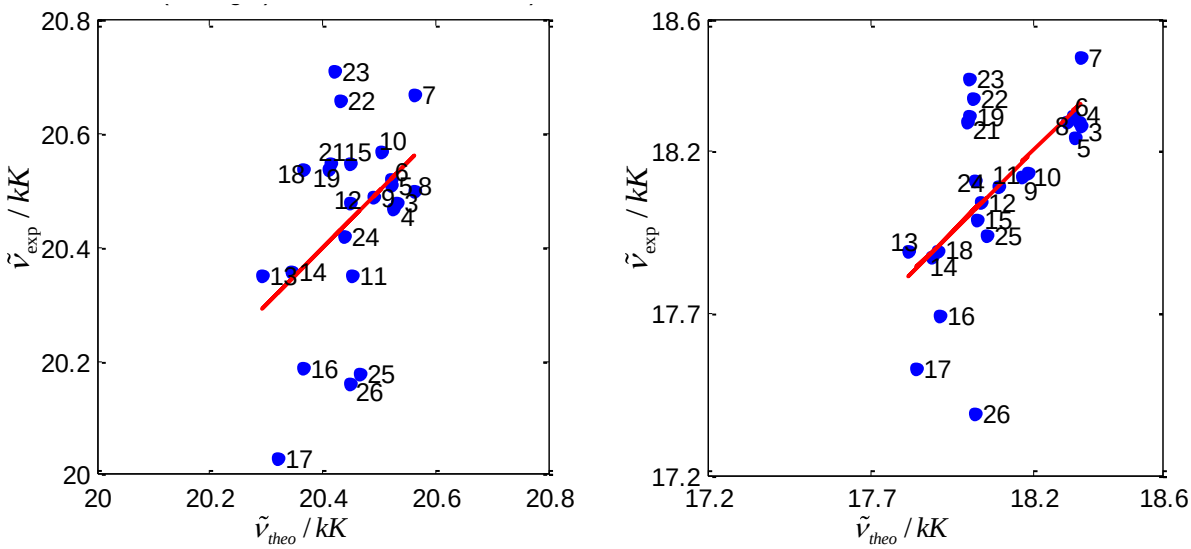

Figure 5-50: Linear solvation energy relationship (LSER) for the absorption (a) and fluorescence (b) maxima of TCPPD using Onsager polarity parameters for 23 solvents.

Table 5-17: LSER coefficients for cyano substitute PPDs using Onsager parameters.

LSER analysis using Onsager parameters										
		PPD (n=21)					PPD (n=21)			
		value	SD	t-value	R		value	SD	t-value	R
Absorption	$\tilde{\nu}_0$	33.29	0.59	56.10	0.732	Fluorescence	29.60	0.75	39.72	0.834
	f(D,n^2)	-1.91	0.43	-4.44			-3.43	0.54	-6.35	
	f(n^2)	-8.90	2.78	-3.20			-14.22	3.49	-4.07	
		MCPPD (n=25)					MCPPD (n=25)			
		value	SD	t-value	R		value	SD	t-value	R
Absorption	$\tilde{\nu}_0$	29.11	0.35	82.15	0.624	Fluorescence	26.11	0.68	38.63	0.816
	f(D,n^2)	-0.92	0.27	-3.35			-3.44	0.52	-6.59	
	f(n^2)	-5.12	1.64	-3.13			-11.78	3.12	-3.78	
		DCPPD (n=25)					DCPPD (n=25)			
		value	SD	t-value	R		value	SD	t-value	R
Absorption	$\tilde{\nu}_0$	26.72	0.33	81.02	0.584	Fluorescence	24.50	0.60	40.79	0.799
	f(D,n^2)	-0.72	0.26	-2.82			-2.87	0.46	-6.19	
	f(n^2)	-4.60	1.52	-3.02			-10.57	2.77	-3.81	
		TCPPD (n=23)					TCPPD (n=23)			
		value	SD	t-value	R		value	SD	t-value	R
Absorption	$\tilde{\nu}_0$	21.33	0.49	43.37	0.432	Fluorescence	19.67	0.70	28.02	0.614
	f(D,n^2)	-0.87	0.42	-2.10			-2.06	0.59	-3.47	
	f(n^2)	-3.52	2.18	-1.62			-5.85	3.11	-1.88	

n = number of solvent used for LSER analysis; R = regression coefficient.

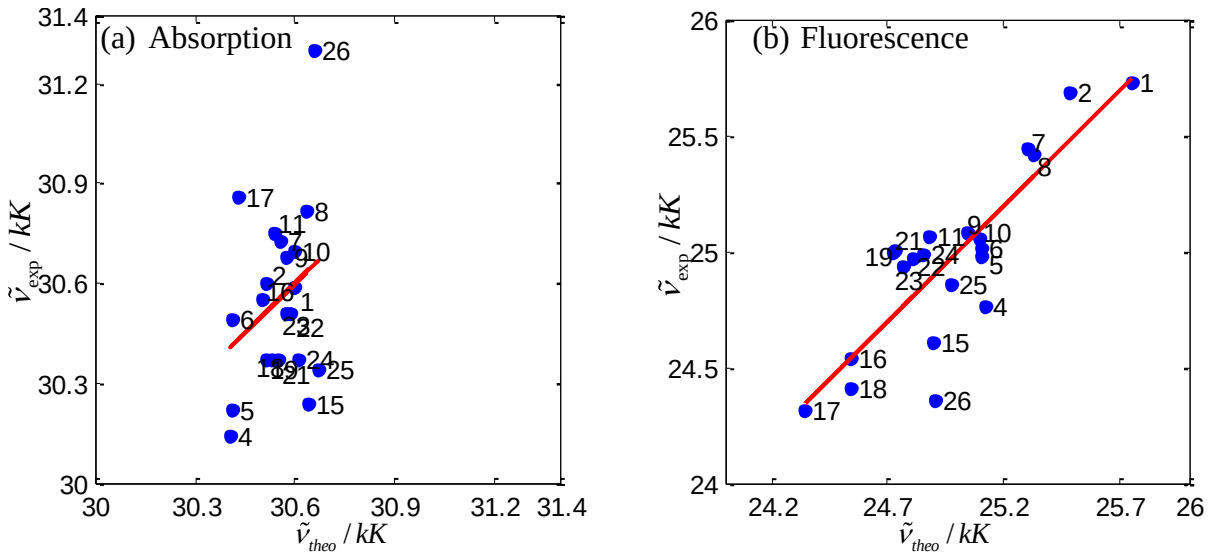

Figure 5-51: Linear solvation energy relationship (LSER) for the absorption (a) and fluorescence (b) maxima of TMPPD using Onsager polarity parameters for 21 solvents.

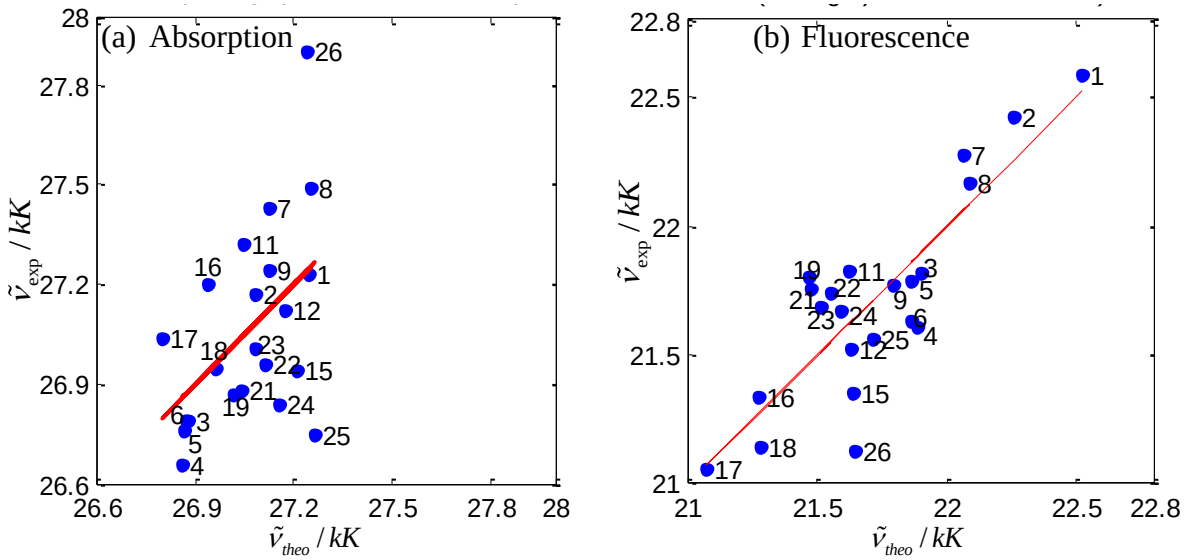

Figure 5-52: Linear solvation energy relationship (LSER) for the absorption (a) and fluorescence (b) maxima of MCTMPPD using Onsager polarity parameters for 22 solvents.

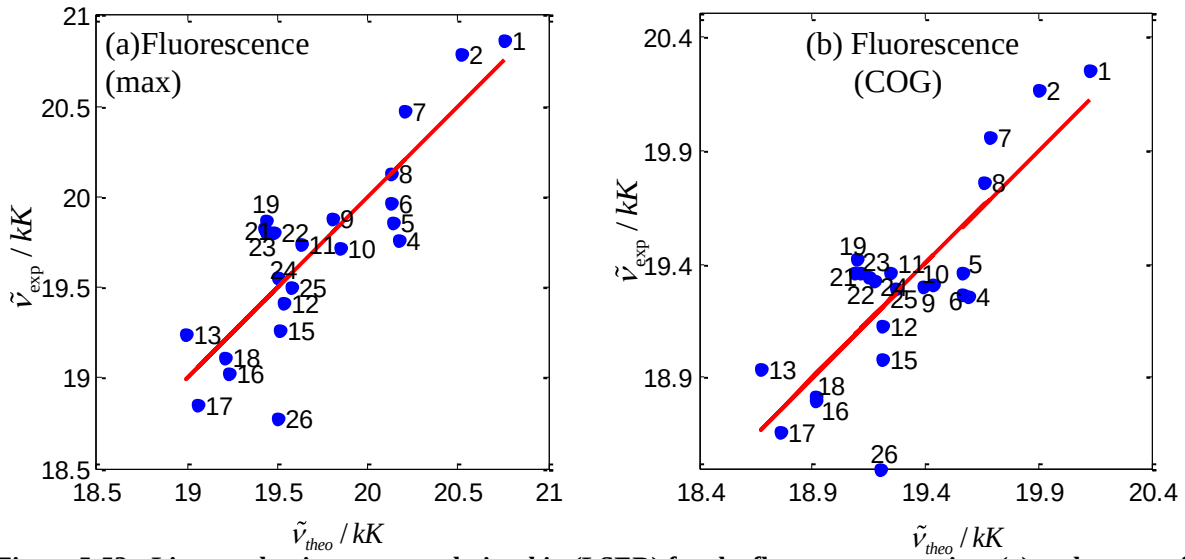

Figure 5-53: Linear solvation energy relationship (LSER) for the fluorescence maxima (a) and center of gravity (b) of DCTMPPD using Onsager polarity parameters for 23 solvents.

Table 5-18: LSER coefficients for cyano substitute TMPPDs using Onsager parameters.

LSER analysis using Onsager parameters											
		TMPPD (n=21)					TMPPD (n=21)				
		value	SD	t-value	R		value	SD	t-value	R
Absorption	$\tilde{\nu}_0$	31.45	0.86	36.61	0.30	Fluorescence	28.51	0.72	39.65	0.84
	$f(D,n^2)$	-0.02	0.61	-0.04			-3.34	0.51	-6.56	
	$f(n^2)$	-4.59	4.03	-1.14			-14.89	3.37	-4.41	
		MCTMPPD (n=22)					MCTMPPD (n=22)				
		value	SD	t-value	R		value	SD	t-value	R
Absorption	$\tilde{\nu}_0$	28.97	0.87	33.15	0.49	Fluorescence	25.35	0.72	35.32	0.84
	$f(D,n^2)$	-0.46	0.61	-0.76			-3.46	0.50	-6.87	
	$f(n^2)$	-9.29	4.06	-2.29			-15.24	3.33	-4.58	
		DCTMPPD (n=23)					DCTMPPD (n=23)				
		value	SD	t-value	R		value	SD	t-value	R
Fluorescence (COG)	$\tilde{\nu}_0$	22.48	0.72	31.34	0.81	Fluorescence (maxima)	23.33	0.82	28.51	0.85
	$f(D,n^2)$	-3.48	0.56	-6.20			-4.58	0.64	-7.16	
	$f(n^2)$	-12.72	3.34	-3.81			-13.87	3.81	-3.64	

n = number of solvent used for LSER analysis; R = regression coefficient.

5.4 LSER analysis using only aprotic solvent

It has been observed from the LSER analysis using both, Kamlet-Taft and Catalan's parameters that the cyano-substituted PPDs have high contribution of the specific interactions for solvatochromic shift in the absorption and emission maxima. Protic solvents are the hydrogen bond donors to the solute molecule. Because of the presence of specific interactions of the hydroxyl solvents (through high hydrogen bond donating ability to the solute molecules), Linear solvation energy relationship (LSER) analyses have been performed for aprotic solvents only (without hydroxyl solvents like water and alcohols) using Onsager polarity parameters as well as combination of ETN and DNN. The plot of the experimentally determined values of absorption and fluorescence maxima versus corresponding theoretically calculated values are shown from Figure A-12 to Figure A-11 (in Appendix). The values for LSER coefficients, obtained from multi-linear regression analysis, are summarized inTable 5-19 (using ETN parameter only), Table 5-20 (using ETN & DNN) and Table 5-21 (using Onsager parameters).

The large improvement in regression coefficients, R, for LSER analysis using ETN parameter (or both ETN and DNN) Table 5-19 and Table 5-20 have been obtained by using

only aprotic solvents compared to those obtained by using all solvents (both protic and aprotic solvents). This is because of fact that that the acidity and polarity of solvent have opposite effect in absorption. So when using aprotic solvents, ETN parameter represents mainly the solvent polarity effects. Also the values of regression coefficients for LSER analysis of absorption as well as emission maxima, using Onsager parameters, are improved when applying to only aprotic solvents, see Table 5-21, compared to those obtained by using both, protic and aprotic solvents. This is because of minimizing of the solvents having specific solvent-solute interactions which can not be described by the Onsager parameters.

Table 5-19: LSER coefficients for cyano substitute PPDs using ETN for aprotic solvents.

LSER analysis for absorption maxima						LSER analysis for fluorescence maxima					
		PPD (n=15)						PPD (n=15)			
		value	SD	t-value	R			value	SD	t-value	R
Absorption	$\tilde{\nu}_0$	31.36	0.15	216.14	0.722	Fluorescence	$\tilde{\nu}_0$	26.52	0.19	138.93	0.830
	ETN	-2.04	0.54	-3.76			ETN	-3.83	0.71	-5.36	
		MCPPD (n=18)						MCPPD (n=18)			
		value	SD	t-value	R			value	SD	t-value	R
Absorption	$\tilde{\nu}_0$	27.84	0.16	175.12	0.723	Fluorescence	$\tilde{\nu}_0$	23.51	0.18	133.68	0.855
	ETN	-2.47	0.59	-4.19			ETN	-4.29	0.65	-6.59	
		DCPPD (n=18)						DCPPD (n=18)			
		value	SD	t-value	R			value	SD	t-value	R
Absorption	$\tilde{\nu}_0$	25.55	0.17	148.64	0.700	Fluorescence	$\tilde{\nu}_0$	22.12	0.19	114.06	0.822
	ETN	-2.49	0.64	-3.92			ETN	-4.15	0.72	-5.78	
		TCPPD (n=16)						TCPPD (n=16)			
		value	SD	t-value	R			value	SD	t-value	R
Absorption	$\tilde{\nu}_0$	20.22	0.23	87.00	0.564	Fluorescence	$\tilde{\nu}_0$	18.08	0.24	75.16	0.725
	ETN	-2.07	0.81	-2.56			ETN	-3.31	0.84	-3.94	

n = number of solvent used for LSER analysis; R = regression coefficient.

Table 5-20: LSER coefficients for cyano substitute PPDs using ETN & DNN for aprotic solvents.

Analysis using ETN and DNN						Analysis using ETN and DNN					
		PPD (n=15)						PPD (n=15)			
		value	SD	t-value	R			value	SD	t-value	R
Absorption	$\tilde{\nu}_0$	31.47	0.12	260.45	0.850	Fluorescence	$\tilde{\nu}_0$	26.70	0.12	217.79	0.945
	ETN	-1.01	0.56	-1.81			ETN	-2.13	0.56	-3.78	
	DNN	-0.87	0.30	-2.95			DNN	-1.44	0.30	-4.78	
		MCPPD (n=18)						MCPPD (n=18)			
		value	SD	t-value	R			value	SD	t-value	R
Absorption	$\tilde{\nu}_0$	28.01	0.08	331.21	0.940	Fluorescence	$\tilde{\nu}_0$	23.68	0.12	199.80	0.946
	ETN	-0.82	0.38	-2.15			ETN	-2.66	0.54	-4.95	
	DNN	-1.46	0.21	-6.84			DNN	-1.45	0.30	-4.85	
		DCPPD (n=18)						DCPPD (n=18)			
		value	SD	t-value	R			value	SD	t-value	R
Absorption	$\tilde{\nu}_0$	25.74	0.08	330.38	0.954	Fluorescence	$\tilde{\nu}_0$	22.32	0.11	204.76	0.955
	ETN	-0.64	0.35	-1.82			ETN	-2.18	0.49	-4.41	
	DNN	-1.65	0.20	-8.38			DNN	-1.75	0.27	-6.35	
		TCPPD (n=16)						TCPPD (n=16)			
		value	SD	t-value	R			value	SD	t-value	R
Absorption	$\tilde{\nu}_0$	20.54	0.10	213.06	0.952	Fluorescence	$\tilde{\nu}_0$	18.42	0.09	214.67	0.976
	ETN	-0.39	0.36	-1.08			ETN	-1.54	0.32	-4.74	
	DNN	-1.79	0.20	-9.01			DNN	-1.90	0.18	-10.70	

n = number of solvent used for LSER analysis; R = regression coefficient.

Table 5-21: LSER coefficients for cyano substitute PPDs using Onsager parameters for aprotic solvents.

LSER analysis using absorption maxima						LSER analysis using fluorescence maxima					
		PPD (n=15)						PPD (n=15)			
		value	SD	t-value	R			value	SD	t-value	R
Absorption	$\tilde{\nu}_0$	33.73	0.63	53.82	0.822	Fluorescence	$\tilde{\nu}_0$	30.27	0.40	75.26	0.968
	$f(D,n^2)$	-1.95	0.45	-4.38			$f(D,n^2)$	-3.51	0.29	-12.26	
	$f(n^2)$	-11.07	2.97	-3.72			$f(n^2)$	-17.58	1.91	-9.21	
		MCPPD (n=18)						MCPPD (n=18)			
		value	SD	t-value	R			value	SD	t-value	R
Absorption	$\tilde{\nu}_0$	29.38	0.31	95.45	0.798	Fluorescence	$\tilde{\nu}_0$	26.56	0.49	54.31	0.936
	$f(D,n^2)$	-0.91	0.24	-3.87			$f(D,n^2)$	-3.70	0.37	-9.91	
	$f(n^2)$	-6.44	1.44	-4.49			$f(n^2)$	-14.02	2.28	-6.14	
		DCPPD (n=18)						DCPPD (n=18)			
		value	SD	t-value	R			value	SD	t-value	R
Absorption	$\tilde{\nu}_0$	26.99	0.27	100.66	0.795	Fluorescence	$\tilde{\nu}_0$	24.88	0.48	51.64	0.915
	$f(D,n^2)$	-0.68	0.20	-3.34			$f(D,n^2)$	-3.05	0.37	-8.28	
	$f(n^2)$	-5.93	1.25	-4.74			$f(n^2)$	-12.46	2.25	-5.54	
		TCPPD (n=16)						TCPPD (n=16)			
		value	SD	t-value	R			value	SD	t-value	R
Absorption	$\tilde{\nu}_0$	21.73	0.38	57.46	0.721	Fluorescence	$\tilde{\nu}_0$	20.05	0.34	58.79	0.922
	$f(D,n^2)$	-1.00	0.31	-3.26			$f(D,n^2)$	-2.37	0.28	-8.55	
	$f(n^2)$	-5.45	1.70	-3.21			$f(n^2)$	-7.63	1.53	-4.98	

n = number of solvent used for LSER analysis; R = regression coefficient.

5.5 *Effect of number of cyano groups*

The effect of cyano groups on the solvent-solute interactions in PPDs and TMPPDs can be underlined in various possible ways and depend on the set of parameters used to study these interactions. Because of the very good regression correlation coefficients for the Kamlet-Taft and Catalan's parameter sets, the LSER coefficients obtained using these parameter sets are discussed in details. LSER analyses obtained using Onsager polarity parameters have lower value of regression coefficients. This indicates the inaptness of the use of these parameters to describe the solvatochromic behaviour of these compounds and hence these are not further discussed.

5.5.1 Comparison for Kamlet-Taft parameters

LSER coefficients for absorption and emission maxima, after applying multiparameter linear regression correlation, using Kamlet-Taft parameters of solvents are summarized in Table 5-9 (for PPDs), Table 5-11 (for TMPPD and MCTMPPD) and Table 5-12 (for DCTMPPD). The comparison of the coefficients for the solvent acidity, basicity and polarity/polarizability terms are performed for all four PPDs (Figure 5-54) and TMPPDs (Figure 5-55 and Figure 5-56) separately in order to see the effect of cyano groups on the solvent-solute interactions. The coefficient of π^* is the least important in absorption as can be seen in Figure 5-54 by its lower values compared to coefficients of α and β in case of PPDs. However the absolute value of *s* is substantially increased for the fluorescence transition for all PPDs, Figure 5-54. All PPDs has some polar character in the ground state. The possible explanation might be the presence of 'syn' configuration of PPDs in the ground state as shown in Scheme 5-4. But the polarities cyano-substituted derivatives of PPD are remarkably increased after the electronic excitation because of some possible internal charge redistribution concentrating negative charge in the CN groups. This enhanced polarity in the excited state manifests itself in a larger response of cyano PPDs fluorescence towards solvent polarity. This means that PPDs have higher dipole moment in the excited state (μ_e) than that of in the ground state (μ_g) as it is usually the case for molecules containing donor and acceptor groups [55, 238].

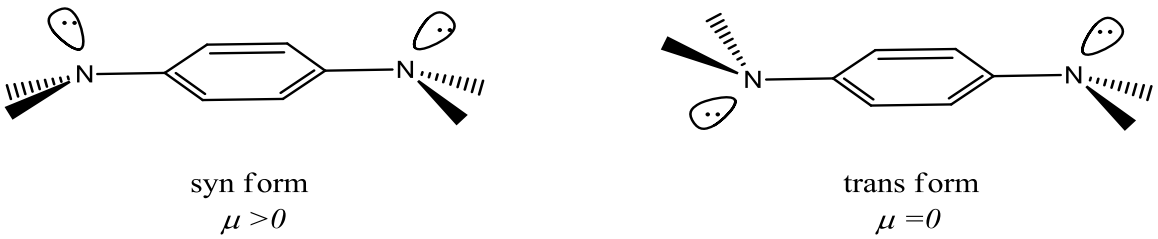

syn form
$\mu > 0$

trans form
$\mu = 0$

Scheme 5-4

It has been found that coefficient of solvent acidity is gradually decreased with increase in number of cyano groups on the PPD in LSER analysis for absorption maxima. The reason of such behaviour is underlined by the fact that the cyano groups are electron withdrawing and as a result the electron density on the amino groups of PPD is decreased with substitution of more cyano groups on the aromatic ring. The lone pair of electrons of the nitrogen atom of the amino groups are not easily available in the presence of more cyano groups on the aromatic ring. Such unavailability of the lone pair of amino group is responsible for inactivity of the solute toward the proton accepting ability from the solvent. So very less interaction of solute molecule containing more cyano groups towards solvent acidity in both

absorption and fluorescence has been observed. The coefficients of solvent basicity term (β) are largely increased by the substitution of cyano group in absorption as well as in emission. This high values for the coefficient of β manifest that the solute molecule has high tendency to donate a proton to the solvent molcules. The value for β coefficient is lowest for PPD and it is dramatically increased in MCPPD and then vary little on further cyano substitution in absorption. In case of emission β coefficient is least for the PPD and highest for the TCPPD. All PPDs have the tendency to interact through hydrogen bonding with the solvent molecule in ground as well as in excited states due to the presence of proton on the amino groups (-NH_2) of the aromatic ring. Thus PPDs show specific interaction with the solvent molecules. Going from PPD to TCPPD, coefficients of acidity term decrease while those of basicity term increase in both absorption and fluorescence.

In TMPPDs, it should be noted that the regression coefficients for the absorption analysis is not reasonably high because the data points are not well spread over the range. Two different set of data points (for protic and aprotic solvents) for the LSER analysis of TMPPD and MCTMPPD have been observed. TMPPDs have no proton on the nitrogen of amino groups, so the contribution for solvent basicity terms β are either very small or have large standard deviation which makes it meaningless. The significant term in the LSER analysis for the absorption maxima of TMPPD is the coefficient of α. None of the solvent parameters have higher contribution in the LSER analysis for absorption maxima of MCTMPPD. LSER analyses of TMPPDs have shown that the solvatochromic shift in the emission maxima is mainly governed by solvent polarity/polarizability with a little contribution of coefficient of α. The high coefficient of polarity for the emission maxima is due to increase in polarity of the molecule in the excited state as discussed for PPDs.

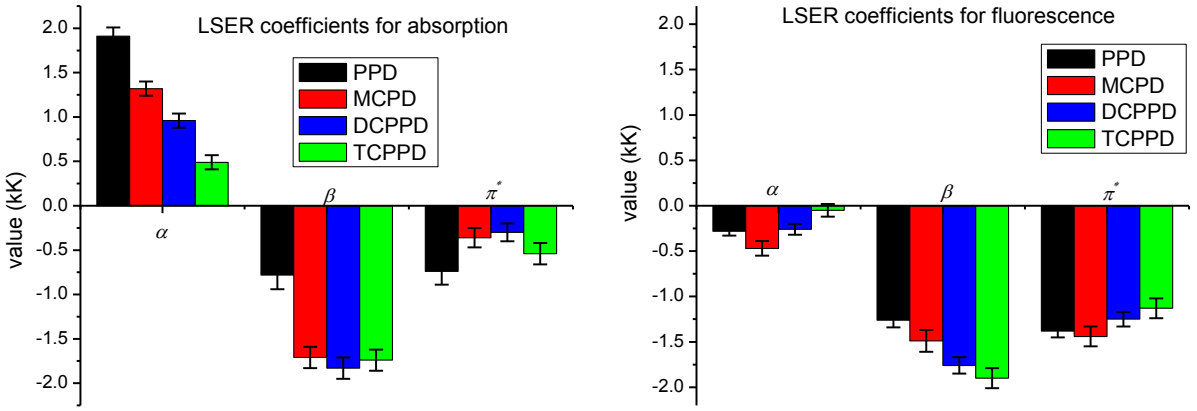

Figure 5-54: Coefficients of LSER analysis of absorption and fluorescence maxima for cyano-substituted PPDs using Kamlet-Taft parameters.

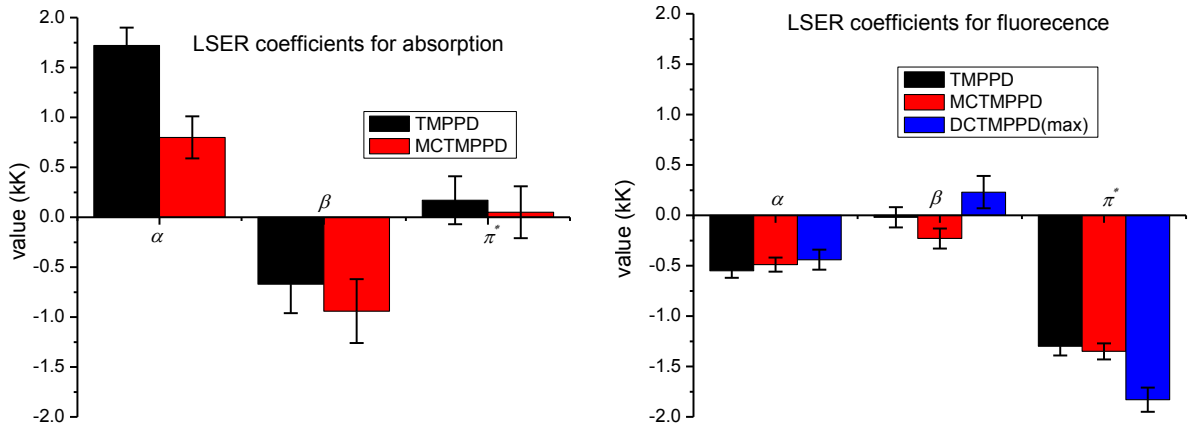

Figure 5-55: Coefficients of LSER analysis of absorption and fluorescence maxima for cyano-substituted TMPPDs using Kamlet-Taft parameters.

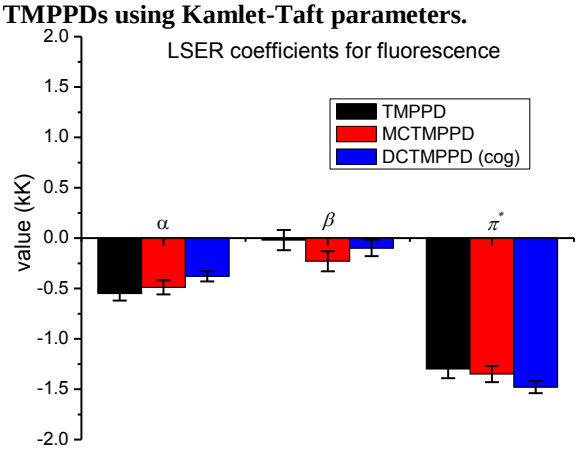

Figure 5-56: Coefficients of LSER analysis of fluorescence maxima for TMPPD & MCTMPPD and fluorescence center of gravity (cog) for DCTMPPD using Kamlet-Taft parameters.

5.5.2 Comparison using Catalan's parameters

The data for the LSER analyses, obtained by using Catalan's parameters have been summarized in Table 5-10 (for PPDs), Table 5-11 (for TMPPD and MCTMPPD) and Table 5-12(for DCTMPPD). The comparison of coefficients of SA, SB, Sdp and Sp for absorption and emission maxima different cyano-substituted PPDs are shown in Figure 5-57 and those of TMPPDs are shown in Figure 5-58 and Figure 5-59 (using the fluorescence centre of gravity for DCTMPPD).

For LSER analysis of absorption maxima, it has been observed that the LSER coefficients of SA vary in same way as coefficients of α for Kamlet-Taft but decrease rapidly with increase in cyano groups in PPDs. The LSER coefficient of SB for PPD is positive (whereas in the Kamlet-Taft analysis the coefficients of β for PPD is -ve) but has very low student's t-value and hence meaningless. The LSER coefficients for SB have been increased in –ve region, in similar way as in Kamlet-Taft analysis, on more cyano substitution. The emission maxima in case Catalan's parameters depend on almost all the parameters (SA, SB, Sdp and Sp). The variation, though relatively small, on going from the PPD to TCPPD using the Catalan's

parameters follow the same pattern as that in Kamlet-Taft analysis. The major contribution in both, absorption and emission maxima with relatively large standard deviation is coefficient of Sp. TMPPDs show negligible contribution of the coefficient of solvent basicity follow the same explanation as in Kamlet-Taft analysis. The absolute values for the coefficients of SA are decreased with substitution of cyano groups on TMPPD for both absorption and fluorescence.

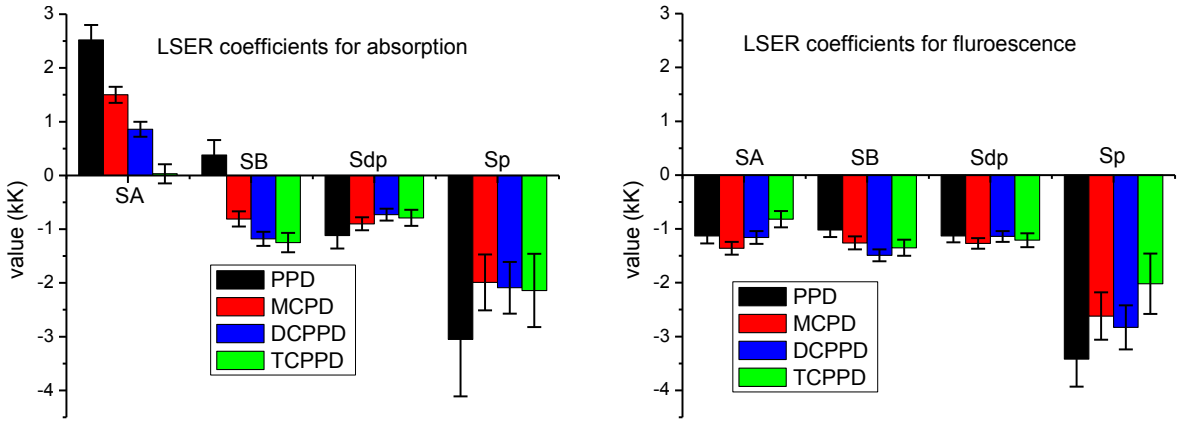

Figure 5-57: Coefficients of LSER analysis of absorption and fluorescence maxima for cyano-substituted PPDs using Catalan's parameters.

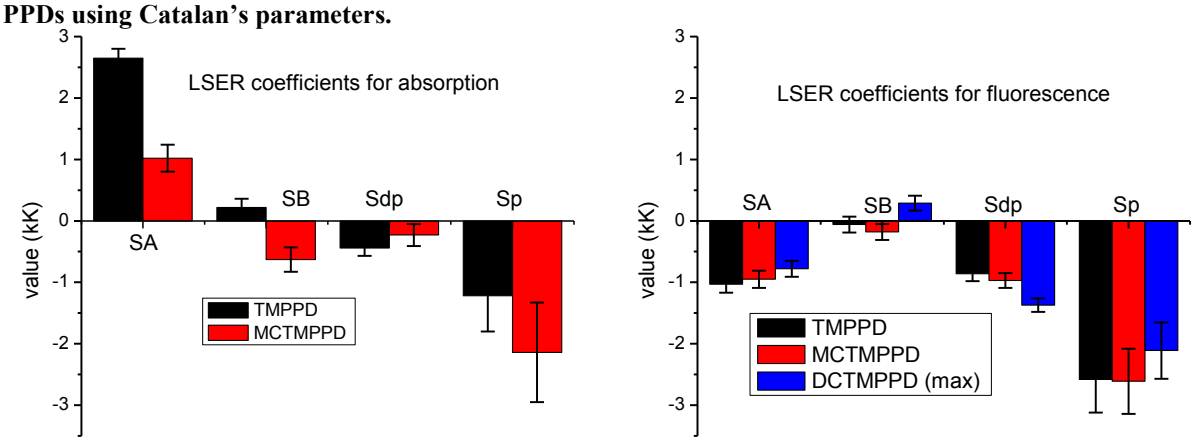

Figure 5-58: Coefficients of LSER analysis of absorption and fluorescence maxima for cyano-substituted TMPPDs using Catalan's parameters.

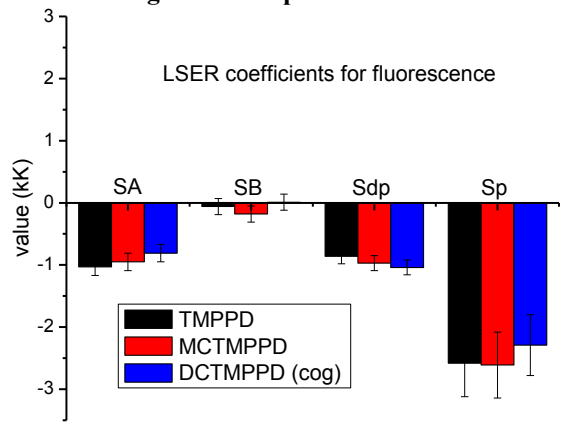

Figure 5-59: Coefficients of LSER analysis of fluorescence maxima for TMPPD & MCTMPPD and fluorescence center of gravity (cog) for DCTMPPD using Catalan's parameters.

5.5.3 Comparison using ETN and DNN parameters

The comparison of LSER coefficients obtained by using ETN and DNN for different PPDs and TMPPDs have been shown from Figure 5-60 to Figure 5-62. LSER analyses of absorption and emission maxima have been compared by using the different set of solvents: (a) all solvents (protic and aprotic) and (b) only aprotic solvents.

It has to be mentioned again that ETN parameter represents both, the solvent polarity and solvent acidity where DNN parameter describe the solvents basicity. An interesting observation is the opposite sign for the values of the ETN coefficients in LSER parameters for the absorption maxima using all solvents (protic+aprotic) and only aprotic solvents as shown in Figure 5-60(a) and Figure 5-60 (b), respectively. As describe earlier ETN value describe polarity as well as the acidity of the solvent so when applying LSER analysis to all solvents, the dominating contribution of solvent acidity (as discussed in previous comparison of Kamlet-Taft and Catalan's parameters) but polarity in more influential when applying to only aprotic solvents. In LSER analysis for absorption maxima, both solvent acidity and polarity behave in opposite direction so is the ETN coefficients.

In fluorescence, both the solvent acidity and polarity behave in similar way so the ETN parameter behaves similar in fluorescence analysis for all solvent and for aprotic solvents only as shown in Figure 5-61. In TMPPDs, the absorption the ETN is positive due to prominent solvent acidity effect while in emission the only governing factor is ETN (solvent acidity and polarity) with no contribution of DNN.

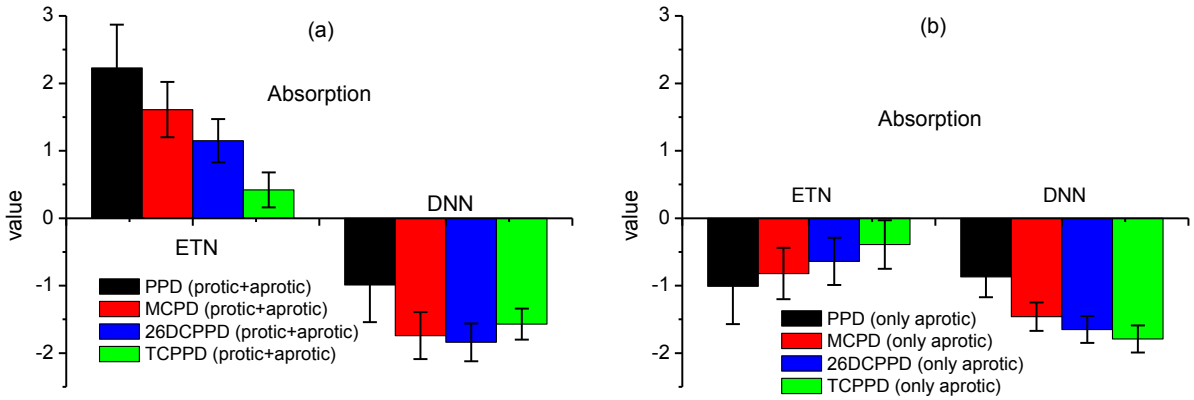

Figure 5-60: Comparison of LSER coefficients for absorption maxima of cyano-substituted PPDs using ETN+DNN parameters for (a) protic+aprotic and (b) only aprotic solvents.

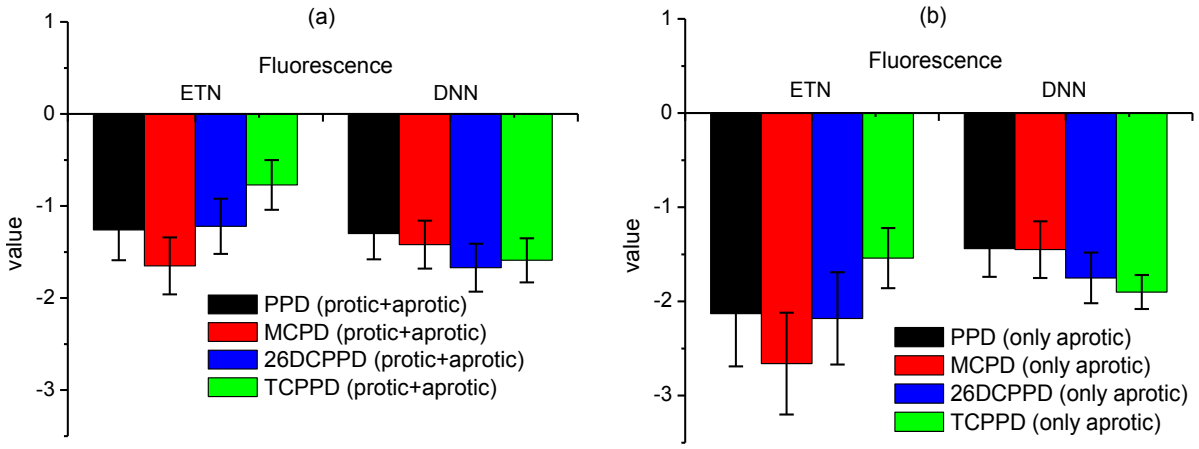

Figure 5-61: Comparison of LSER coefficients for fluorescence maxima of cyano-substituted PPDs using ETN+DNN parameters for (a) protic+aprotic and (b) only aprotic solvents.

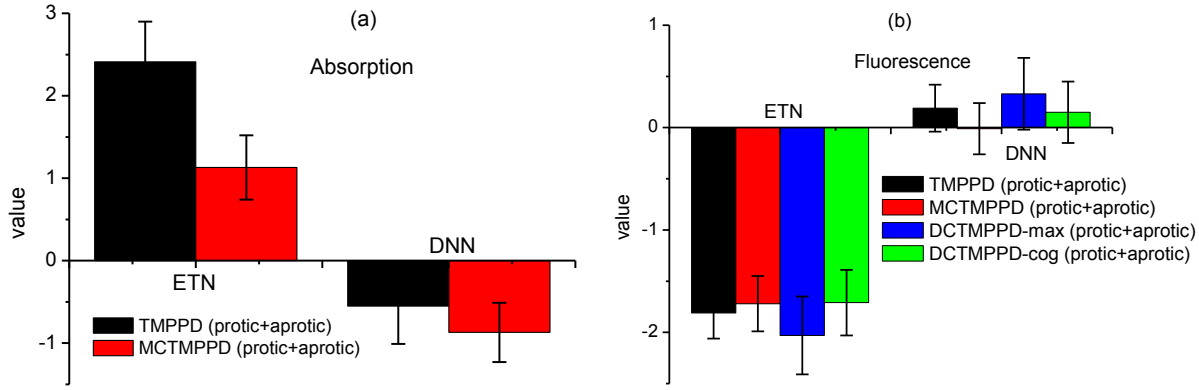

Figure 5-62: Comparison of LSER coefficients for (a) absorption and (b) fluorescence maxima of cyano-substituted TMPPDs using ETN+DNN parameters for different protic and aprotic solvents.

5.6 Comparison of Kamlet-Taft and Catalan's parameters

The coefficients of solvent acidity and basicity term for different PPDs and TMPPD obtained from the LSER analyses using Kamlet-Taft and Catalan's parameters have been compared to each other. It has been observed that in LSER correlations for absorption maxima, the coefficients of SA term are higher compared to that of α for PPD and TMPPD. On increasing the number of cyano groups, from PPD to TCPPD, the coefficients of SA are decreases more rapidly compared to those of α and for TCPPD there is almost no contribution from the solvent acidity according to Catalan's parameters.

In case of coefficient of solvent basicity, the coefficients of β value are always higher compared to corresponding coefficients of SB in absorption as shown in Figure 5-63. For LSER coefficients in emission maxima, the coefficients for SA are much higher than those of α in all the compounds see Figure 5-64. The value for the coefficient for SA is almost three times higher than that of α in case of MCPPD and four times higher in PPD and

26DCPPD. In case of TCPPD the contribution of coefficient of α is insignificant but the coefficient of SA term has its share in solvatochromic analysis. The coefficients of basicity terms for the emission analysis behave almost in same fashion as in absorption analysis, i.e. coefficients for SB is relatively smaller than those of β as shown in Figure 5-64.

Such a difference in the LSER coefficient obtained by using Kamlet-Taft and Catalan's parameters is due to the different parameterization of solvent properties, especially for protic solvents.

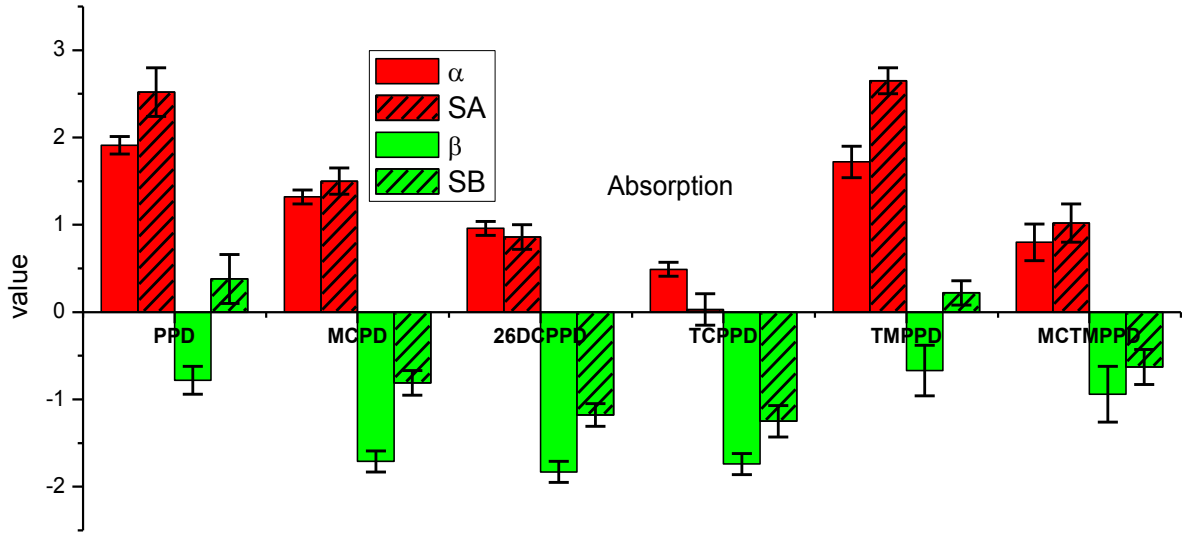

Figure 5-63: Comparison of solvent acidity and basicity parameters of Kamlet-Taft and Catalan for absorption.

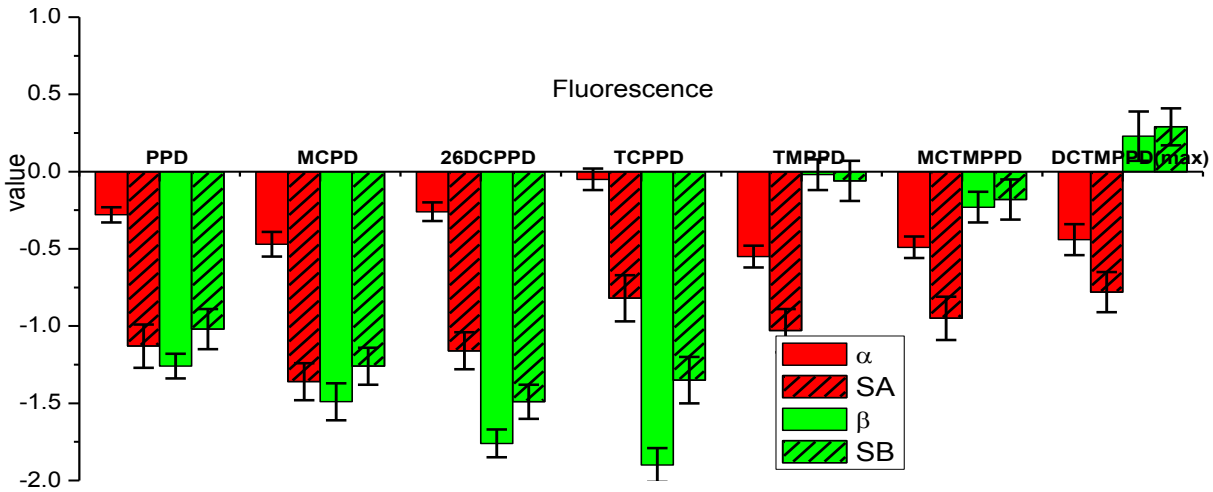

Figure 5-64: Comparison of solvent acidity and basicity parameters of Kamlet-Taft and Catalan for fluorescence.

5.6.1 Absorption and fluorescence maxima

The theoretical values for absorption and emission maxima have been calculated from LSER analysis using different parameter sets. Three different parameters set Kamlet-Taft, Catalan's

parameters and ETN+DNN have been applied to obtain the theoretical values. The theoretically values of $\tilde{\nu}_o$ have been plotted for different number of cyano groups substituted on the aromatic ring of PPD; e.g. 0 for PPD, 1 for MCPPD, 2 for 26DCPPD, 4 for TCPPD) as are shown in Figure 5-65 (a) for absorption maxima and in Figure 5-65 (b) for emission maxima. From Figure 5-65 (a) and Figure 5-65 (b), one can estimate the region for the $\tilde{\nu}_o$ for absorption and emission maxima for the PPD containing three cyano groups.

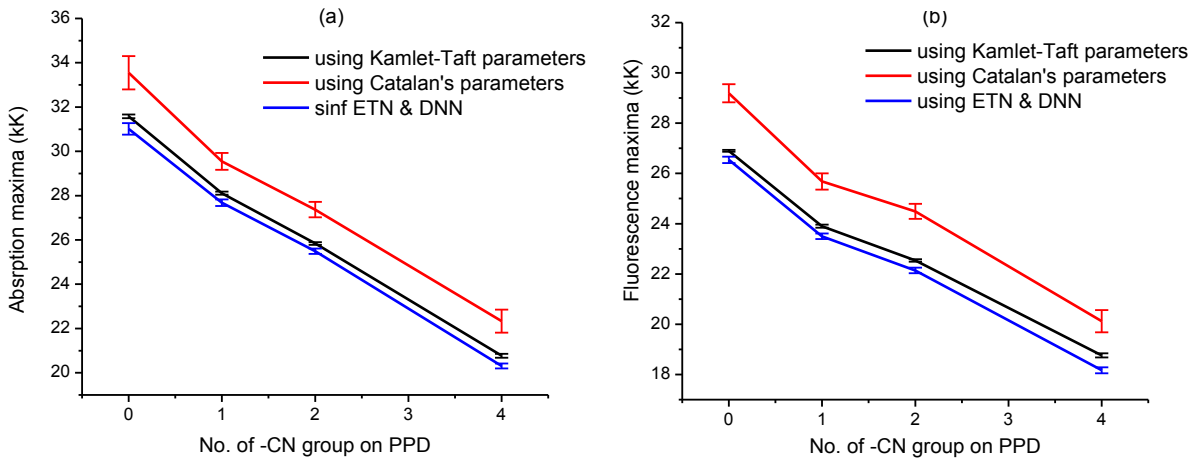

Figure 5-65: Theoretically calculated values of $\tilde{\nu}_o$ for (a) absorption and (b) fluorescence of different cyano-substituted PPDs using different parameter sets.

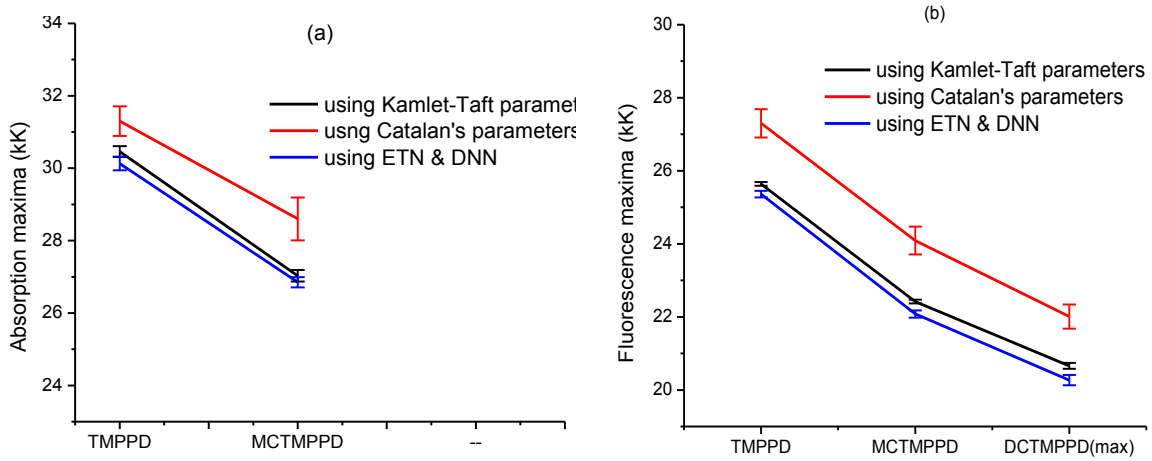

Figure 5-66: Theoretically calculated values of $\tilde{\nu}_o$ for (a) absorption and (b) fluorescence of different cyano-substituted TMPPDs using different parameter sets.

The $\tilde{\nu}_o$ values for TMPPDs have been plotted for the absorption and fluorescence maxima and shown in Figure 5-66. It can be seen clearly, that the theoretical value obtained from Catalan's parameters have higher values compare to those obtained from other to parameters set in case of the absorption as well as emission maxima. The theoretical values can be

verified by measuring the fluorescence and excitation maxima for the gas phase sample at very low pressure.

5.7 Effect of methylation of amino groups of PPD

Comparison of the PPDs with corresponding counter part of methylated derivatives (TMPPDs) has been studied. Such comparison of the LSER coefficients for absorption maxima have been shown in Figure 5-67 (a) and Figure 5-67 (b) for Kamlet-Taft and Catalan's parameters, respectively.

It should be noted that LSER analysis for absorption maxima in case of TMPPDs have relatively lower regression coefficients (in case MCMPPD) and data points are not well distributed over the range shown in Figure 5-37 (a and b) and Figure 5-38 (a and b). The absolute value of coefficients of acidity terms (α and SA) either remain the same or decrease a little for TMPPDs compare to PPDs in absorption values. The small decrease in TMPPDs might be due to steric reason after methyl substitution on the amino groups. The coefficients of basicity terms (β and SB) are decreased due to unavailability of the protons of amino groups after methylation. The coefficients of polarity term (π^* and Sdp) has also been lowered on methylation of PPDs showing that PPDs are more polar (may exist in syn forms) in behaviour compare to TMPPDs.

LSER analysis for emission maxima are shown in Figure 5-68 (using Kamlet-Taft parameters) and Figure 5-69 (using Catalan's parameters). Figure 5-70 show the LSER analysis for emission using fluorescence centre of gravity (cog) instead of maxima (max) for DCTMPPD. Very small variation in values for the LSER coefficients for acidity (α and SA) and polarity (π^* and Sdp) terms have been observed that which can be explained on the same lines as was done in the absorption. But dramatic decreases in the coefficients of the basicity terms (β and SB) on methylation have been observed. The values for these coefficients change to almost zero for TMPPDs which are much higher (usually most influential) in PPDs. This effect is due to fact the protons of the amino groups, which are very active, in PPDs are replaced by methyl groups giving the corresponding TMPPDs.

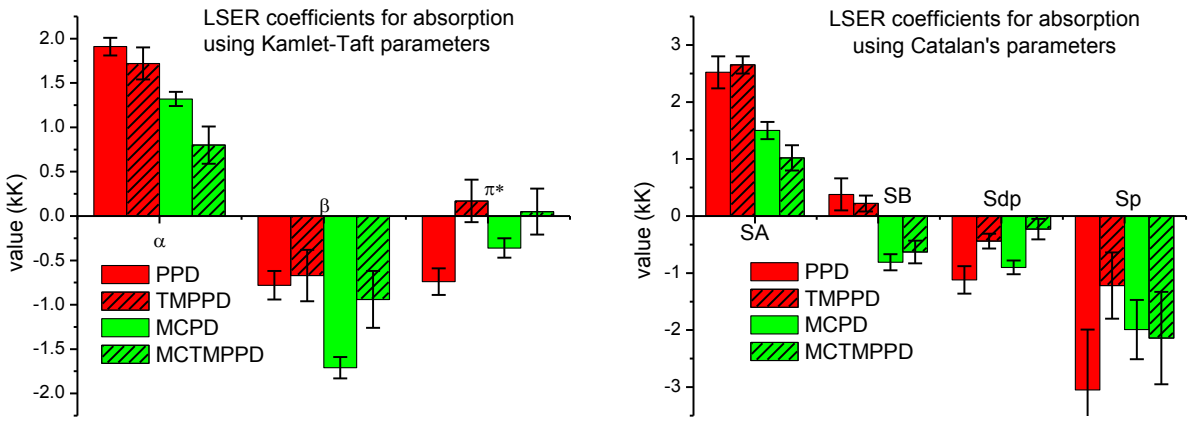

Figure 5-67: Coefficients of LSER analysis of absorption maxima for PPD, MCPPD, TMPPD and MCTMPPD using (a) Kamlet-Taft and (b) Catalan's parameters.

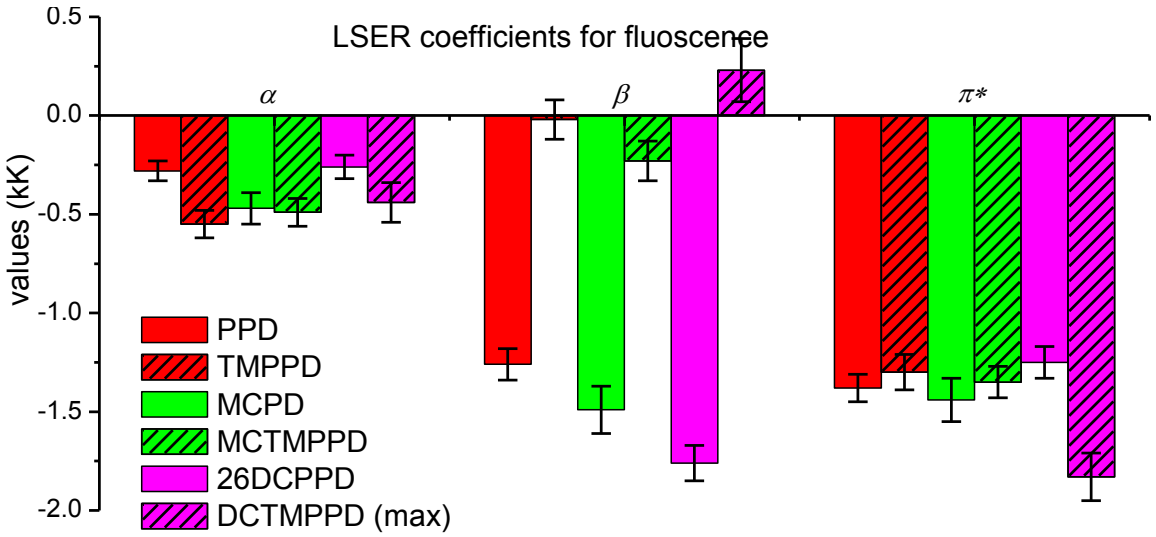

Figure 5-68: Coefficients of LSER analysis of fluorescence maxima for PPD, MCPPD, 26DCPPD, TMPPD, MCTMPPD and DCTMPPD (max) using Kamlet-Taft parameters.

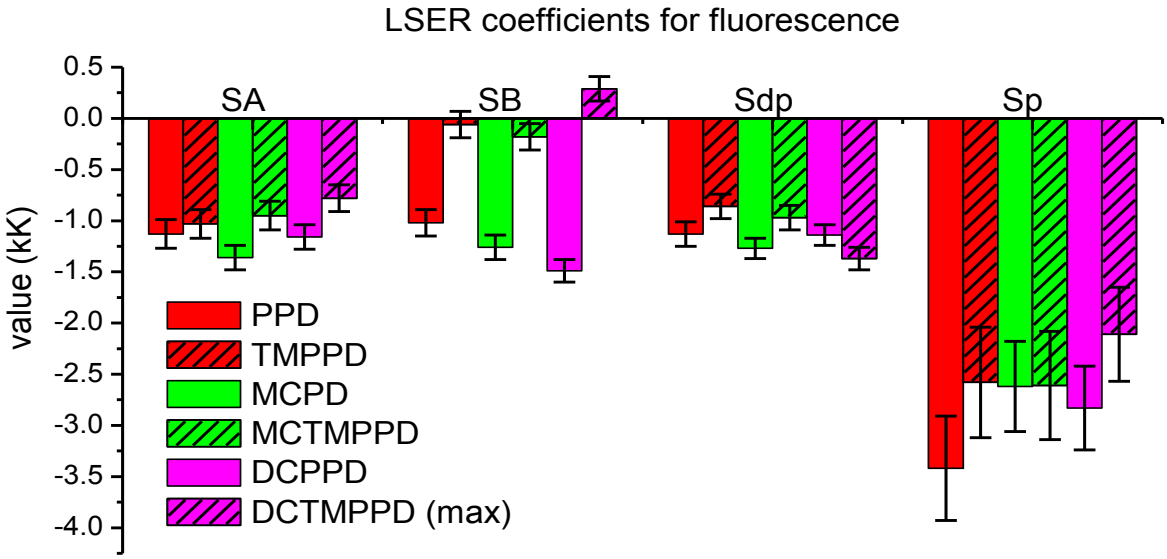

Figure 5-69: Coefficients of LSER analysis of fluorescence maxima for PPD, MCPPD, 26DCPPD, TMPPD, MCTMPPD and DCTMPPD (max) using Catalan's parameters.

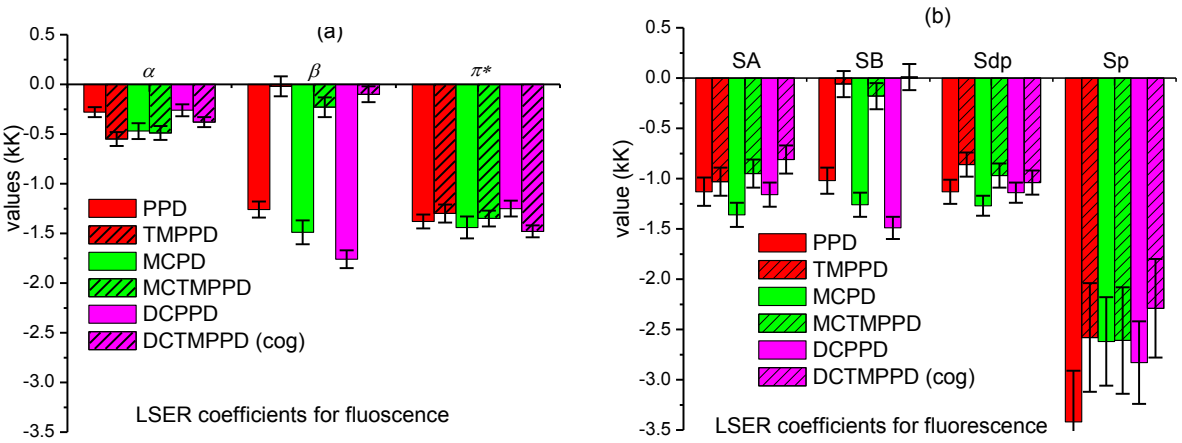

Figure 5-70: Coefficients of LSER analysis of fluorescence maxima for PPD, MCPPD, 26DCPPD, TMPPD, MCTMPPD and DCTMPPD (cog) using (a) Kamlet-Taft parameters (b) Catalan's parameters.

5.7.1 Comparison of photophysical properties

Photophysical properties like Stokes shift,0-0 transition energy E_{00}, fluorescence lifetime τ, fluorescence quantum yield Φ, radiative rate constant k_r and non-radiative rate constant k_{nr} measured in different solvents have been compared for PPDs (from Figure 5-71 to Figure 5-73) and TMPPDs (from Figure 5-74 to Figure 5-76). It has been observed that the Stokes shift is larger and span over wide range(~ 4600 cm^{-1} to 8300 cm^{-1}) in different solvents for PPD compared to small and narrow spaced in case TCPPD (~ 2000 cm^{-1} to 3000 cm^{-1}). The Stokes shift data for TMPPD (Figure 5-74) has interesting observations. The Stokes shift from TMPPD to MCTMPPD is either remains the same or slightly decreases while from MCTMPPD to DCTMPPD value of Stokes shift increases for all the solvents.

The E_{00} in different solvents is decreased with increase of cyano groups in both PPDs and TMPPDs.

Both, the fluorescence lifetime and fluorescence quantum yields have been increased largely after the substitution of the cyano group(s) on the aromatic ring of PPD and TMPPD as shown in Figure 5-72 and Figure 5-75, respectively. The distinct behaviour (very fluorescence lifetime and quantum yields) of mono-cyano derivative of PPD and TMPPD in the protic solvents has been observed. This effect might be due to enhanced hydrogen bonding between the solvent and solute molecules in protic solvents and a large increase in the non-radiative rate constants k_{nr} have been observed for MCPPD and MCTMPPD in protic solvents as shown in Figure 5-73 and Figure 5-76, respectively.

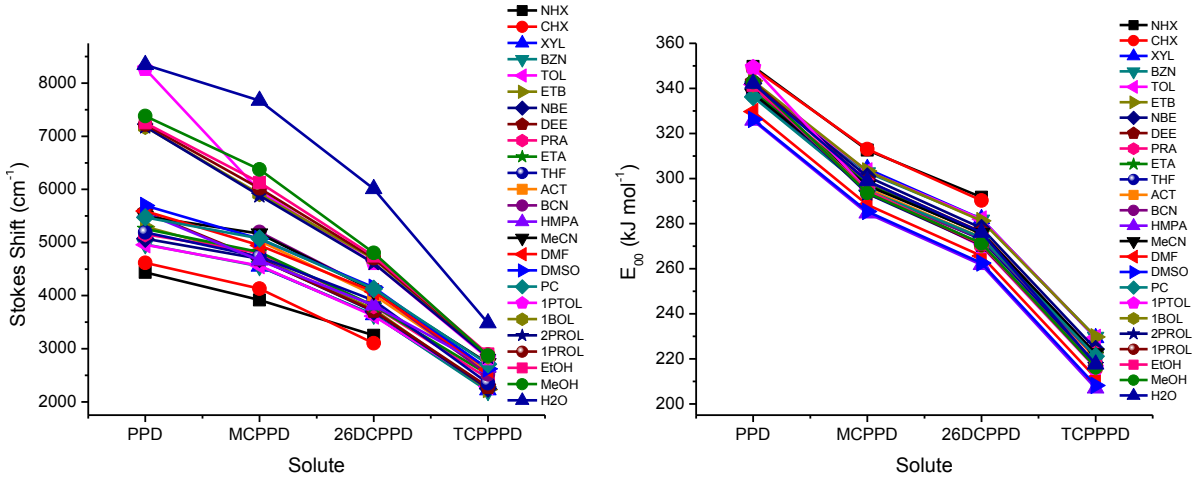

Figure 5-71: Stokes shift and E_{00} of cyano-substituted PPDs in different solvents.

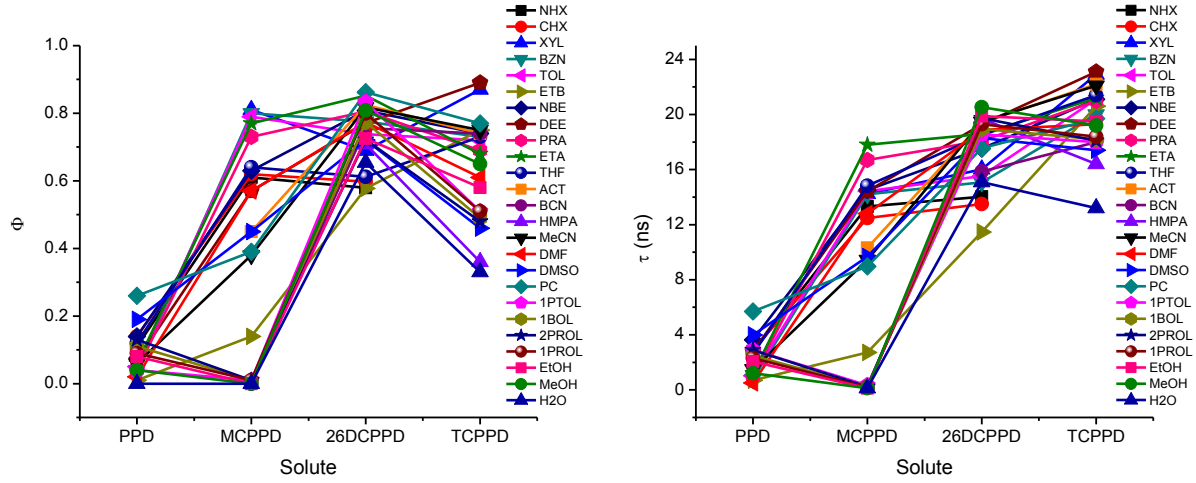

Figure 5-72: Fluorescence quantum yield (Φ) and fluorescence lifetime (τ) of cyano-substituted PPDs in different solvents.

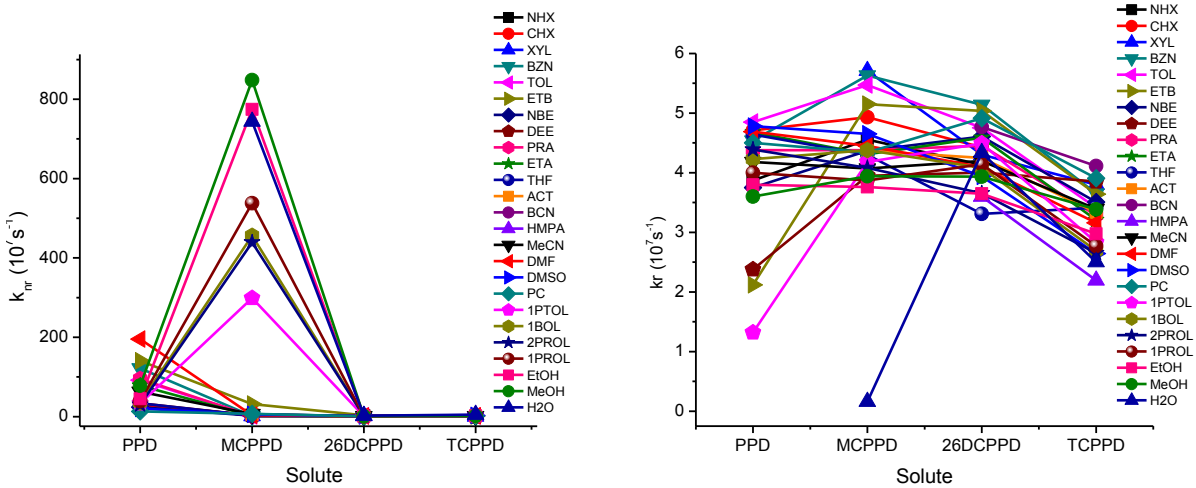

Figure 5-73: Radiative (k_r) and non-radiative rate constants (k_{nr}) of cyano-substituted PPDs in different solvents.

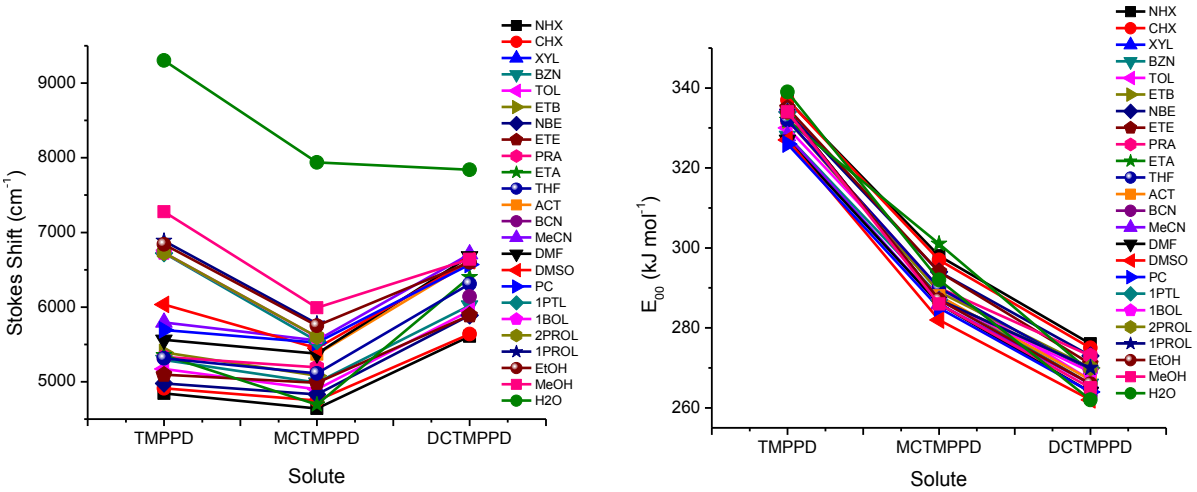

Figure 5-74: Stokes shift and E_{00} of cyano-substituted TMPPDs in different solvents.

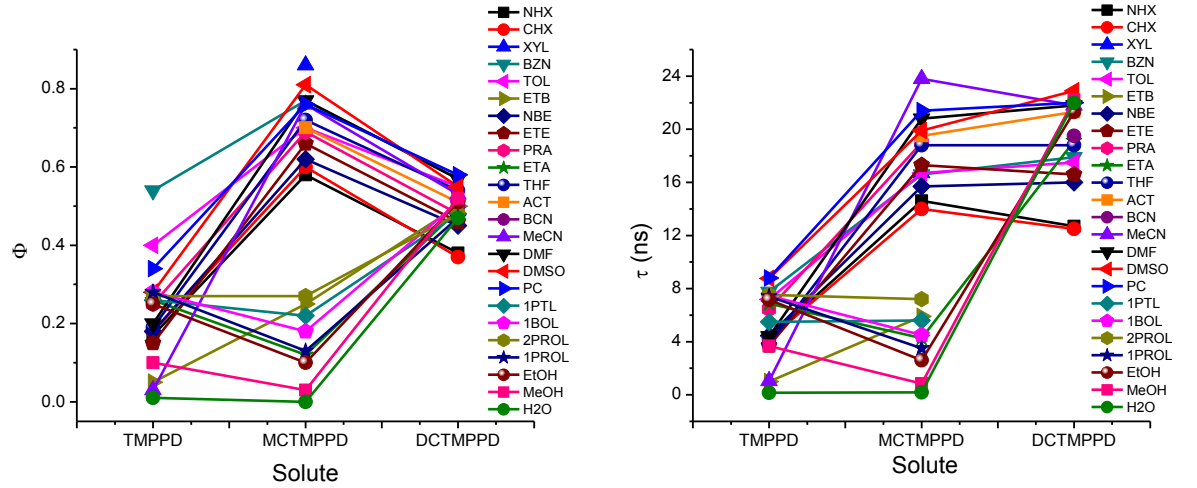

Figure 5-75: Fluorescence quantum yield (Φ) and fluorescence lifetime (τ) of cyano-substituted TMPPDs in different solvents.

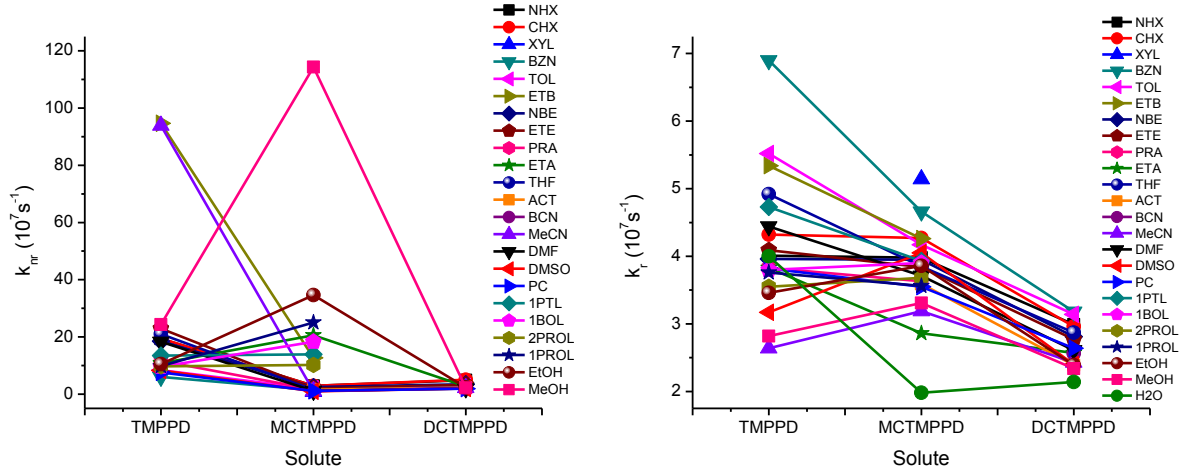

Figure 5-76: Radiative (k_r) and non-radiative rate constants (k_{nr}) of cyano-substituted TMPPDs in different solvents.

5.8 Electrochemical properties

Different electrochemical properties like redox potential values and diffusion coefficients for the cyano substitute PPDs (MCPPD, 26DCPPD and TCPPD) and TMPPDs (MCTMPPD and DCTMPPD) have been measured. All redox potential in the present study are reported versus Ag/AgCl.

Cyclic voltammetric studies for the various cyano-substituted PPDs and TMPPDs have been performed at room temperature (298 K). All cyclic voltammograms (CVs) have been studied in acetonitrile using 0.1 M tetrabutylammonium hexafluorophosphate ($TBAPF_6$) in acetonitrile as supporting electrolyte with Pt as working electrode and Ag/AgCl as reference electrode. Both PPD and TMPPD (and there derivatives) can form di-cations by losing two electrons at different potential as shown in Scheme 5-5.

$$M \underset{}{\overset{-e}{\rightleftharpoons}} M^{+} \overset{-e}{\rightleftharpoons} M^{2+}$$

Scheme 5-5

M corresponds to PPD or TMPPD. In the present study we have seen electrochemical oxidations of the cyano-substituted PPDs are irreversible within the time frame of potential scan where as the cyano-substituted TMPPDs have undergone reversible oxidations. This attributes the fact of the hydrogen atom abstraction from the amino group ($-NH_2$) of PPDs which is not present in methylated derivatives.

Redox potential

The standard redox potential in case of reversible systems have been determined by the method reported by Fukuzumi *et al.* [239]. Activation free energy for one electron transfer between oxidants and reductants can be expressed as a function of redox potential of oxidant and reductants. Two such equations, eq. 5-3 and eq. 5-4, have been obtained on the basis of Rehm-Weller and Marcus free energy relationships.

$$E_{ox}^{p} = E_{ox}^{o} + \frac{1-2\beta}{[\beta(1-\beta)]^{1/2}} \Delta G_0^{\neq} \qquad 5\text{-}3$$

$$E_{ox}^{p} = E_{ox}^{o} + 4(1-2\beta)\Delta G_0^{\neq} \qquad 5\text{-}4$$

where $\beta = \dfrac{1.857RT}{F(E_{ox}^{p} - E_{ox}^{p/2})}$

The value of is also calculated from the dependence of peak potential E_{ox}^{p} on scan rate *v* as given by eq. 5-5 (i.e from the slop of E_{ox}^{p} versus *log v*).

$$E_{ox}^{p} = \frac{2.3RT}{2\beta F}\log v + const. \qquad 5\text{-}5$$

The slope of either $\frac{1-2\beta}{[\beta(1-\beta)]^{1/2}}$ or $4(1-2\beta)$ versus the peak potential E_{ox}^{p} give the value of standard oxidation potential.

For reversible system the formal potential has been calculated from eq. 5-6.

$$E_{ox}^{o} = \frac{E_{pa} + E_{pc}}{2} \qquad 5\text{-}6$$

E_{pa} and E_{pc} are corresponding anodic and cathodic peak potential for reversible system.

Diffusion coefficient

The diffusion coefficients have been calculated using Randles-Sevcik equation for reversible (eq. 5-7) and irreversible (eq. 2-66) system .

$$i_p = (2.69\times10^5)n^{3/2}ACD^{1/2}v^{1/2} \qquad 5\text{-}7$$

$$i_p = \left(2.99\times10^5\right)n(n\beta)^{1/2}ACD^{1/2}v^{1/2} \qquad 5\text{-}8$$

where temperature is 298 K, i_p is expressed in ampere, A expressed in cm^2, D in cm^2s^{-1}, C in $molcm^{-3}$, v in Vs^{-1}.

The diffusion coefficient D is calculated from the slope of i_p (A) versus v (V s^{-1}).

5.9 Electrochemistry of cyano-substituted PPDs

Cyclic voltammograms of the PPD and its cyano-substituted derivatives (MCPPD, 26DCPPD and TCPPD) have been obtained at room temperature (298 K). PPD has reversible one electron transfer in as shown in Figure 5-77(a). The peak current varies linearly as shown in Figure 5-77(b). The 2nd oxidation peak of PPD is reversible at low scan rate and has lost its shape with increase in the scan rate as shown by Figure 5-78.

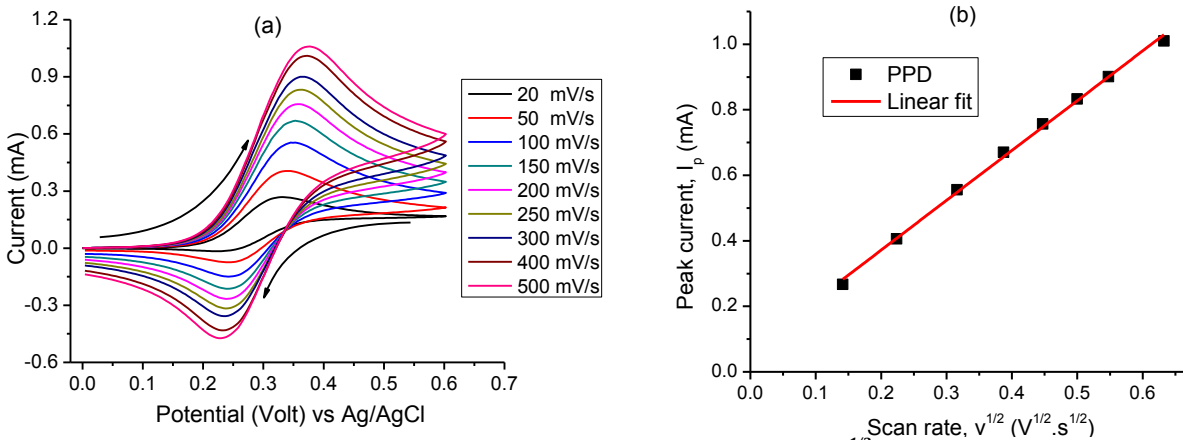

Figure 5-77: (a) CVs of PPD at different scan rates. (b) Plot of scan rate ($v^{1/2}$) versus peak current (I_p) for PPD.

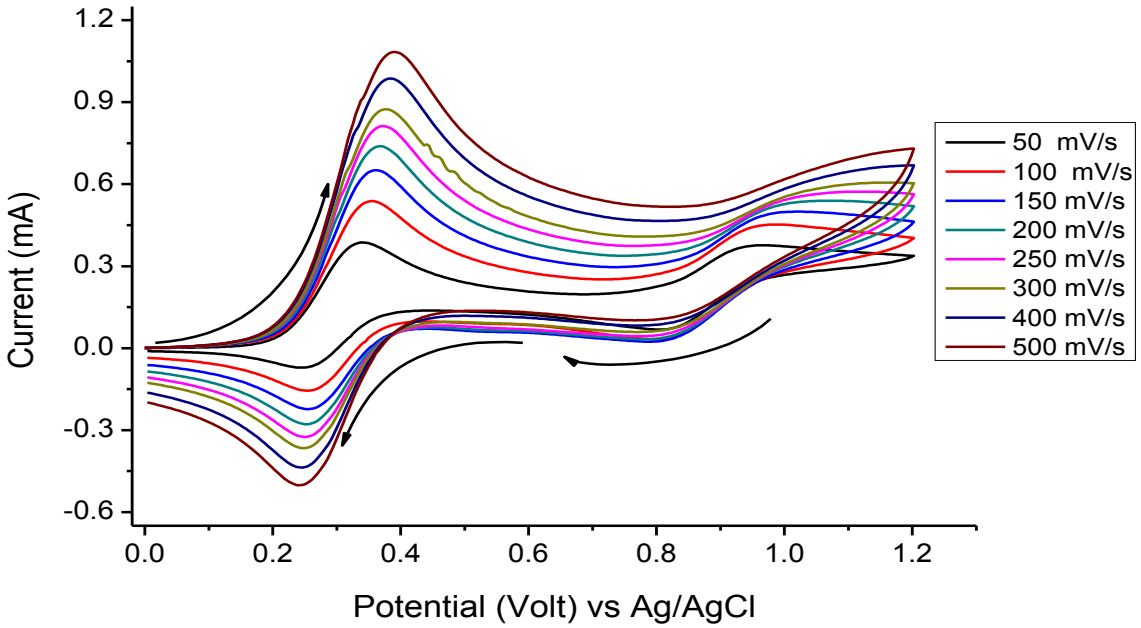

Figure 5-78: Cyclic voltammogram of PPD at different scan rates.

In case of MCPPD first oxidation peak is irreversible for the all scan rates (20 to 500 mV s^{-1}) but the 2nd peak somehow shows very little reversible peak at 1.15 V only for 20 mV s^{-1} (shown in the inset of Figure 5-80). Another interesting observation is shift in the 2nd oxidation peak with scan rate is quite unusual. The reduction peaks at 0.72 V and -0.43 V corresponds to the product form through chemical reaction of the oxidised species. Peak current I_p changes linearly with square root of the scan rate (shown in Figure 5-79 (a)) for the first oxidation peak and is used to calculate the electrochemical parameters. Only two oxidation peaks have been observed in case of MCPPD.

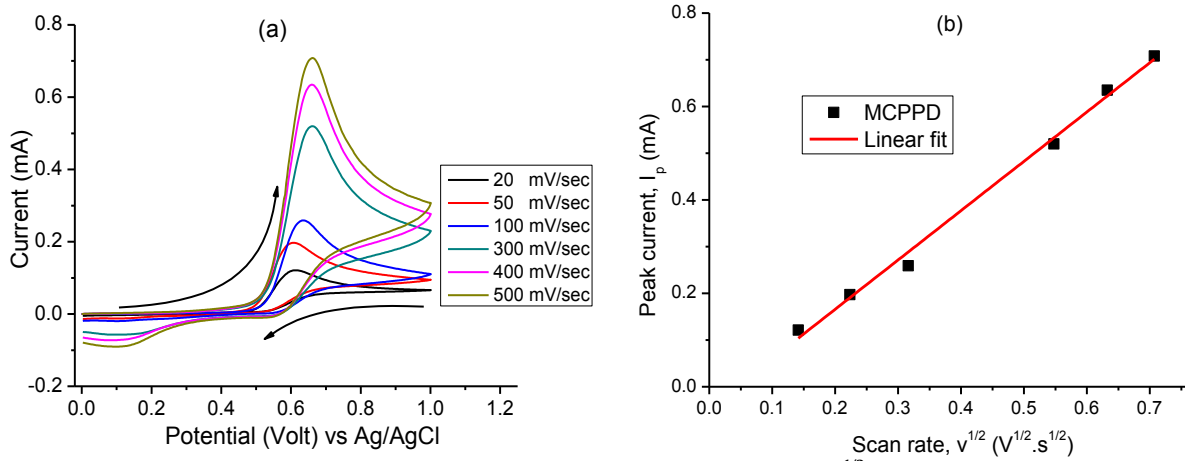

Figure 5-79: CVs of MCPPD at different scan rates (a). Plot of scan rate ($v^{1/2}$) versus peak current (I_p) for MCPPD (b).

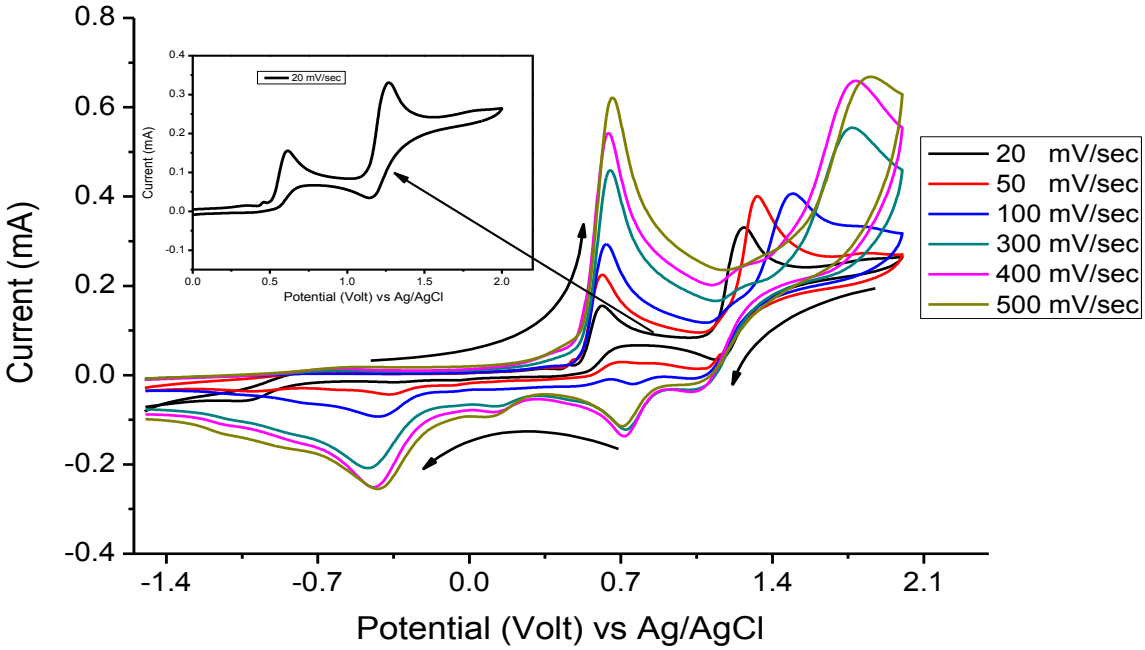

Figure 5-80: Cyclic voltammogram of MCPPD at different scan rates.

Cyclic voltammograms for 26DCPPD at different scan rate have been shown in Figure 5-81 (for 1st oxidation potential) and Figure 5-82 (whole voltage range -2.2 to 2 V). Figure 5-81 (a) have shown the similar reversible behaviour as in case of MCPPD and a linear change in peak current with square root of scan rate is shown in Figure 5-81 (b). 26DCPPD has also shown a little reversible peak for 2nd oxidation peak at 20 mV s^{-1}. One interesting feature is the irreversible reduction peak at -1.95 V (for 100 mV s^{-1}) which is not present in MCPPD. Two different scan directions are shown in Figure 5-83for the scan rate of 500 mV s^{-1}. This figure shows that small reduction (at 0.98 V and -0.29 V) and small oxidation (at –0.83 V and -0.43 V) peaks are due to products formed in irreversible oxidation (around 1.0 V and 1.7 V) and irreversible reduction (around -2.0 V) processes, respectively. Altogether there are three irreversible peaks in 26DCPPD, two oxidations (at 0.9 V and 1.7 V) and one reduction (at -2.0 V).

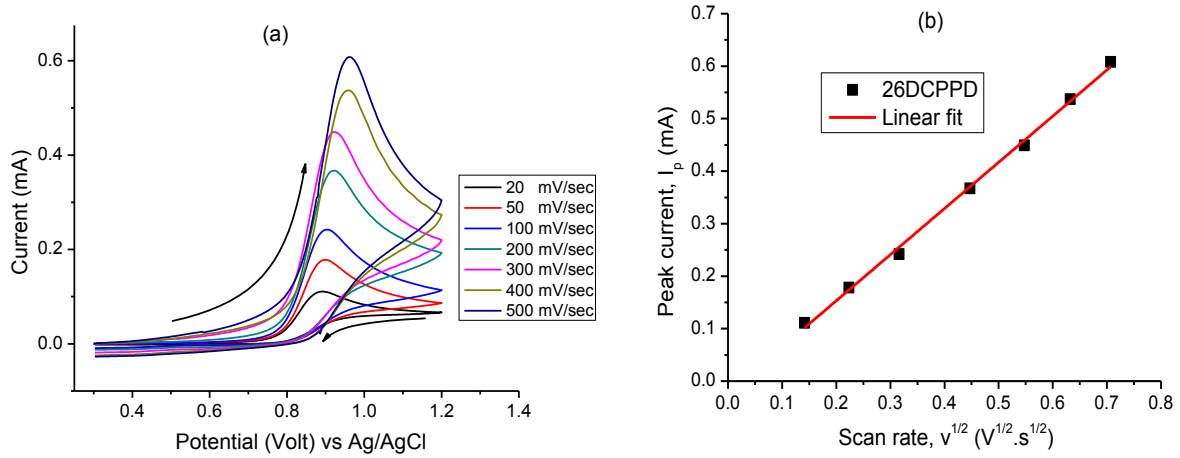

.

Figure 5-81: (a) CVs of DCPPD at different scan rates. (b) Plot of scan rate ($v^{1/2}$) versus peak current (I_p) for DCPPD.

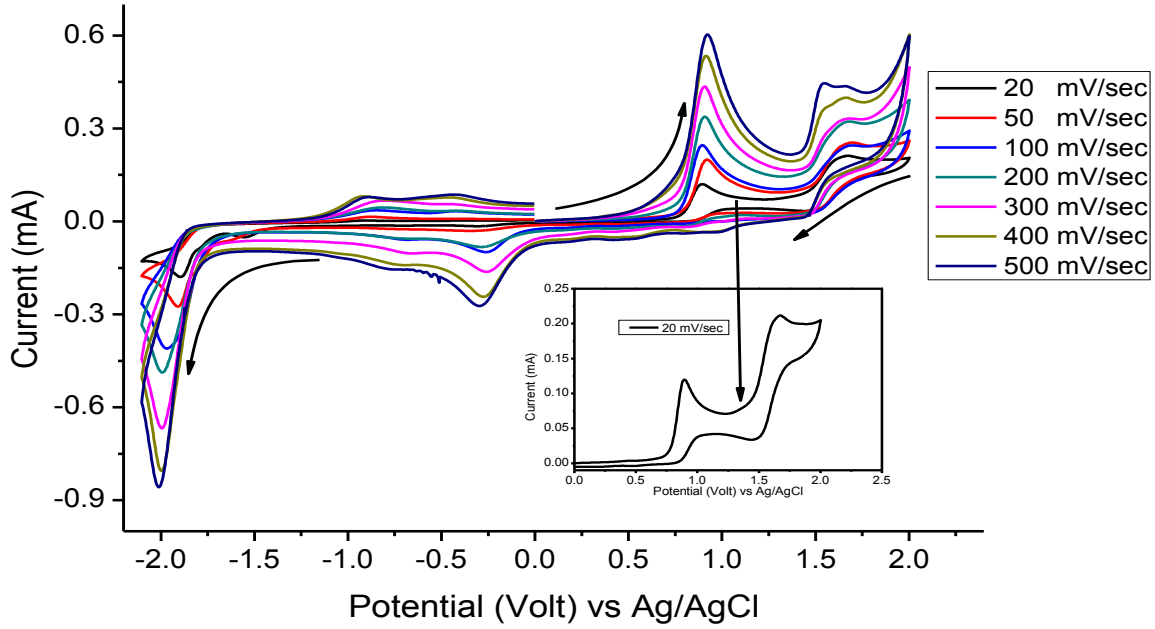

Figure 5-82: Cyclic voltammogram of 26DCPPD at different scan rates.

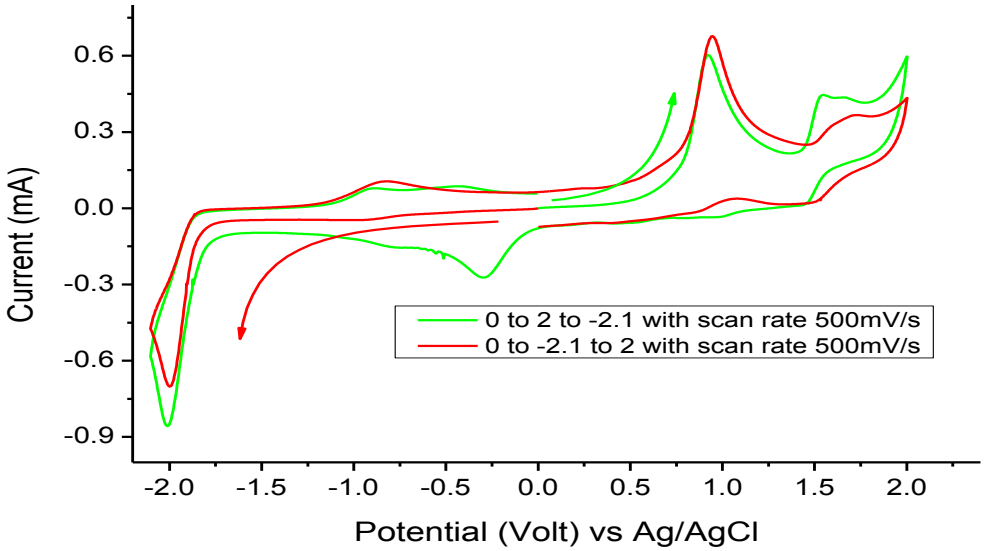

Figure 5-83: Cyclic voltammogram of 26DCPPD at 500 mV s^{-1} in two different scan directions.

TCPPD has shown only one oxidation peak at 1.5 V (in Figure 5-84a) which is in contrast to the other cyano-substituted PPDs (all PPDs have two oxidation peaks). One more interesting feature is that it has two reduction peaks (-0.8 V and 1.8 V). One of the reduction peaks is reversible as shown in Figure 5-85 (a). The peak current for both, the irreversible oxidation and reversible reduction varies linearly with the squire root of the scan root shown in Figure 5-84 (b) and Figure 5-85(b), respectively.

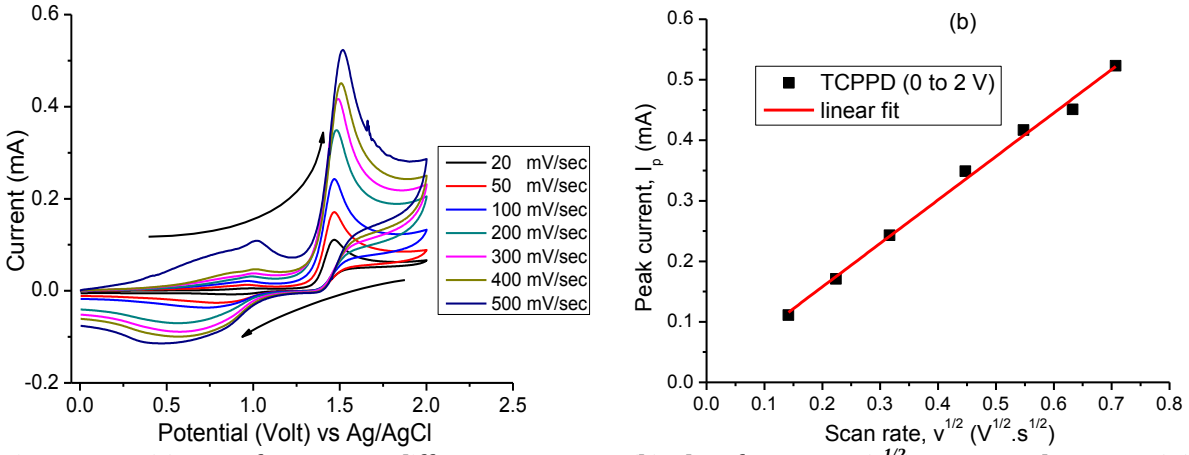

Figure 5-84: (a) CVs of TCPPD at different scan rates. (b) Plot of scan rate ($v^{1/2}$) versus peak current (I_p) for TCPPD for the potential range of 0 to 2 V.

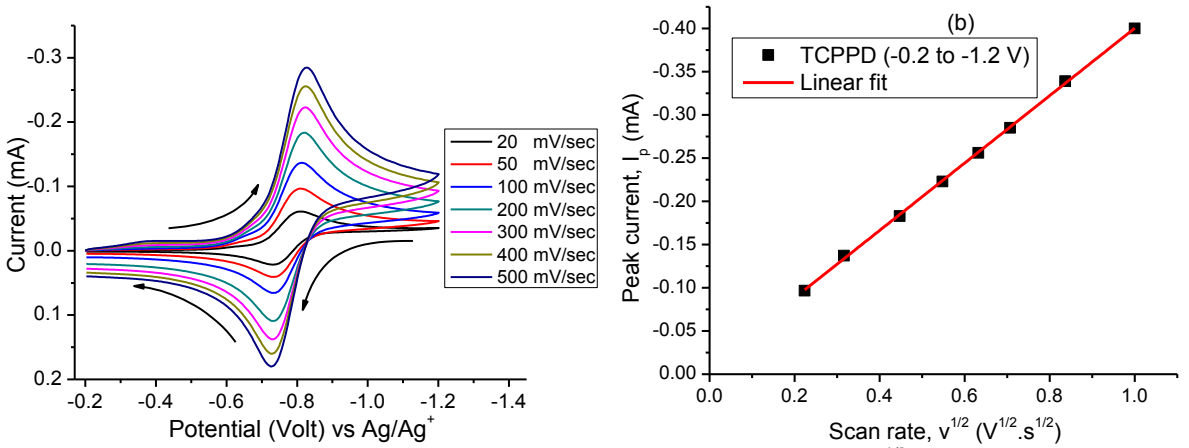

Figure 5-85: (a) CVs of TCPPD at different scan rates. (b) Plot of scan rate ($v^{1/2}$) versus peak current (I_p) for TCPPD for the potential range of -0.2 to -1.2 V.

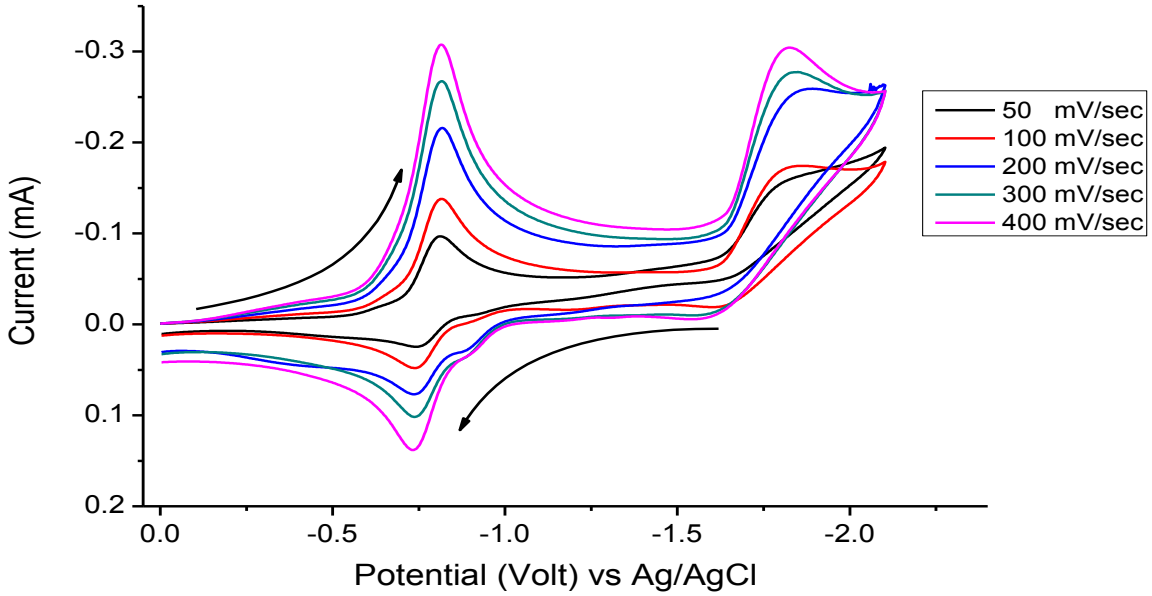

Figure 5-86: Cyclic voltammogram of TCPPD at different scan rates.

All the electrochemical oxidation process for the cyano-substituted PPDs is irreversible. The oxidation peak potential is gradually increased with the increase in number of cyano groups attached to aromatic ring of PPD. This is explained in terms of the fact that the availability of the electrons on the amino groups ($-NH_2$) is decreased due to electron acceptor substitution of the cyano (-CN). The more the number of cyano groups attached on the aromatic ring, the less favourable is the oxidation of the PPD. In case of TCPPD, where four cyano groups decrease the reduction potential to -0.8 V and oxidation potential is 1.5 V. PPD and MCPPD have only undergone two steps oxidation processes but in 26DCPPD there are two oxidation peaks and one reduction peak. Further increase in cyano substitution led to two reduction peaks and one oxidation peak as seen in TCPPD. The values of the standard oxidation potential and diffusion coefficients for PPDs and its cyano-substituted derivatives are summarized in Table 5-22.

5.9.1 Electrochemistry of cyano-substituted TMPPDs

TMPPD itself and its cyano-substituted derivatives undergo two sequential reversible oxidation processes. The Cyclic voltammograms of TMPPD, MCTMMPD and DCTMPPD for the range 1st oxidation potential range (1st electron transfer) as well as the linear variation of peak current versus square root of scan rate for these compounds are shown in Figure 5-87, Figure 5-89 and Figure 5-91 respectively.

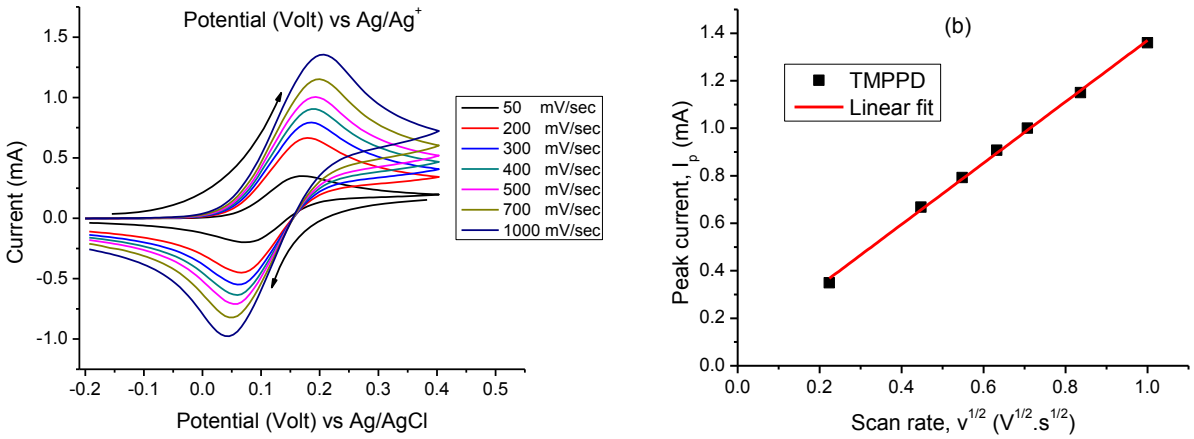

Figure 5-87: (a) CVs of TMPPD at different scan rates. (b) Plot of scan rate ($v^{1/2}$) versus peak current (I_p) for TMPPD for the potential range of -0.2 to 0.4 V.

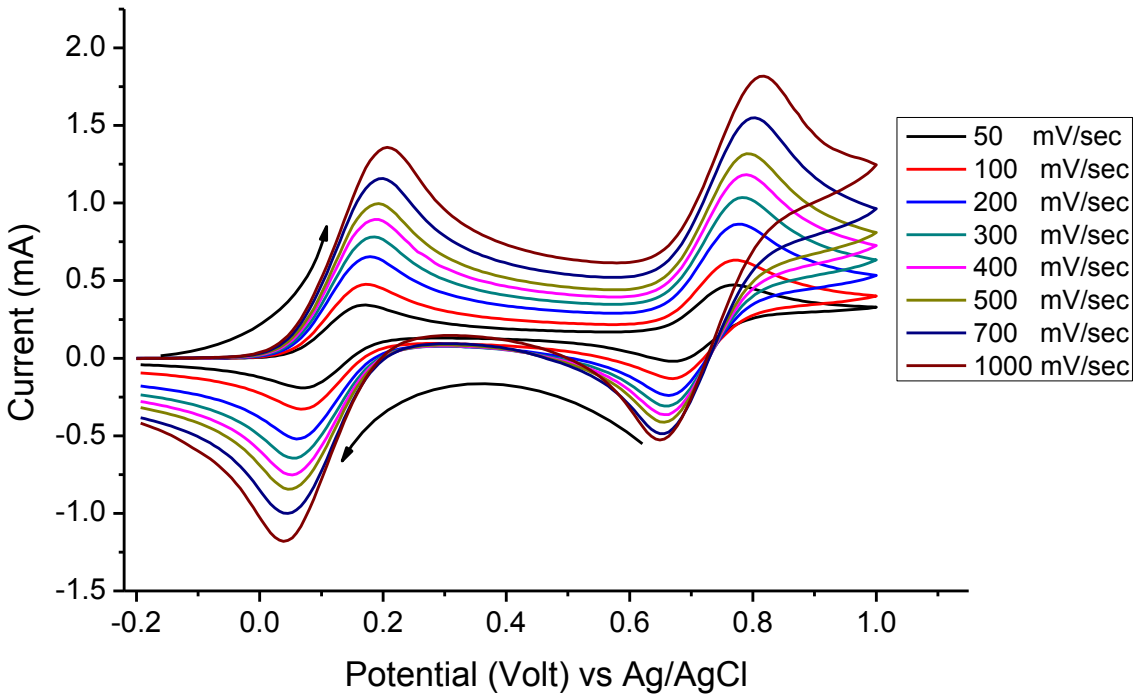

Figure 5-88: Cyclic voltammogram of TMPPD at different scan rates.

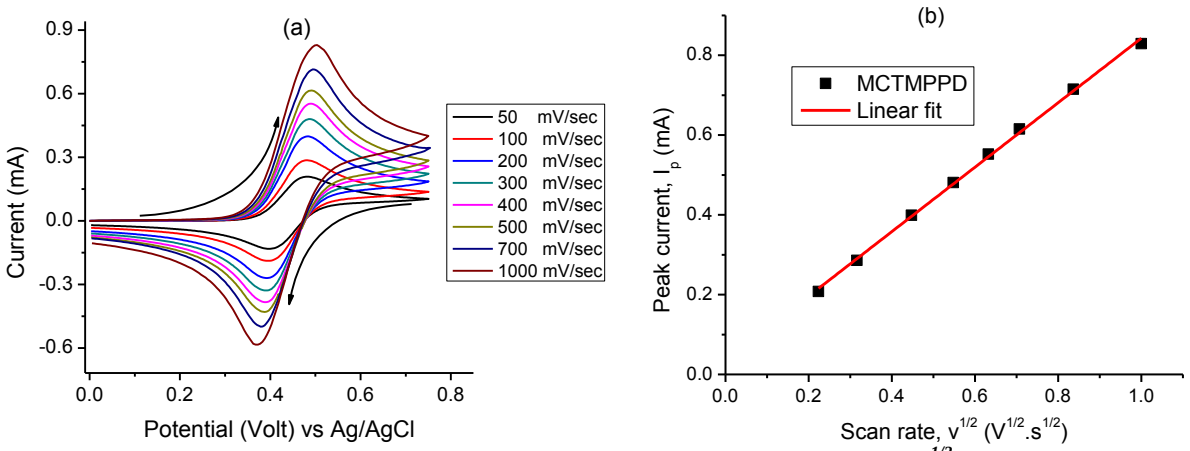

Figure 5-89: (a) CVs of MCTMPPD at different scan rates. (b) Plot of scan rate ($v^{1/2}$) versus peak current (I_p) for MCTMPPD for the potential range of 0 to 0.75 V.

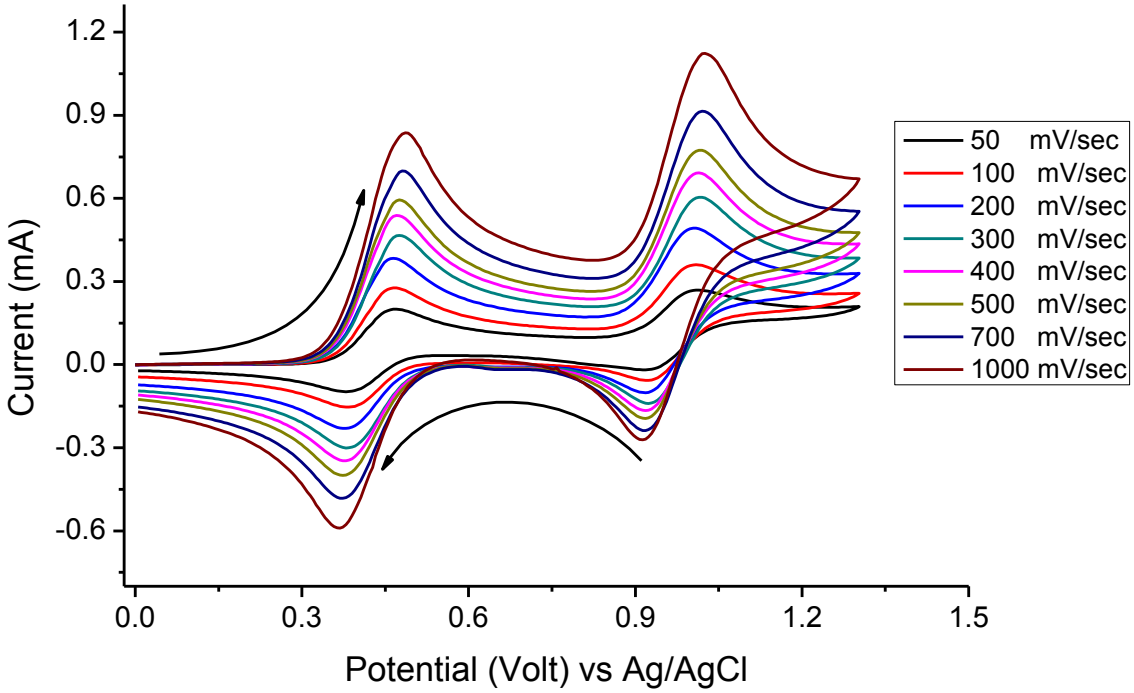

Figure 5-90: Cyclic voltammogram of MCTMPPD at different scan rates.

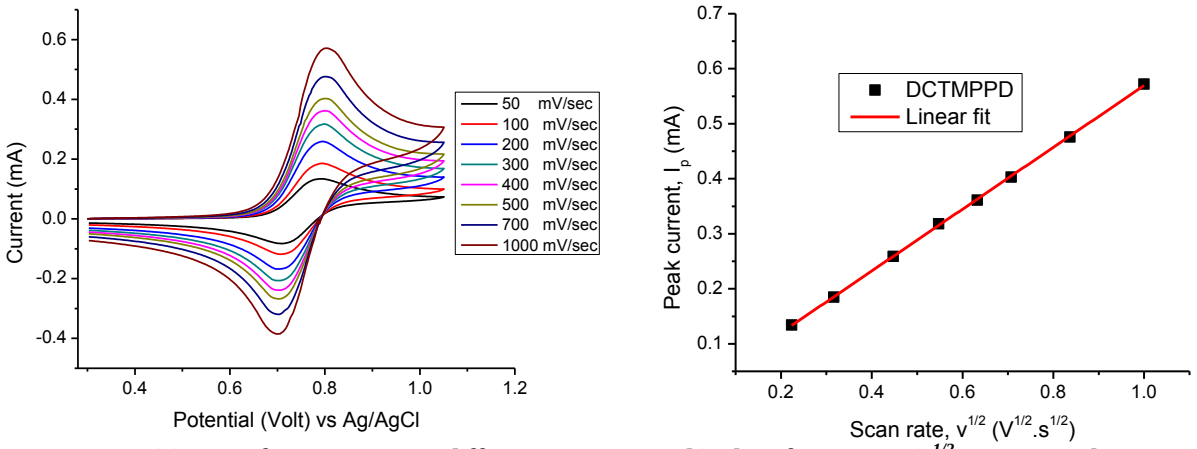

Figure 5-91: (a) CVs of DCTMPPD at different scan rates. (b) Plot of scan rate ($v^{1/2}$) versus peak current (I_p) for DCTMPPD for the potential range of 0.3 to 1.05 V.

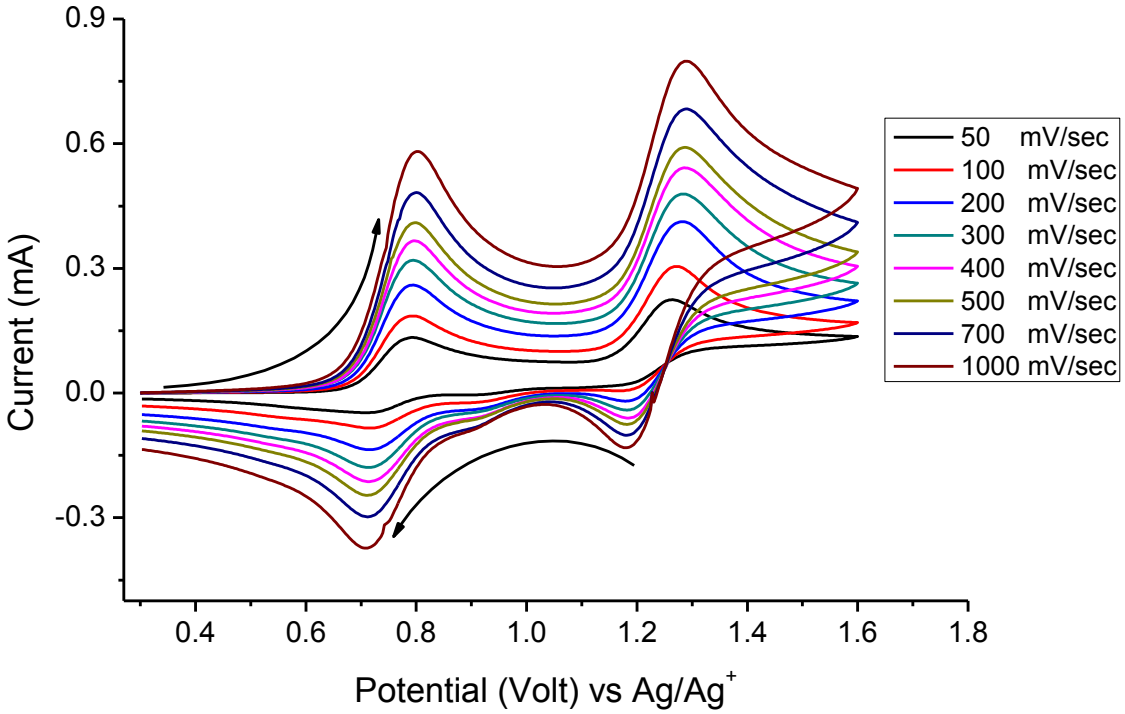

Figure 5-92: Cyclic voltammogram of DCTMPPD at diff erent scan rates.

No reduction process has been observed for any of the cyano-substituted TMPPDs in acetonitrile containing 0.1M $TBAPF_6$ system. All three TMPPDs behave in similar way except that the oxidation potential goes to higher value with more number of cyano substitutions i.e. the oxidation potential of TMPPD is 0.12 V, MCTMPPD is 0.44 and DCTMPPD is 0.75. The cyclic voltammograms for both oxidation step for TMPPD. MCTMPPD and DCTMMPD are shown in Figure 5-88, Figure 5-90 and Figure 5-92. The electrochemical parameters for the 1st oxidation process for TMPPDs are reported in Table 5-22.

Table 5-22: Electrochemical kinetic parameters for the cyano-substituted PPDs and TMPPDs at 298 K in acetonitrile containing 0.1 M $TBAPF_6$.

PPDs/ TMPPDs	Reduction/ oxidation	reversible/ irreversible	Conc. (m M)	$E_1^{o(b)}$ (V)	$D_1^{(a)}$ (10^5 cm^2s^{-1})	E_2^o (V)
PPD	PPD/ PPD^+	reversible	5.18	0.3	17.5	0.95*
MCPPD	MCPPD/ $MCPPD^+$	irreversible	2.51	0.7	50.2	1.27**
26DCPPD	DCPPD/ $DCPPD^+$	irreversible	2.69	0.98	33.6	1.67**
26DCPPD	DCPPD/ $DCPPD^-$	irreversible	2.69	-1.95	33.6	--
TCPPD	TCPPD/ $TCPPD^+$	irreversible	1.2	1.5	133.6	---
TCPPD	TCPPD/ $TCPPD^-$	reversible	1.2	0.78	21.9	-1.82***
TMPPD	TMPPD/ $TMPPD^+$	reversible	4.26	0.12	20.8	0.73(b)
MCTMPPD	MCTMPPD/ $MCTMPPD^+$	reversible	2.99	0.44	16.6	0.97(b)
DCTMPPD	DCTMPPD/ $DCTMPPD^+$	reversible	1.75	0.75	23.3	1.23(b)

(a) Diffusion coefficients are calculated for the 1st oxidation or 1st reduction process
(b) Redox potential of reversible systems are obtained by using eq. 5-9 and Eq. 5-10 for the irreversible systems.
* 2nd oxidation peak potential at 50 mVs^{-1}; ** 2nd oxidation peak potential at 20 mVs^{-1}
*** 2nd reduction peak potential at 400 mVs^{-1} and this peak is irreversible.

5.10 ESR Study of MCTMPPD & DCTMPPD

ESR studies have been applied to investigate the electron self exchange in cyano-substituted PPDs and TMPPDs. Both PPDs and TMPPDs have been oxidized chemically using nitrosyl perchlorate ($NOClO_4.H_2O$). The concentration of nitrosyl perchlorate is $5x10^{-4}$ M. Both MCPPD and DCPPD have been converted into very light brown color on oxidation but the radicals are not stable (show irreversible oxidation in CV) and no ESR signals have been observed. MCTMPPD and DCTMPPD forms blue color stable radicals and are measureable using ESR spectroscopy. The concentration of MCTMPPD and DCTMPPD vary from $5x10^{-4}$ M to $3x10^{-2}$ M while the concentration of oxidizing agent remains the same ($5x10^{-4}$ M) to measure the self exchange kinetics. The radical of DCTMPPD has been measured only at concentration of $5x10^{-4}$ M because at higher concentration the radical of DCTMPPD is not stable and concentration of radical is decreasing rapidly with time. The ESR spectra without any self exchange process ($5x10^{-4}$ M of DCTMPPD) along with the simulated spectra are shown in shown in Figure 5-93 and corresponding parameters were obtained from the

simulation as given in Table 5-23. The radical cation of DCTMPPD has 4 nitrogen atoms with two equivalent nitrogen of the –CN groups and two non-equivalent atoms of dimethylamino, $–N(CH_3)_2$ groups. There are 14 hydrogen atoms, two sets of 6 hydrogen atoms on each $–N(CH_3)_2$ group and two equivalent hydrogen atoms of aromatic ring. The number of lines obtained theoretically, if no overlapping is considered, are 3x3x5x7x7x3=6615. All ESR spectra have been obtained at room temperature (295.5 K).

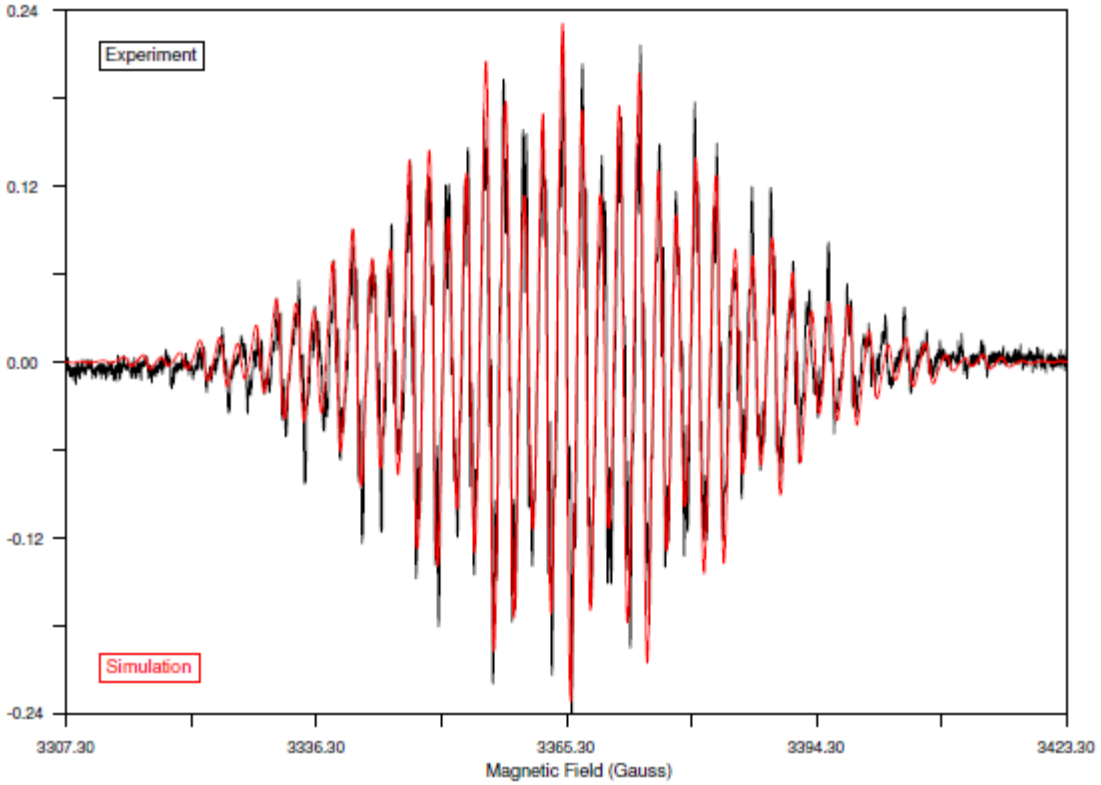

Figure 5-93: ESR spectrum of DCTMPPD (5x10-4 M) in acetonitrile at 295.5 K.

Table 5-23: ESR parameter of DCTMPPD

Nuclei	Coupling constant	Spin	Number of atoms
a_{N1} (N-CH_3)	6.47	1	1
a_{N2} (N-CH_3)	6.46	1	1
a_N (CN)	0.18	1	2
a_{H1} (N-$(CH_3)_2$)	8.94	0.5	6
a_{H2} (N-$(CH_3)_2$)	8.91	0.5	6
a_H (Ar)	2.116	0.5	2
Line width = 0.503	Lorenntzian = 100.2		G-shift = 0
	Simulation correlation = 0.912		

The ESR spectrum of MCTMPPD cation radical without any self exchange process ($5x10^{-4}$ M of MCTMPPD) is shown in Figure 5-94. Different attempts have been made to simulate the ESR spectra of MCTMPPD radical but are unsuccessful. MCTMPPD is relatively less symmetrical compared to DCTMPPD. There are 3 nitrogen atom, none of them is equivalent, 15 hydrogen atoms, two non equivalent sets of 6 hydrogen atom on each of $-N(CH_3)_2$ groups and three non-equivalent hydrogen atoms on the aromatic ring. The total number of lines estimated for MCTMPPD are 3x3x3x7x7x2x2x2= 10584. MCTMPPD radical is stable compared to that of DCTMPPD at higher concentrations. The ESR spectrum no self exchange process ($5x10^{-4}$ M of MCTMPPD) is shown at the top of Figure 5-95. So in order to have an idea about the ESR parameter, ENDOR measurements will be performed. In Figure 5-95, it can be clearly seen that the line broadening occurs with the increase in concentration of the MCTMPPD upto $2x10^{-2}$ M. Going to further higher concentration does not change the spectra but the intensity of signal is very much decrease with time and much noisy spectrum was obtained. Determination of the ESR parameters are on the way but not completed yet. Once the hyperfine coupling constants for different atoms are known, the self exchange kinetic can be studied for MCTMPPD.

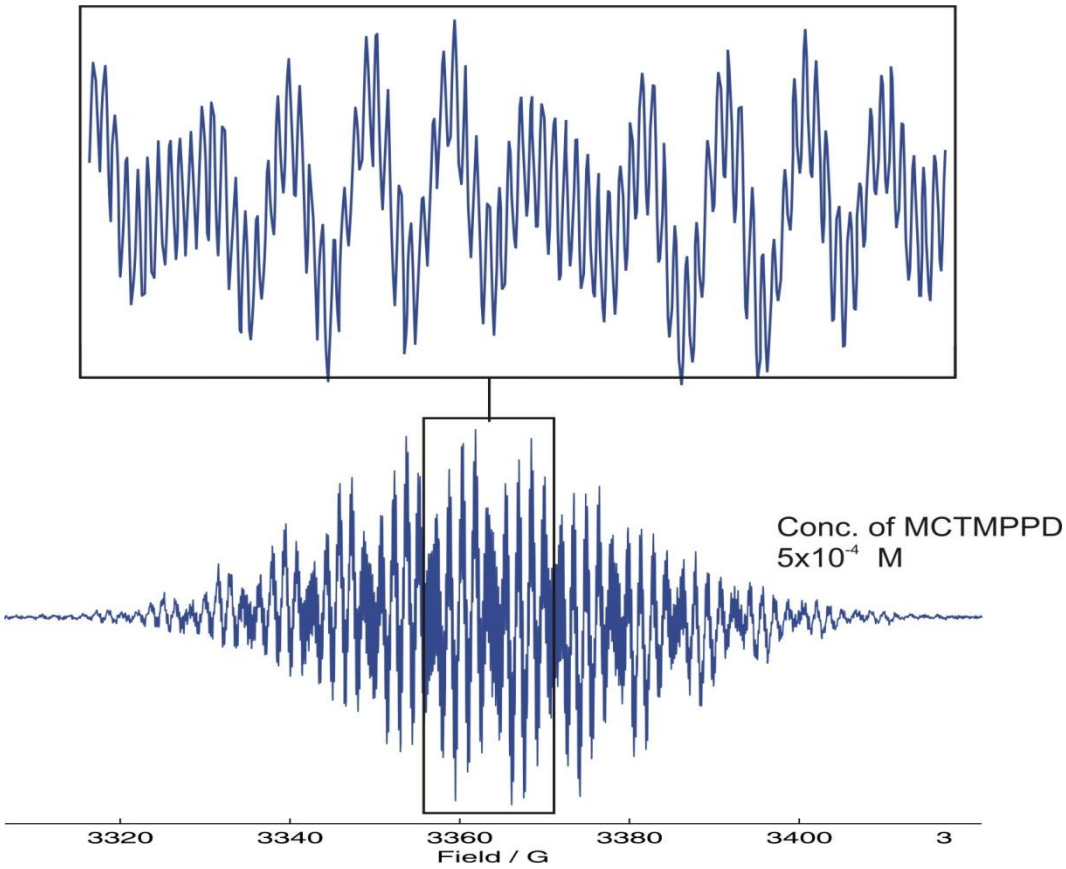

Figure 5-94: ESR spectrum of $5x10^{-4}$ M MCTMPPD with $5x10^{-4}$ M nitrosyl perchlorate.

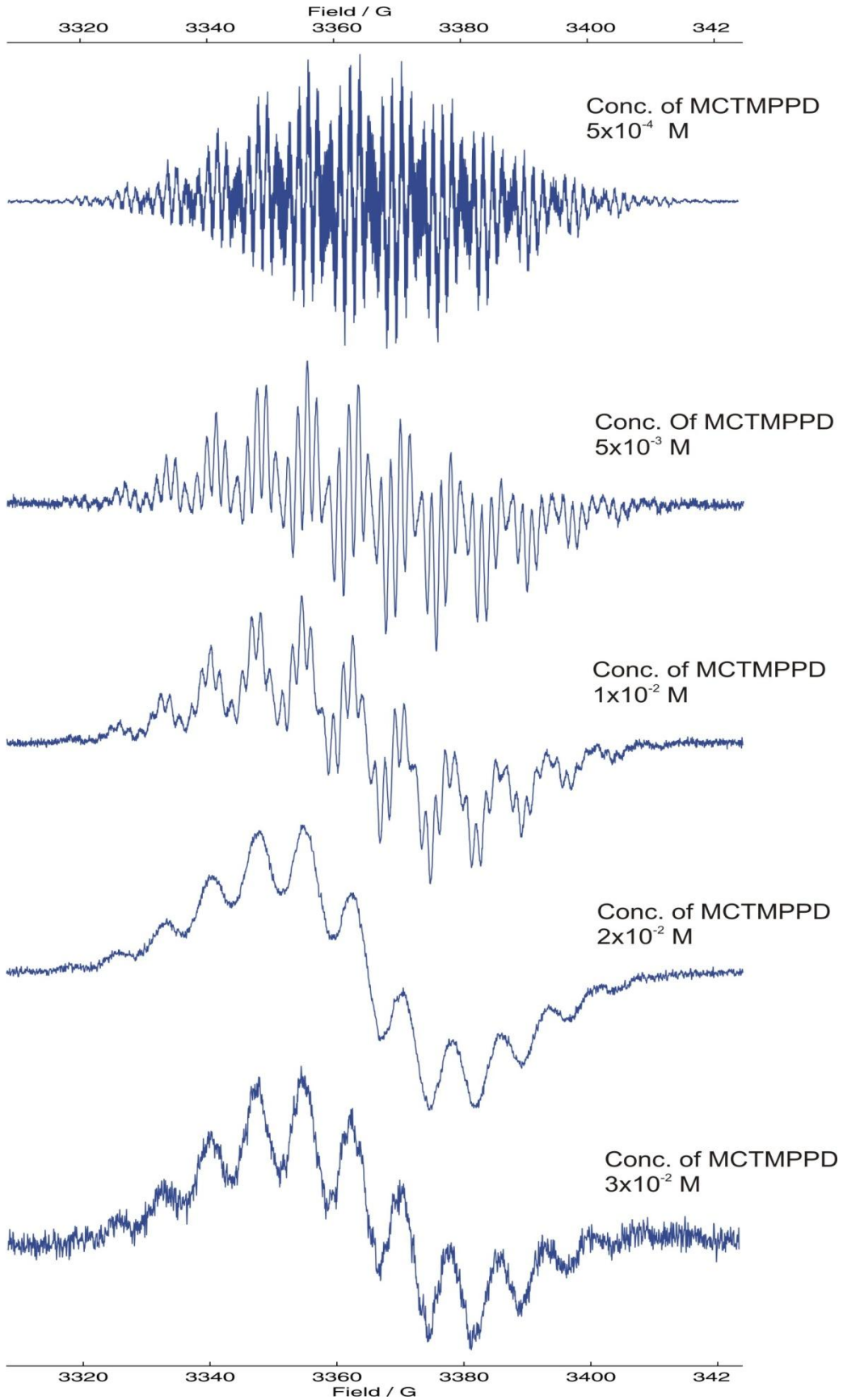

Figure 5-95: ESR spectra of MCTMPPD at different concentrations and 5x10-4 M nitrosyl perchlorate at 295.5 K.

6 CONCLUSIONS AND OUTLOOK

Photophysical properties were investigated in about 25 solvents for each of the cyano-substituted PPDs and TMPPDs. The aim to use large number of solvents is to have an insight for the solvent effect on the photophysical properties. These photophysical and electrochemical properties are compared with respect to gradual increase in number of cyano-substitution on the aromatic ring of PPD and TMPPD. Also the comparisons of photophysical properties for the each PPD with corresponding tetramethylated derivatives (TMPPD) were analyzed. Different solvent parameter sets have been applied though multiparameter regression analysis

6.1 Conclusions

New cyano-substituted aromatic compounds were synthesized. The commonly used Rosenmund–von Braun reaction, for the replacement of halogen groups (-Cl or –Br in present work) with cyano groups, did not work even using long reaction times the presence of different polar solvents like HMPA, DMF, DMSO etc. Methylation of the cyano-substituted PPDs is not trivial as for the PPD (especially when the aromatic ring is highly electron deficient).

Solvatochromic studies for PPDs and TMPPD have revealed the following conclusions:

For the absorption maxima, multiparameter regression analyses have shown that the influence of solvent acidity on the absorption maxima is decreased and that of solvent basicity is increased with increasing the number of cyano groups. The effect of solvent basicity is opposite compare to that of solvent acidity. The LSER coefficients of solvent acidy have positive sign (shift the absorption maxima to higher values) where the LSER coefficients of solvent basicity (β and SB) have negative sign (shift the absorption maxima to lower values). When using Kamlet-Taft parameters, the LSER coefficients of α were reduce on going from PPD to TCPPD and this decrease in coefficient of α was gradual with increasing number of cyano groups. The same behavior was observed when using Catalan's parameters. The LSER coefficients of SA in absorption were changed from 2.52 (for PPD) to 0.03 (for TCPPD). This is due to the fact that electron density on the amino groups (due to lone pair of $–NH_2$) is shifted to the ring because of substitution of cyano groups on aromatic ring. So the result is decrease in coefficients of α and SA. The LSER coefficients of β and

SB have higher values for more number of cyano groups. In Kamlet-Taft analysis, the coefficients of β have higher values for cyano-substituted PPDs compare to PPD. Substitution of first cyano group on PPD shift the value of coefficient β from -0.78 to -1.74 but further substitutions of cyano groups did not change this value much. When applying Catalan's parameters, the value of the SB coefficient for PPD was positive which was changed to negative for MCPPD and further increase in magnitude was observed on more cyano group substitutions. Such increase in coefficients of β and SB with more cyano groups indicated that the proton of amino groups ($-NH_2$) are more readily available for hydrogen bonding with solvent molecules in the ground state. This is again linked to shift of electron density toward cyano groups. In short, the absorption maxima are mainly influence by solvent acidity in PPD but in TCPPD the solvent basicity is major candidate which govern the solvent-solute interactions. The values for the coefficients of polarity terms (for using, both Kamlet-Taft and Catalan's parameters) were not changing much compared to change in the coefficients of acidity and basicity terms. The low student t-values for coefficients of π^* pointed toward the meaningless behavior for polarity term. The specific solute-solvent interactions are changing much on going from PPD to TCPPD and mainly govern absorption maxima of PPDs.

In case of fluorescence maxima, all the coefficients of polarity, acidity and basicity terms have negative values (shift the emission maxima to lower value). But the values of the acidity terms increase from PPD to MCPPD and then decrease with increase in number of cyano groups. Such an effect is observed for both, Kamlet-Taft and Catalan's parameters. In case of Kamlet-Taft parameters, the values of coefficients of α are lower and have lower student t-values. So this makes it meaningless. The absolute values for coefficients of solvent basicity (β and SB) terms increase with increase in number of cyano groups. The coefficients for polarity terms did not change much among the PPDs. Emission of PPDs are primarily governed by the solvent basicity and polarity terms.

In absorption analysis, the solvatochromism of TMPPD is governed only by solvent acidity. The LSER analysis of absorption maxima have scattered points in case of MCTMPPD[26] and all LSER coefficients have very low student t-values. This is due to the fact that the substitution of cyano group on TMPPD decreases coefficient of α but no contribution of due to β (because of substitution of methyl groups on nitrogen atom of amino) and coefficient of

[26] Such behavior has been also observe in absorption of DCTMPPD.

π^* is also very small. In LSER analysis for the emission maxima of TMPPDs, the only parameter that governs the solvatochromic shift is the polarity term.

On comparison of PPDs with corresponding TMPPDs, it has been found that almost all term behave in similar fashion except for the coefficients of solvent basicity terms. In TMPPDs, large diminutions in the coefficient for β and SB terms have been observed in both absorption and emission due to absence of any proton which can interact with solvent molecules.

LSER analysis using ETN and DNN parameters were studied using all solvents (protic + aprotic) and only aprotic solvents. Also the analysis is performed using only ETN parameter and combination of ETN & DNN parameters. In PPDs, it was found that single ETN parameter was not able correlate the theoretical and experimental values for both absorption and emission maxima. When solvent basicity term (Donor number, DNN) was used in combination with ETN, nice correlations were found for both absorption and emission maxima. This suggests the presence of high impact of solvent basicity term in solute-solvent interaction in PPDs, which is inline with previous finding using Kamlet-Taft and Catalan's analysis. Using the combination of ETN and DNN in TMPPDs did not demonstrate any improvement in the LSER coefficients compared to those obtained using ETN only. This observation highlights the absence of any specific interactions due to solvent basicity.

LSER analysis using ETN values for only aprotic solvents have revealed that the PPDs correlated in much better ways in absorption analysis. This is due to the fact that the acidity and polarity are behaving with opposite sign in PPDs. So when only aprotic solvents are used the ETN parameters mainly represent solvent polarity but when using all solvents, ETN parameters represent both solvent acidity and polarity contributions and former is dominant for absorption maxima of PPDs.

Onsager analysis using all solvents did not give good correlation for PPDs because of high specific interactions. Though the contributions of specific interaction were subtracted before using Onsager parameters, but still this correlation was not very successful. Much improved LSER correlations (for fluorescence maxima) using Onsager parameters were obtained when using only aprotic solvents. This illustrates the fact that Onsager parameters are not applicable on absorption maxima of the PPDs having only specific interactions and partially valid for fluorescence maxima.

Photophysical properties of PPDs and TMPPDs were compared on the basis of increase in number cyano groups substituted on aromatic ring. It has been found that both; absorption

and emission maxima in different solvent are red shifted with increase in number of cyano groups. The fluorescence lifetime and quantum yield are much increased after the substitution of first cyano group (as in MCPPD compared to that of PPD). Further substitution did not improve these quantities. One interesting observation is that fluorescence lifetime and quantum yield of mono cyano species (MCPPD and MCTMPD) are very much reduce in protic solvents compared to those in aprotic solvent. This may be due to some hydrogen bonding effect in MCPPD and MCTMPPD. The non-radiative rate constants k_{nr} have much higher values in protic solvents for MCPPD and MCTMPPD.

Absorption and emission spectra of TCHQ in H_2O at different concentration disclose the highly acidic nature of TCHQ. Due to presence of four cyano groups, the aromatic ring is highly electron deficient and very much willing to donate its hydroxyl proton. TCHQ exists in three different forms, i.e. TCHQ, $TCHQ^-$ and $TCHQ^{-2}$, at different pH/H_o values as well as in different solvents. There exist two ground state pKa values at 0.9 and 3.8 but only one pK_a^* value -1.1. TCHQ is a strong acid and has capacity to donate its proton to the solvent very efficiently. The donating ability of TCHQ depends on the solvent used and is related to hydrogen bond accepting ability (β) of the solvent. Ethers are the only solvent which contains only the neutral species in the ground state. In neutral water and DMSO no neutral TCHQ is detected. All the three forms of TCHQ (neutral TCHQ, $TCHQ^-$ and $TCHQ^{2-}$) are fluorescent. Both absorption and emission characteristics of TCHQ and its deprotonated forms ($TCHQ^-$ and $TCHQ^{2-}$) depend on the medium in which these are studied. Solvatochromic study for neutral TCHQ is difficult to study because of either difficulty to have neutral specie at low concentrations.

The cyclic voltammetry measurements show a gradual increase in the oxidation potential from PPD to TCPPD (also in TMPPD to DCTMPPD). In DCPPD, a reduction peak at -1.95 V (vs Ag/AgCl) and two reduction peaks in TCPPD at -0.8 V (vs Ag/AgCl) and -1.8 V (vs Ag/AgCl) has been found. The behavior of PPDs is such that the oxidation potential values are increased and reduction potentials are decreased with increasing the number of cyano groups substituted on the aromatic ring. Such effect is related with electron withdrawing effect of cyano groups. On comparison of PPDs and TMPPDs, it has been found that oxidation is reversible in TMPPDs and is irreversible in PPDs. The radicals formed during oxidation of PPDs are unstable and undergo chemical reaction (probably deprotonation) very fast.

6.2 Outlooks

Because of long reaction times (and mixture of products formed) for substitution of halogen atom with cyano group on PPD and TMPPDs, microwave synthetic techniques can be a better alternative to improve the reaction yield.

Stable radical of MCTMPPD is obtained by chemical oxidation and ESR spectrum of MCTMPPD radical is highly splitted. Estimation of coupling constants with simulation was unsuccesful. The ENDOR measurements are required to have an idea about the values of coupling constants. The radicals of cyano-substituted PPDs are highly unstable and unable to record ESR spectra for these. The electrochemical generation of radical using a flow arrangement can give the ESR parameters.

Cyano-substituted derivative of both, PPDs and TMPPDs can be used as in the study of electron transfer, energy transfer and proton transfer processes in the excited state.

The electrochemical properties of TMPPD and MCTMPPD are not very much different. Both of these give stable radicals and oxidation potential are close to each other. But there is high difference in fluorescence quantum yield and fluorescence lifetime. MCTMPPD can be a better replacement of TMPPD in various studies where high fluorescence lifetime and fluorescence quantum yield is beneficial or required. Cyano-substituted TMPPDs form stable radical and can be used as precursor in molecular magnets.

TMPPD is very well studied in literature in various aspects like photo-ionization, magnetic field effects, homogeneous electron transfer and heterogeneous electron transfer studies. MCTMPPD can be studied for similar aspect as in TMPPD.

Because of interesting photophysical and electrochemical properties of cyano substitute PPDs and TMMDPs, one could think of using them as building blocks in polymers for organic electronics.

The intriguing results in pK_a^* studies of DCPPD, open the path of another study, for the time-resolved study for the fluorescence of DCPPD in aqueous solution at different pH values. Such a study would help to have better understanding of anomalous behavior of DCPPD in exited state in aqueous solution. Such investigations can also be made for MCPPD.

Due to interesting absorption and emission behavior of TCHQ, a systematic study of absorption and emission characteristics of hydroquinone and its cyano-substituted derivatives (mono-, di-, tri-cyano) can be designed to underline the interesting photophysical

properties of these compounds. The extreme sensitivity of TCHQ from moisture can make it interesting probe for moisture monitoring/measurements.

These are just few interesting aspects for these cyano-substituted aromatic compounds but still many more are waiting for potential findings to unveil their applications in various fields of chemistry in general and in photochemistry in particular.

A. Appendix

A-1 Emission spectra of TCHQ in different solvents excited at various wavelengths

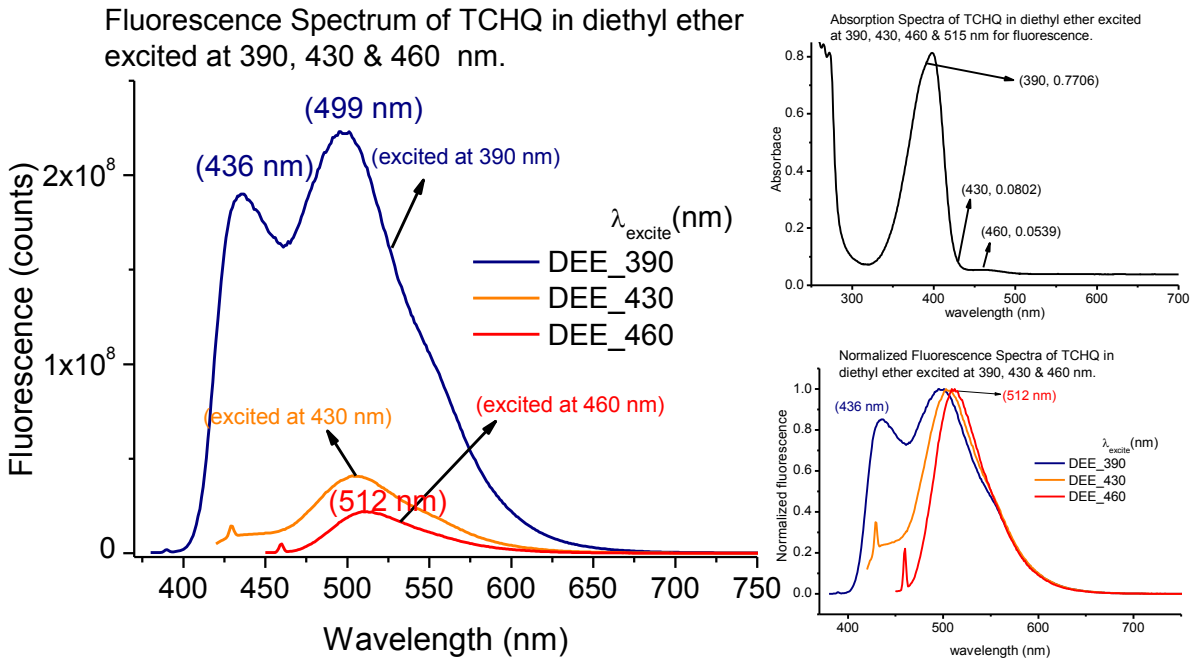

Figure A-1: Absorption, fluorescence and normalized fluorescence spectra of TCHQ in diethyl ether excited at 390, 430 and 460 nm.

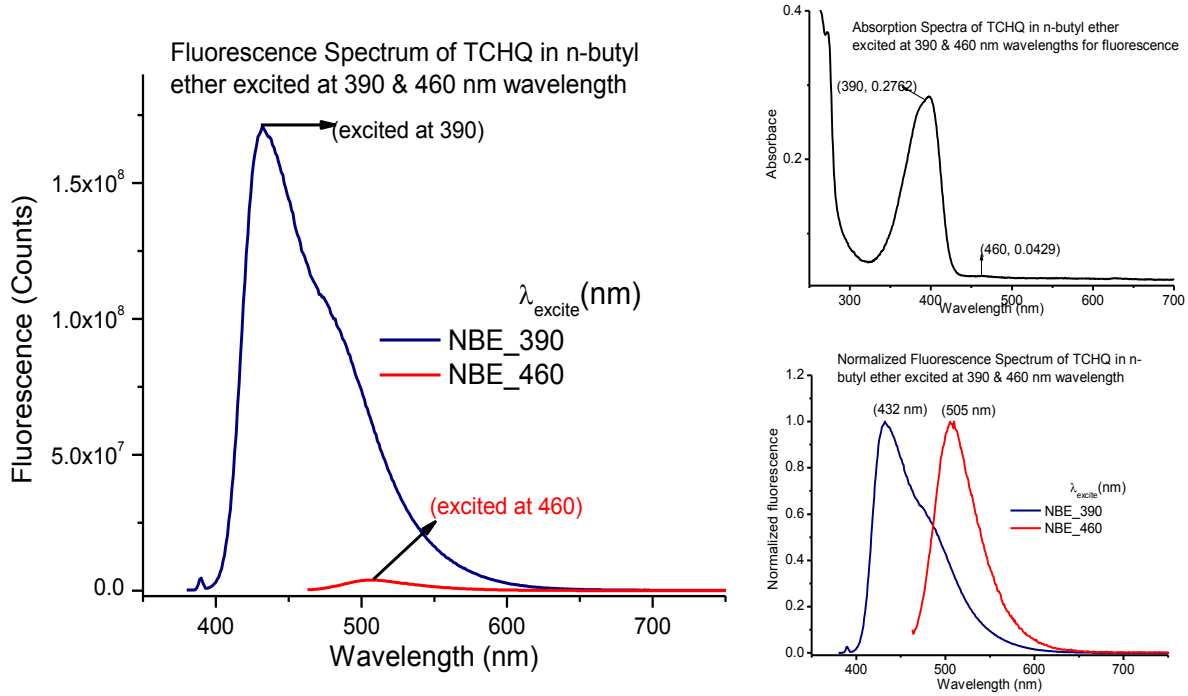

Figure A-2: Absorption, fluorescence and normalized fluorescence spectra of TCHQ in n-butyl ether excited at 390 and 460 nm.

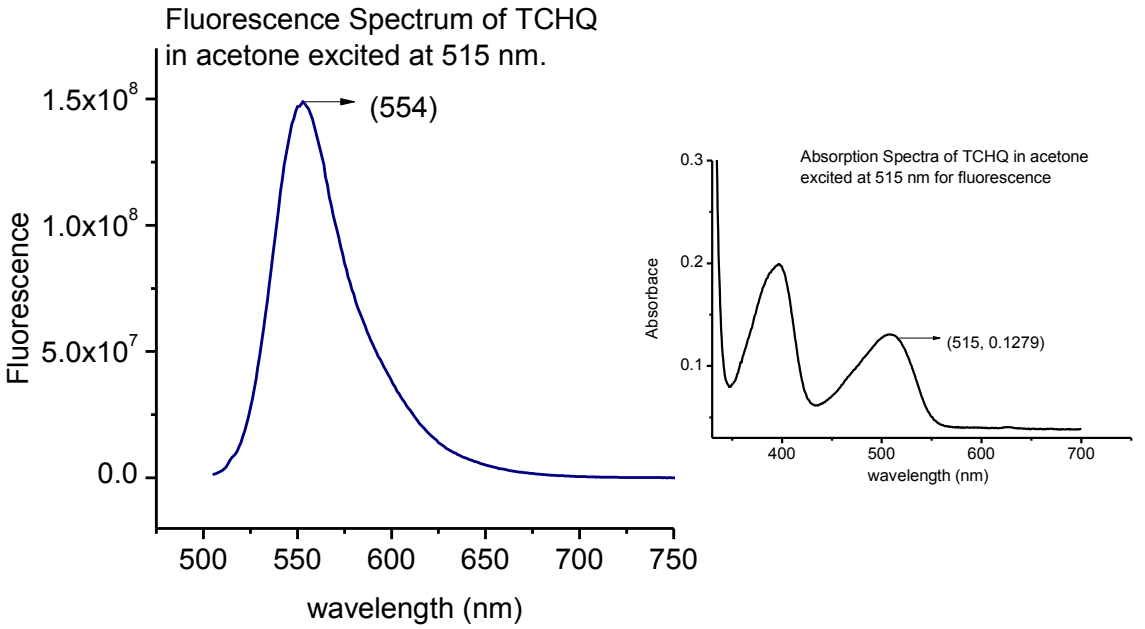

Figure A-3: Absorption, fluorescence and normalized fluorescence spectra of TCHQ in acetone excited at 515 nm.

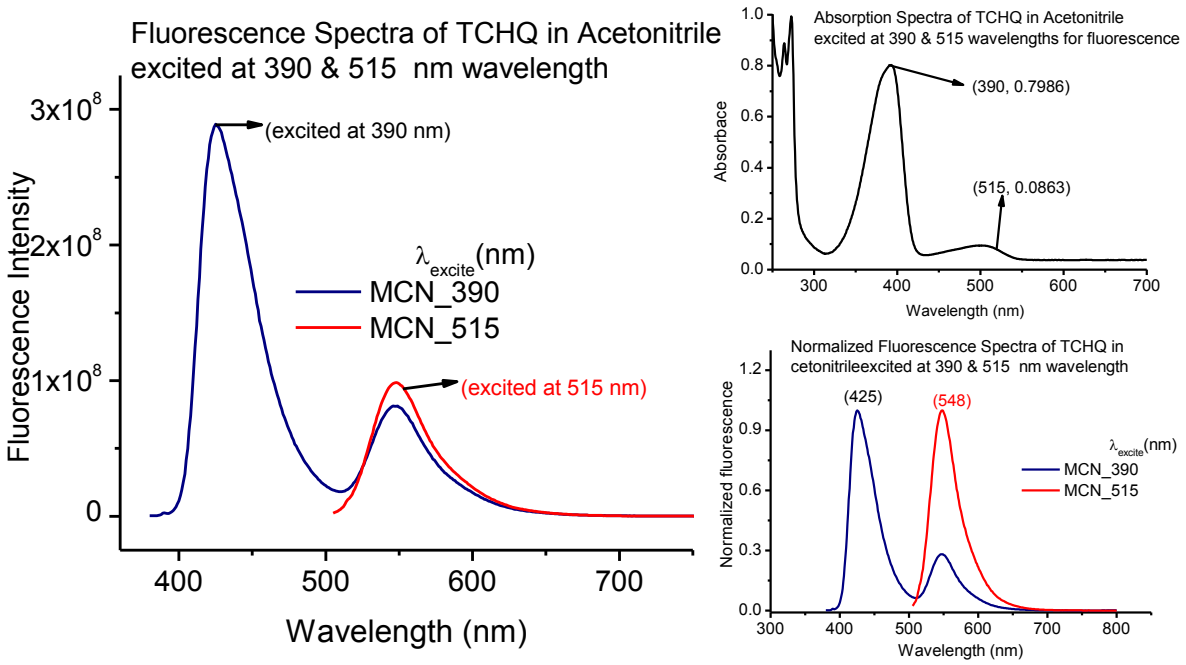

Figure A-4: Absorption, fluorescence and normalized fluorescence spectra of TCHQ in acetonitrile excited at 390 and 515 nm.

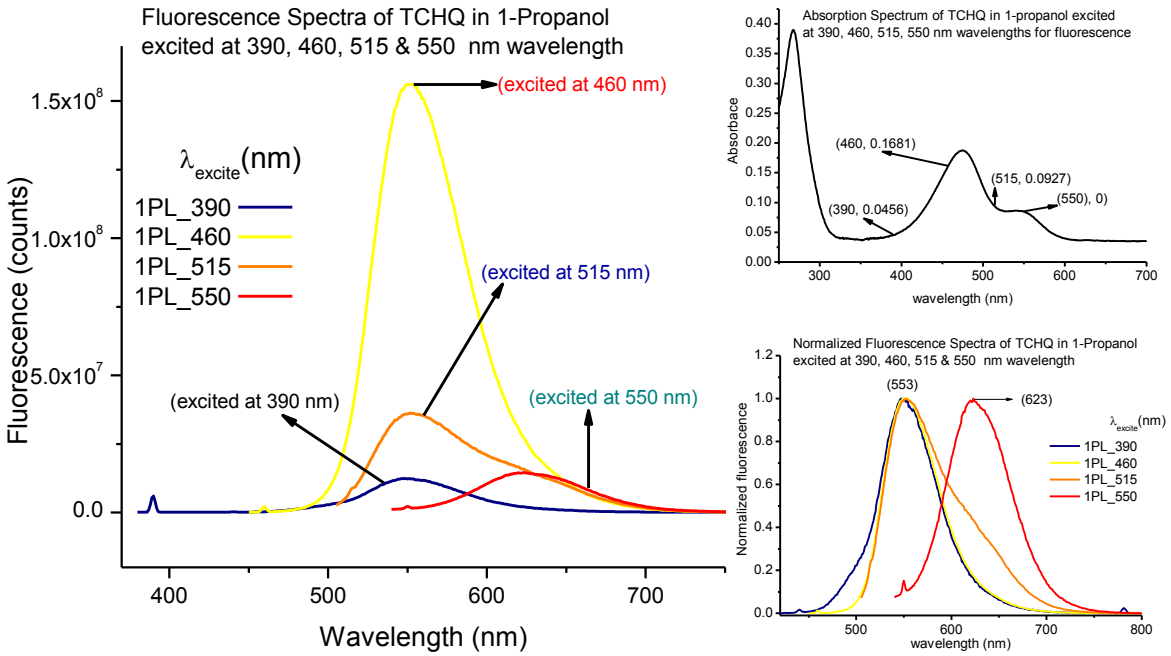

Figure A-5: Absorption, fluorescence and normalized fluorescence spectra of TCHQ in 1-propanol excited at 390, 460, 515 and 550 nm.

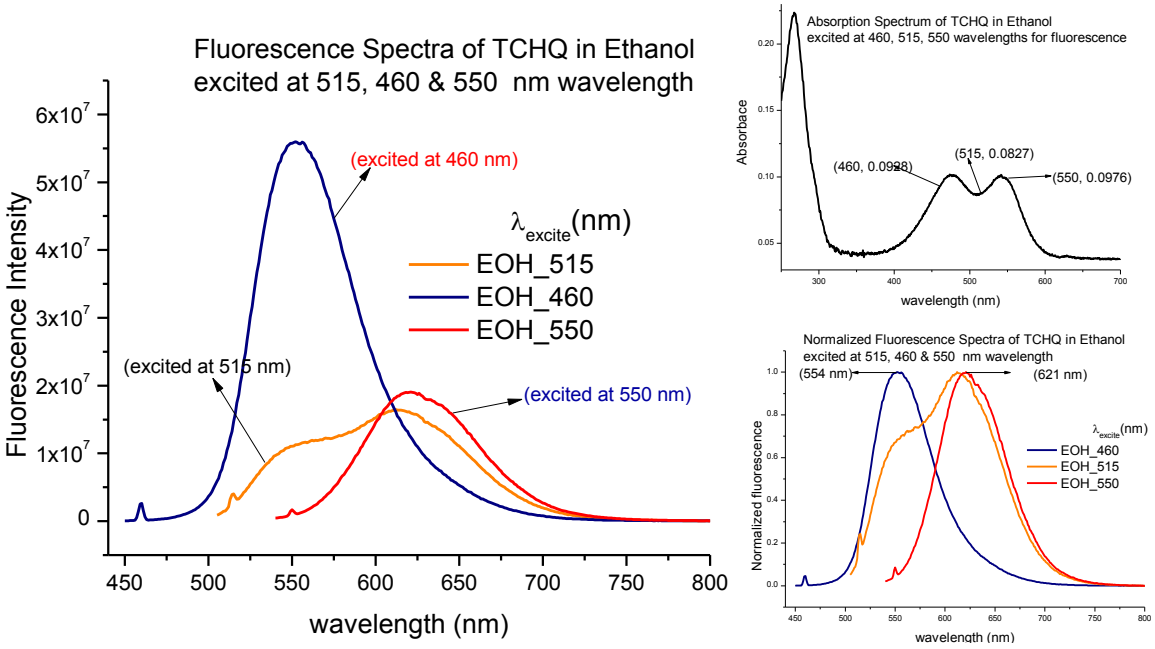

Figure A-6: Absorption, fluorescence and normalized fluorescence spectra of TCHQ in ethanol excited at 460, 515 and 550 nm.

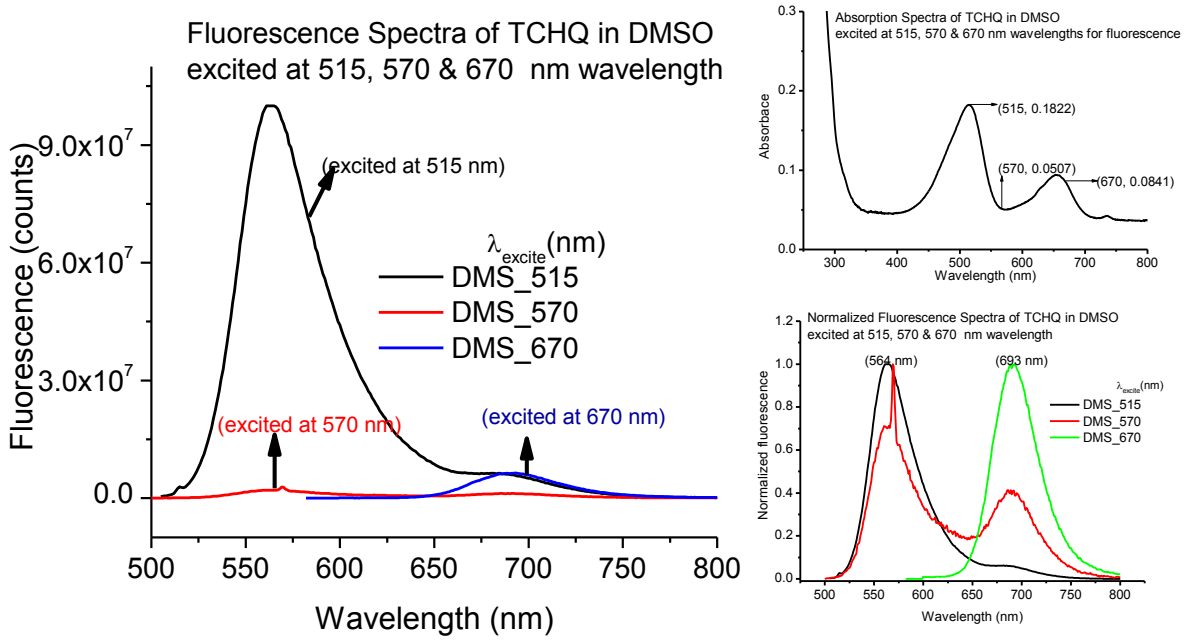

Figure A-7: Absorption, fluorescence and normalized fluorescence spectra of TCHQ in DMSO excited at 515, 570 and 670 nm.

A-2 LSER analysis of cyano-substituted PPDs using Onsager parameters for protic solvents only.

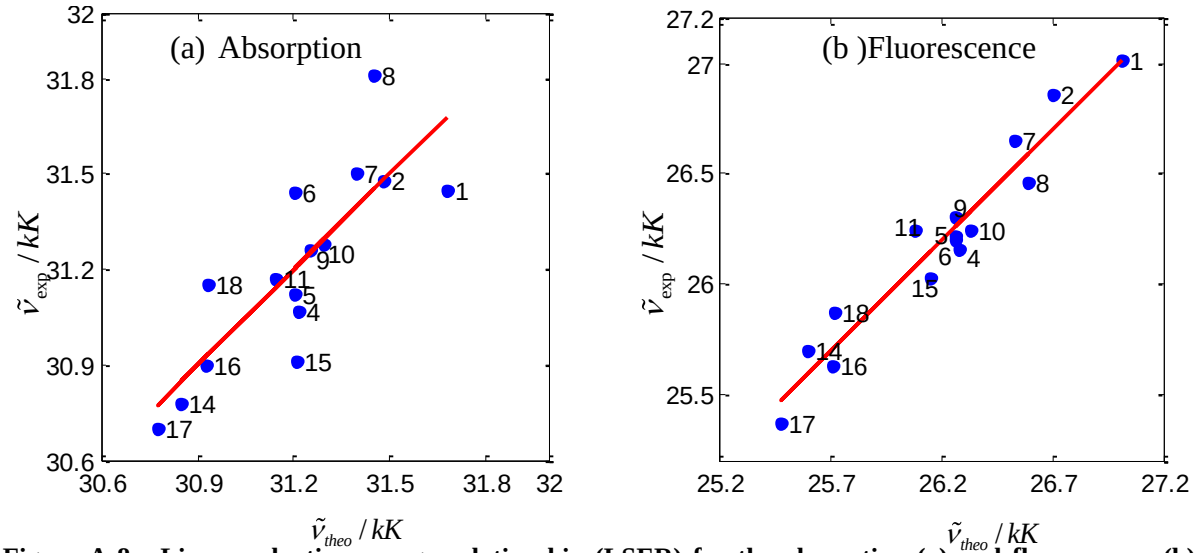

Figure A-8: Linear solvation energy relationship (LSER) for the absorption (a) and fluorescence (b) maxima of PPD using Onsager polarity parameters for aprotic solvents (15 solvents).

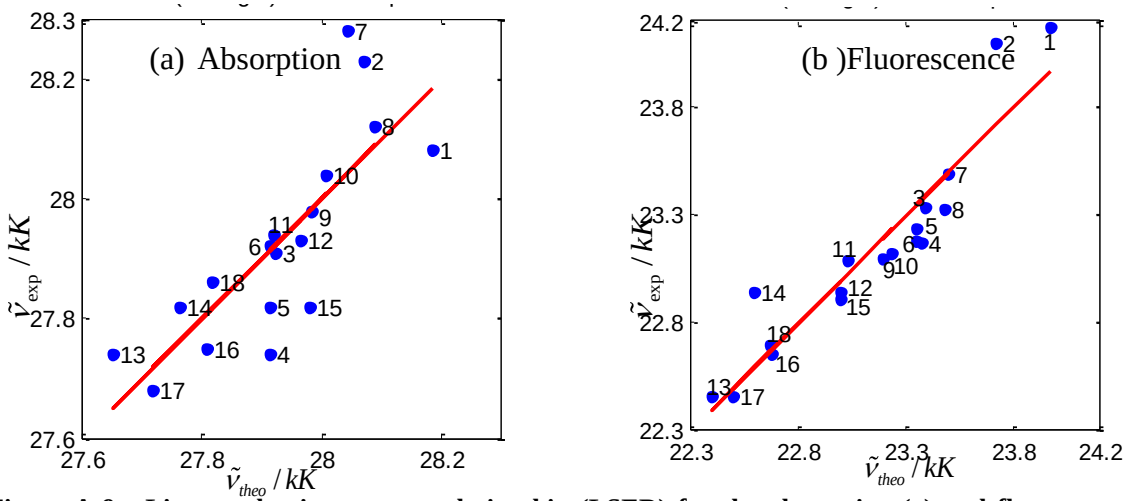

Figure A-9: Linear solvation energy relationship (LSER) for the absorption (a) and fluorescence (b) maxima of MCPPD using Onsager polarity parameters for aprotic solvents (18 solvents).

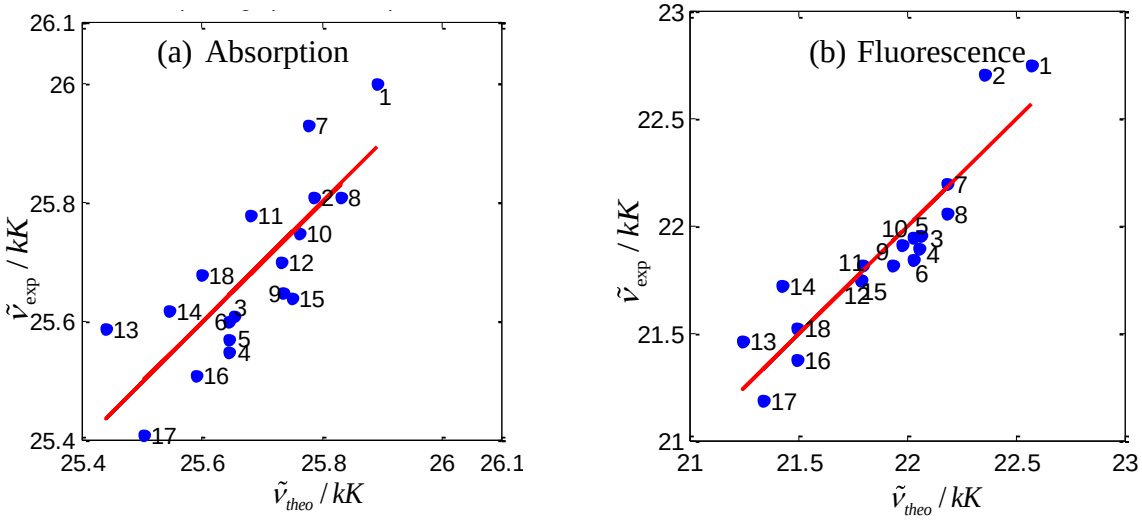

Figure A-10: Linear solvation energy relationship (LSER) for the absorption (a) and fluorescence (b) maxima of DCPPD using Onsager polarity parameters for aprotic solvents (18 solvents).

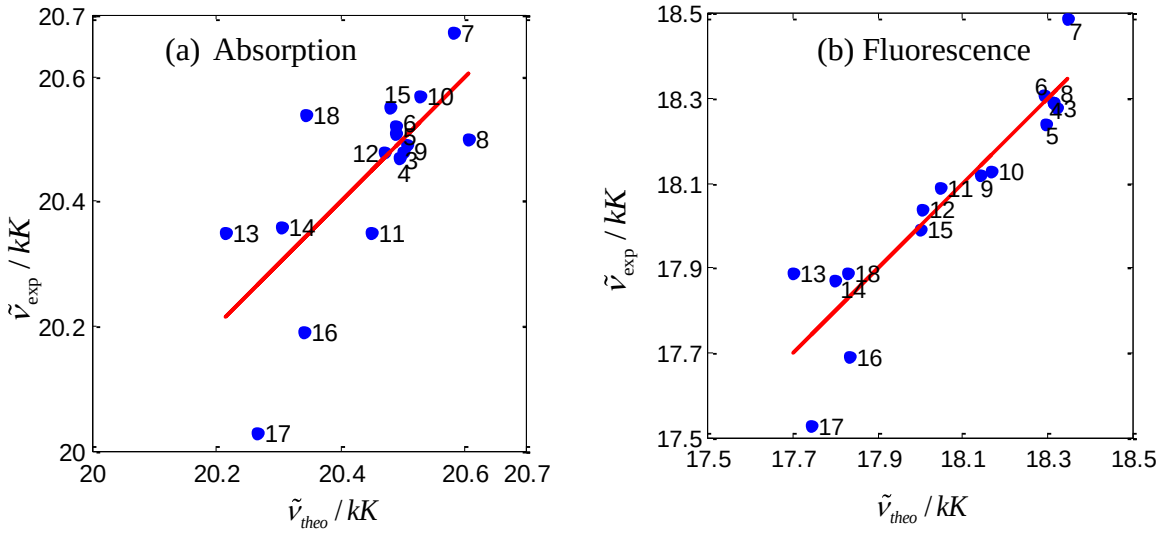

Figure A-11: Linear solvation energy relationship (LSER) for the absorption (a) and fluorescence (b) maxima of TCPPD using Onsager polarity parameters for aprotic solvents (16 solvents).

A-3 LSER analysis of cyano-substituted PPDs using ETN and DNN parameters for protic solvents only.

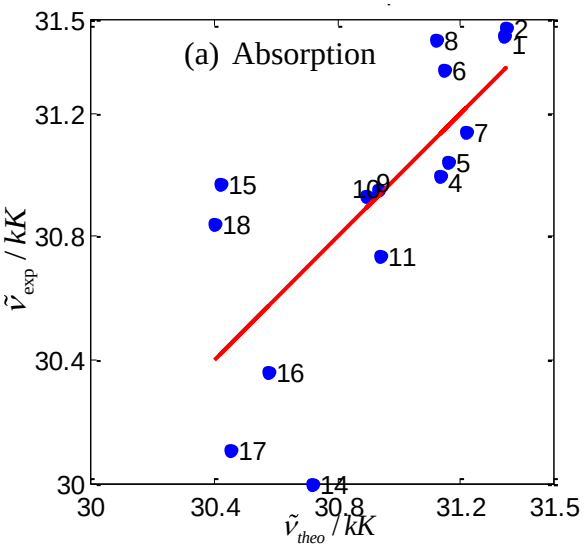

(a) LSER analysis for the absorption maxima ($\tilde{\nu}_{abs}$) of PPD using ETN parameter.

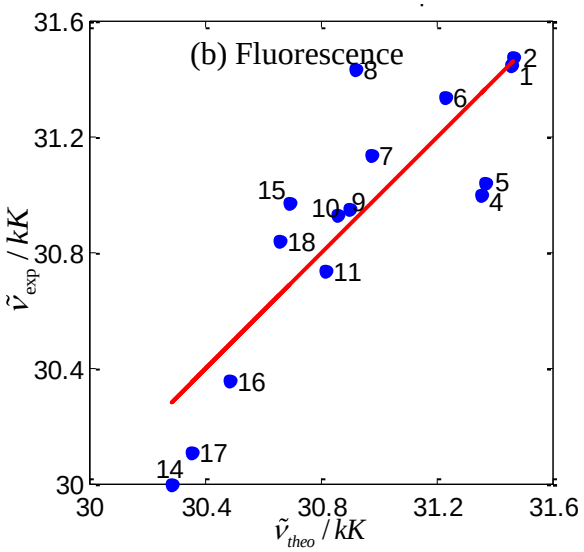

(a) LSER analysis for the absorption maxima ($\tilde{\nu}_{abs}$) of PPD using ETN & DNN.

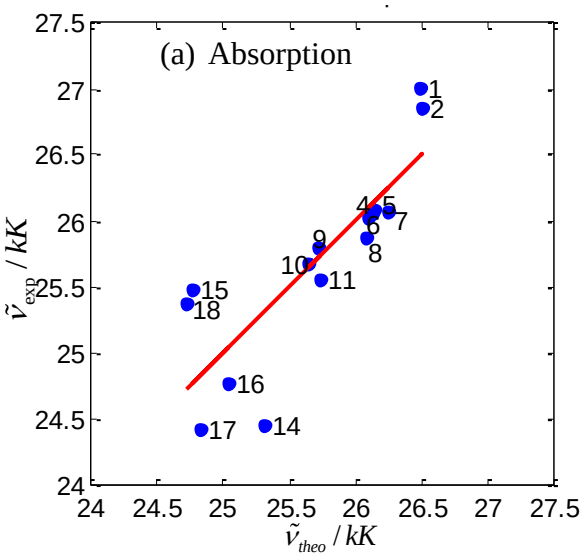

(b) LSER analysis for the fluorescence maxima ($\tilde{\nu}_{flu}$) of PPD using ETN parameter.

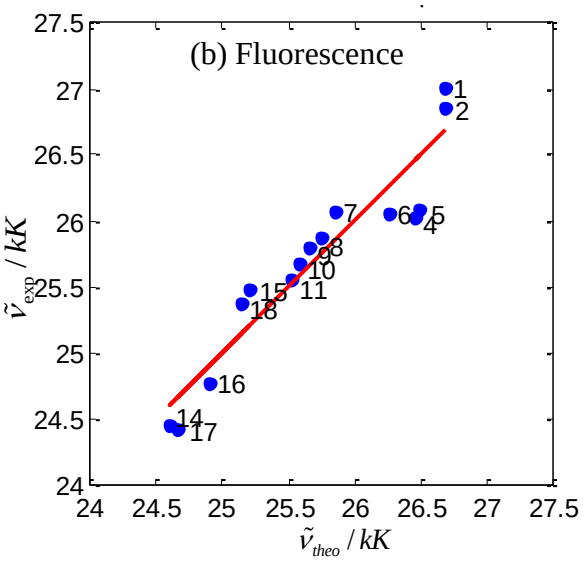

(a) LSER analysis for the fluorescence maxima ($\tilde{\nu}_{flu}$) of PPD using ETN & DNN.

Figure A-12: Linear solvation energy relationship (LSER) for the absorption (a and c) and fluorescence (b and d) maxima of PPD using ETN (a and b) as well as ETN+DNN (c and d) parameters for aprotic solvents (15 solvents).

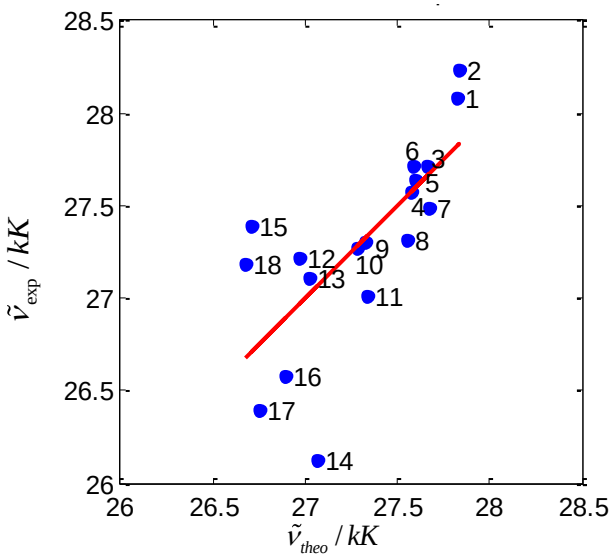

(a) LSER analysis for the absorption maxima ($\tilde{\nu}_{abs}$) of MCPPD using ETN parameter.

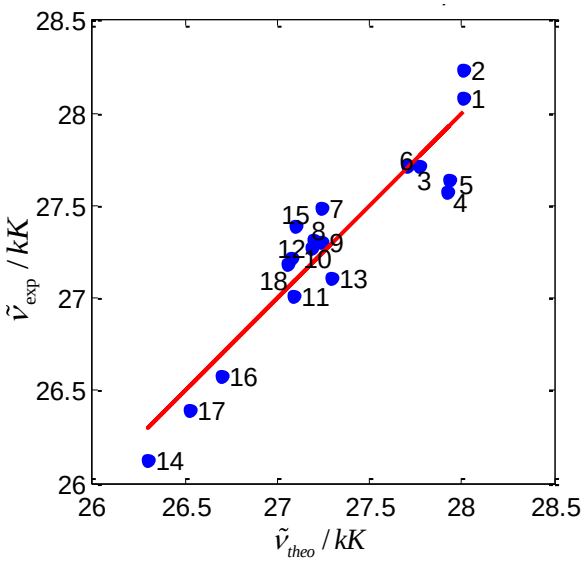

(a) LSER analysis for the absorption maxima ($\tilde{\nu}_{abs}$) of MCPPD using ETN & DNN.

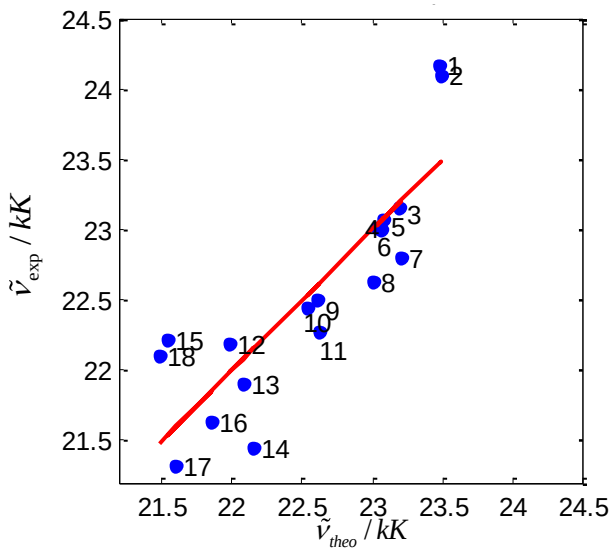

(a) LSER analysis for the fluorescence maxima ($\tilde{\nu}_{flu}$) of MCPPD using ETN parameter.

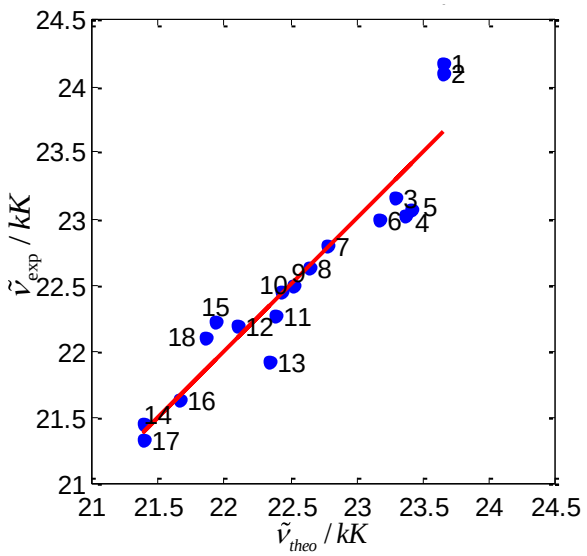

(b) LSER analysis for the fluorescence maxima ($\tilde{\nu}_{flu}$) of MCPPD using ETN & DNN.

Figure A-13: Linear solvation energy relationship (LSER) for the absorption (a and c) and fluorescence (b and d) maxima of MCPPD using ETN (a and b) as well as ETN+DNN (c and d) parameters for aprotic solvents (18 solvents).

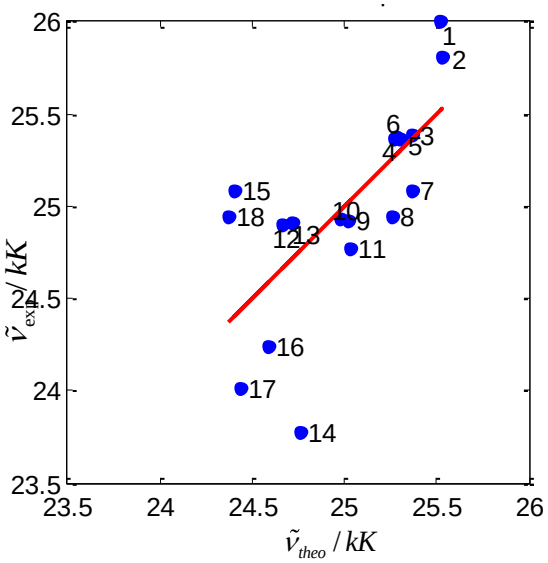

(a) LSER analysis for the absorption maxima ($\tilde{\nu}_{abs}$) of DCPPD using ETN parameter.

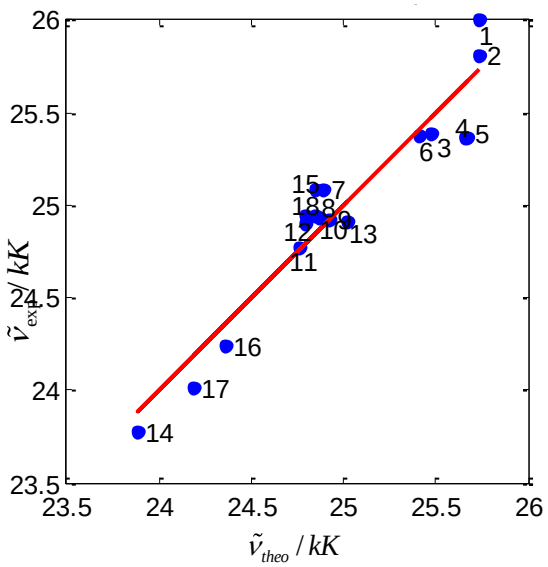

(a) LSER analysis for the absorption maxima ($\tilde{\nu}_{abs}$) of DCPPD using ETN & DNN.

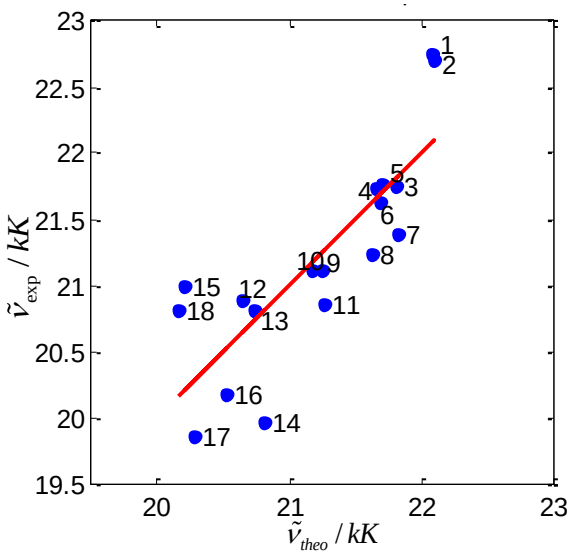

(a) LSER analysis for the fluorescence maxima ($\tilde{\nu}_{flu}$) of DCPPD using ETN parameter.

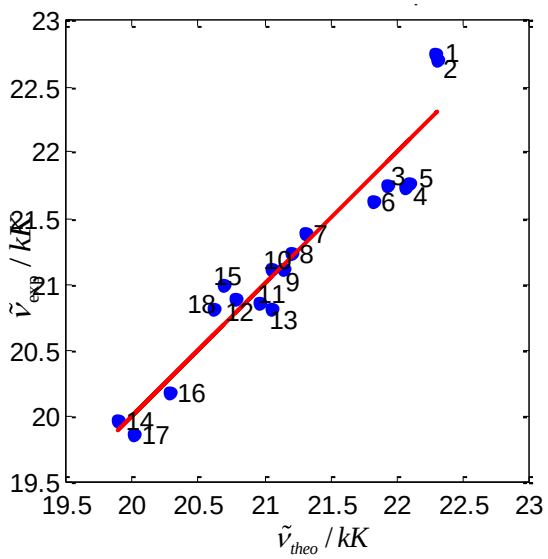

(a) LSER analysis for the fluorescence maxima ($\tilde{\nu}_{flu}$) of DCPPD using ETN & DNN.

Figure A-14: Linear solvation energy relationship (LSER) for the absorption (a and c) and fluorescence (b and d) maxima of DCPPD using ETN (a and b) as well as ETN+DNN (c and d) parameters for aprotic solvents (18 solvents).

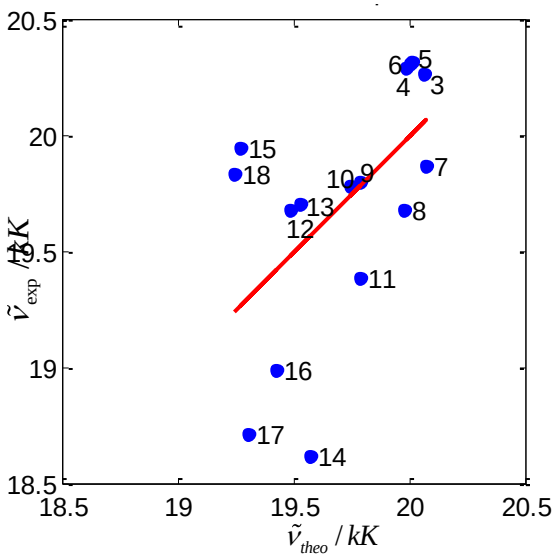

(a) LSER analysis for the absorption maxima ($\tilde{\nu}_{abs}$) of TCPPD using ETN parameter.

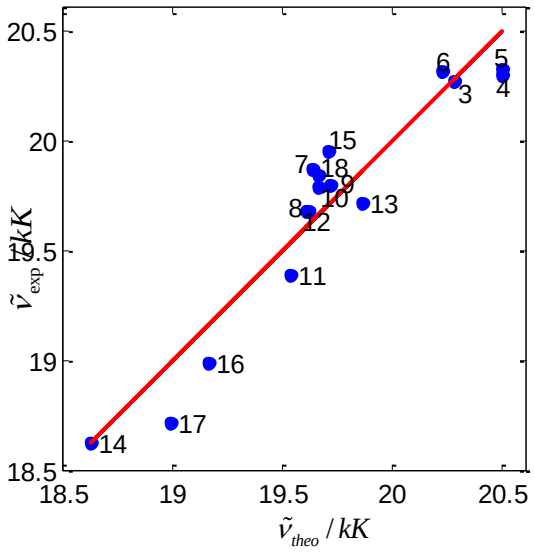

(a) LSER analysis for the absorption maxima ($\tilde{\nu}_{abs}$) of TCPPD using ETN & DNN.

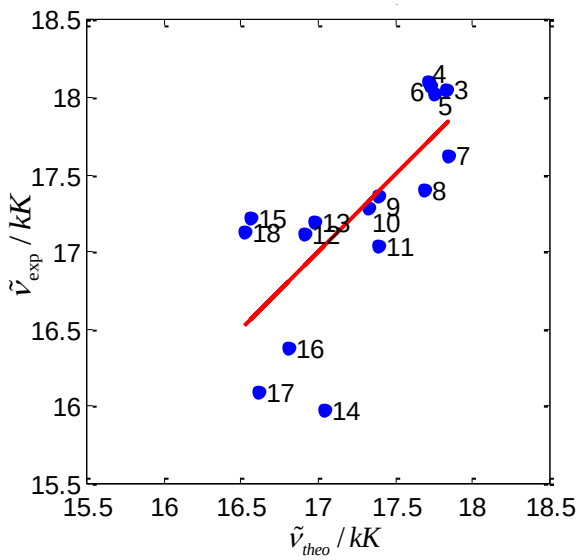

(a) LSER analysis for the fluorescence maxima ($\tilde{\nu}_{flu}$) of TCPPD using ETN parameter.

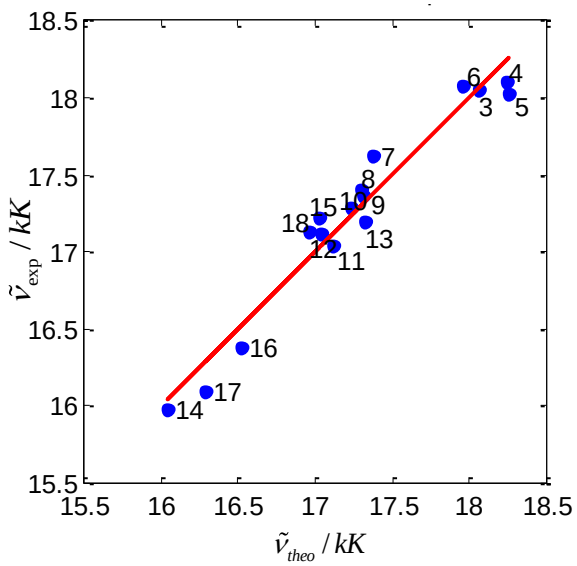

(a) LSER analysis for the fluorescence maxima ($\tilde{\nu}_{flu}$) of TCPPD using ETN & DNN.

Figure A-15: Linear solvation energy relationship (LSER) for the absorption (a and c) and fluorescence (b and d) maxima of TCPPD using ETN (a and b) as well as ETN+DNN (c and d) parameters for aprotic solvents (16 solvents).

A-4 Solvents Parameters used in LSER analysis.

Table A-1: Solvent parameters: di-electric constant (ε), refractive index (nD) , Onsager f(n2), f(D) and f(D,n2), Reichardt (ETN and ET(30)), Gutmanns's donor number (DNN), Kamlet-Taft (α, β and π*) and Catalan (SA, SB, Sdp and Sp) parameters.

Ref. No.	Solvents	$\varepsilon^{(a)}$	$n_D^{(a)}$	f(D)	$f(n^2)$	$f(D,n^2)$	ETN	DNN	α	β	π^*	SA	SB	Sdp	Sp
1	n-Hexan	1.880	1.372	0.185	0.185	0.000	0.009	0.00	0	0	-0.11	0	0.056	0	0.616
2	Cyclohexan	2.020	1.424	0.202	0.203	-0.001	0.006	0.00	0	0	0	0	0.073	0	0.683
3	p-Xylene	2.264	1.493	0.229	0.225	0.003	0.07	0.13	0.00	0.12	0.45	0.00	0.16	0.18	0.78
4	Benzene	2.274	1.498	0.230	0.227	0.003	0.11	0.00	0.00	0.10	0.55	0.00	0.12	0.27	0.79
5	Toluene	2.381	1.494	0.240	0.226	0.014	0.10	0.00	0.00	0.11	0.49	0.00	0.13	0.28	0.78
6	Ethylbenzene	2.395	1.493	0.241	0.225	0.016	0.11	0.15	0.00	0.12	0.53	0.00	0.14	0.24	0.77
7	n-Butylether	3.040	1.397	0.288	0.194	0.094	0.07	0.49	0.00	0.46	0.18	0.00	0.64	0.18	0.67
8	Diethyl ether	4.197	1.350	0.340	0.177	0.163	0.12	0.49	0.00	0.47	0.24	0.00	0.56	0.39	0.62
9	Propyl acetate	6.000	1.383	0.385	0.189	0.196	0.21	0.41	0.00	0.40	0.53	0.00	0.55	0.56	0.67
10	Ethyl acetate	6.020	1.370	0.385	0.184	0.201	0.23	0.44	0.00	0.45	0.45	0.00	0.53	0.64	0.65
11	THF	7.580	1.405	0.407	0.197	0.210	0.21	0.52	0.00	0.55	0.55	0.00	0.58	0.77	0.70
12	Acetone	20.560	1.356	0.464	0.179	0.285	0.36	0.44	0.08	0.48	0.62	0.00	0.48	0.91	0.65
13	Benzonitrile	25.200	1.526	0.471	0.235	0.236	0.33	0.31	0.00	0.37	0.88	0.05	0.28	0.85	0.85
14	HMPA	29.300	1.457	0.475	0.214	0.261	0.32	1.00	0.00	1.00	0.87	0.00	0.81	1.10	0.74
15	Acetonitrile	35.940	1.342	0.479	0.174	0.306	0.46	0.36	0.19	0.40	0.66	0.04	0.29	0.97	0.65
16	DMF	36.710	1.428	0.480	0.205	0.275	0.39	0.69	0.00	0.69	0.88	0.03	0.61	0.98	0.76
17	DMSO	46.450	1.478	0.484	0.220	0.264	0.44	0.77	0.00	0.76	1.00	0.07	0.65	1.00	0.83
18	PC	64.920	1.420	0.489	0.202	0.287	0.47	0.39	0.00	0.40	0.83	0.11	0.34	0.94	0.75
19	1-Pentanol	13.900	1.408	0.448	0.198	0.250	0.59	0.64	0.84	0.86	0.40	0.32	0.86	0.59	0.69
21	1-Butanol	17.510	1.397	0.458	0.194	0.264	0.59	0.75	0.84	0.84	0.47	0.34	0.81	0.66	0.67
22	2-Propanol	19.920	1.375	0.463	0.186	0.277	0.55	0.93	0.76	0.84	0.48	0.28	0.83	0.81	0.63
23	1-Propanol	20.450	1.384	0.464	0.189	0.275	0.62	0.77	0.84	0.90	0.52	0.37	0.78	0.75	0.66
24	Ethanol	24.550	1.359	0.470	0.181	0.289	0.65	0.82	0.86	0.75	0.54	0.40	0.66	0.78	0.63
25	Methanol	32.660	1.327	0.477	0.168	0.309	0.76	0.77	0.98	0.66	0.60	0.61	0.55	0.90	0.61
26	Water	78.304	1.333	0.490	0.170	0.320	1.00	0.46	1.17	0.47	1.09	1.06	0.03	1.00	0.68

Solvent data and solvent parameters are taken from ref. [35-42, 70-71, 106, 135, 138]

(a) At 25 ^{o}C; THF = tetrahydrofuran; HMPA =Hexamethylphosphoramide ; DMF = Dimethylformamide; DMSO = Dimethyl sulfoxide; PC = Propylene carbonate

ACRONYMS

The acronyms used for various solvent are given in Table 3-2 and those for cyano-substituted derivatives of both, PPDs and TMPPDs are given in Table 3-1.

TCHQ	2,3,5,6-tetracyanohydroquinone
DCNB	1,4-dicyanobenzene
25DClPPD	2,5-dichloro-p-phenylendiamine
25DCPPD	2,5-dicyano-p-phenylendiamine
TCNE	Tetracyanoethylene
ICT	Intramolecular charge transfer
TICT	Twisted intramolecular charge transfer
KAT	Kamlet, Abound and Taft
CV	Cyclic voltammetry
LD	Laser diode
LED	Light emitting diode
LSER	Linear solvation energy relationship
ESR	Electron spin resonance
ENDOR	Electron nuclear double-resonance
CIDEP	Chemically induced dynamic electron polarization

BIBLIOGRAPHY

1. Poulos, A.T., C.K. Kelly, and R. Simone, *Photoinduced electron transfer in the p-phenylenediamine-paraquat molecular complex.* The Journal of Physical Chemistry, 1981. **85**(7): p. 823-828.
2. Pearson, A.J. and W. Xiao, *Fluorescent Photoinduced Electron Transfer (PET) Sensing Molecules with p-Phenylenediamine as Electron Donor.* The Journal of Organic Chemistry, 2003. **68**(13): p. 5361-5368.
3. Sharma, S.N., Z.S. Pillai, and P.V. Kamat, *Photoinduced Charge Transfer between CdSe Quantum Dots and p-Phenylenediamine.* The Journal of Physical Chemistry B, 2003. **107**(37): p. 10088-10093.
4. Hirata, Y. and S. Araki, *Photoinduced electron transfer of N,N,N',N'-tetramethyl-p-phenylenediamine and maleic anhydride in 2-propanol.* Chem. Phys. Lett., 2007. **437**(1-3): p. 28-31.
5. Honma, H., H. Murai, and K. Kuwata, *CIDEP study on photooxidation of N,N,N',N'-tetramethyl-p-phenylenediamine by maleic anhydride. Enhanced S--T-1 mixing by radical-ion pair system.* Chem. Phys. Lett., 1992. **195**(2-3): p. 239-242.
6. Honma, H., H. Murai, and K. Kuwata, *CIDEP Study of Radical-Ion Pair Systems: Photooxidation Reactions of N,N,N',N'-tetramethyl-p-phenylenediamine by Maleic Anhydride in Alcohol Solution.* The Journal of Physical Chemistry, 1994. **98**(10): p. 2571-2575.
7. Grampp, G. and G. Stiegler, *ESR-spectroscopic investigations on the radical cations of p-phenylenediamines and related compounds. The determination of the various spin polarization parameters.* Z. Phys. Chem. (Munich), 1984. **141**(2): p. 185-200.
8. Grampp, G. and P. Pluschke, *The correlations and quantum chemical interpretations of some molecular properties of several p-phenylenediamines and related compounds.* Collect. Czech. Chem. Commun., 1987. **52**(4): p. 819-29.
9. Sacher, M. and G. Grampp, *Magnetic field effects on the luminescence of para-phenylenediamine derivatives.* Ber. Bunsen-Ges., 1997. **101**(6): p. 971-974.
10. Moressi, M.B., M.A. Zón, and H. Fernández, *Solvent effects on the heterogeneous kinetics of N,N,N',N'-tetramethyl p-phenylendiamine (TMPD) in nonaqueous binary solvent mixtures. The role of the preferential solvation phenomenon.* Electrochimica Acta, 2000. **45**(10): p. 1669-1682.
11. Grampp, G. and W. Jaenicke, *ESR-Spectroscopic Investigation of the Homogeneous Electron Transfer Reactions between Substituted p-Phenylenediamines and Quinonediimines, and the Validity of Marcus' Theory. I. Measurements at 293 K.* Berichte der Bunsengesellschaft für physikalische Chemie, 1984. **88**(4): p. 325-334.
12. Melchior, M.T. and A.H. Maki, *Electron spin resonance study of P-phenylene-diamine positive ion.* The Journal of Chemical Physics, 1961. **34**(2): p. 471-476.
13. Tachikawa, H. and A.J. Bard, *Electrogenerated chemiluminescence. XII. Magnetic field effects on ECL in the tetracene--TMPD system; evidence for triplet--triplet annihilation of tetracene.* Chem. Phys. Lett., 1973. **19**(2): p. 287-289.
14. Kapturkiewicz, A. and W. Jaenicke, *Comparison between heterogeneous and homogeneous electron transfer in p-phenylenediamine systems.* Journal of the Chemical Society, Faraday Transactions 1: Physical Chemistry in Condensed Phases, 1987. **83**(9): p. 2727-2734.
15. Michaelis, L., M.P. Schubert, and S. Granick, *Free radicals of the type of Würster's salts.* J. Am. Chem. Soc., 1939. **61**: p. 1981-92.

16. Umezawa, Y., F. Yajima, and S. Fujiwara, *Polarographic study of the electron transfer reaction between Co(III) complexes and N,N,N',N'-tetramethyl-p-phenylenediamine(TMPD) in aqueous solution.* Journal of Inorganic and Nuclear Chemistry, 1974. **36**(11): p. 2535-2537.
17. Rees, N.V., et al., *The high speed channel electrode applied to heterogeneous kinetics: The oxidation of 1,4-phenylenediamines and related species in acetonitrile.* Journal of Electroanalytical Chemistry, 2002. **534**(2): p. 151-161.
18. Clegg, A.D., et al., *Experimental validation of Marcus theory for outer-sphere heterogeneous electron-transfer reactions: The oxidation of substituted 1,4-phenylenediamines.* ChemPhysChem, 2004. **5**(8): p. 1234-1240.
19. Rogers, E.I., et al., *Electrochemical Kinetics of Ag|Ag+ and TMPD|TMPD+• in the Room-Temperature Ionic Liquid [C4mpyrr][NTf2]; toward Optimizing Reference Electrodes for Voltammetry in RTILs.* The Journal of Physical Chemistry C, 2007. **111**(37): p. 13957-13966.
20. Long, J.S., et al., *Oxidation of several p-phenylenediamines in room temperature ionic liquids: Estimation of transport and electrode kinetic parameters.* Journal of Physical Chemistry C, 2008. **112**(17): p. 6993-7000.
21. Sakurai, H., et al., *Synthesis and characterization of p-phenylenediamine derivatives bearing an electron-acceptor unit.* J. Org. Chem., 2005. **70**(7): p. 2754-2762.
22. Chiu, K.Y., et al., *Substituent effects on the electrochemical and spectral characteristics of N,N,N',N'-tetraaryl-p-phenylenediamine derivatives.* Journal of Electroanalytical Chemistry, 2005. **578**(2): p. 283-287.
23. Michaelis, L., M.P. Schubert, and S. Granick, *The free radicals of the type of wurster's salts.* J. Am. Chem. Soc., 1939. **61**(8): p. 1981-1992.
24. Schwarzenbacher, G., et al., *Investigation of 2,6-disubstituted N,N,N',N'-tetramethyl-p-phenylenediamines as precursors/building blocks for molecular magnets.* J. Mater. Chem., 2002. **12**(3): p. 534-539.
25. Wüster, C. and R. Sendter, Ber. Dtsch. Chem. Ges, 1803. **12**.
26. Bamfield, P., Chromic Phenomena: Technological Applications of Colour Chemistry (The Royal Society of Chemistry UK), 2001.
27. Zachariasse, K.A., et al., *Counterintuitive absence of an excited-state intramolecular charge transfer reaction with 2,4,6-tricyanoanilines. experimental and computational results.* J. Phys. Chem. A, 2009. **113**(12): p. 2693-2710.
28. Oshima, J., et al., *Extreme fluorescence sensitivity of some aniline derivatives to aqueous and nonaqueous environments: Mechanistic study and its implication as a fluorescent probe.* J. Phys. Chem. A, 2006. **110**(14): p. 4629-4637.
29. Oshima, J., T. Yoshihara, and S. Tobita, *Water-induced fluorescence quenching of mono- and dicyanoanilines.* Chem. Phys. Lett., 2006. **423**(4-6): p. 306-311.
30. Rosspeintner, A., et al., *Photophysical properties of 2,6-dicyano-N,N,N',N'-tetramethyl-p-phenylenediamine.* Journal of Photochemistry and Photobiology A: Chemistry, 2006. **183**(1-2): p. 225-235.
31. Angulo, G., et al., *Spectroscopic characteristics of a novel highly fluorescent p-phenylenediamine: Tetracyano-p-phenylenediamine.* Journal of Photochemistry and Photobiology A: Chemistry, 2008. **199**(2-3): p. 204-210.
32. Berlman, I.B., Handbook of Fluorescence Spectra of Aromatic Molecules, 1971.
33. Darmanyan, A.P., W. Lee, and W.S. Jenks, *Charge Transfer Interactions in the Generation of Singlet Oxygen O2(1Δg) by Strong Electron Donors.* The Journal of Physical Chemistry A, 1999. **103**(15): p. 2705-2711.

34. Manoharan, R. and S.K. Dogra, *Spectral Characteristics of Phenylenediamines and Thier Various Protonated Species.* Bulletin of the Chemical Society of Japan, 1987. **60**: p. 4409-4415.
35. Kamlet, M.J. and R.W. Taft, *The solvatochromic comparison method. I. The β-scale of solvent hydrogen-bond acceptor (HBA) basicities.* J. Am. Chem. Soc., 1976. **98**(2): p. 377-383.
36. Taft, R.W. and M.J. Kamlet, *The solvatochromic comparison method. 2. The α-scale of solvent hydrogen-bond donor (HBD) acidities.* J. Am. Chem. Soc., 1976. **98**(10): p. 2886-2894.
37. Kamlet, M.J., J.L. Abboud, and R.W. Taft, *The solvatochromic comparison method. 6. The π^* scale of solvent polarities.* J. Am. Chem. Soc., 1977. **99**(18): p. 6027-6038.
38. Kamlet, M.J., et al., *Linear solvation energy relationships. 23. A comprehensive collection of the solvatochromic parameters, π*, α, and β, and some methods for simplifying the generalized solvatochromic equation.* J. Org. Chem., 1983. **48**(17): p. 2877-2887.
39. Catalán, J., et al., *Progress towards a generalized solvent polarity scale: The solvatochromism of 2-(dimethylamino)-7-nitrofluorene and its homomorph 2-fluoro-7-nitrofluorene.* Liebigs Ann., 1995(2): p. 241-252.
40. Catalán, J., et al., *A generalized solvent basicity scale: The solvatochromism of 5-nitroindoline and its homomorph 1-methyl-5-nitroindoline.* Liebigs Annales, 1996(11): p. 1785-1794.
41. Catalán, J. and C. Díaz, *A generalized solvent acidity scale: The solvatochromism of o-tert-butylstilbazolium betaine dye and its homomorph o,o'-di-tert-butylstilbazolium betaine dye.* Liebigs Annales, 1997(9): p. 1941-1949.
42. Catalán, J., *Toward a generalized treatment of the solvent effect based on four empirical scales: Dipolarity (SdP, a new scale), polarizability (SP), acidity (SA), and basicity (SB) of the medium.* J. Phys. Chem. B, 2009. **113**(17): p. 5951-5960.
43. Reichardt, C., *Empirical parameters of solvent polarity as linear free-energy relationships.* Angew Chem (Int Ed Engl), 1979. **18**(2): p. 98-110.
44. Vazquez, C., et al., *Cyanil. Synthesis and characterization of the strongest isolated electron acceptor and its reduced forms.* J. Org. Chem., 1993. **58**(1): p. 65-81.
45. Reichardt, C., *Solvatochromism, thermochromism, piezochromism, halochromism, and chiro-solvatochromism of pyridinium N-phenoxide betaine dyes.* Chemical Society Reviews, 1992. **21**(3): p. 147-153.
46. Reichardt, C., *Solvatochromic dyes as solvent polarity indicators.* Chemical Reviews, 1994. **94**(8): p. 2319-2358.
47. Gutmann, V., *Solvent effects on the reactivities of organometallic compounds.* Coordination Chemistry Reviews, 1976. **18**(2): p. 225-255.
48. Malval, J.-P., B. Graff, and P. Jaques, *Solvatochromism of thioxanthone (TX) in the light of CAS PT2 computations.* . EPA Newsletter, 2009: p. 37-53.
49. Suppan, P. and N. Ghoneim, Solvatochromism (The Royal Society of Chemistry, Cambridge), 1997.
50. Mansha, A., et al., Unpublished results.
51. Witt, O.N., *Zur Kenntniss des Baues und der Bildung färbender Kohlenstoffverbindungen.* Berichte der deutschen chemischen Gesellschaft, 1876. **9**(1): p. 522-527.
52. Woodward, R.B., *Structure and the Absorption Spectra of α,β-Unsaturated Ketones.* Journal of the American Chemical Society, 1941. **63**(4): p. 1123-1126.

53. Fieser, L.F., M. Fieser, and S. Rajagopalan, *Absorption spectroscopy and the structures of the diosterols.* The Journal of Organic Chemistry, 1948. **13**(6): p. 800-806.
54. Strickler, S.J. and R.A. Berg, *Relationship between absorption intensity and fluorescence lifetime of molecules.* The Journal of Chemical Physics, 1962. **37**(4): p. 814-822.
55. Valeur, B., Molecular Fluorescence Principles and Applications (WILEY-VCH), 2002.
56. Stokes, G.G., *On the Change of Refrangibility of Light.* Philosophical Transactions of the Royal Society of London, 1852. **142**: p. 463-562.
57. Auzel, F., *Upconversion and Anti-Stokes Processes with f and d Ions in Solids.* Chemical Reviews, 2003. **104**(1): p. 139-174.
58. Rurack, K., *Fluorescence Quantum Yields: Methods of Determination and Standards*, in *Standardization and Quality Assurance in Fluorescence Measurements I*, U. Resch-Genger, Editor. 2008, Springer Berlin Heidelberg. p. 101-145.
59. Crosby, G.A. and J.N. Demas, *Measurement of photoluminescence quantum yields. Review.* The Journal of Physical Chemistry, 1971. **75**(8): p. 991-1024.
60. Resch-Genger, U., Standardization and Quality Assurance in Fluorescence Measurements I: Techniques (Springer), 2008.
61. Monte, C., et al., *Linking fluorescence measurements to radiometric units.* Metrologia, 2006. **43**(2).
62. DeRose, P.C., E.A. Early, and G.W. Kramer, *Qualification of a fluorescence spectrometer for measuring true fluorescence spectra.* Review of Scientific Instruments, 2007. **78**(3).
63. De Mello, J.C., H.F. Wittmann, and R.H. Friend, *An improved experimental determination of external photoluminescence quantum efficiency.* Advanced Materials, 1997. **9**(3): p. 230-232.
64. DeRose, P.C. and U. Resch-Genger, *Recommendations for Fluorescence Instrument Qualification: The New ASTM Standard Guide.* Anal. Chem., 2010. **82**(5): p. 2129-2133.
65. Resch-Genger, U., K. Hoffmann, and A. Hoffmann, *Standardization of Fluorescence Measurements: Criteria for the Choice of Suitable Standards and Approaches to Fit-for-Purpose Calibration Tools.* Annals of the New York Academy of Sciences, 2008. **1130**(1): p. 35-43.
66. DeRose, P.C., et al., *Need for and Metrological Approaches Towards Standardization of Fluorescence Measurements from the View of National Metrology Institutes*, in *Standardization and Quality Assurance in Fluorescence Measurements I*, U. Resch-Genger, Editor. 2008, Springer Berlin Heidelberg. p. 33-62.
67. Reichardt, C., Solvents and Solvent Effects in Organic Chemistry (WILEY-VCH Verlag GmbH & Co. KGaA, Weinheim), 2003. 3rd edition.
68. Hantzsch, A., *Über die Halochromie und »Solvatochromie« des Dibenzal-acetons und einfacherer Ketone, sowie ihrer Ketochloride.* Berichte der deutschen chemischen Gesellschaft (A and B Series), 1922. **55**(4): p. 953-979.
69. Sheppard, S.E., *The Effects of Environment and Aggregation on the Absorption Spectra of Dyes.* Reviews of Modern Physics, 1942. **14**(2-3): p. 303.
70. Marcus, Y., The Properties of Solvents; Wiley Series in Solution Chemistry, 1998. **4**.
71. Wypych, G., *Hanbook of Solvents (ChemTec Publishing, Canada).* 2001.
72. Gutmann, V., A. Steininger, and E. Wychera, *Donorstärken in 1,2-Dichloräthan.* Monatshefte für Chemie / Chemical Monthly, 1966. **97**(2): p. 460-467.

73. Laurence, C. and J.-F. Gal, *Lewis Basicity and Affinity Measurement: Definitions and Context*. Lewis Basicity and Affinity Scales. 2009: John Wiley & Sons, Ltd.
74. Jensen, W.B., *The Lewis acid-base concepts : an overview / William B. Jensen*. 1980, New York :: Wiley.
75. Parker, A.J., *The effects of solvation on the properties of anions in dipolar aprotic solvents.* Quarterly Reviews, Chemical Society, 1962. **16**(2): p. 163-187.
76. Alexander, R., et al., *Solvation of ions. XI. Solubility products and instability constants in water, methanol, formamide, dimethylformamide, dimethylacetamide, dimethyl sulfoxide, acetonitrile, and hexamethylphosphorotriamide.* Journal of the American Chemical Society, 1967. **89**(15): p. 3703-3712.
77. Alexander, R., et al., *Solvation of ions. XIV. Protic-dipolar aprotic solvent effects on rates of bimolecular reactions. Solvent activity coefficients of reactants and transition states at 25°.* Journal of the American Chemical Society, 1968. **90**(19): p. 5049-5069.
78. Alexander, R. and A.J. Parker, *Solvation of ions. XII. Changes in the standard chemical potential of anions on transfer from protic to dipolar aprotic solvents.* Journal of the American Chemical Society, 1967. **89**(22): p. 5549-5551.
79. Clare, B.W., et al., *Solvation of ions. IX. The effect of anion solvation on acid dissociation constants in methanol, water, dimethylformamide, and dimethyl sulfoxide.* Journal of the American Chemical Society, 1966. **88**(9): p. 1911-1916.
80. Coniglio, B.O., et al., *Solvation of ions. Part VII. Solvation of transition states for S_N2 and S_NAr reactions of azide and thiocyanate ions in methanol and dimethylformamide.* Journal of the Chemical Society B: Physical Organic, 1966: p. 152-160.
81. Cook, D., et al., *Solvation of ions. Part VIII. S_N2 reactions of phenoxide and carboxylate anions with methyl iodide in methanol and in dimethylformamide.* Journal of the Chemical Society B: Physical Organic, 1966: p. 404-409.
82. Mac, Y.C., et al., *Solvation of ions. Part X. Kinetic and thermodynamic properties of bimolecular reactions between anions and cations and between dipoles in protic and dipolar aprotic solvents.* Journal of the Chemical Society B: Physical Organic, 1967: p. 525-530.
83. Parker, A.J., *Solvation of ions. Part VI. Activity coefficients of anions in methanol relative to dimethylformamide.* Journal of the Chemical Society A: Inorganic, Physical, Theoretical, 1966: p. 220-228.
84. Parker, A.J. and D. Brody, *Salvation of Ions. Part IV.[1] the electronic absorption spectra of some group VI anions and their conjugate acids in protic and dipolar aprotic Solvents.* Journal of the Chemical Society (Resumed), 1963: p. 4161-4167.
85. Parker, A.J., et al., *Correlation of solvent effects on rates of solvolysis and S_N2 reactions.* Journal of Organic Chemistry, 1978. **43**(10): p. 1843-1854.
86. Chastrette, M. and J. Carretto, *Statistical study of solvent effects-II. Analysis of some empirical parameters of solvent polarity.* Tetrahedron, 1982. **38**(11): p. 1615-1618.
87. Chastrette, M., et al., *Approach to a general classification of solvents using a multivariate statistical treatment of quantitative solvent parameters.* Journal of the American Chemical Society, 1985. **107**(1): p. 1-11.
88. Exner, O., *How to get wrong results from good experimental data: A survey of incorrect applications of regression.* Journal of Physical Organic Chemistry, 1997. **10**(11): p. 797-813.
89. Exner, O. and K. Zvára, *Coefficient of determination in some atypical situations: Use in chemical correlation analysis.* Journal of Physical Organic Chemistry, 1999. **12**(2): p. 151-156.

90. Bohle, M., W. Kollecker, and D. Martin, *Anwendung der Faktoranalyse in der organischen Chemie.* Zeitschrift für Chemie, 1977. **17**(5): p. 161-168.
91. Cramer Iii, R.D., *BC(DEF) parameters. 2. An empirical structure-based scheme for the prediction of some physical properties.* Journal of the American Chemical Society, 1980. **102**(6): p. 1849-1859.
92. Cramer Iii, R.D., *BC(DEF) parameters. 1. The intrinsic dimensionality of intermolecular interactions in the liquid state.* Journal of the American Chemical Society, 1980. **102**(6): p. 1837-1849.
93. Lippert, E., *Dipole moment and electronic structure of excited molecules.* Z. Naturforsch., 1955. **10a**: p. 541-5.
94. Lippert, E., *Spektroskopische bestimmungen des dipolmomentes aromatischer verbindungen im ersten angeregten singulettzustand.* Z. Elektrochem., 1957. **61**: p. 962-975.
95. Mataga, N., Y. Kaifu, and M. Koizumi, Bulletin of the Chemical Society of *Japan*, 1956. **29**: p. 465-470.
96. McRae, E.G., *Theory of solvent effects on molecular electronic spectra. Frequency shifts.* J. Phys. Chem., 1957. **61**(5): p. 562-572.
97. Bayliss, N.S. and E.G. McRae, *Solvent Effects in Organic Spectra: Dipole Forces and the Franck–Condon Principle.* The Journal of Physical Chemistry, 1954. **58**(11): p. 1002-1006.
98. Onsager, L., *Electric moments of molecules in liquids.* Journal of the American Chemical Society, 1936. **58**(8): p. 1486-1493.
99. Suppan, P., *Excited-state dipole moments from absorption/fluorescence solvatochromic ratios.* Chem. Phys. Lett., 1983. **94**(3): p. 272-275.
100. Rettig, W., *Application of a simplified microstructural solvent interaction model to the solvatochromism of twisted intramolecular charge transfer (TICT) states.* Journal of Molecular Structure, 1982. **84**(3-4): p. 303-327.
101. Brand, L. and J.R. Gohlke, *Fluorescence Probes for Structure.* Annual Review of Biochemistry, 1972. **41**(1): p. 843-868.
102. Lakowicz, J.R., Principles of Fluorescence Spectroscopy (Springer), 2006.
103. Liptay, W., *Die lösungsmittelabhägigkeit der wellenzahl von elektronenbanden und chemisch-physikalischen grundlagen.* Z. Naturforsch., 1965. **20 A**: p. 1441-1471.
104. Bakhshiev, N.G., *A New Generalized Spectral Luminescent Method for Determining Dipole Moments of Molecules in the Ground and Excited States.* Optics and Spectroscopy (English translation of Optika i Spektroskopiya), 2000. **88**(2): p. 190-194.
105. Kawski, A., *On the estimation of excited-state dipole moments from solvatochromic shifts of absorption and fluorescence spectra.* Zeitschrift fur Naturforschung - Section A Journal of Physical Sciences, 2002. **57**(5-6): p. 255-262.
106. Reichardt, C., Solvents and Solvent Effects in Organic Chemistry (WILEY-VCH Verlag GmbH & Co. KGaA, Weinheim), 2003.
107. Beck, S.C. and D.T. Cramb, *Condensed Phase Dispersive Interactions of Benzo[a]pyrene with Various Solvents and with DNA: A Twist on Solvatochromism.* The Journal of Physical Chemistry B, 2000. **104**(12): p. 2767-2774.
108. Ravi, M., A. Samanta, and T.P. Radhakrishnan, *Excited State Dipole Moments from an Efficient Analysis of Solvatochromic Stokes Shift Data.* The Journal of Physical Chemistry, 1994. **98**(37): p. 9133-9136.
109. Lippert, E., et al., *Umwandlung von Elektronenanregungsenergie.* Angewandte Chemie, 1961. **73**(21): p. 695-706.

110. Nikolay, G.B. and et al., *Experimental Determination of the Dipole Moments of Organic Molecules in Excited Electronic States.* Russian Chemical Reviews, 1969. **38**(9): p. 740.
111. Grabowski, Z.R., K. Rotkiewicz, and W. Rettig, *Structural Changes Accompanying Intramolecular Electron Transfer: Focus on Twisted Intramolecular Charge-Transfer States and Structures.* Chemical Reviews, 2003. **103**(10): p. 3899-4031.
112. Zachariasse, K.A., *Comment on "Pseudo-Jahn-Teller and TICT-models: a photophysical comparison of meta-and para-DMABN derivatives" [Chem. Phys. Lett. 305 (1999) 8] The PICT model for dual fluorescence of aminobenzonitriles.* Chem. Phys. Lett., 2000. **320**(1,2): p. 8-13.
113. Zachariasse, K.A., et al., *Intramolecular charge transfer in aminobenzonitriles: requirements for dual fluorescence.* Pure Appl. Chem., 1993. **65**(8): p. 1745-50.
114. Rettig, W., B. Bliss, and K. Dirnberger, *Pseudo-Jahn-Teller and TICT-models: a photophysical comparison of meta- and para-DMABN derivatives.* Chem. Phys. Lett., 1999. **305**(1,2): p. 8-14.
115. Rettig, W., *TICT states and beyond: Reaction dimensionality and application to photosynthesis.* Journal of Chemical Sciences, 1992. **104**(2): p. 89-104.
116. Kosower, E.M., et al., *Intramolecular donor-acceptor systems. Radiative and nonradiative processes for the excited states of 2-N-arylamino-6-naphthalenesulfonates.* J. Am. Chem. Soc., 1975. **97**(8): p. 2167-2178.
117. Kosower, E.M. and H. Dodiuk, *Intramolecular donor-acceptor systems. 3. A third type of emitting singlet state for N-alkyl-6-N-arylamino-2-naphthalenesulfonates. Solvent modulation of substituent effects on charge-transfer emissions.* J. Am. Chem. Soc., 1978. **100**(13): p. 4173-4179.
118. Dodiuk, H. and E.M. Kosower, *Multiple fluorescences. 4. The protonated form of N-alkyl-2-N-arylamino-6-naphthalenesulfonates.* J. Am. Chem. Soc., 1977. **99**(3): p. 859-865.
119. Hermant, R.M., et al., *Systematic study of a series of highly fluorescent rod-shaped donor-acceptor systems.* J. Am. Chem. Soc., 1990. **112**(3): p. 1214-1221.
120. Mes, G.F., et al., *Excited-state dipole moment and solvatochromism of highly fluorescent rod-shaped bichromophoric molecules.* J. Am. Chem. Soc., 1984. **106**(22): p. 6524-6528.
121. Rao, C.N.R., S. Singh, and V.P. Senthilnathan, *Spectroscopic studies of solute-solvent interactions.* Chemical Society Reviews, 1976. **5**: p. 297-316.
122. Liptay, W., *Electrochromism and Solvatochromism.* Angewandte Chemie International Edition in English, 1969. **8**(3): p. 177-188.
123. Suppan, P., *Invited review. Solvatochromic shifts. The influence of the medium on the energy of electronic states.* J. Photochem. Photobiol., A, 1990. **50**(3): p. 293-330.
124. Buncel, E. and S. Rajagopal, *Solvatochromism and solvent polarity scales.* Accounts of Chemical Research, 1990. **23**(7): p. 226-231.
125. Tomasi, J., B. Mennucci, and R. Cammi, *Quantum mechanical continuum solvation models.* Chemical Reviews, 2005. **105**(8): p. 2999-3093.
126. Katritzky, A.R., et al., *QSPR treatment of solvent scales.* Journal of Chemical Information and Computer Sciences, 1999. **39**(4): p. 684-691.
127. Laurence, C., et al., *The empirical treatment of solvent-solute interactions: 15 Years of π.* J. Phys. Chem., 1994. **98**(23): p. 5807-5816.
128. Kosower, E.M., *The effect of solvent on spectra. I. A new empirical measure of solvent polarity: Z-values.* J. Am. Chem. Soc., 1958. **80**(13): p. 3253-3260.
129. Knauer, B.R. and J.J. Napier, *The nitrogen hyperfine splitting constant of the nitroxide functional group as a solvent polarity parameter. The relative importance*

for a solvent polarity parameter of its being a cybotactic probe vs.Its being a model process. J. Am. Chem. Soc., 1976. **98**(15): p. 4395-4400.
130. Brooker, L.G.S., et al., *Color and constitution. XIII. Merocyanines as solvent property indicators.* J. Am. Chem. Soc., 1965. **87**(11): p. 2443-2450.
131. Nigam, S. and S. Rutan, *Principles and applications of solvatochromism.* Applied Spectroscopy, 2001. **55**(11).
132. Reichardt, C., Solvents and Solvent Effects in Organic Chemistry (WILEY-VCH), 2002.
133. Grunwald, E. and S. Winstein, *The correlation of solvolysis rates.* J. Am. Chem. Soc., 1948. **70**(2): p. 846-854.
134. Dong, D.C. and M.A. Winnik, *The Py scale of solvent polarities.* Can. J. Chem., 1984. **62**: p. 2560-2565.
135. Catalán, J. and H. Hopf, *Empirical treatment of the inductive and dispersive components of solute-solvent interactions: The solvent polarizability (SP) scale.* European Journal of Organic Chemistry, 2004(22): p. 4694-4702.
136. Catalán, J., et al., *On solvent basicity: Analysis of the SB scale.* J. Phys. Chem. A, 1997. **101**(28): p. 5183-5189.
137. Dimroth, K., et al., Justus Liebigs Ann. Chem, 1963. **661**(null): p. 1.
138. Marcus, Y., *The properties of organic liquids that are relevant to their use as solvating solvents.* Chemical Society Reviews, 1993. **22**(6): p. 409-416.
139. Reichardt, C., *Solvents and solvent effects: An introduction.* Organic Process Research and Development, 2007. **11**(1): p. 105-113.
140. Brooker, L.G.S., G.H. Keyes, and D.W. Heseltine, *Color and Constitution. XI.1 Anhydronium Bases of p-Hydroxystyryl Dyes as Solvent Polarity Indicators.* J. Am. Chem. Soc., 1951. **73**(11): p. 5350-5356.
141. Catalán, J., *Use of the SPP scale for the analysis of molecular systems with dual emissions resulting from the solvent polarity.* Journal of Fluorescence, 1996. **6**(1): p. 15-22.
142. Bollinger, J.-C., G. Yvernault, and T. Yvernault, *Enthalpies de complexation de quelques phosphoramides avec le chlorure d'antimoine(V). Influence de la structure sur le nombre donneur selon Gutmann.* Thermochimica Acta, 1983. **60**(2): p. 137-147.
143. Castro, G.T., O.S. Giordano, and S.E. Blanco, *Determination of the pK_a of hydroxy-benzophenones in ethanol-water mixtures. Solvent effects.* Journal of Molecular Structure: THEOCHEM, 2003. **626**: p. 167-178.
144. Perkampus, H.H., UV-VIS Spectroscopy and Its Applications (Springer), 1992.
145. Benesi, H.A. and J.H. Hildebrand, *A spectrophotometric investigation of the interaction of iodine with aromatic hydrocarbons.* J. Am. Chem. Soc., 1949. **71**(8): p. 2703-2707.
146. Chattopadhyay, N., *Determination of pK^* in excited state proton transfer (ESPT) reaction: a rearrangement of Weller's equation; advantage of dual luminescence.* J. Photochem. Photobiol., A, 1995. **88**(1): p. 1-4.
147. Van Stam, J. and J.E. Löfroth, *The protolysis of singlet excited β-naphtol: A two-day laboratory experiment to introduce photophysics.* J. Chem. Educ., 1986. **63**(2): p. 181-184.
148. Förster, T., Z. Elektrochem., 1950. **54**(1): p. 42-46.
149. Grabowski, Z.R. and W. Rubaszewska, *Generalised Förster cycle. Thermodynamic and extrathermodynamic relationships between proton transfer, electron transfer and electronic excitation.* Journal of the Chemical Society, Faraday Transactions 1: Physical Chemistry in Condensed Phases, 1977. **73**: p. 11-28.

150. Tsutsumi, K., S. Sekiguchi, and H. Shizuka, *Proton-transfer reactions in the excited state of phenanthrylamines by nanosecond spectroscopy and fluorimetry.* Journal of the Chemical Society, Faraday Transactions 1: Physical Chemistry in Condensed Phases, 1982. **78**(4): p. 1087-1101.
151. Shizuka, H., et al., *Direct measurement of proton dissociation in thhe excited state of protonated 1-aminopyrene with picosecond pulses.* Chem. Phys. Lett., 1979. **62**(2): p. 408-411.
152. Shizuka, H. and K. Tsutsumi, *Excited state pK^*_a values of aromatic amines by dynamic analyses.* Journal of Photochemistry, 1978. **9**(3): p. 334-335.
153. Bard, A.J. and L.R. Faulkner, Electrochemical Methods Fundamentals and Applications (John Wiley & Sons, Inc.), 2001.
154. Heinze, J., *Cyclic voltammetry - 'electrochemical spectroscopy'.* Angewandte Chemie - International Edition in English, 1984. **23**(11): p. 831-847.
155. Matsuda, H. and Y. Ayabe, *Zur Theorie der Randles-Sevčikschen Kathodenstrahl-Polarographie.* Zeitschrift für Elektrochemie, Berichte der Bunsengesellschaft für physikalische Chemie, 1955. **59**(6): p. 494-503.
156. Nicholson, R.S., *Theory and application of cyclic voltammetry for measurement of electrode reaction kinetics.* Anal. Chem., 1965. **37**(11): p. 1351-1355.
157. Nicholson, R.S. and I. Shain, *Theory of stationary electrode polarography single scan and cyclic methods applied to reversible, irreversible, and kinetic systems.* Anal. Chem., 1964. **36**(4): p. 706-723.
158. Lavagnini, I., R. Antiochia, and F. Magno, *An extended method for the practical evaluation of the standard rate constant from cyclic voltammetric data.* Electroanalysis, 2004. **16**(6): p. 505-506.
159. Klingler, R.J. and J.K. Kochi, *Electron-transfer kinetics from cyclic voltammetry. Quantitative description of electrochemical reversibility.* J. Phys. Chem., 1981. **85**(12): p. 1731-1741.
160. Delahay, P., *Theory of Irreversible Waves in Oscillographic Polarography.* J. Am. Chem. Soc., 1953. **75**(5): p. 1190-1196.
161. Vogel, A.I. and G. Svehla, Vogel's Textbook Of Macro And SemiMicro Qualitative Inorganic Analysis (Longman London) 1979.
162. Paul, M.A. and F.A. Long, *H_o and related indicator acidity functions.* Chemical Reviews, 1957. **57**(1): p. 1-45.
163. Grilij, J., *Synthesis and photophysical characterization of tetracyano-p-phenylenediamine.* (Diplomarbeit) Institute o f Physical & Theoretical Chemistry, Graz University of Technology, Austria, 2004.
164. Rosspeintner, A., *Kinetics of photoinduced electron transfer reactions between 2,6-dicyano-N,N,N',N'-tetramethylp-phenylenediamine and various quenchers.* Master Thesis, Technical University Graz, 2002.
165. Webster, O.W., M. Brown, and R.E. Benson, *Tetracyano-p-phenylenediamine.* J. Org. Chem., 1965. **30**(9): p. 3250-2.
166. Landgraf, S., *Application of semiconductor light sources for investigations of photochemical reactions.* Spectrochimica Acta - Part A: Molecular and Biomolecular Spectroscopy, 2001. **57**(10): p. 2029-2048.
167. Justinek, M., *Set-up of a Single Photon Timing equipment and the fluorescence quenching of rubrene by organic radicals.* Master Thesis, Technical University Graz, 1999.
168. Kubista, M., et al., *Experimental correction for the inner-filter effect in fluorescence spectra.* Analyst, 1994. **119**(3): p. 417-419.

169. Dhami, S., et al., *Phthalocyanine fluorescence at high concentration: dimers or reabsorption effect?* Photochemistry and Photobiology, 1995. **61**(4): p. 341-346.
170. Angulo, G., G. Grampp, and A. Rosspeintner, *Recalling the appropriate representation of electronic spectra.* Spectrochimica Acta - Part A: Molecular and Biomolecular Spectroscopy, 2006. **65**(3-4): p. 727-731.
171. Fery-Forgues, S. and D. Lavabre, *Are Fluorescence Quantum Yields So Tricky to Measure? A Demonstration Using Familiar Stationery Products.* J. Chem. Educ., 1999. **76**(9): p. 1260-1264.
172. Birks, J.B., Photophysics of Aromatic Molecules (Wiley monographs in chemical physics), 1970.
173. Kirkbright, G.F., *Determination of absolute fluorescence quantum efficiency of quinine bisulfate in aqueous medium by optoacoustic spectrometry.* Anal. Chem., 1977. **49**(12): p. 1850-1852.
174. Reynolds, G.A. and K.H. Drexhage, *New coumarin dyes with rigidized structure for flashlamp-pumped dye lasers.* Optics Communications, 1975. **13**(3): p. 222-225.
175. Kubin, R.F. and A.N. Fletcher, *Fluorescence quantum yields of some rhodamine dyes.* J. Lumin., 1982. **27**(4): p. 455-462.
176. Long, J.S., et al., *Oxidation of Several p-Phenylenediamines in Room Temperature Ionic Liquids: Estimation of Transport and Electrode Kinetic Parameters.* The Journal of Physical Chemistry C, 2008. **112**(17): p. 6993-7000.
177. Sharp, M., *Determination of the charge-transfer kinetics of ferrocene at platinum and vitreous carbon electrodes by potential steps chronocoulometry.* Electrochimica Acta, 1983. **28**(3): p. 301-308.
178. Bhat, M.A., et al., *Outer Sphere Electroreduction of CCl4 in 1-Butyl-3-methylimmidazolium Tetrafluoroborate: An Example of Solvent Specific Effect of Ionic Liquid.* The Journal of Physical Chemistry B, 2009. **113**(9): p. 2848-2853.
179. Jacob, S.R., et al., *Variable-Temperature Microelectrode Voltammetry: Application to Diffusion Coefficients and Electrode Reaction Mechanisms.* The Journal of Physical Chemistry B, 1999. **103**(15): p. 2963-2969.
180. Mowry, D.T., *The Preparation of Nitriles.* Chemical Reviews, 1948. **42**(2): p. 189-283.
181. Braun, C.L., T.W. Scott, and A.C. Albrecht, *Multiphoton ionization of N,N,N'.N'-tetramethyl-p-phenylenediamine: the condensed-phase two-photon ionization spectrum.* Chem. Phys. Lett., 1981. **84**(2): p. 248-252.
182. Fernández, H. and M.A. Zón, *Determination of the kinetic and activation parameters for the electro-oxidation of N,N,N', N'-tetramethyl-p-phenylenediamine (TMPD) in acetonitrile (ACN) by chronocoulometry and other electrochemical techniques.* Journal of Electroanalytical Chemistry, 1990. **283**(1-2): p. 251-270.
183. Honma, H., H. Murai, and K. Kuwata, *CIDEP study on photooxidation of N,N,N',N'-tetramethyl-p-phenylenediamine by maleic anhydride. Enhanced S-T_{-1} mixing by radical-ion pair system.* Chem. Phys. Lett., 1992. **195**(2-3): p. 239-242.
184. Cataldo, F., *On the polymerization of p-phenylenediamine.* European Polymer Journal, 1996. **32**(1): p. 43-50.
185. Sacher, M. and G. Grampp, *Magnetic field effects on the luminescence of p-phenylenediamine derivatives.* Berichte der Bunsengesellschaft/Physical Chemistry Chemical Physics, 1997. **101**(6): p. 971-974.
186. Lawrence, N.S., et al., *Voltammetric investigation of hair dye constituents: Application to the quantification of p-phenylenediamine.* Analyst, 2001. **126**(11): p. 1897-1900.

187. Lü, J.-M., et al., *14N/15N Isotope Effect on the Electron Transfer Process between N,N,N',N'-Tetramethyl-p-phenylenediamine and Wurster's Blue.* The Journal of Physical Chemistry A, 2001. **105**(29): p. 6971-6975.
188. Ito, A., et al., *Polycationic states of oligoanilines based on Wurster's blue.* European Journal of Organic Chemistry, 2009(26): p. 4441-4450.
189. Rosenmund, K.W. and E. Struck, *Das am Ringkohlenstoff gebundene Halogen und sein Ersatz durch andere Substituenten. I. Mitteilung: Ersatz des Halogens durch die Carboxylgruppe.* Berichte der deutschen chemischen Gesellschaft (A and B Series), 1919. **52**(8): p. 1749-1756.
190. v. Braun, J. and G. Manz, *Fluoranthen und seine Derivate. III. Mitteilung.* Justus Liebigs Annalen der Chemie, 1931. **488**(1): p. 111-126.
191. Ellis, G.P. and T.M. Romney-Alexander, *Cyanation of aromatic halides.* Chemical Reviews, 1987. **87**(4): p. 779-794.
192. Veauthier, J.M., et al., *The Synthesis of Polynitrile Aromatic and Oligopyridine Ligands via Palladium-Catalyzed Cyanation of Aryl Halides.* ChemInform, 2006. **37**(8): p. no-no.
193. Cassar, L., et al., *Phase-transfer catalysis in the nickel-catalyzed cyanation of aryl halides.* Journal of Organometallic Chemistry, 1979. **173**(3): p. 335-339.
194. Schareina, T., A. Zapf, and M. Beller, *Improving palladium-catalyzed cyanation of aryl halides: development of a state-of-the-art methodology using potassium hexacyanoferrate(II) as cyanating agent.* Journal of Organometallic Chemistry, 2004. **689**(24): p. 4576-4583.
195. Cassar, L., S. Ferrara, and M. Fo, *Nickel-Catalyzed Cyanation of Aromatic Halides*, in *Homogeneous Catalysis II*. 1974, American Chemical Society. p. 252-273.
196. Friedman, L. and H. Shechter, *Dimethylformamide as a Useful Solvent in Preparing Nitriles from Aryl Halides and Cuprous Cyanide; Improved Isolation Techniques1a.* The Journal of Organic Chemistry, 1961. **26**(7): p. 2522-2524.
197. Vagin, S., et al., *Synthesis and Properties of an Unsymmetrical Triazole-Functionalized (Phthalocyaninato)zinc Complex.* European Journal of Organic Chemistry, 2005. **2005**(15): p. 3271-3278.
198. Newman, M. and H. Boden, *Notes- N-Methylpyrrolidone as Solvent for Reaction of Aryl Halides with Cuprous Cyanide.* The Journal of Organic Chemistry, 1961. **26**(7): p. 2525-2525.
199. Luo, F.-T., V.K. Ravi, and C. Xue, *The novel reaction of ketones with o-oxazoline-substituted anilines.* Tetrahedron, 2006. **62**(40): p. 9365-9372.
200. Bacon, R.G.R. and H.A.O. Hill, *210. Metal ions and complexes in organic reactions. Part I. Substitution reactions between aryl halides and cuprous salts in organic solvents.* Journal of the Chemical Society (Resumed), 1964: p. 1097-1107.
201. Suzuki, H. and T. Hanafusa, *A Convenient Synthesis of Highly Substituted Benzonitriles and Benzenepolynitriles1.* Synthesis, 1974. **1974**(01): p. 53,55.
202. Olah, G.A., et al., *Recent aspects of nitration: New preparative methods and mechanistic studies (A Review).* Proceedings of the National Academy of Sciences of the United States of America, 1982. **79**(14): p. 4487-4494.
203. Olah, G.A. and S.J. Kuhn, *3,5-dinitro-o-tolunitrile.* Organic Syntheses, Coll. Vol., 1973. **5**: p. 480.
204. Bourne, E.J., et al., *313. Studies of trifluoroacetic acid. Part V. Trifluoroacetic anhydride as a condensing agent in reactions of nitrous and nitric acids.* Journal of the Chemical Society (Resumed), 1952: p. 1695-1696.

205. Coon, C.L., W.G. Blucher, and M.E. Hill, *Aromatic nitration with nitric acid and trifluoromethanesulfonic acid.* The Journal of Organic Chemistry, 1973. **38**(25): p. 4243-4248.
206. Arya, D.P. and D.J. Jebaratnam, *Towards the development of non-enediyne approaches for mimicking enediyne chemistry: Design, synthesis and activity of a 1,4-bisdiazonium compound.* Tetrahedron Letters, 1995. **36**(25): p. 4369-4372.
207. Staab, H.A. and H. Haffner, *Orientierungseffekte auf Charge-Transfer-Wechselwirkungen, VIII. Diastereomere 4,7-Dimethoxy-12,15-dinitro[2.2]paracyclophane.* Chemische Berichte, 1977. **110**(10): p. 3358-3365.
208. Bennett, G.M. and R.L. Wain, *Organic molecular compounds. Part II.* Journal of the Chemical Society (Resumed), 1936: p. 1108-1114.
209. Senear, A.E., et al., *The synthesis of potential antimalarials. Some substituted N-phenylsulfonamides.* J. Org. Chem., 1946. **11**(4): p. 378-383.
210. Gottschlich, A. and K. Leverenz, *2,6-dicyano-4-nitroaniline and process for producing it*. 1968.
211. McGill, C.K. and A. Rappa, *Advances in the Chichibabin Reaction*, in *Advances in Heterocyclic Chemistry*, R.K.F.R.S. Alan, Editor. 1988, Academic Press. p. 1-79.
212. Kos, N.J., H.C. Van der Plas, and B. Van Veldhuizen, *Pyrimidines. 77. The Chichibabin reaction of purines with potassium amide in liquid ammonia.* The Journal of Organic Chemistry, 1979. **44**(18): p. 3140-3143.
213. Pozharskii, A.F. and et al., *Advances in the Study of the Chichibabin Reaction.* Russian Chemical Reviews, 1978. **47**(11): p. 1042.
214. Shreve, R.N., et al., *Amination in the Heterocyclic Series By Sodium Amide.* Industrial & Engineering Chemistry, 1940. **32**(2): p. 173-178.
215. Ottmann, G. and H. Hooks, *Chlorination of Aromatic N-Sulfinylamines.* The Journal of Organic Chemistry, 1965. **30**(3): p. 952-954.
216. Welcher, R., D. Berets, and L. Sentz, *Stability of Cyanogen.* Industrial & Engineering Chemistry, 1957. **49**(10): p. 1755-1758.
217. Brotherton, T.K. and J.W. Lynn, *The Synthesis And Chemistry Of Cyanogen.* Chemical Reviews, 1959. **59**(5): p. 841-883.
218. Middleton, W.J., et al., *Cyanocarbon Chemistry. III.1 Addition Reactions of Tetracyanoethylene.* J. Am. Chem. Soc., 1958. **80**(11): p. 2783-2788.
219. Hünig, S., et al., *N,N,N'N'-tetramethyl-p-phenylenediamine.* Organic Syntheses, Coll. Vol., 1973. **5**: p. 1018
220. Sorokin, Vladimir I., Valery A. Ozeryanskii, and Alexander F. Pozharskii, *A Simple and Effective Procedure for the N-Permethylation of Amino-Substituted Naphthalenes.* European Journal of Organic Chemistry, 2003. **2003**(3): p. 496-498.
221. Doornbos, T. and J. Strating, *The complete n-alkylation of 1,4-diamino-2,5-dibromobenzene and of 1,4-diamino-2,5-dimethoxybenzene.* Organic Preparations and Procedures, 1969. **1**(4): p. 287 - 303.
222. Li, Z., et al., *Synthesis of Structurally Identical Fluorine-18 and Iodine Isotope Labeling Compounds for Comparative Imaging.* Bioconjugate Chemistry, 2003. **14**(2): p. 287-294.
223. Allen, J.G., J. Burdon, and J.C. Tatlow, *1177. Aromatic polyfluoro-compounds. Part XXVII. Reactions of pentafluoro-aniline, -N-methylaniline, and -NN-dimethylaniline with nucleophiles.* Journal of the Chemical Society (Resumed), 1965: p. 6329-6336.
224. Pine, S.H. and B.L. Sanchez, *Formic acid-formaldehyde methylation of amines.* The Journal of Organic Chemistry, 1971. **36**(6): p. 829-832.
225. Billman, J.H., A. Radike, and B.W. Mundy, *Alkylation of Amines. I1.* J. Am. Chem. Soc., 1942. **64**(12): p. 2977-2978.

226. Thomas, D.G., J.H. Billman, and C.E. Davis, *Alkylation of Amines. II. N,N-Dialkylation of Nuclear Substituted Anilines.* J. Am. Chem. Soc., 1946. **68**(5): p. 895-896.
227. Bucsis, L. and K. Friedrich, *Polycyanbenzole V: Ein einfacher Zugang zum Tetracyanhydrochinon. Darstellung der 1,4-Dihalogen-tetracyanbenzole.* Chemische Berichte, 1976. **109**(7): p. 2462-2468.
228. Heqedus, L.S., et al., *Synthesis of 2,5-disubstituted 3,6-diamino-1,4-benzoquinones.* The Journal of Organic Chemistry, 1982. **47**(13): p. 2607-2613.
229. Chattopadhyay, N., *Determination of pK^* in excited state proton transfer (ESPT) reaction: a rearrangement of Weller's equation; advantage of dual luminescence.* J. Photochem. Photobiol., A, 1995. **88**(1): p. 1-4.
230. Siva Kumar, P., S. Kothai Nayaki, and M. Swaminathan, *Photophysical behaviour of 2,6-diaminoanthraquinone in different solvents and at various pH.* Spectrochimica Acta - Part A: Molecular and Biomolecular Spectroscopy, 2007. **68**(3): p. 651-655.
231. Nayaki, S.K. and M. Swaminathan, *Excited state solvatochromic and prototropic behaviour of 4-aminodiphenylamine and 4,4'-diaminodiphenylamine-A comparative study by electronic spectra.* Spectrochimica Acta - Part A: Molecular and Biomolecular Spectroscopy, 2006. **64**(3): p. 631-636.
232. Kothai Nayaki, S. and M. Swaminathan, *Unusual luminescence characteristics of aminobiphenyls.* Spectrochimica Acta - Part A: Molecular and Biomolecular Spectroscopy, 2002. **58**(13): p. 2931-2940.
233. Kothai Nayaki, S. and M. Swaminathan, *Spectral characteristics of 2-aminodiphenylamine in different solvents and at various pH values.* Spectrochimica Acta - Part A: Molecular and Biomolecular Spectroscopy, 2001. **57**(7): p. 1361-1367.
234. Swaminathan, M. and S.K. Dogra, Can. J. Chem., 1983. **61**: p. 1064.
235. Manoharan, R. and S.K. Dogra, *Acidity constants in the excited states: Absence of an excited-state prototropic equilibrium for the monocation-neutral pair of 2,3-diaminonaphthalene.* J. Phys. Chem., 1988. **92**(18): p. 5282-5287.
236. Manaoharan, R. and S.K. Dogra, *Spectral Characteristics of Phenylenediamines and Their Various Protonated Species.* Bull. Chem. Soc. Jpn.
, 1987. **60**: p. 4409-4415.
237. Rotkiewicz, K. and Z.R. Grabowski, *Excited states of aminoanthracenes. An experimental approach to electron density distribution.* Trans. Faraday Soc., 1969. **65**: p. 3263-3278.
238. Seliskar, C.J. and L. Brand, *Electronic spectra of 2-aminonaphthalene-6-sulfonate and related molecules. II. Effects of solvent medium on the absorption and fluorescence spectra.* J. Am. Chem. Soc., 1971. **93**(21): p. 5414-5420.
239. Fukuzumi, S., et al., *One-electron oxidation potential of an NADH model compoun and a dimer rhodium(I) complex in irreversible systems. A convenient determination from the fluorescence quenching by electron acceptors.* Bull. Chem. Soc. Jpn., 1983. **56**: p. 2220-2227.